Halogen ⋯ Halogen Interactions in Host – Guest Systems

Francoise Mystere Amombo Noa

Thesis presented for the degree of

DOCTOR OF PHILOSOPHY

in the Department of Chemistry

University of Cape Town

August 2017

University of Cape Town

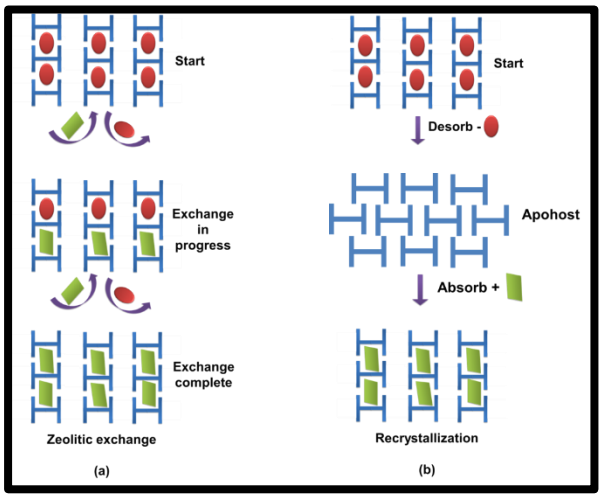

The copyright of this thesis vests in the author. No quotation from it or information derived from it is to be published without full acknowledgement of the source. The thesis is to be used for private study or non-commercial research purposes only.

Published by the University of Cape Town (UCT) in terms of the non-exclusive license granted to UCT by the author.

University of Cape Town

Hard Work Beats Talent When Talent Fails To Work.

(Kevin Durant)

Declaration

I, Francoise Mystere Amombo Noa, declare that the contents of this thesis represent my own work, and that the thesis has not previously been submitted for academic examination towards any qualification. Furthermore, it represents my own ideas and not necessarily those of the University of Cape Town.

FM Amombo Noa	**11 August 2017**
Signed	Date

Declaration_Inclusion Publications

"I confirm that I have been granted permission by the University of Cape Town's Doctoral Degrees Board to include the following publication(s) in my PhD thesis, and where co-authorships are involved, my co-authors have agreed that I may include the publication(s)"

I confirm that I have been granted permission by the University of Cape Town's Doctoral Degrees Board to include the following publication(s) in my PhD thesis, and where co-authorships are involved, my co-authors have agreed that I may include the publication(s):

a. Amombo Noa, F.M.; Bourne, S. A.; Nassimbeni, L. R. *Cryst. Growyh Des*. 2015, 15 (7), 3271 – 3279.*

b. Amombo Noa, F. M.; Bourne, S. A.; Su, H.; Nassimbeni, L. R. *Cryst. Growth Des*. 2016, 16 (3), 1636 - 1642.*

c. Amombo Noa, F. M.; Bourne, S. A.; Su, H.; Weber, E.; Nassimbeni, L. R. *Cryst. Growth Des*. 2016, 16 (8), 4765 – 4771.*

d. Amombo Noa, F. M.; Bourne, S. A.; Su, H.; Nassimbeni, L. R. *Cryst. Growth Des*. 2017, 17 (4), 1876 – 1883.*

e. Amombo Noa, F. M.; Bourne, S. A.; Su, H.; Nassimbeni, L. R. *Cryst. Growth Des*. 2017, 17 (9), 4647 – 4654.*

SIGNATURE: FM Amombo Noa DATE: 11/08/2017

STUDENT NAME: FM Amombo Noa STUDENTNUMBER: AMMFRA002

Acknowledgments

I will like to express my gratitude to my supervisors: Professor Luigi R. Nassimbeni and Professor Susan A. Bourne for their guidance, encouragement and motivation during the PhD course.

I owe special thanks to Dr. Hong Su for her assistance on single crystal X-ray diffraction data collection.

I am grateful for Dr. Leigh Loots for her training in using computer programs to solve troublesome crystal data.

I will like to also thank the University of Cape Town (UCT) and the National Research Foundation (NRF) for their financial support.

I am very fortunate to have met friends at the UCT chemistry department. It has been a great experience.

Special thanks to the past and present members of the Supramolecular Chemistry research group for their help and support.

Finally to my parents, for their unconditional love and their belief in me.

Dedication

To my dearest parents Vincent and Rosalie

For their endless love

Publications and Conferences

Parts of this thesis have been published:

1. Amombo Noa, F.M.; Bourne, S. A.; Nassimbeni, L. R. *Cryst. Growyh Des*. 2015, 15 (7), 3271 – 3279.

   Title: Halogen Bonding in Host – Guest Compounds: Structures and Kinetics of Enclathration and Desolvation.
2. Amombo Noa, F. M.; Bourne, S. A.; Su, H.; Nassimbeni, L. R. *Cryst. Growth Des*. 2016, 16 (3), 1636 -1642.

   Title: Guest Exchange in Halogenated Host – Guest Compounds: Structures and Kinetics.
3. Amombo Noa, F. M.; Bourne, S. A.; Su, H.; Weber, E.; Nassimbeni, L. R. *Cryst. Growth Des*. 2016, 16 (8), 4765 – 4771.

   Title: Hydrogen Bonding *versus* Halogen Bonding in Host – Guest Compounds.
4. Amombo Noa, F. M.; Bourne, S. A.; Su, H.; Nassimbeni, L. R. *Cryst. Growth Des*. 2017, 17 (4), 1876 – 1883.

   Title: Secondary Interactions in Halogenated Werner Clathrates.
5. Amombo Noa, F. M.; Bourne, S. A.; Su, H.; Nassimbeni, L. R. *Cryst. Growth Des*. 2017, 17 (9), 4647 – 4654.

   Title: Halogen – Bonding, Isomorphism, Polymorphism and Kinetics of Enclathration in Host – Guest Compounds.

Parts of this thesis have been presented at the following conferences:

6. The 29th European Crystallographic Meeting (ECM29), Rovinj, Croatia: 23 – 28 August 2015.

   Title: Halogen Bonding in Host – Guest Compounds: Structures and Kinetics of Enclathration and Desolvation (oral presentation).
7. The Science Postgraduate Student Council Symposium, University of Cape Town, South Africa: 31 August 2016.

   Title: Guest Exchange in Halogenated Host – Guest Compounds: Structures and Kinetics (oral presentation).
8. The First Pan African Conference on Crystallography (PCCr1), University of Dschang, Cameroon: 6 – 10 October 2016.

   Title: Guest Exchange on Selected Halogenated Host – Guest Compounds: Structures and Kinetics (poster presentation).
9. 23rd International Conference on the Chemistry of the Organic Solid State (ICCOSS XXIII), Stellenbosch, South Africa: 02 – 07 April 2017.

   Title: Halogen and Hydrogen Bonding in Host – Guest Compounds (poster presentation).
10. 24th Congress and General Assembly of the International Union of Crystallography (IUCr – 2017), Hyderabad, India: 21 - 28 August 2017.

    Title: Hydrogen Bonding and Secondary Interactions in Halogenated Complexes (poster presentation).

ABSTRACT

Halogen ⋯ Halogen Interactions in Host – Guest Systems

For a few decades now, halogen bonds which are non-covalent interactions, have gained a lot of interest in the science community due to their applications in diverse research areas. Halogen bonding (XB) is an interaction that occurs between electron deficient halogen compounds and electron donors. This is an established non-covalent interaction in the solid and gaseous phase.

In this thesis, the work presented deals with the investigation of halogen bond interactions in host-guest complexes utilising both experimental and theoretical techniques.

Two host compounds, tetrakis-4-(bromophenyl)ethylene and its iodo-analogue were synthesised for the studies reported in Chapter 3, 4 and 5.

Chapter 3, deals with the classification of halogen ⋯ halogen interactions using halogenated methanes as guest solvents. Here, the inclusion complexes can be classified into different types of halogen bonds depending on their geometry. Type I, which are of van der Waals in nature usually have X ⋯ X distances greater than the sum of their van der Waals radii. Type II_a and II_b are interactions which are considered to be attractive and their X ⋯ X distances are usually shorter than those of type I. The compounds obtained in Chapter 3 were used to study both the kinetics of desolvation and the kinetics of enclathration for the solid host-methyl iodide vapour reactions, to obtain their rate law and determine activation energies.

In Chapter 4, the two hosts mentioned above were utilised to form inclusion compounds with a series of halogenated compounds for guest exchange reactions. The structures of the starting inclusion compounds were exposed to the vapours of the second incoming guests to form intermediate complexes and final compounds, which were used to analyse the halogen ⋯ halogen interactions in their structures. NMR spectroscopy was performed on selected

crystals to monitor the guest exchange experiment and the rate law of each exchange reaction was established.

Tetrakis-4-(bromophenyl)ethylene and its iodo-analogue were also used as host compounds in Chapter 5. Here, halogen···halogen interactions are also classified and two novel polymorphs of tetrakis-4-(iodophenyl)ethylene with 3-picoline (3PIC) are reported. Kinetics of enclathration by suspension was conducted on two of the bromo-host inclusion compounds (with 3-bromopyridine and 3-picoline) at 25 °C and 35 °C.

Competition between hydrogen and halogen bonding was performed in Chapter 6, using three similar but subtly different host compounds with halogenated substituted pyridines as guests. IR spectroscopy and Hirshfeld surface analysis were utilised for further characterisation of these inclusion compounds.

The synthesis of halogenated Werner clathrates containing Cl^-, Br^- and I^- in Chapter 7, was conducted with various guests of substituted pyridines. Compounds, which were derived from NiI_2 yielded ionic complexes, forming iodide anions. Iodine was added to these complexes to form tri-iodide anions. The Werner clathrates obtained with the 4-picoline (4PIC) could also be directly synthesised by the exposure of $NiCl_2$/$NiBr_2$ to the vapour of 4PIC. Kinetics of enclathration of these two solid-vapour reaction compounds were also analysed.

All the structures in this study were elucidated using single crystal X-ray diffraction. Thermal analyses such as thermogravimetry (TG), hot stage microscopy (HSM) and differential scanning calorimetry (DSC) were used for the determination of the thermal behaviour of the new compounds. Variable temperature powder X-ray diffraction was also carried out for the characterisation of the new compounds.

Abbreviations and Compound Codes

H-bond	Hydrogen bond
X-bond	Halogen bond
CH_3I	Iodomethane
CH_2Cl_2	Dichloromethane
CH_2I_2	Diiodomethane
$CHCl_3$	Chloroform
CCl_4	Carbon tetrachloride
DCE	1, 2-dichlorethane
MeI	Methyl iodide
BEN	Benzene
PIP	Piperidine
2BrPY	2-bromopyridine
3BrPY	3-bromopyridine
3ClPY	3-chloropyridine
3PIC	3-picoline
DSC	Differential scanning calorimetry
TG	Thermogravimetric analysis
HSM	Hot-Stage microscopy
IR	Infra-Red
NMR	Nuclear Magnetic Resonance

Table of contents

Chapter II: Materials and Experimental Methods

List of Figures

List of Tables

The other figures and tables in this study are embedded into the publications.

CHAPTER I: INTRODUCTION

"Mankind is divisible into two great classes: Hosts and Guests."

-Max Beerbohm (b. 1872), Hosts and Guests

1.1 Molecular Chemistry in the Direction of Supramolecular Chemistry

Molecular chemistry is dependent on the covalent bond and understanding its properties, its formation and breaking between pairs of atoms, has given rise to the synthesis of the vast array of molecular compounds which are the products of our great science. Since the synthesis of urea by Wöhler[1] in 1828, synthetic methods in organic and organometallic chemistry have developed a series of very sophisticated methods which allow one to construct pre-designed molecules via controlled steps.[2,3]

By comparison, supramolecular chemistry relies on secondary interaction between molecules.

The term supramolecular chemistry was first introduced by Jean-Marie Lehn in 1978 as ''chemistry of molecular assemblies and of the intermolecular bond,''[4] although the term itself made a much earlier appearance (in Webster's Dictionary in 1903).[5] It can also be defined as the chemistry of the intermolecular bond, covering the structures and functions of the entities formed by association of two or more chemical species.[6-11] Traditionally phrases such as ''chemistry of the non-covalent bond'', and ''non-molecular chemistry'' or even ''lego chemistry'' were utilized to describe this field. [5]

Supramolecular chemistry is involved in diverse disciplines and fields, with a complete control over supramolecules which is comprised of two or more molecules, guests and hosts, interacting with each other in a noncovalent manner. Figure 1.1 illustrates the comparison between molecular and supramolecular chemistry.

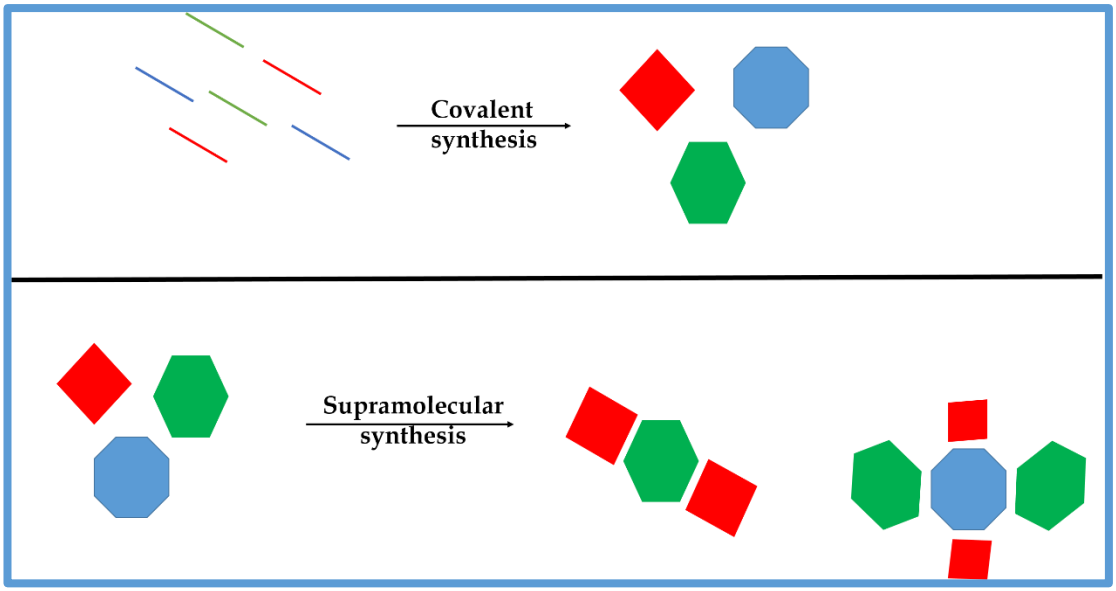

Figure 1.1 Comparison between the scope of molecular and supramolecular chemistry.

1.2 Halogen Bonding Definition

Since this thesis deals with halogen⋯ halogen interactions in host-guest chemistry, a brief introduction to this topic follows: A halogen bond R_a-X⋯Y-R_b is a highly directional, electrostatically driven non covalent interaction which occurs when there is evidence of a net attraction between an electrophilic region on a halogen atom and the nucleophilic region of a molecule. On the other hand, the halogen bond has been defined by Desiraju[12] as "A nonbonded interaction between an electrophilic halogen atom and an electronegative species". Halogen atoms are partially negatively charged species. This effect can be explained by the anisotropic nature of the electron density ρ(r) around the halogen nucleus, giving rise to a larger atomic radius in the equatorial region followed with smaller atomic radius in the polar region.[13-15] However, computational quantum mechanical and database studies of organo-halogens and dihalogens with some electron donors atoms (oxygen and nitrogen) suggested that the main attractive forces of the halogen

bond interaction is due to the electrostatic interaction between the polarised halogen atom and the electron donor.[16,17]

An International Union of Pure and Applied Chemistry (IUPAC) project recommended in 2013 that the halogen bond be defined as ''A halogen bond R-X···Y-Z occurs when there is evidence of net attractive interaction between an electrophilic region on a halogen atom X belonging to a molecule or a molecular fragment R-X (where R can be another atom including X, or a group of atoms) and a nucleophilic region of a molecule or molecular fragment, Y-Z''.[18] Useful features of halogen bond are given below:

a) The formation of a halogen bond is usually accompanied by an increase in the length of the R-X covalent bond.
b) The distance between the halogen atom donor X and acceptor atom Y is sometimes less than the sum of the van der Waals radii of X and Y.
c) Electrostatic, dispersion and polarization are the primarily forces involved in the formation of halogen bond. These forces play relative roles and may vary from one case to the other.
d) The halogen atom X can participate more than one halogen bond.
e) Halogen transfer reactions and other reactive phenomena are involved in halogen bonds.
f) The R-X···Y angle has the habit of being linear 180 ^{o} and the halogen atom X tends to align in the same direction of the axis of the n-lone pair on Y or the π bond electron pair in Y-Z.
g) The halogen bond strength decreases with the increase of an electronegative atom X and/or decreases with the electron withdrawing ability of R.
h) The bond critical point and a bond path connection between X and Y are usually illustrated by the electron density topology of the halogen bond.
i) There is an association between the formation of a halogen bond with the formation of new vibration modes, Raman absorptions, and

changes in the IR, NMR signals of R-X and Y-Z and blue shifts in UV visible spectrum of the halogen bond donor.

1.3 Halogen Bonding in History

Halogen bonding was first discussed in 1863 by Guthries[19] in the synthesis of NH_3I_2. This complex was made by addition of I_2 to a saturated solution of ammonium nitrate, which showed a quick decomposition into ammonia and I_2 when exposed to air. Lachman, in 1903 had proved that I_2 complexes in solvents show different colours, from brown in alcohols, red-brown in toluene, red in ethylene bromide and violet in chloroform.[20] This colour change was also explained by Krüss *et* al [21] suggesting that it is due to the different molecular weights of I_2; where I_2 solution is most likely to be violet, but $(I_2)_n$ (n > 1) forms a brown solution.

A study was also conducted into the different colours observed in I_2 solutions and a conclusion was drawn that the position of absorption bands in the visible region move gradually from violet to brown coloured solutions.[22] Also the 1: 1 I_2 with aromatic π electron donating molecules studied by Benesi *et* al [23] in 1949 rusing UV-Vis spectra revealed that there is a shift in absorption band in the visible region followed with an intense new band in the ultraviolet region and colour changes indicating the formation of the I_2 complexes with hydrocarbons in non-polar solvents. All the spectrophotometric studies had added toward the theory of charge-transfer complexes between electron donors and electron acceptors.[24- 26]

The theory of quantum mechanics of resonance complex was explained by Mulliken[27] using halogen bonding as a charge-transfer interaction.

The first crystallographic study of halogen bonding was conducted in 1950 by Hassel and co-workers[19] using the molecules of bromine and *p*-dioxane.[28] This crystallographic study elucidated a Br⋯O distance of 2.71 Å which is less

than the sum of the van der Waals radii for a bonded Br to oxygen (3.35 Å) and a C-Br ⋯ O angle of 180° (Figure 1.2).

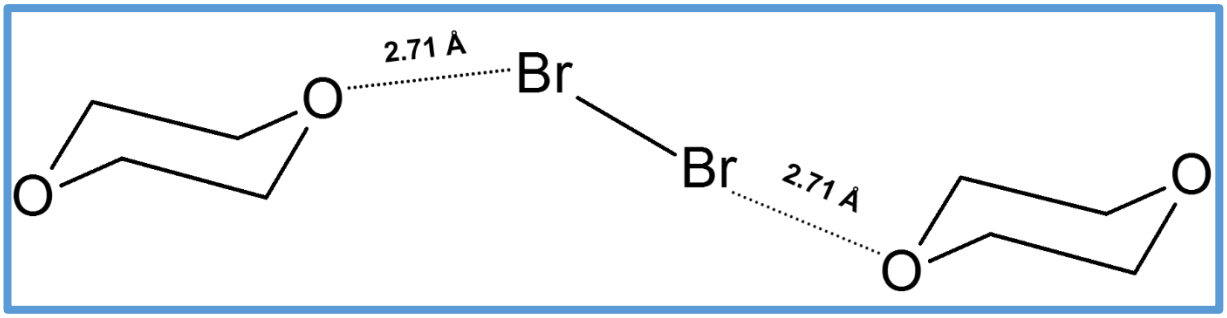

Figure 1.2 Halogen bonding in 1,4-dioxane and bromine structure. The first X-ray crystallographic evidence of a halogen bond.[28]

Hassel was awarded the Nobel prize in chemistry in 1969, for his discovery that halogens can act as electrophilic electron acceptors, and self-assemble towards highly directionally organised crystalline charge transfer complexes in the presence of electron donors.[29,30]

Several other halogenated molecules were studied using crystallography and spectroscopy with various Lewis bases.[29,31]

Around 1990 and 2000, other molecules rather than dihalogen molecules were studied as halogen bond donors, and their interaction properties were experimentally[32-34] and theoretically[17,35-38] examined. This study examined the geometric and energetic properties characterization of halogen bonds.

The term ''halogen bond'' was first used by Dumas in the context of the studies of complexes formed by CCl_4, CBr_4, $SiCl_4$ and $SiBr_4$ with organic solvents such as anisole, di-n-butyl ether, pyridine, tetrahydrofuran and tetrahydropyran.[39]

An advanced explanation of halogen bonding using the δ-hole concept was established by Politzer and co-workers.[13,14,40] Politzer suggested that the term 'δ-hole' donates the positive halogen surface region and that the halogen bond

is an electrostatically driven attractive interaction between a positive δ-hole on a covalently-bonded halogen atom and a negative site. The dependence of the magnitude and presence of the δ-hole on the halogen is due to the electron withdrawing power of the rest of the molecule.

The study of molecular electrostatic potential by Brinck[41,42] illustrated that in CH_3Br, CBr_4 and CCl_4 the halogen atoms have areas of positive electrostatic potential on the outer part of their surfaces, where the other sides of the halogen have the negative potential. Plots of CF_4, CF_3Cl and CF_3Br and CF_3I are given in Figure 1.3 using molecular electrostatic potential to illustrate the concept of δ-hole.

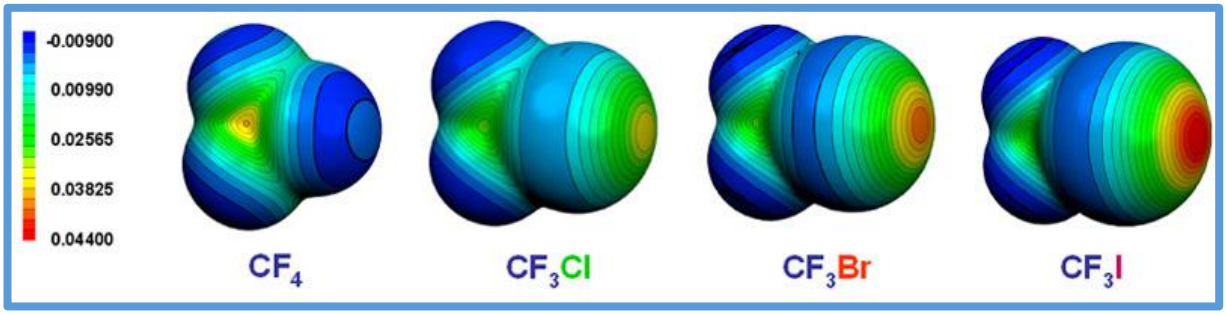

Figure 1.3 Molecular electrostatic potential of CF_4, CF_3Cl, CF_3Br and CF_3I showing the δ-hole in red.[14]

1.4 Halogen Bonding versus Hydrogen Bonding

Many studies (experimental and theoretical) have shown the intriguing similarities between halogen and hydrogen bonds. Both halogen and hydrogen bonds are classified as short range, electrostatically driven, non-covalent interactions which occur between a covalently bound, electropositive halogen or hydrogen and an electron donor. These interactions (halogen and hydrogen bonding) have long been recognised.[29, 43-45]

These two bonds are both highly directional interactions, and differ slightly; whereby halogen bonds are nearly linear with the R-X···D angle close to

180 °, whereas hydrogen bonds are more non-linear with the R-H···D angles less than 180 °.[46]

Metrangolo and co-workers showed the parallel between the energetic, geometric and spectroscopic features of halogen bonds and hydrogen bonds.[44] There is also a competition in the formation of the bond between halogen and hydrogen bonding.[43,47] They have similar bond strength ranging from 1 to 40 kcal/mol.[44,48] Competition studies between these two interactions have been carried out using computational calculations,[49-51] gas phase experiments[45] and in supramolecular crystals.[34, 52-54] In this thesis, competition study has been performed exploring the hydrogen and halogen bonding in host-guest compounds.[55]

The first competition study between halogen bonding and hydrogen bonding was in solution and was accomplished by Di Paolo *et* al, and found that these two interactions play a role in the mechanism of action of volatile anaesthetics.[56] Certain molecules are able to co-crystallize with both halogen and hydrogen bond donors.[34]

In spectroscopic studies, halogen bond systems exhibit blue shifts as well as red shifts similar to hydrogen bonded systems.[37,57]

Parallels have been drawn between halogen bonding and hydrogen bonding, but total replacement of the hydrogen bonding to halogen bonding was not particularly successful.[58,59]

Halogen bonding did show it competence[60] and even prevail over hydrogen bonding.[34,61,62] A lot of information regarding the strength of halogen bonding is computational and most of these studies are based on experimental evidence.

1.5 Nature and Strength of the Halogen Bond

Till this day, there is a debate concerning the source of the nature of halogen bond.[63] Quantum theory has played a major role in understanding the nature of halogen bond with the formation of complexes utilizing basically electrostatic forces in weakly halogen bonded compounds and more covalent forces in strongly halogenated bonded molecules.[64,65]

A study using the symmetry adapted perturbation theory has demonstrated that, with the increase in size of the halogen atom, the electrostatic and dispersive interactions also contribute to the increase in the strength of the interactions which become more dominant with iodine.[66]

The nature of halogen⋯ halogen interactions, particularly in Cl⋯ Cl interactions has received a fair amount of study over the decade. A database survey of halogen⋯oxygen interactions was conducted, illustrating that these interactions (X⋯ O) followed the halogen bond strength. This goes in the order Cl (27%) < Br (34%) < I (39%).[67]

When using Lewis base, the strength of a halogen bond (A-X⋯Lewis base) increases; when X is less electronegative, A is more electron withdrawing group and X is more polarizable.[63,67] The C-X⋯Lewis base angle (maximum 180 º) correlates with the strength of halogen bonding.[68] The strength of a halogen bond increases in the order N > O > S when using electron withdrawing atoms.[69] In addition, as the halogen electronegativity decreases (F > Cl > Br > I), the strength of C-X⋯H hydrogen bond decreases.[69]

1.6 Halogen ··· Halogen Interactions and Other Noncovalent Interactions Displayed by Halogen Atoms

The tendency for the formation of halogen bonds among the halogens is as follows: F << Cl < Br < I. Halogen ··· halogen interaction is another kind of interaction which is exhibited by halogen atoms and a lot of studies in the crystallographic field have been conducted containing halogenated molecules.[70-72]

Studies have been conducted by Desiraju *et* al[73] and Pedireddi *et* al[74] utilizing the Cambridge Structural Database (CSD)[75] as a tool, indicating that there are two types of interactions, type I and type II. Type II, however can be split into type II_a and II_b, following a study derived from experimental charge density analysis.[70] The outcome of the three types of geometries are shown in Figure 1.4.[76] Type I angles θ_1 and θ_2 are usually equal ($\theta_1 = \theta_2$), type II_a have $\theta_1 = 180\ ^{o}$ and $\theta_2 = 90\ ^{o}$. Type II_b, angles θ_1/θ_2 sometimes deviated from the ideal values of $180\ ^{o}/120\ ^{o}$.

The majority of type I cases arise from interactions across a crystallographic centre of symmetry with a linear C-X ··· X-C system, and are seldom observed. This type I is a symmetrical interaction through van der Waals interaction between two halogen atoms. Type II are usually unsymmetrical interactions, and are deemed to arise due to polarized halogen atoms, which increase from Cl through Br to I. Researchers, such as Price *et* al[77] and Lommerse *et* al[17] have proven that the interactions become stronger for more readily polarizable halogen atoms (Br and I).

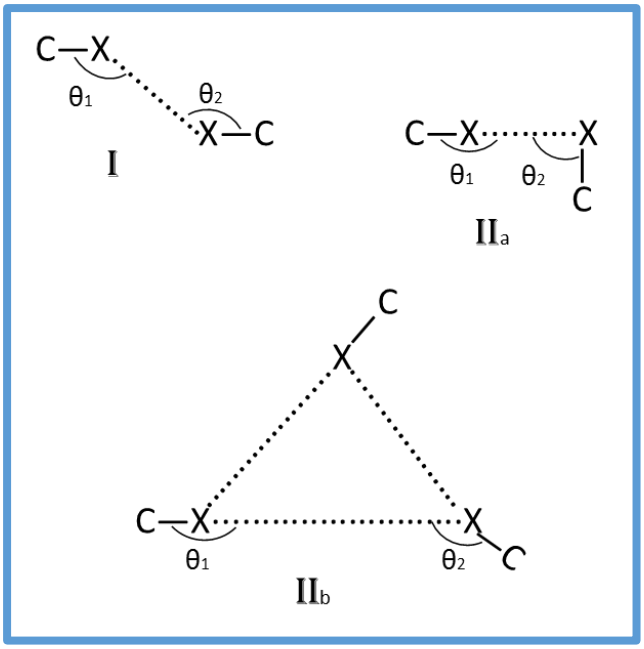

Figure 1.4 Halogen ⋯ Halogen Interactions.[76]

There are other interactions exhibited by halogens beyond the traditional C-X ⋯ Lewis base halogen bond. The π – system also functions as a Lewis base in the formation of halogen bonding in an orthogonal position with respect to the halogen atom, which is shown in Figure 1.5. [78-80] The C-X ⋯ π is an interaction dominated by dispersion and electrostatic interaction between the position region on the C-X axis and the negative electrostatic potential of the π – system which plays a non-negligible role.[81,82] There are similarities between the strength of C-H ⋯ π and C-X ⋯ π.[82]

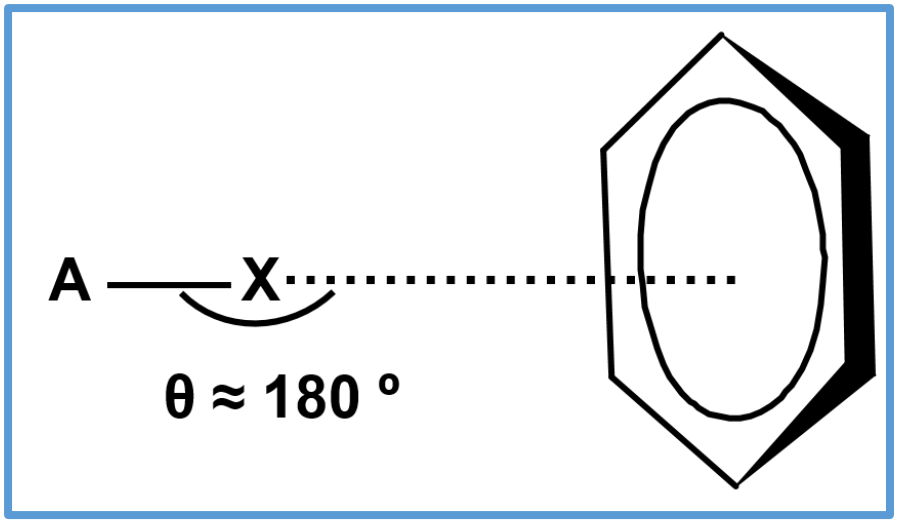

Figure 1.5 Schematic representation of a noncovalent interaction between a halogen atom and a benzene ring.

1.7 Halogen Bonding and Crystal Engineering

Crystal engineering is a branch of supramolecular chemistry which deals with the design of materials with specific properties. In the case of crystalline solids two main ideas are pertinent: self-assembly and the concept of synthons. Self-assembly is a spontaneous process, under thermodynamic control, which allows small entities to combine to form larger products.[83]

In supramolecular chemistry, a synthon is a structural unit within part of a supramolecule, which are assembled with the aid of intermolecular interactions via synthetic pathways.[84] It can be difficult to predict how these interactions are going to interact in a crystal structure due to the nature of the crystallization process. Formation of clusters by molecules increases in size until a critical formation of a nucleus. This occurs at the initial stage of the growth of the crystal.

However, it can be possible to predict a crystal structure of a small cluster, which does not relate to the structure of large clusters or the crystal morphology.

Over the last decade, halogen bonds have been used in the construction of a range of supramolecular architectures in the solid state, and play a prominent role in crystal engineering. Halogen bonds can link several molecules to form discrete supramolecules or functional materials such as: anion-organic frameworks,[85,86] conducting materials or magnetic molecular materials[87,88] and crystalline assemblies[89,90] with applications in liquid crystals.[91]

Halogen bonding has many applications in crystal engineering that have been reviewed. [88, 92-95] These involved several complexes connected by halogen bonds to form 1D, 2-dimensional (2D), and 3-dimensional (3D) networks of halogen bonding linked molecules or halogen bond networks.[95] A study, focusing on structures formation, between perfluorocarbon (PFC) and hydrocarbon (HC) compounds, is illustrated in Figure 1.6.[96] The I···N halogen bond in the structure was the main cause for the stabilisation of the complex between perfluorocarbon and hydrocarbon molecules.

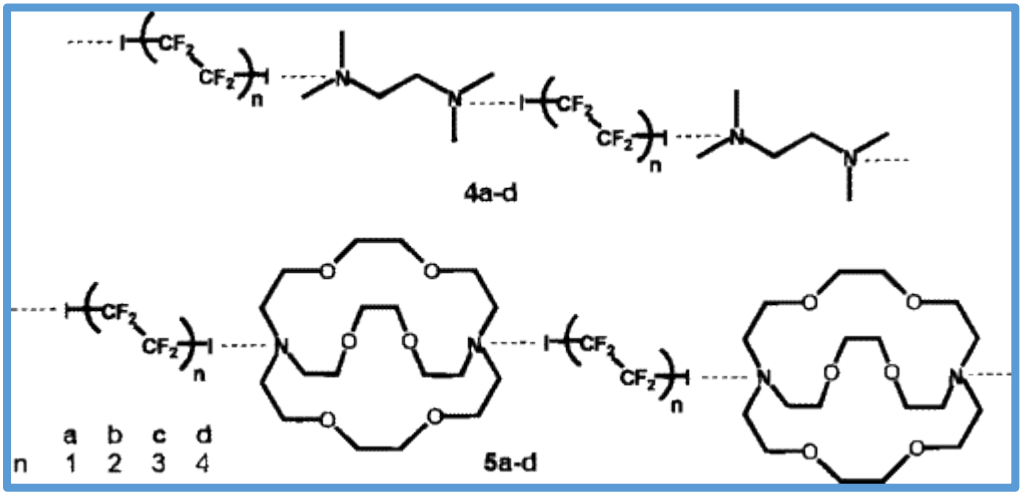

Figure 1.6 Halogen bonding in perfluorocarbon and hydrocarbon compounds.

Recently, halogen bonded complex 1D networks have been utilized to characterize anions and polyanions. Mixtures of nickel iodide, 3-picoline/4-picoline methanol/water, acetonitrile and iodine were synthesised by crystallisation. These formed supramolecular anions and polyanions. Figure 1.7, is an example of one of the halogen-bonded structures, in which the resulting crystalline compound (salt), has a $\mathbf{[Ni(H_2O)_2(3PIC)_4]^{2+}}$ cation and two iodide anions. This structure crystallizes in *C*2/*c* with Z = 4 and the Ni^{2+} ion located on a diad at Wyckoff position *e*. The coordination of the Ni ions remains as octahedral, with the two water molecules at the axial positions. The waters are hydrogen-bonded to the I^- anions.[97]

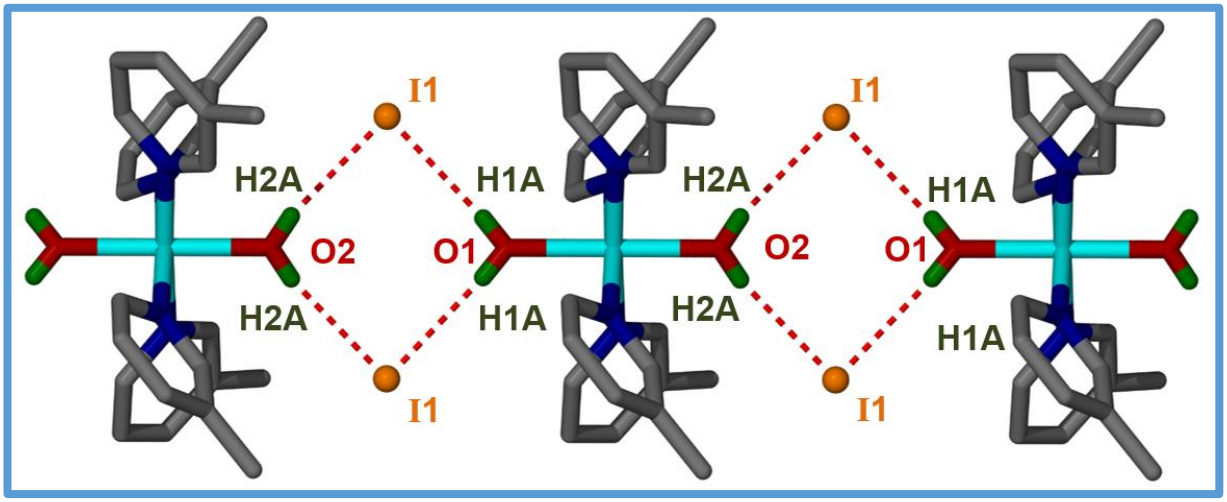

Figure 1.7 Hydrogen bonding ribbon of Diaquatetra(3-methylpyridine)nickel (II) diiodide.[97]

Halogen bonding and hydrogen bonding demonstrated simultaneous action for the construction of co-crystal networks. A study by Aakeröy and co-workers using 2, 3, 5, 6-tetrafluoro-4-iodobenzaldehyde oxime showed the ability of halogen atoms to act as both donors and acceptors generating in a 2D networks. This is illustrated in Figure 1.8.[53]

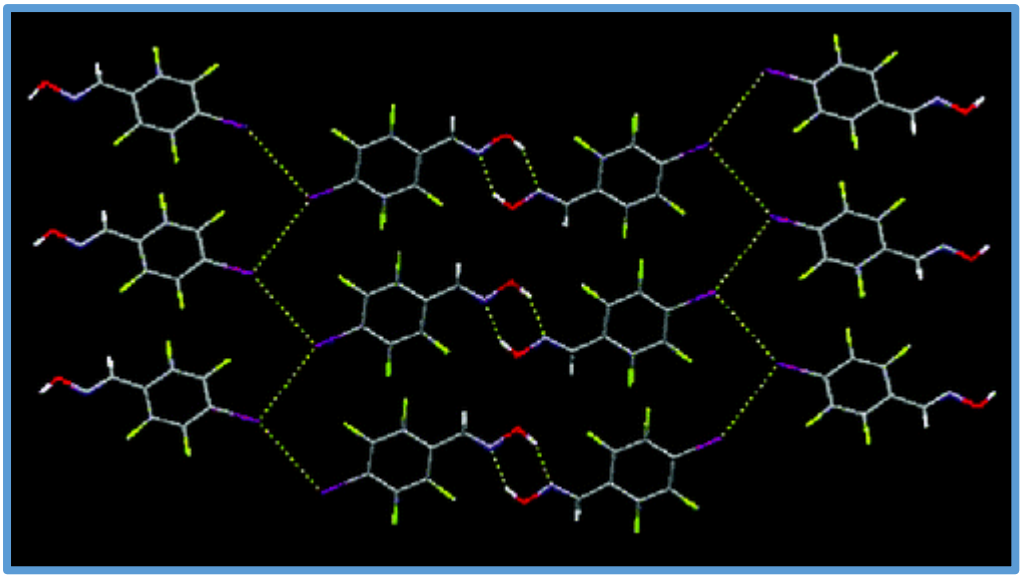

Figure 1.8 2D sheet generated through a combination of self-complementary hydrogen bonds and I···I interactions.[53]

The 3D architectures are formed by utilizing tetradentate modules. A 3D network example was formed with adamantoid crystal structure. The network was realised by the usage of tetradentate molecules bonded to two halogen bond donor sites and two halogen bond acceptor sites. The main interaction is the I···O connection. There are two of those I···O which are significantly below the van der Waals radii sum (I···O; 3.303 (11) and 3.379 (13) Å). These compounds have spaces in their centres which makes them porous and allows penetration by solvents.[98] The complex of tetraphenyl phosphonium iodide diiodoacetylene and/or tetrakis(4-pyridyl)pentaerythritol 1, 6-diiodoperfluorohexane also showed the presence of 3D networks via halogen bonds (Figure 1.9).[99, 100]

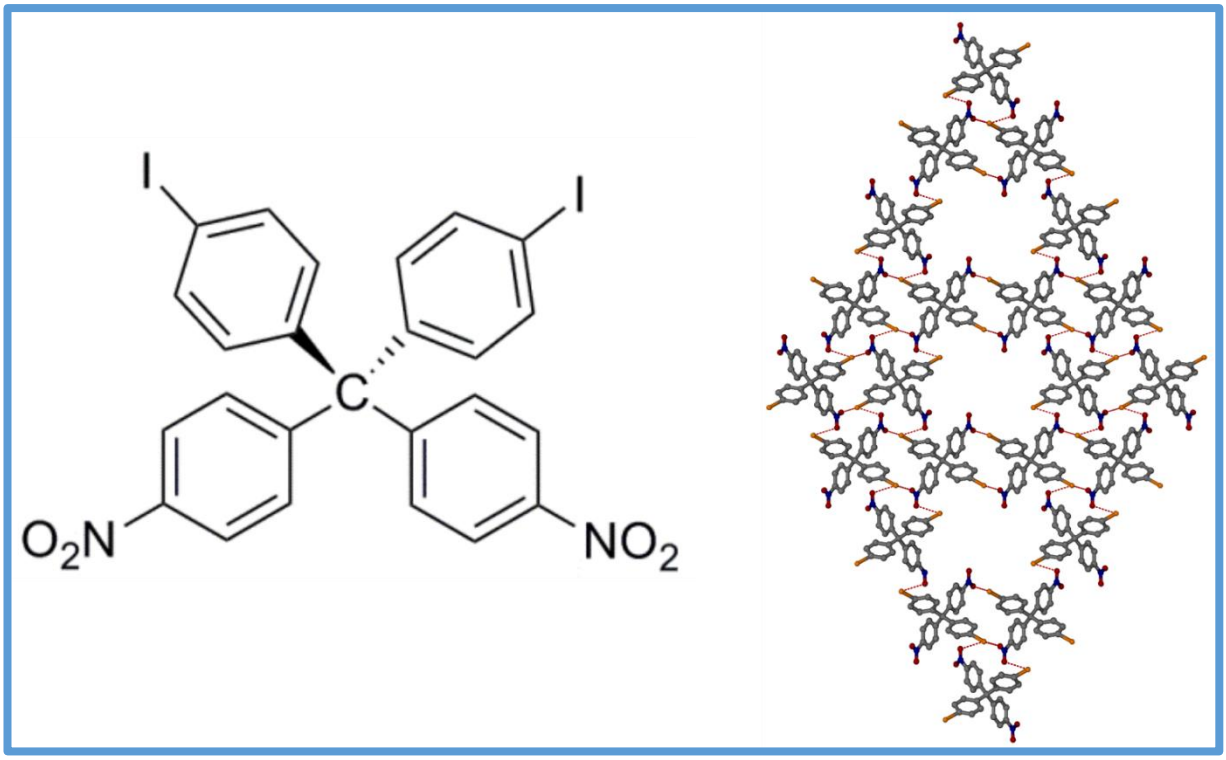

Figure 1.9 4′, 4′-Diiodo-4″, 4″-dinitrotetraphenylmethane and the structure of adamantoid, showing the I···O interactions.[98]

1.8 Hydrogen Bonding Definition

Hydrogen bonding has played and continues to play an important role in molecular self-assembly.[101-104] The Hydrogen bond was defined by Pauling in his book "The Nature of the Chemical Bond" according to which "Under certain conditions a hydrogen atom is attracted by rather strong forces to two atoms, instead of one atom. This may be considered as a bond between them; and it is called the hydrogen bond".[105]

In 1960, Pimental and McClellan described hydrogen bonding as: "There is evidence of a bond, and there is evidence that this bond involves an atom of hydrogen bonded to another atom".[106] Hydrogen bond was defined by a task group of International Union for Pure and Applied Chemistry (IUPAC) as being "The hydrogen bond is an attractive interaction between a hydrogen atom from a molecule or a molecular fragment R-H in which R is more

electronegative than H, and an atom or a group of atoms in the same or a different molecule, in which there is evidence of bond formation".[107] The IUPAC committee has recommended some criteria useful as evidence and some typical characteristics that define a weak interaction as a hydrogen bond. There are six of these criteria for a R-H···Y-Z:

a) Electrostatics, charge-transfer and dispersion are the forces involved in the formation of the hydrogen bond.
b) The covalent bond R-H is polarized and there is a strength increase with the increase in electronegativity of R in H···Y bond.
c) The stronger the R-H···Y is, the shorter the H···Y distance is; R-H···Y angle is usually closer to 180 °.
d) A red shift in the infrared R-H stretching frequency is the result of an increase in the R-H length in hydrogen bond formation. This bond length R-H also has an effect where there is an increase in the infrared absorption cross-section for the R-H stretching vibration. There is usually a strong H···Y bond link to a greater lengthening of the R-H···Y bond in hydrogen bonding. The association between new vibrational modes and the formation of the hydrogen bond is automatically generated.
e) R-H···Y leads to characteristic signatures in NMR which pronounced proton deshielding for hydrogen atom in the R-H, through hydrogen bond spin-spin couplings between R and Y; and enhancements of nuclear overhauser.
f) The detection of a hydrogen bonding is done experimentally by: the Gibbs energy of formation for a R-H···Y must be greater than the thermal energy of the system.

An IUPAC working group[108] suggested that typical characteristics for a hydrogen bond are:

a) There must be a strong correlation between the pK_a of R-H and pK_b of Y-Z and the energy of the hydrogen bond formed between them.

b) In proton transfer reactions (R-H ⋯ Y → R ⋯ H-Y) hydrogen bonding is considered as a partially activated precursor.
c) Networks in hydrogen bonds usually show cooperativity which deviate from pair wise additivity in the properties of hydrogen bond.
d) Crystal structures packing modes, are influenced by R-H ⋯ Y which are usually directional.
e) The extent of charge transfer between the donor and the acceptor, and the energy of interaction of the hydrogen bond are usually in good correlation.
f) The analysis of the electron density topology of a hydrogen bonded system generally illustrated a bond path connecting H and Y and a (3, -1) bond critical point between H and Y.

1.9 Hydrogen Bonding and History

Hydrogen bonding (H-bonding) is the most important of all directional interactions in a determined structure. The use of hydrogen bond (H-bond) has an influence on the crystal packing and has also been established in crystal engineering.[109-116] These hydrogen interactions are usually effects of charge dipole or dipole-dipole sources. The hydrogen bond can also arise from electrostatic forces; charge transfer and dispersion interactions also play and important role. The charge transfer interaction is distinguished by the R-H bond lengthening upon the formation of complex, and can be the main source for a red shift in the infrared R-H stretching frequency. The electrostatic interaction between an electron rich site H-bonding with the lone pair electrons of a heteroatom (N, O, Cl^-, I^-; called the hydrogen bond acceptor) and a hydrogen atom (H-bond donor) which is generally electron deficient. This interaction is usually represented as follow: A-H ⋯ B/B ⋯ H-A (where A is the electron withdrawing species which is covalently bound to the H (hydrogen) atom and B is a Lewis base. This representation of H-bonding is illustrated in Figure 1.10.

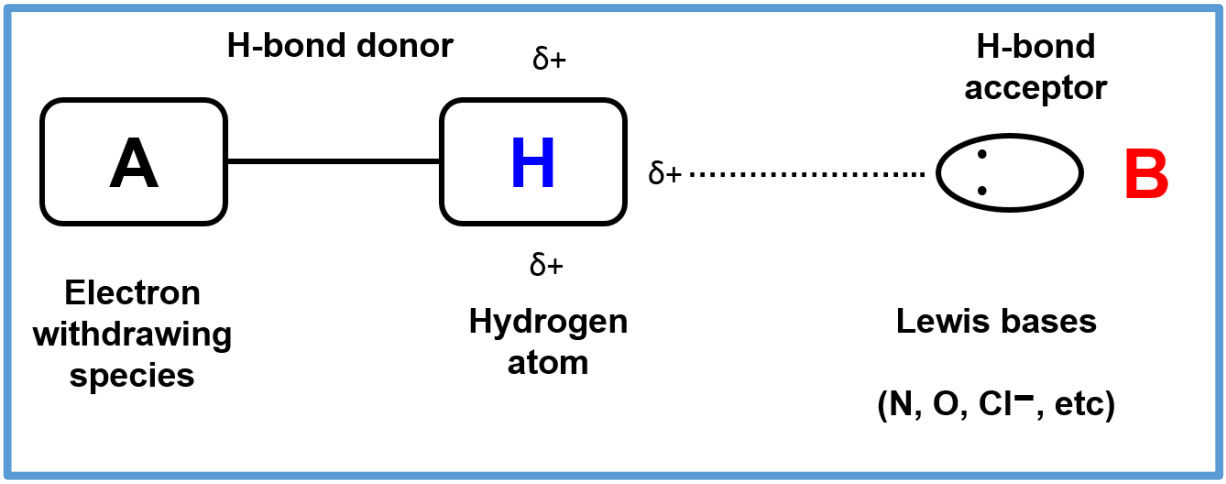

Figure 1.10 Hydrogen bonding: interactions between attraction and an electron rich Lewis base (H-bond acceptor) and an electron deficient H atom (H-bond donor).

In 1892, Nernst noted that, there are weak interactions between molecules containing hydroxyl group.[117] The first proper description of H-bonding however, came ten years later after the concept of "Nebenvalenz" meaning minor valence; and "Innerekomplexsalzbildung", which was established by Werner[118] and Hantzsch[119] describing the inter and intra-molecular of H-bonding. In Werner study, he illustrated that, ammonium salts has a configuration in which a proton remains between the molecule of ammonia and the ion. The name mesohydric form was the label given by Oddo *et al*[120] to describe intramolecular hydrogen bonds. This was utilized to explain the properties of some *o*-hydroxyazo derivatives of eugenol.

A study proposing a hydrogen bonded structure of trimethyl ammonium hydroxide was in a good agreement with Werner, thus for the accountability of its slight dissociation with comparison to tetramethyl ammonium hydroxide.[121] A year after the above research, Pfeiffer made a proposal of an intramolecular hydrogen bond, which was between hydroxyl and carbonyl functional groups in 1-hydroxyanthraquinone.[122]

The history of H-bond continues, when Latimer and co-workers[123] recognised the unusual properties of water and ice caused by the existence of the hydrogen bondings between H_2O molecules. This research showed that free

pair of electrons on one of the H_2O molecule can be able to exert enough force on the hydrogen held by a pair of electrons on another H_2O molecule to play a bridging role between the two molecules. This Lewis dot formalism was the first truly description called "Interaction bond". Lewis was the first one to quote the hydrogen bond.[124] The anion structure of $[F: H: F]^-$ was proposed by Pauling[125] using the residual entropy of ice with the concept of hydrogen bonding.[126]

A lot of theoretical and experimental resources have been discovered in 1936, applications of H-bond theory allowed to better understand its nature and behaviour in complex organic substances as: cellulose, gels, sugars, starch, proteins and other related substances.[127] Pauling and co-workers made a number of discoveries on the role of H-bonding in the function and structure of biomolecules and the description of elements of protein structure such as alpha helix and beta sheet.[128,129] The structure of DNA double helix was also elaborated by Watson and Crick.[130] H-bonding can have multiple electron rich sites that interact with a single hydrogen bond donor.[131] An H-bond is bifurcated when two electron rich sites interact with one donor, and can also be trifurcated when three acceptors bond to one donor. This is shown in Figure 1.11.

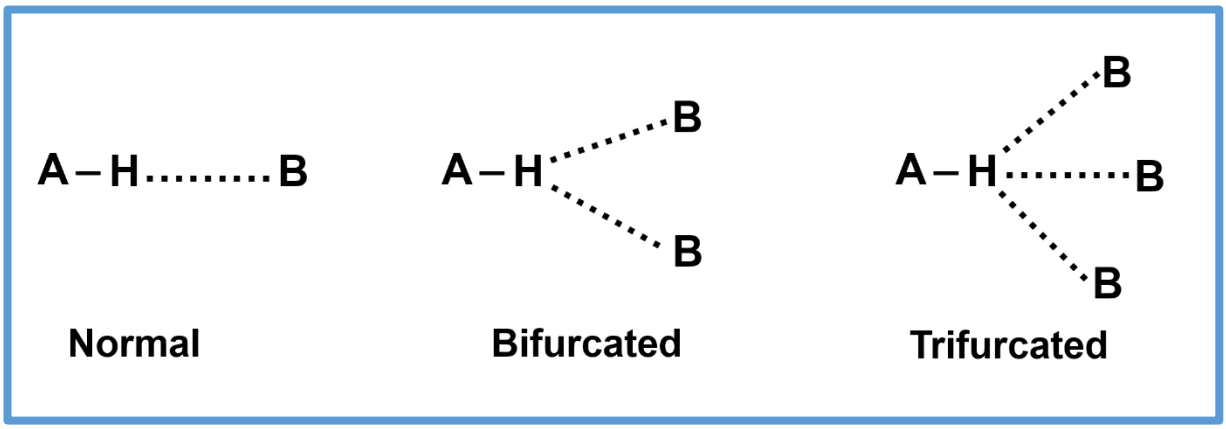

Figure 1.11 Multiple Lewis bases forming H-bonds with a single hydrogen atom.

H-bond energy cannot be measured in the solid state directly but can be obtained in the gas phase with estimated dissociation energies of 0.8 kJ/mol to 160 kJ/mol.[131] The strongest H-bonds can occur when one of the species is charged. $[F\text{-}H\text{-}F]^-$ is a structure with a strong dissociation energy (163 kJ/mol),[132,133] which is a greater magnitude than weak covalent bonds. This dissociation energy of 163 kJ/mol in $[F\text{-}H\text{-}F]^-$ is higher than that of the F-F covalent bond which is 150 kJ/mol.[102]

Hydrogen bonds can be classified as strong, moderate and weak. Strong hydrogen bonds often occur with shorter distance, and tend to form linear bonding.[134] These strong interactions are also affected by van der Waals interactions and charge-transfer, which contribute to the energy of stabilisation. The effects of stabilisation, however diminish with distance.[135] Hydrogen bonds can be also moderate with a dissociation energy of 10 kJ/mol to 40 kJ/mol. This type of H-bond is formed between uncharged species with a highly electronegative atom. This is the case of water molecules bonded to each other with a dissociation energy ranging from 19 kJ/mol to 21 kJ/mol in the gas phase.[131] The dissociation energy of weak hydrogen bonds are less than 10 kJ/mol and generally involve alkyl donors. This interaction is not directional as opposed to other electrostatic interactions.[131]

1.10 Nature and Strength of Hydrogen Bond

Hydrogen bonding is a special case of van der Waals bonding in which a hydrogen atom has an important role. Depending on the nature of the acceptor and donor group; the strength of hydrogen bond is displayed. The weaker hydrogen bonds are difficult to distinguish from van der Waals interactions; and the strongest hydrogen bonds are usually stronger than the weakest covalent bonds.[136] Hydrogen bond has many faces and gives rise to its own classification on the basic of energetic criteria. The strength of H-bond is characterised by:

- An intermolecular energy of the order of 20 kJ/mol or less (weak H-bond).
- A complexation energy from 20 – 50 kJ/mol (medium H-bond).
- A strong hydrogen bond with the interaction energy ranging from 80 – 150 kJ/mol.

Distinct energy decomposition schemes have been utilized for the decomposition of hydrogen bond energy into the energy terms. The first decomposition schemes was discussed by Kollman *et al*[137,138], where the total hydrogen bonding energy is broken into three contributions; the first one is electrostatic energy, the second contribution is the delocalisation energy and the third one is a conservative estimate of the correlation energy. Other studies on decomposition scheme, where the interaction energy is calculated within the Hartree-Fock theory of one electron approximation, were also conducted.[139,140] Another study on the analysis of different hydrogen bonded complexes was performed, showing that, there is a distance dependence on the energy components of hydrogen bonds.[141]

Electrostatic contribution is an important factor responsible for the classification of the hydrogen bond. It is observed in strong H-bonds and in weak H-bonds, dispersive interactions are dominant. The analysis of structural and spectroscopic data of a large number of O-H···O-H bondings showed an electrostatic covalent hydrogen bond model.[142] According to this model, weak hydrogen bonds are more electrostatic in nature. The covalent character of a bond depends on the strength of the interaction; as the strength of the interaction increases, the covalent bond increases. This phenomenon makes the very strong hydrogen bonds to be three-centre four-electron covalent bonds. This study of the weak H-bond being electrostatic in nature was also confirmed by Desiraju[48] where he claimed that the stronger hydrogen bonds are characterized by charge-transfer from the acceptor to proton donating bond, and the weak H-bond is electrostatic.

Other researchers illustrated that delocalization and electrostatic interaction energy are the most significant tool of attraction in terms of hydrogen bonding.[143,144]

1.11 Importance of Hydrogen Bonding in Crystal Engineering

Because of its potential applications in crystal engineering, the H-bond has been a tool of attraction. These applications can be the design of new materials, molecular recognition, small molecule inclusion, catalysis and sensor analysis.[145-151] Hydrogen bonding has been recognized as the master key in crystal engineering. It is the most used interaction due to its strength and directionality.[152,153] H-bond is the most reliable design tool in the non-covalent assembly of molecules. Hydrogen bonding still remains at the forefront of crystal engineering strategies. Crystal engineering is an interdisciplinary subject in which several of aspects of solid state supramolecular chemistry have been developed. The use of non-covalent interactions such as hydrogen bond, halogen bond, van der Waals interactions, π···π interaction and H···π in crystal engineering has been conducted. Hydrogen bonding is ubiquitous in nature and has played a significant role in the preparation of organic crystals. Depending on the strength some hydrogen bonds are stronger than weak covalent bonds and its directionality strategies; especially strong H-bonds as: O-H···O, O-H···N and N-H···O interactions.

The focus of crystal engineering in the exploitation of hydrogen bonding has been performed on same functional group or homosynthons. This is the example of OH···OH, COOH···COOH, $CONH_2$···$CONH_2$, etc…[84] There are also complementary functional groups which target the hererosynthon architecture. This heterosynthon can occur in structure with functional groups as carboxylic acid···pyridine[154] phenol···pyridine[155] acid···amide[154] bonding.

Figure 1.12 shows the heterosynthon between the carboxylic acid of vanillic acid hydrogen bonded to the imidazole nitrogen of caffeine.[154]

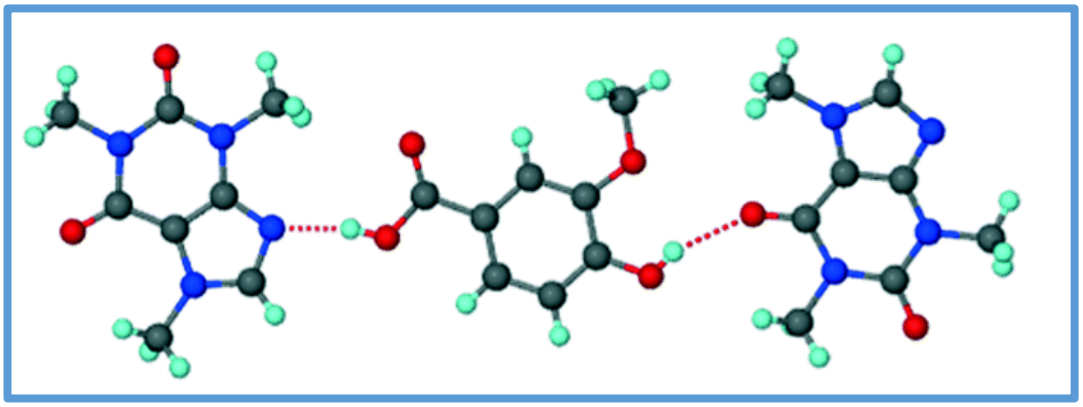

Figure 1.12 Hydrogen bonding on the caffeine vanillic acid structure showing the heterosynthon interaction.

H-bond was also found to have applications in synthetic material science. The investigation of the charge transport in the five-ring quinacridone and the four-ring epindolidione was illustrated, showing that the hydrogen bonding reinforce the intermolecular π stacking in support of the mobilities up to 1.5 cm^2/Vs with T80 lifetimes which is comparable with the most stable organic semiconducting materials. This is shown in Figure 1.13.[156]

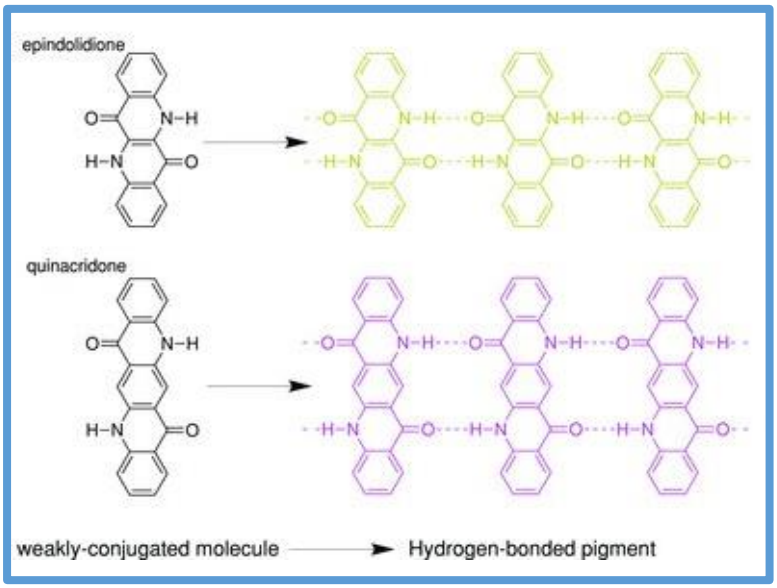

Figure 1.13 H-bonding between epindolidione/quinacridone molecules illustrating the template of intermolecular π stacking.

There are also other combinations of functional groups such as COOH $\cdots O_{nitro}$, C-H $\cdots N_{pyridyl}$ bonding among other possible interactions. George *et* al [157] showed that crystal engineering of ureas adopt the N-H $\cdots$ O tape α-network via I $\cdots O_2N$ synthon, which stabilizes the structure.

1.12 Organic Host Compounds Studied

The careful control of the overall architecture of organic crystalline molecules is the topic of intense interest, aiming to obtain desirable and useful properties. Halogen bonding has advantages in recycling and resolution processes which are an important segment in synthetic chemistry in terms of economic and environmental areas. In this research, the host compounds tetrakis(bromophenyl)ethylene and its iodoanalogue were chosen because they are reactive in terms of halogen bonding.[158] The compounds were first used by Toda *et* al with various guest molecules such as acetone, tetrahydrofuran,[159] p-xylene,[160] 1,1,2,2-tetrachloroethane[158] and C_{60} fullerence/toluene solvate.[161]

These two host compounds have proven to form chiral inclusion complex crystals with different achiral guest compounds in which the achiral host molecules are arranged in a chiral form.[159] Figure 1.14 shows the host conformation, where X is either Br or I.

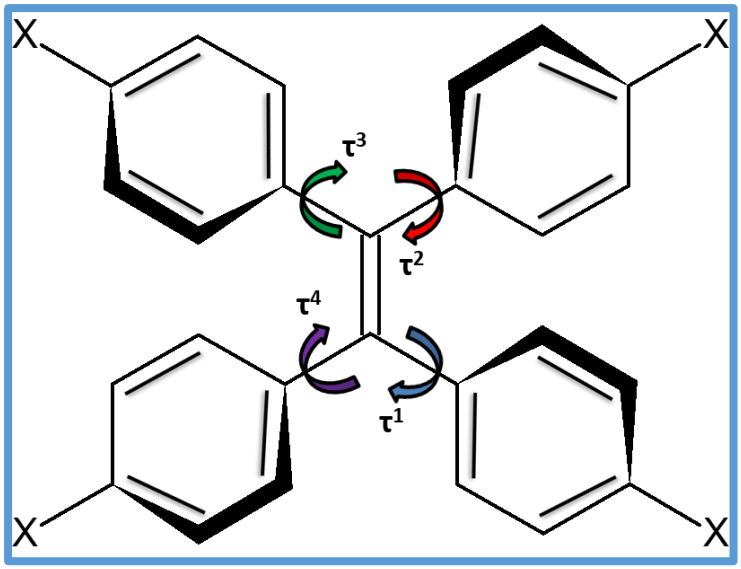

Figure 1.14 Propeller conformation of the host compounds.

Three similar host compounds (Figure 1.15) were all synthesised by Weber *et al*[162-164] and were also utilised in this thesis for the comparison between hydrogen and halogen bonding.

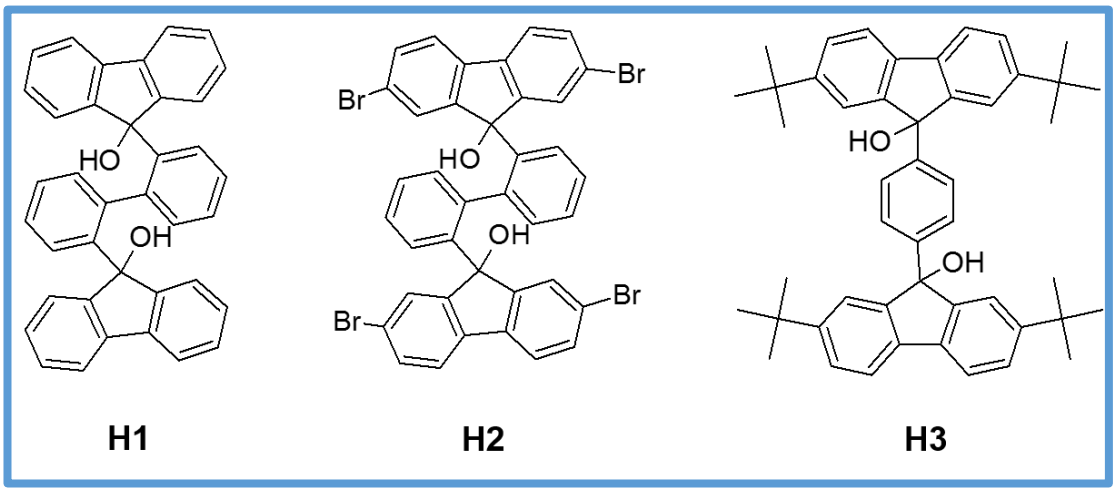

Figure 1.15 schematic representation of **H1**: 9, 9′-(Biphenyl-2,2′-diyl)difluoren-9-ol, **H2**: 2,2′,7,7′-tetrabromo-9,9′-(biphenyl-2,2′-diyl)difluoren-9-ol and **H3**: 2,2′,7,7′-tetra-tert-butyl-9,9′-(1,4-phenylene)difluoren-9-ol.

1.13 Werner Clathrates as Host Compounds

Werner clathrates are coordination complexes, and can be represented by the general formula MX_2A_4, where M is a divalent cation (Cr, Co, Fe, Hg, Mn, Ni, Fe), X denotes anionic ligands (NCS^-, NCO^-, NO_3^-, Cl^-, Br^-, I^-) and A is usually a neutral base, which are substituted pyridines, α-arylakylamines or isoquinoline. Werner clathrates have received great attention from many researchers in the past few years, due to their ability to entrap a wide range of compounds including noble gases[165-175] and condensed aromatic hydrocarbons.[165-176] The guest molecule in Werner clathrates is retained by steric barriers formed by the host molecule lattice. These complexes are also selective as their selectivity for molecules as possible guests differ according to the shape of the molecule.

The properties of Werner clathrates were investigated with the intention to use them for separation in petroleum fractions, and can be employed in clathrate chromatography in the analysis of compound mixtures and the accurate determination of isomers.[165-177]

The freedom of rotation of the Ni-N coordination bonds is the main reason why clathrates can be formed by inorganic complexes. Among various Werner clathrates, $[Ni(NCS)_2(4\text{-}MePy)_4]$ has been the most studied inclusion and illustrated general properties for the MX_2A_4 group. The guest component in this type of enclathration is located in layers, channels or cages. There is restriction of the conformational freedom of pyridine ring when they rotate around the Ni-N bonds. An example of a general Werner clathrate is shown in Figure 1.16.

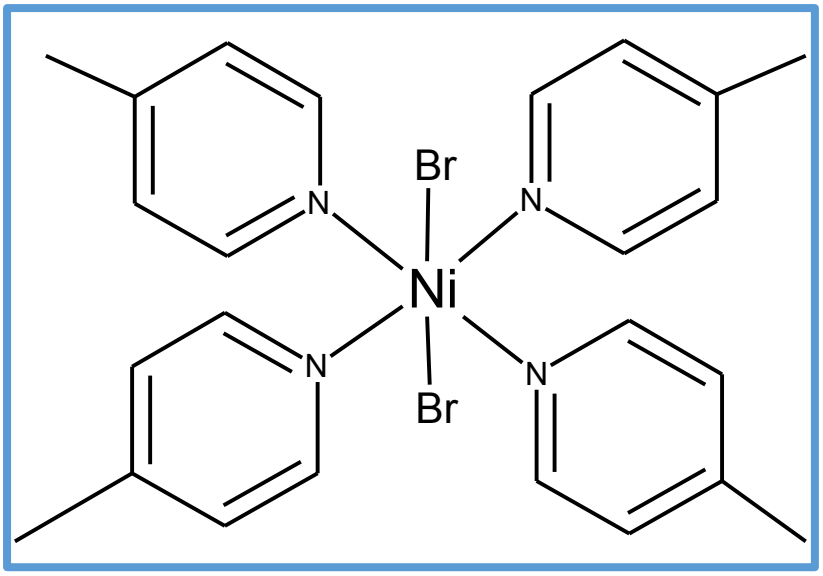

Figure 1.16 A schematic representation of a Werner clathrate complex.

The four torsion angles in these clathrates are usually independent of one another when the host molecules are located in general positions. In the case where the host molecules are on a centre of inversion or on a diad, there are two pairs of symmetry related angles. When the host molecule is on a diad, the axis is normally found to lie between the pyridine bases, but sometimes, it is found to pass through a pair of *trans*-pyridines.

The propeller conformation is obtained for the host compounds when the four torsion angles values are all positive (+ + + +) or all negatives (- - - -). The conformation where two of the torsion angles are positive and two negative (+ + - -) is found when the host component sits on a centre of symmetry. This conformation is not more commonly observed than the previous one because it is of higher potential energy. The other conformation (+ - + -) has not been found in any studies.

Fundamental research on the physical chemistry of these clathrates bas been conducted by Lipkowski, who reviewed their fundamental properties[178,179] outlined their structures and thermodynamics of the enclathration process. These complexes are generally synthesised by the decomposition of $NiCl_2$ with thiocyanate salt, and by the addition of the aromatic ligand.

The host [Ni(NCS)$_2$(4-methylpyridine)$_4$] has been revisited and its polymorphic phases and reactivity towards guest components has been studied.[180] Solid – solid grinding methods and solid solution were utilised to synthesise both $NiCl_2$ and $CoCl_2$ complexes with xylene isomers included as guest molecules.[181]

Recently, halogenated Werner clathrates containing Cl, Br and I were synthesised and characterised by single x-ray diffraction, solid-vapor kinetics of formation and thermal analysis.[97] In this study, complexes deriving from NiI_2 were found to be ionic. This research is explained in chapter 6.

1.14 Polyiodide Compounds

French chemist Courtois was the first to discover iodine in 1811 during the manufacture of potassium nitrate.[182,183] The element (I) was named after the Greek word for violet.[184] Iodine belongs to group 17 of the periodic table among the halogens. Iodine has 7 valence electrons in its highest energy level. This allows it to react with other elements by gaining an electron in order to fulfil the octect rule and become the anion I^-. This element exists at ambient conditions as a solid structure of diatomic molecules I_2, which have long I-I distance of approximately 2.7 Å.[185] Iodine can form polyiodide compounds due to its large atomic size and high electron affinity. Polyiodide was discovered by Pelletier and Caventou[186] when they illustrated that the addition of iodine to strychnine resulted in a crystalline compound of strychnine tri-iodide. The properties of iodine and its polyiodide compounds are distinct. Diatomic I_2 has characteristics of donor - acceptor features.[187] The molecules of iodine which are Lewis acid acceptors have strong affinity for iodide ion I^- which have energy of approximately 180 kJ/mol when compared to weak halogen$\cdots$ halogen interactions as Cl$\cdots$ Cl between chlorocarbons which are 5 kJ/mol.[44]

Polyiodides have gained much attention due to their interesting structural chemistry. Polyiodide compounds can contain up to 29 iodine atoms.[75,188] Polyiodides have various applications in several areas. One of the applications is the blue starch – iodine complex which was discovered already around 1814,[189] and can also be used as a sensitive analytical test for iodine.[190,191] Another amazing application of iodine is an appropriate antidote for the poisoning when it is in the form of a solution of iodine in potassium iodide (KI_3).[192] There are different structures of polyiodides which can form simple discrete units to very complex 2D and 3D networks. The first structural determination of a polyiodide compound was ammonium tri-iodide [$(NH_4)I_3$)].[193] Solid polyiodides have gained much attention for their unique electrical properties, which include acting as insulators, this depends on their structure and composition.[194,195]

Materials with magnetic properties containing polyiodide species have been studied.[196] The Nobel prize in chemistry (2000) was awarded to Alan J. Heeger, Alan G. MacDiarmid and Hideki Shirakawa for their novel preparation of conductive polymers using polyiodides.[197] Iodine-iodide clusters are built up by the I_3^- ion and discrete I_2 molecules which are connected together by medium strong to weak halogen – halide interactions. A study was conducted using various levels of Density Functional Theory (DFT) illustrating the influence of the electrostatic environment on tri-iodide interactions in dimer of $I_3^- \cdots I_3^-$. This research has shown that the chemical environment is vital for the correct modelling of these kinds of interactions.[198] Iodine – rich iodides are numerous and the structures of these compounds have been characterized.[199,200] Similar results were obtained when metal – iodide complexes interact with I_2. Strong interaction between iodine and transition metal – iodides are formed. These compounds may or may not comprise stabilized ligands.[201] The nature of the M-I $\cdots$ I-M moiety, where M is a transition metal has been of great interest. The formation of M-I $\cdots$ I-M structures by I $\cdots$ I interactions occurs by the formation of metal iodides via an

oxidative addition reaction of iodine (I_2). This is the case of the Pt(II)-I···I-Pt(II) interaction formed by the addition of I_2 to Pt(II) complexes.[202]

In our work, Werner clathrates containing polyiodides showed that the initial NiI_2 in the synthesis is replaced by $Ni(CH_3CN)_2$ and the detached I^- ion formed I_3^- in addition of I_2.[97]

Another computational investigation using DFT methods, illustrated that the theoretical method to study the electronic structure to obtain dyes and their adducts with I^- and I_3^- was conducted and that there was good agreement between the computational calculations and the experimental absorption bands were assigned to [dye^+I^-] compounds.[203] Polyiodides properties mentioned above show potential technical applications in various areas.

1.15 Aim of the Thesis

The overall aim of the project was to investigate the aspect of halogen···halogen interactions in host-guest systems with various tools. In particular, the objectives of this project were to:

- Investigate the geometry and statistical distribution of halogen···halogen interactions in the solid state, by mapping the parameters of R-X···X-R' systems in the Cambridge Structural Database (CSD) and in the new structures elucidated in this project. This was necessary in order to determine which compounds with halogen atoms such as Cl, Br and I form halogen···halogen interactions in the solid state.
- Characterise interactions between volatile guests like CH_3I and halogenated host compounds such as tetrakis-(4-bromophenyl) ethylene and its iodo-analogue.
- Perform guest exchange experiments of the obtained compounds to see if these new complexes would store the incoming volatile guests.
- Measure kinetics of enclathration between selected solid-host compounds and volatile halogenated guests. This experiment will be carried out on an especially constructed balance which is fully computerized and using thermogravimetric analysis.
- Measure kinetics of enclathration in aqueous suspension of selected guest solvents.
- Measure kinetics of decomposition of selected halogenated host –guest systems in order to obtain their activation energies and infer the mechanism of the reactions.
- Synthesise and characterise novel halogenated Werner hosts and study their interactions with halogenated guests.

An understanding of intermolecular interactions is required for the design of new solid forms with predetermined connectivity. Halogen bonds and hydrogen bonds are similar when dealing with synthetic tools. Looking at the similarities and differences of these two interactions in the same environment is quite advantageous when it comes to molecular recognition. The resultant structures from this research will be analysed with respect to halogen and hydrogen bonding found in these compounds by comparing the two interactions where possible.

1.16 Thesis Layout

The thesis consists of eight Chapters, Chapter 1 which is the general introduction to the study, followed by the experimental chapter, which describes the host compounds and the methods and instruments used (chapter 2). The results are presented from chapter 3 to 7 and chapter 8 is the general conclusion.

The thesis presents the results in the form of publications. I was the one who did all the experimental work:

a) The synthesis of the tetrakis-4-(bromophenyl)ethylene and the tetrakis-4-(iodophenyl)ethylene host compounds and their purifications.
b) Crystal growth and characterisation by thermal gravimetry, IR, NMR and structure solution and refinement.
c) The kinetics of desorption and evaluation of activation energies.
d) The kinetics of enclathration by stirred suspension.
e) The interpretation of the structural and thermal results.

1. Prof. L. R. Nassimbeni was the main supervisor who authorised the papers in conjunction with myself.

2. Prof. S. A. Bourne was the co-supervisor who provided scientific and editorial input into the papers.
3. Dr. Hong Su was responsible for the single crystal data X-ray collections, and assisted with data manipulation, especially with regards to absorption problems caused by very heavy atoms (iodine, bromine) and handling of decomposing crystals.
4. Prof. Edwin Weber supplied the host compounds which were employed in paper 3 (chapter 6).

Chapter 3, describes inclusion compounds of the two hosts tetrakis-4-(bromophenyl)ethylene and its iodoanalogue with a series of volatile halogenated methanes. The crystal structures were utilised for the characterisation of the halogen⋯halogen interactions and in the case of five isomorphous structures, these correlates with their activations of desorption. The packing of structures was studied by Hirschfeld surfaces analysis and the stability of these compound was measured by Differential Scanning Calorimetry (DSC). The kinetics of enclathration of the solid-vapor CH_3I reaction was measured and the kinetic law established.

In Chapter 4, guest exchange reactions of a series of halogenated inclusion compounds were carried out with a view to understanding the mechanism of these processes. The structures of the starting host-guest compounds, their intermediates and of the final products were elucidated. The halogen⋯halogen interactions were analysed. The kinetics of the exchange were followed by NMR spectroscopy and the rate laws established. The stoichiometry and thermal stabilities of the compounds were characterised by thermal gravimetry and differential thermal analysis.

Chapter 5, shows the synthesis of eight inclusion compounds of the hosts tetrakis(4-bromophenyl) ethylene and its iodoanalogue with substituted pyridines. The obtained compounds were characterised by X-ray diffraction, thermal analysis and kinetics of enclathration by suspension. The iodo host

yielded two polymorphs with 3-picoline. These polymorphs showed different void topologies in their DSC profiles.

Chapter 6 illustrates the work of three similar yet contrasting host compounds in order to study their propensity for hydrogen bonding versus halogen bonding with halogenated guests.

Chapter 7 deals with the synthesis of eight Werner hosts which contain Cl^-, Br^-, and I^- and their enclathration of various guests. Their structures have been elucidated and correlated with their thermal decomposition as measured by TG and DSC. Two of the hosts have also been synthesised by direct exposure of the $NiCl_2$/$NiBr_2$ to the vapour of 4-picoline, and the kinetics of these solid – vapor reactions have been analysed.

Chapter 8 summarises the main conclusions from all the obtained results.

1.17 References

1. Wöhler, F. *Ann. Phys*. 1828, 88 (2), 253 – 256.
2. Walvogel, S. R. *Angew. Chem. Int. Ed*. 2005, 44 (32), 5005 – 5006.
3. Lehn, J-M. *Angew. Chem. Int. Ed.* 1988, 27 (11), 89 – 112.
4. Lehn, J-M. *Supramolecular Chemistry: Concepts and Perspectives; VCH: Weinheim,* 1995.
5. Atwood, J. L.; Steed, J. W. *Encyclopedia of Supramolecular Chemistry. Marcel Dekker, Inc. New York, Basel.* 2004, Vol. 2, pp. 1401.
6. Lehn, J-M. *Struct. Bonding*. 1973, 16, 1.
7. Lehn, J-M. *Pure. Appl. Chem.* 1978, 50, 871.
8. Lehn, J-M. *Science*. 1985, 227, 849.
9. Lehn, J-M.; Atwood, J. L.; Davies, J. E.; MacNicol, D. D.; Vögtle, F. *Comprehensive supramolecular Chemistry. Wiley & Sons, New York*. 1991.
10. Steed, J. W.; Atwood, J. L. *Supramolecular Chemistry. John Wiley & Sons. Chichester*. 2000.
11. Steed, J. W.; Turner, D. R.; Wallace, K. J. *Core Concepts in Supramolecular Chemistry and Nanochemistry. Singapore; John Wiley & Sons*. 2007.
12. Desiraju, G. R. *Crystal Engineering: The Design of Organic Solids; Elsevier: Amsterdam,* 1989.
13. Murray, J. S.; Paulsen, K.; Politzer, P. *Proc. India Acad. Sci Ser. Chim.* 1994, 106, 267 – 275.
14. Clark, T.; Hennemann, M.; Murray, J. S.; Politzer, P. *J. Mol. Model.* 2007, 13, 291 – 296.
15. Politzer, P.; Lane, P.; Concha, M. C.; Ma, Y. G.; Murray, J. S. *J. Mol. Model.* 2007, 13, 305 – 311.
16. Ramasubbu, N.; Parthasarathy, R.; Murray, R. P. *J. Am. Chem. Soc.* 1986, 108 (15), 4308 - 4314.
17. Lommerse, J. P. M.; Stone, A. J.; Taylor, R.; Allen, F. H. *J. Am. Chem. Soc.* 1996, 118 (13), 3108 - 3116.

18. Desiraju, G. R.; Ho, P. S.; Kloo, L.; Legon, A. C.; Marquardt, R.; Metrangolo, P.; Politzer, P. A.; Resnati, G.; Rissanen, K. *Appl. Chem.* 2013, 85, 1711.
19. Guthries, F. *J. Am. Chem. Soc.* 1863, 16, 239 – 244.
20. Lachman, A. *J. Am. Chem. Soc.* 1903, 25 (1), 50 – 55.
21. Krüss, J.; Thiele, H. *Zfschu. Anorg. Chem.* 1894, 7, 25.
22. Walker, O. J. *Trans. Faraday Soc.* 1935, 31, 1432 – 1438.
23. Benesi, H. A.; Hildebrand, J. H. *J. Am. Chem. Soc.* 1949, 71, 2703 – 2707.
24. Mulliken, R. S. *J. Am. Chem. Soc*. 1950, 72 (1), 606 – 608.
25. Mulliken, R. S. *J. Phys. Chem*. 1952, 56 (7), 801 – 822.
26. Mulliken, R, S. *J. Am. Chem. Soc*. 1952, 74 (3), 811 – 824.
27. Mulliken, R. S.; Person, W. B. *Molecular Complexes: A Lecture and Reprint Volume, Wiley – Interscience, New York*. 1969.
28. Hassel, O.; Hvoslef, J. *Acta. Chem.* 1954, 74 (3), 811 – 824.
29. Hassel, O. *Science*. 1970, 170 (3957), 497 – 502.
30. Hassel, O. *Structural Aspects of Interatomic Charge – Transfer Bonding. In Nobel Lectures, Chemistry 1963 – 1970, Elsevier Publishing Company: Amsterdam*. 1972, pp. 314 - 329.
31. Mulliken, R. S. *Science.* 1967, 157, 130 – 160.
32. Bai, H.; Ault, B. S. *J. Mil. Struct.* (TheoChem). 1990, 238, 223 – 230.
33. Peebles, S. A.; Fowler. P. W.; Legon, A. C. *Chem. Phys. Lett.* 1995, 240, 130 – 134.
34. Corradi, E.; Meille, S. V.; Messina, M. T.; Metrangolo, P.; Resnati, G. *Angew. Chem. Int. Ed*. 2000, 39, 1782 – 1786.
35. Romaniello, P.; Lelj, F. *J. Phys. Chem. A*. 2002, 106, 9114 – 9119.
36. Valerio, G.; Raos, G.; Meille, S. V.; Metrangolo, P.; Resnati, G. *J. Phys. Chem. A*. 2000, 104, 1617 – 1620.
37. Wang, W.; Wong, N-B.; Zheng, W.; Tian, A. *J. Phys. Chem. A*. 2004, 108, 1799 -1805.
38. Zou, J-W.; Jiang, Y-J.; Guo, M.; Hu, G-X.; Zhang, B.; Liu, H-C.; Yu, Q-S. *Chem. Eur. J.* 2005, 11, 740 – 751.

39. Dumas, J-M.; Peurichard, H.; Gomel, M. J. *J. Chem. Res. Synop.* 1978, 54 – 55.
40. Politzer, P.; Murray, J. S.; Clark, T. *Phys. Chem. Chem. Phys*. 2013, 15, 11178 - 11189.
41. Brinck, T.; Murray, J. S.; Politzer, P. *Int. J. Quantum Chem.* 1992, 44 (19), 57 – 64.
42. Brinck, T.; Murray, J. S.; Politzer, P. *Int, J. Quantum Chem*. 1993, 48 (2), 73 – 88.
43. Metrangolo, P.; Resnati, G. *Science.* 2008, 321, 918 – 919.
44. Metrangolo, P.; Neukirch, H.; Pillati, T.; Resnati, G. *Acc. Chem. Res.* 2005, 38 (5), 386 – 395.
45. Legon, A. C. *Angew. Chem. Int. Ed.* 1999, 38 (18), 2687 - 2714.
46. Shields, Z. P.; Murray, J. S.; Politzer, P. *Int. J. Quantum Chem.* 2010, 110, 2823 -2832.
47. Peter, P.; Jane, S. M.; Pat, L. *Int, J. Quantum Chem.* 2007, 107, 3046 - 3056.
48. Desiraju, G. R. *Acc. Chem. Res.* 2002, 35, 565 – 573.
49. Alkorta, I.; Blanco, F.; Solimannejad, M.; Elguero, J. *J. Phys. Chem. A*. 2008, 112, 10856 - 10863.
50. Zhou, P-P.; Qui, W-Y.; Liu, S.; Jin, N-Z. *Phys. Chem. Chem. Phys*. 2011, 13, 7408 – 7418.
51. Li, Q-Z.; Jing, B.; Li, R.; Liu, Z-B.; Li, W-Z.; Luan, F.; Cheng, J-B.; Gong, B-A.; Sun, J-Z. *Phys. Chem. Chem. Phys.* 2011, 13, 2266 – 2271.
52. Aakeröy, C. B.; Desper, J.; Helfrich, B. A.; Metrangolo, P.; Pillati, T.; Resnati, G.; Stevenazzi, A. *Chem. Commun.* 2007, 41, 4236 – 4238.
53. Aakeröy, C. B.; Fasulo, M.; Schultheiss, N.; Desper, J.; Moore, C. *J. Am. Chem. Soc.* 2007, 129 (45), 13772 – 13773.
54. Aakeröy, C. B.; Chopade, P. D.; Ganser, C.; Desper, J. *Chem. Commun.* 2011, 47 (16), 4688 - 4690.
55. Amombo Noa, F. M.; Bourne, S. A.; Su, H.; Nassimbeni, L. R. *Cryst. Growth Des.* 2016, 16, 4765 - 4771.
56. Di Paolo, T.; Sandorfy, C. *Nature*. 1974, 252, 471 – 472.

57. Murray, J. S.; Concha, M. C.; Lane, P.; Hobza, P.; Politzer, P. *J. Mol. Model.* 2008, 14, 699.
58. Tawarada, R.; Seio, K.; Sekine, M. *J. Org. Chem.* 2008, 73, 383 – 390.
59. Kraut, D. A.; Churchill, M. J.; Dawson, P. E.; Herschlag, D. *ACS Chem. Biol.* 2009, 4, 269 – 273.
60. Groth, P.; Hassel, O. *Acta Chem. Scand.* 1964, 18, 402 – 408.
61. Di Paolo, T.; Sandorfy, C. *Can. J. Chem.* 1974, 52, 3612 – 3622.
62. Di Paolo, T.; Sandorfy, C. *Chem. Phys. Lett.* 1974, 26, 466 – 469.
63. Politzer, P.; Murray, J. S.; Clark, T. *Phys. Chem. Chem. Phys.* 2010, 12, 7748 -7757.
64. Lu, Y-X.; Zou, J-W.; Wang, Y-H.; Jiang, Y-J.; Yu, Q-S. *J. Phys. Chem. A.* 2007, 111, 10781 - 10788.
65. Lu, Y-X.; Zou, J-W.; Wang, Y-H.; Yu, Q-S. *J. Mol. Struct. (Theochem).* 2006, 776, 83 – 87.
66. Riley, K. E.; Hobza, P. *J. Chem. Theory. Comput.* 2008, 4, 232 – 242.
67. Auffinger, P.; Hays, F. A.; Westhof, E.; Ho. P. S. *Proc, Natl. Acad. Sci. USA.* 2004, 101, 16789 – 16794.
68. Riley, K. E.; Murray, J. S.; Politzer, P.; Concha, M. C.; Hobza, P. *J. Chem. Theory. Comput.* 2008, 5, 155 – 163.
69. Lu, Y-X.; Wang, Y-H.; Zhu, W. *Phys. Chem. Chem. Phys.* 2010, 12, 4543 – 4551.
70. Bui. T. T. T.; Dahaoui, S.; Lecomte, C.; Desiraju, G. R.; Espinosa, E. *Angew. Chem. Int. Ed.* 2009, 48, 3838 – 3841.
71. Nayak, S. K.; Reddy, M. K.; Row, T. N. G.; Choppa, D. *Cryst. Growth Des.* 2011, 11, 1578 – 1596.
72. Hathwar, V. R.; Row, T. N. G. *J. Phys. Chem. A.* 2010, 114, 13434 – 13441.
73. Desiraju, G. R.; Parthasarathy, R. *J. Am. Chem. Soc.* 1989, 111, 8725 – 8726.
74. Pedireddi, V. R.; Reddy, D. S.; Goud, B. S.; Craig, D. C.; Rae, A. D.; Desiraju, G. R. *J. Chem. Soc. Perkin Trans. 2.* 1994, 2353 – 2360.
75. Allen, F. H. *Acta. Crystallogr., Sect. B.* 2002, 58, 380 – 388.

76. Amombo Noa, F. M.; Bourne, S. A.; Nassimbeni, L, R. *Cryst. Growth Des.* 2015, 15, 3271 – 3279.
77. Price, S. L.; Stone, A. J.; Lucas, J.; Rowland, R. S; Thornley, A. E. *J. Am. Chem. Soc.* 1994, 116, 4910 – 4918.
78. Legon, A. C. *Phys. Chem. Chem. Phys.* 2010, 12, 7736 – 7747.
79. Shishkin, O. V. *Chem. Phys. Lett.* 2008, 458, 96 – 100.
80. Duarte, D.; De las Vallejos, M.; Peruchena, N. *J. Mol. Model.* 2010, 16, 737 – 748.
81. Wallnoeffer, H. G.; Fox, T.; Liedl, K. R.; Tautermann, C. S. *Phys. Chem. Chem. Phys.* 2010, 12, 14941 – 14949.
82. Zhao, Q.; Feng, D.; Sun, Y.; Hao, J.; Cai, Z. *J. Mol. Model.* 2011, 17, 1935 – 1939.
83. Lindoy, L. F.; Atkinson, I. M. *Self-assembly in Supramolecular Chemistry Systems, Cambridge, UK. The Royal Society of Chemistry Cambridge.* 2000.
84. Desiraju, G. R. *Angew. Chem. Int. Ed.* 1995, 34, 2311 – 2327.
85. Yamamoto, H. M.; Yamaura, J-I.; Kato, R. J. *J. Am. Chem. Soc.* 1998, 120, 5905 – 5913.
86. Lieffrig, J.; Jeannin, O.; Fourmigué, M. *J. Am. Chem. Soc.* 2013, 135, 6200 – 6210.
87. Fourmigué, M. *Halogen Bonding in Conducting or Magnetic Molecular Materials, Metrangolo, P.; Resnati, G (Eds), Honding Bonding: Fundamentals and Applications: Structure and Bonding. Berlin, UK, Springer.* 2008, pp. 181 -207.
88. Fourmigué, M. *Curr. Opin. Solid State Mater. Sci*. 2009, 13, 36 – 45.
89. Metrangolo, P.; Carcenac, Y.; Lahtinen, M.; Pilati, T.; Rissanen, K.; Vij, A.; Resnati, G. *Science.* 2009, 323, 1461 – 1464.
90. El-Sheshtawy, H. S.; Bassil, B. S.; Assaf, K. I.; Kortz, U.; Nau, W. M. *J. Am. Chem. Soc.* 2012, 134 (48), 19935 – 19941.
91. Bruce, D. W. *Halogen-bonded Liquid Crystals. Metrangolo, P.; Resnati, G (Eds). Halogen Bonding: Fundamentals and Applications: Structure and Bonding*. 2008, pp. 161 – 180.

92. Rissanen, K. *Cryst. Eng. Comm.* 2003, 10, 1107 – 1113.
93. Metrangolo, P.; Pilati, T.; Resnati, G.; Stevanazzi, A. *Curr. Opin. Colloid Interface Sci.* 2003, 8, 215 – 2 22.
94. Metrangolo, P.; Resnati, G.; Pilati, T.; Liantonio, R.; Meyer, F. *J. Polym. Sci, Part A: Polym. Chem.* 2007, 45, 1 – 15.
95. Metrangolo, P.; Resnati, G.; Pilati, T.; Biella, S. *Halogen Bonding Fundamentals and Applications, Eds. Metrangolo, P.; Resnati, G. Springer, Berlin*. 2008, Vol. 126, pp. 105 – 136.
96. Amico, V.; Meille, S. V.; Corradi, E.; Messina, M. T.; Resnati, G. *J. Am. Chem. Soc.* 1998, 120, 8261 – 8262.
97. Amombo Noa, F. M.; Bourne, S. A.; Su, H.; Nassimbeni, L. R. *Cryst. Growth Des.* 2017, 17, 1876 – 1883.
98. Thaimattam, R.; Sharma, C. V. K.; Clearfield, A.; Desiraju, G. R. *Cryst. Growth Des.* 2001, 1, 103 -106.
99. Ghassemzadeh, M.; Harms, K.; Dehnicke, K. *Chem. Ber.* 1996, 126, 259 – 265.
100. Metrangolo, P.; Meyer, F.; Pilati, T.; Prosperpio, D. M.; Resnati, G. *Chem. Eur. J.* 2007, 13, 5765 – 5772.
101. Bernstein, J.; Etter, M. C.; Leiserowitz, L. *Structure Correlation,* Vol. 2, VCH, 1994.
102. Aakeröy, C. B.; Seddon, K. R. *Chem. Soc. Rev.* 1993, 22, 397 – 407.
103. Kojic-Prodic, B.; Stefanic, Z.; Zinic, M. *Croat. Chem. Acta.* 2004, 77, 415 – 425.
104. Nangia, A.; Desiraju, G. R. NATO Sci. Ser., Ser. 1999, C519, 193 – 208.
105. Pauling, L. *The Nature of the Chemical Bond.* Cornell University Press: Ithaca, 1939.
106. Pimentel, G. C.; McClellan, A. L. *The hydrogen Bond.* Freeman, W. H: San Francisco, 1960.
107. Arunan, E.; Desiraju, G. R.; Klein, R. A.; Sadlej, J.; Scheiner, S.; Alkorta, I.; Clary, D. C.; Crabtree, R. H.; Dannenberg, J. J.; Hobza, P.; Kjaergaard, H. G.; Legon, A. C.; Mennucci, B.; Nesbitt, D. J. *Defining the Hydrogen*

Bond: An account (IUPAC Technical Report). *Pure Appl. Chem.* 2011, 83, 1637 – 1641.

108. Arunan, E.; Desiraju, G. R.; Klein, R. A.; Sadlej, J.; Scheiner, S.; Alkorta, I.; Clary, D. C.; Crabtree, R. H.; Dannenberg, J. J.; Hobza, P.; Kjaergaard, H. G.; Legon, A. C.; Mennucci, B.; Nesbitt, D. J. *Pure Appl. Chem.* 2011, 83, 1619 – 1636.
109. Nishio, M. *CrystEngComm*. 2004, 6, 130 – 158.
110. Ward, M. D. *Struct. Bonding (Berlin, Ger).* 2009, 132, 1 – 23.
111. Braga, D.; Grepioni, F. *J. Chem. Soc., Dalton Trans.* 1999, 1 – 8.
112. Burrows, A. D. *Struct. Bonding (Berlin, Ger)*. 2004, 108, 55 – 96.
113. Braga, D.; Maini, L.; Polito, M.; Grepioni, F. *Struct. Bonding (Berlin Ger)*. 2004, 111, 1 – 32.
114. Brammer, L. *Perspect. Supramol. Chem*. 2003, 7, 1 – 75.
115. Aakeröy, C. B.; Leinen, D. S. *NATO Sci. Ser., Ser.* 1999, C538, 89 – 106.
116. Aakeröy, C. B. *NATO ASI Ser., Ser.* 1999, C539, 303 – 324.
117. Nernst, W. *Z. Phys. Chem.* 1892, 8, 110 -139.
118. Werner, A. *Justus Liebigs Ann. Chem.* 1902, 322, 261 -296.
119. Hantzsch, A. *Ber. Dtsch. Chem. Ges.* 1910, 43, 3049 – 3076.
120. Oddo, G.; Puxeddu, E. *Gazz. Chim. It.* 1906, 36, 1 – 48.
121. Moore, T. S.; Winmill, T. F. *J. Chem. Soc., Trans.* 1912, 101, 1635 – 1676.
122. Pfeiffer, P.; Fischer, P.; Kuntner, J.; Monti, P.; Pros, Z. *Justus Liebigs Ann. Chem.* 1913, 398, 137 – 196.
123. Latimer, W. M.; Rodebush, W. H. *J. Am. Chem. Soc*. 1920, 42, 1419 – 1433.
124. Lewis, G. N. *Valence and Structure of Atoms and Molecules. The Chemical Catalog Co., Inc.: New York*, 1923.
125. Pauling, L. *J. Am. Chem. Soc.* 1931, 53, 1367 – 1400.
126. Pauling, L. *J. Am. Chem. Soc.* 1935, 57, 2680 – 2684.
127. Huggins, M. L. *J. Org. Chem.* 1936, 1, 407 – 456.
128. Pauling, L.; Corey, R. B. *J. Am. Chem. Soc*. 1950, 72, 5349.
129. Pauling, L.; Corey, R. B. *Proc. Natl. Acad. Sci. USA*. 1951, 37, 205 – 211.
130. Watson, J. D.; Crick, F. H. C. *Nature*. 1953, 171, 737 – 738.

131. Steiner, T. *Angew. Chem. Int. Ed.* 2002, 41, 48 – 76.
132. Gronert, S. *J. Am. Chem. Soc.* 1993, 115, 10258 -10266.
133. Legon, A. C.; Millen, D. J.; North, H. M. *Chem. Phys. Lett*. 1987, 135, 303 – 306.
134. Jeffrey, G. A. *An Introduction to Hydrogen Bonding, University Press, Oxford,* 1997.
135. Maitland, G. C. R.; Rigby, M.; Smith, B. E.; Wakeham, W. A. *Intermolecular Forces: Their Origin and Determination, Clarendon Press, Oxford,* 1981.
136. Desiraju, G. R.; Steiner, T. *The Weak Hydrogen Bond: In Structure Chemistry and Biology. Oxford University Press: New York*, 2001.
137. Kollman, P. A.; Allen, L. C. *Theor. Chim. Acta*. 1970, 18, 399 – 403.
138. Kollman, P. A.; Allen, L. C. *Chem. Rev*. 1972, 72, 283 – 303.
139. Kitaura, K.; Morokuma, K. *Int. J. Quantum Chem*. 1976, 10, 325 – 340.
140. Morokuma, K. *Acc. Chem. Res*. 1977, 10, 294 – 300.
141. Umeyama, H.; Morokuma, K. *J. Am. Chem. Soc.* 1977, 99, 1316 – 1332.
142. Gilli, G.; Gilli, P. *J. Mol. Struct.* 2000, 552, 1 – 3.
143. Grabowski, S. J. *Chem. Rev.* 2011, 111, 2597 – 2625.
144. Grabowski, S. J.; Sokalski, W. A.; Dyguda, E.; Leszczynski, J. *J. Phys. Chem.* 2006, B110, 6444 – 6446.
145. Kondo, M.; Yoshitomi, T.; Seki, K.; Matsuzaka, H.; Kitagawa, S. *Angew. Chem. Int. Ed. Engl*. 1997, 36, 1725 – 1727.
146. Li, H.; Eddaoudi, M.; O'keeffe, M.; Yaghi, O. M. *Nature*. 1999, 402, 276 – 279.
147. Kosal, M. E.; Chou, J. –H.; Wilson, S. R.; Suslick, K. S. *Nat. Matter.* 2002, 1, 118 – 121.
148. Albrecht, M.; Lutz, M.; Spek, A. L.; van Koten, G. *Nature*. 2000, 406, 970 – 974.
149. Pedireddi, V. R. *Cryst. Growth Des.* 2001, 1, 383 – 385.
150. Broder, C. K.; Davidson, M. G.; Forsyth, V. T.; Howard, J. A. K.; Lamb, S.; Mason, S. A. *Cryst. Growth Des.* 2002, 2, 163 – 169.

151. Zaman, M. B.; Udachin, K. A.; Ripmeester, J. A. *Cryst. Growth Des.* 2004, 4, 585 – 589.

152. Legon, A. C.; Millen, D. J. *Acc. Chem. Res.* 1987, 20 (10), 39 -46.

153. Wood, P. A.; Allen, F. H.; Pidcock, E. *CrystEngComm.* 2009, 11 (8), 1563 – 1571.

154. Jacobs, A.; Amombo Noa, F. M. *CrystEngComm.* 2015, 17, 98 – 106.

155. Vishweshwar,P.; Nangia,A.; Lynch, V. M. *CrystEngComm.* 2003, 5, 164 – 168.

156. Głowacki, E. D.; Irimia-Vladu, M.; Kaltenbrunner, M.; Gsiorowski, J.; White, M. S.; Monkowius, U.; Romanazzi, G.; Suranna, G. P.; Mastrorilli, P.; Sekitani, T.; Bauer, S.; Someya, T.; Torsi, L.; Sariciftci, N. S. *Adv. Mater.* 2013, 25 (11), 1563 -1569.

157. George, S.; Nangia, A.; Lam, C. –K.; Mak, T. C. W.; Nicoud, J. –F. *Chem. Commun*. 2004, 1202 – 1203.

158. Tanaka, K.; Fujimoto, D.; Toda, F. *Tetrahedron Letters*. 2000, 41, 6095-6099.

159. Tanaka, K.; Fujimoto, D.; Altreuther, A.; Oeser, T.; Irngartinger, H.; Toda, F. *J. Chem. Soc., Perkin Trans*. 2000, 2, 2115-2120.

160. Tanaka, K.; Fujimoto, D.; Oeser, T.; Irngartinger, H.; Toda, F. *Chem. Commun*. 2000, 413 - 414.

161. Tanaka, K.; Caira, M. R. *J. Chem. Res.* 2002, 642.

162. Weber, E.; Skobridis, K.; Wierig, A.; Stathi, S.; Nassimbeni, L. R.; Niven, M. L. *Angew. Chem, Int. Ed. Engl.* 1993, 32, 606 - 608.

163. Bourne, S. A.; Nassimbeni, L. R.; Niven, M. L.; Weber, E.; Wierig, A. *J. Chem. Soc., Perkin Trans*. 2. 1994, 1215 - 1222.

164. Weber, E.; Dörpinhaus, N.; Csöregh, I. *J. Chem. Soc., Perkin Trans. 2*. 1990, 2167-2177.

165. Cartraud, P.; Cointot, A.; Renaud, A. *J. Chem. Soc., Faraday Trans. 1*. 1981, 77, 1561 – 1567.

166. Flipper, J. L.; Karle, J.; Karle, I. L. *J. Am. Chem.* 1970, 92, 3749 – 3755.

167. Flipper, J. L.; Karle, J. *J. Phys. Chem.* 1971, 75, 3566 – 3567.

168. MacNicol, D. D.; Wilson, F. B. *Chem. Commun*. 1971, 786.
169. Powell, H. M. *J. Chem. Soc.* 1948, 61 – 73.
170. Faraday, M. *Quart. J. Sci*. 1823, 15, 71.
171. Schaflautl, C. *J. Prakt. Chem.* 1841, 21, 129 – 157.
172. Hoffman, K. A.; Kuspert, F. *Z. Anorg. Allg. Chem.* 1897, 15, 204 – 224.
173. Weber, E.; Josel, H. P. *J. of Incl. Phenom.* 1983, 1, 79 – 85.
174. Pedersen, C. J. *J. Am. Chem. Soc*. 1967, 89, 2495 – 2496.
175. Allison, S. A.; Bauer, R. M. *J. Chem. Soc. A*, 1969, 1717 – 1723.
176. Schaeffer, W. D.; Dorsey, W. S.; Skinner, D. A.; Christain, C. G.*J. Am. Chem. Soc*. 1957, 79, 5870 – 5876.
177. Kemula, W.; Sybilska, D. *Nature*. 1960, 185, 237 – 238.
178. Lipkowski, J. *In Inclusion Compounds; Atwood, J. L.; Davies, J. E. D.; MacNicol, D. D.; Eds; Academic Press: New York,* 1984, Vol. 1, Chapter 3.
179. Lipkowski, J. *In Comprehensive Supramolecular Chemistry; Atwood, J. L.; Davies, J. E. D.; MacNicol, D. D.; Vögtle, F., exec. Eds; Elsevier: Oxford,* 1996, Vol. 6, Chapter 20.
180. Soldatov, D. V.; Enright, G. D.; Ripmeester, J. A. *Cryst. Growth Des.* 2004, 4, 1185 – 1194.
181. Batisai, E.; Lusi, M.; Jacobs, T.; Barbour, L. J. *Chem. Commun*. 2012, 481, 12171 -12173.
182. Weeks, M. E. *In Discovery of the Elements; J. Chem. Educ*: Easton, PA, 1945.
183. Courtois, B. *Ann. Chim*. 1813, 91, 304 – 310.
184. Gay Lussac, J. L. *Ann. Chim*. 1814, 91, 5 – 160.
185. Wells, A. F. *Structural Inorganic Chemistry. 5th Eds:* Clarendon Press, Oxford University Press, New York, 1984.
186. Pelletier, P.; Caventou, J. B. *Ann. Chim*. 1819, 10, 164.
187. Bent, H. A. *Chem. Reviews.* 1968, 68 (5), 587 – 648.
188. Loos, K. R.; Jones, A. C. *J. Phys. Chem*. 1974, 78 (22), 2306 – 2307.
189. Teitelbaum, R. C.; Ruby, S. L.; Marks, J. *J. Am. Chem. Soc.* 1980, 102, 3522 – 3523.
190. Colin, J. J.; de Claubry, H. G. *Ann. Chim.* 1814, 90, 87 – 92.

191. Greenwood, N. N.; Earnshaw, A. *In Chemistry of the Elements:* Pergamon Press, 1990, Chapter 17.
192. Jörgensen, S. M. *J. F. Prakt. Chem*. 1870, 2, 433.
193. Mooney, R. C. L. *Z. Kristallogr*. 1935, 90, 143.
194. Coppens, P. *Structural Aspects of Iodine – Containing Low – Dimensional Materials, in Extended Linear Chain Compounds:* Miller, J.; Eds: Springer US, 1982, pp. 333 – 356.
195. Marks, T.; Kalina, D. *Highly Conductive Halogenated Low – Dimensional Materials, in Linear Chain Compoundds:* Miller, J.; Ed: Springer US, 1982, pp. 197 – 331.
196. Allen, D. W.; Berridge, R.; Bricklebank, N.; Forder, S. D.; Palacio, F.; Coles, S. J.; Hursthouse, M. B.; Skabara, P. J. *Inorg. Chem.* 2003, 42, 3975 – 3977.
197. "The Nobel prize in chemistry 2000". Nobel Media AB 2014. Web page: http://www.nobelprize.org/nobel_prizes/chemistry/laureates/2000/ ,accessed on 13 February 2017.
198. Groenewald, F.; Esterhuysen, C.; Dillen, J. *Theor. Chem. Acc.* 2012, 131 (10), 1 – 12.
199. Blake, A. J.; Devillanova, F. A.; Gould, R. O.; Li, W. – S.; Lippolis, V.; Parksons, S.; Radek, C.; Schröder, M. *Chem. Soc. Rev*. 1998, 27, 195 – 206.
200. Lu, J. Y.; Zhang, Y.; Cmaidalka, J. E. *CrystEngComm*. 2002, 4, 213 – 214.
201. Svensson, P. H.; Kloo, L. *Chem. Rev*. 2003, 103 (5), 1649 – 1684.
202. Westra, A. N.; Bourne, S. A.; Esterhuysen, C.; Koch, K. R. *Dalton Trans*. 2005, 2162 – 2172.
203. Lobello, M. G.; Fantacci, S.; de Angelis, F. *J. Phys. Chem C.* 2011, 115 (38), 18863 – 18872.

CHAPTER II

Materials and Experimental Methods

2.1 Materials

- Tetrakis(4-bromophenyl)ethylene was synthesized by exposing tetraphenylethylene to bromine vapour in a desiccator for a day. The product obtained was recrystallized from a 50/50 (v/v) mixture of ethanol and chloroform[1] to yield the desired product as illustrated in Figure 2.1.[1,2]

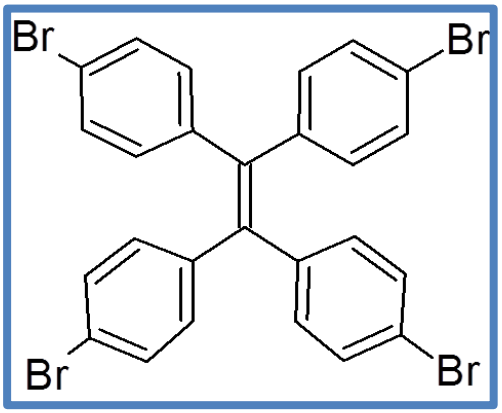

Figure 2.1 Chemical structure of tetrakis(4-bromophenyl)ethylene.

- Tetrakis(4-iodophenyl)ethylene was prepared by mixing a suspension of tetraphenylethylene (8.3 g, 25.0 mmol), iodine (12.7 g, 50.0 mmol) and bis-[trifluoroacetoxy]phenyl iodine (26.2 g, 60.0 mmol) in distilled chloroform (30.0 ml) and stirring at room temperature for 12 hours. The reaction mixture was filtered, washed with a little hexane until the iodine colour disappeared from solution. The resulting product was dried and recrystallized from toluene to give colourless prismatic crystals (Figure 2.2).[1,2]

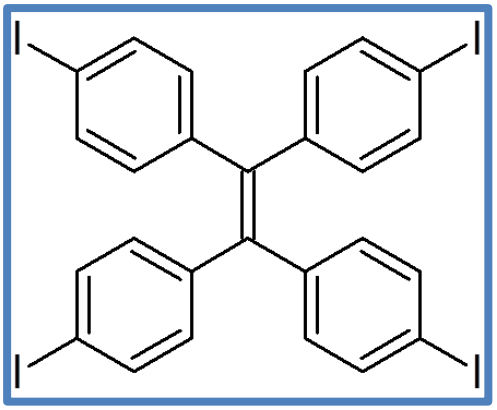

Figure 2.2 Chemical structure of tetrakis(4-iodophenyl)ethylene.

The three compounds 9,9′-(Biphenyl-2,2′-diyl)difluoren-9-ol, 2,2′,7,7′-tetrabromo-9,9′-(biphenyl-2,2′-diyl)difluoren-9-ol and 2,2′,7,7′-tetra-tert-butyl-9,9′-(1,4-phenylene)difluoren-9-ol were supplied by Weber, who used the following procedures:

- 9,9′-(Biphenyl-2,2′-diyl)difluoren-9-ol[3]: this compound was synthesised by slowly adding a solution of *n*BuLi (53.1 ml, 85 mmol, 1.6N in *n*-hexane) under argon at 0 °C to 2, 2′-dibromobiphenyl (10.5 g, 38 mmol) in 70 ml of dry diethyl ether. The reaction was stirred for 2 h and a solution of fluorenone (13.8 g, 77 mmol) in dry diethyl ether was added dropwise. The mixed solution was further stirred for another 2h at room temperature and heated at reflux for 15h, and subsequently hydrolysed (NH_4Cl solution). The precipitated product was filtered, the ethereal phase was separated off, dried with $MgSO_4$ and evaporated to dryness in a vacuum. More product was precipitated when methanol was added to the oily residue and a yield of 13.8 g (70%) was obtained (Figure 2.3).[3]

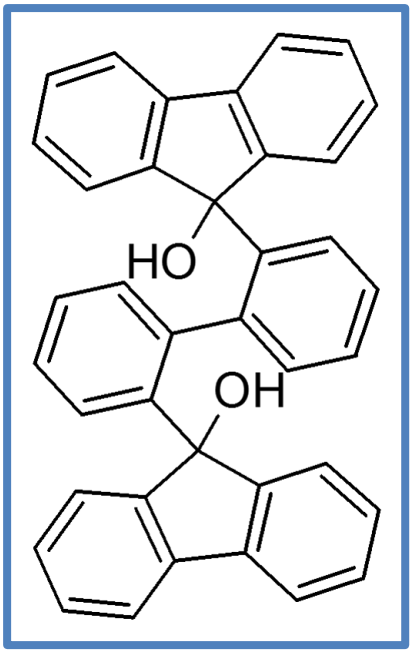

Figure 2.3 Chemical structure of 9, 9′-(Biphenyl-2,2′-diyl)difluoren-9-ol.

- 2,2′,7,7′-tetrabromo-9,9′-(biphenyl-2,2′-diyl)difluoren-9-ol was synthesized by adding fluorenone in portion as a solid in dry tetrahydrofuran (THF)to give a solution that was heated under reflux for 24 hours. The formed solid precipitate which did not dissolve on quenching with saturared aqueous ammonium chloride (NH_4Cl) solution was collected and treated with hot methanol (MeOH) for the removal of impurities. The latter was recrystallized from dimethylformamide (DMF) to yield 22% of colorless crystals (Figure 2.4).[4]

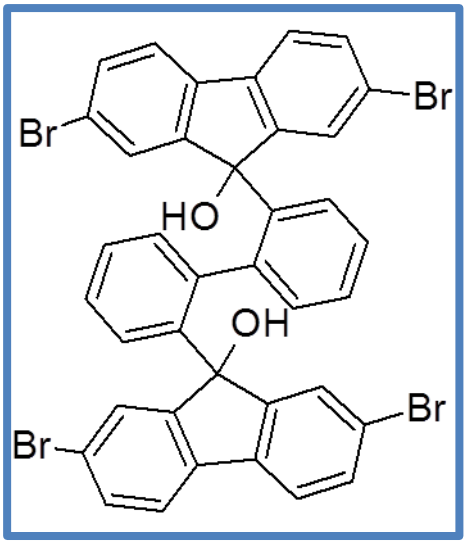

Figure 2.4 Chemical structure of 2,2′,7,7′-tetrabromo-9,9′-(biphenyl-2,2′-diyl)difluoren-9-ol.

- 2,2′,7,7′-tetra-tert-butyl-9,9′-(1,4-phenylene)difluoren-9-ol: the starting ketones was obtained by oxidation of the corresponding fluorenones with oxygen (O_2).[5,6] The bis(fluorenol) was synthesized by treatment of the above ketone with the corresponding aryllithium reagents. These were prepared by treatment of the appropriate aryl bromide with nBuLi under usual condition (Figure 2.5).[7]

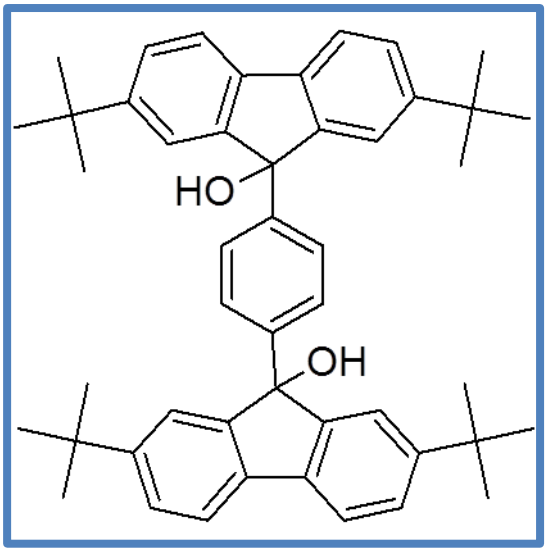

Figure 2.5 Chemical structure of 2,2′,7,7′-tetra-tert-butyl-9,9′-(1,4-phenylene)difluoren-9-ol.

2.2 Crystal Growth

Inclusion complexes were obtained by dissolving the host compounds in excess of the solvent guests, heated and stirred on a hot plate. The solutions were filtered and allowed to evaporate at room temperature.

2.3 Syntheses of Nickel Complexes

Compounds used for the synthesis of nickel complexes were purchased from Sigma-Aldrich.

- $[Ni(OH_2)_2(4\text{-}Ipy)_4]\bullet 2I\bullet 3(4Ipy)$: The complex was prepared by dissolving 40 mg (0.128 mmol) of NiI_2 in distilled water , 105 mg (0.512 mmol) of 4-iodopyridine (4-Ipy) in MeOH, and the two mixtures were added in a vial. The solution was allowed to evaporate slowly at ambient temperature.

- $[Ni(ACN)_2(3PIC)_4]\bullet 2I_3$ and $[Ni(ACN)_2(4PIC)_4]\bullet 2I_3$: These compounds were obtained by dissolving NiI_2 (40 mg) in distilled water and iodine (I_2: 32.51 mg) in acetonitrile. The two solutions were mixed and excess of 3-picoline/4-picoline (3PIC/4PIC) was added to the blend. Brown crystals were yielded from the solutions after three days.

- $[Ni(OH_2)_2(3PIC)_4]\bullet 2I$ and $[Ni(OH_2)_2(4PIC)_4\bullet 4I\bullet (4PIC)_4\bullet 5H_2O$: NiI_2 (40 mg, 0.128 mmol) was dissolved in distilled water, then excess of 3PIC/4PIC was added to the solution along with little of MeOH. The mixture was heated at approximately 60 °C, filtered and left to evaporate at room temperature. Blue crystals were obtained after six days.

- $2[NiBr_2(4PIC)_4]$, $2[NiCl_2(4PIC)_4]\bullet H_2O$ and $2[NiCl_2(3Brpy)_4]\bullet 3Brpy$: 40 mg (0.128 mmol) of $NiBr_2$/$NiCl_2$ was dissolved in distilled water, then

excess of 3-Bromopyridine/4-picoline and MeOH was added to the solution. Blue crystals yielded after a week due slow evaporation.

2.4 Characterisation

2.4.1 Thermal Analysis

Thermogravimetry (TG) was performed on a Q500 (TA Instruments) thermal balance between 25 and 450 °C and Differential Scanning Calorimetry (DSC) was conducted on a Q200 series instrument in the temperature range of 20 to 450 °C. These experiments were done at a heating rate of 10 °C /min under a dry nitrogen purge gas at a flow rate of 60 mL /min.

2.4.2 Thermogravimetry (TG)

The study of chemical changes in a material via the measurement of a sample weight as a function of temperature or time is conducted by thermogravimetry (TG). This technique is capable of establishing the stoichiometry of an inclusion complex as well as measuring kinetics of desorption by isothermal thermogravimetric analysis (TGA); the mass loss of a sample is measured with time at a fixed temperature. It is also adequate for analysis of quantitative thermal reactions with mass changes as evaporation, gas absorption, decomposition, desorption and dehydration.[8]

TG instrument components are a furnace, electronic balance, sample holder, temperature programmer, an enclosure for the establishment of the desired atmosphere, and direct display of the resultant data on a computer screen.

2.4.3 Differential Scanning Calorimetry (DSC)

DSC is an instrument developed to a high degree of complexity. It measures melting temperature, latent heat of melting, reaction energy and temperature, crystalline phase transition temperature and energy, glass transition

temperature, oxidation induction times, denaturisation temperatures and heat capacity changes following a transition.

This technique can also be employed in the measurement of amount of energy absorbed or released by a sample while being heated or cooled. DSC gives a quantitative and qualitative data on endothermic and exothermic processes. The sample is placed in a suitable pan and sits in a DSC cell along with an empty reference pan placed on a symmetric platform.[9]

There are two types of DSC instruments widely used:

- Heat Flux DSC (eg. TA DSC and Mettler DSC): Here, the sample and reference undergo the same rate of heating from a single source. The difference in temperatures in both sample and reference pans is recorded and converted to a power difference (ΔP), this gives the difference in heat flow.
- Power compensated DSC (Perkin-Elmer system): The sample and reference are heated separately and the pan temperatures are detected using thermocouples attached to the disk platforms.

2.4.4 Non-isothermal Kinetics

Kinetics of decomposition were investigated non-isothermally using a thermogravimetric technique.[10,11] Crystals were crushed to keep sample size uniform for each experiment performed. The non-isothermal weight loss was recorded at different heating rates (2, 4, 8, 16 and 32 °C/min) up to 300 °C. The rate of these experiments can be obtained by the equation:

$$dC/dT = A/\beta . f(C)e^{-Ea/RT} \quad \ldots\ldots\ldots\ldots (2.1)$$

Where C is the mass loss of the sample, β is the heating rate.

The above equation can be reduced to:

$$d\log\beta/d(1/T) = (0.457/R)E_a \quad \ldots\ldots\ldots (2.2)$$

The curves obtained were examined by plotting $-\log\beta$ *vs* T^{-1}.

Where T is the absolute temperature, and a straight line with a slope: $-(0.457E_a)/R$.

These above parameters were used to calculate the activation energy of the studied compound.

2.4.5 Solvent Sorption Kinetics

The kinetics of enclathration was carried out in a specially constructed balance in which a powdered sample of the host compound was exposed to the vapour of the volatile guest. This apparatus (Figure 2.6) allows the sorption to be determined under controlled conditions of temperature and vapour pressure. The mass gain is automatically recorded as a function of time and the data were converted to the extent of reaction α.

$$\alpha = (m_t - m_o)/(m_\infty - m_o) \quad \text{..... (2.3)}$$

Where m_o, m_t and m_∞ are the masses at the start, during and at the end of the experiment respectively. The α-time curves may then be fitted to an appropriate rate law[12] and the rate constant thus evaluated.

This balance was constructed by Professor L. J Barbour (University of Stellenbosch) who also wrote the software for the kinetics analysis.

Figure 2.6 Balance for monitoring the uptake of solvent vapours.

2.4.6 Hot Stage Microscopy (HSM)

HSM is a combination of microscopy and thermal analysis. This technique enables one to study and physically characterise materials as a function of temperature and time. HSM allows one to visually observe thermal events which are difficult to discern using DSC or TG. These events can be correlated with the physical changes (melting point, guest desorption, polymorphic transitions, etc) occurring in a crystal upon heating when using other thermal analysis techniques such as TG and DSC.

Crystals were submerged in silicone oil when subjected to the heating process under a Nikon SMZ-10 microscope fitted with a Linkam THMS 600 hot stage connected to a Linkam TP92 temperature controlling system.

However, since the temperature measuring device is not as close to the sample as in the TG & DSC, the temperature associated with the thermal events were slightly different from those observed in the DSC and TG. Crystals when analysed on the DSC/TG were crushed but not while using HSM. This factor

may also affect the onset temperatures observed for the thermal events. The experiments on the HSM were performed at atmospheric pressure.

2.5 Spectroscopy Studies

2.5.1 Fourier Transform Infrared Spectroscopy (FT-IR)

IR spectroscopy uses the fact that molecules absorb specific frequencies which can characterise their structures. This technique is used to identify and analyse the frequency of the vibrations from the bonds in the molecule.

In this study, IR experiments were carried out on a Perkin-Elmer FT-IR C88996 spectrometer. Samples were scanned over a range of 440-4400 cm^{-1} at 2 cm^{-1} spectral resolution.

One of the important advantages of this technique is that samples can be analysed in any state: solid, liquid or gas.[13]

2.5.2 Proton NMR Spectroscopy

Proton NMR experiments were carried out on a Bruker Ultrashield 300^{+} or 400^{+} spectrometer. The ^{1}HNMR spectra were recorded and used to determine or confirm the stoichiometry of the inclusion complexes. Compounds were dissolved with deuterated chloroform, $CDCl_3$, or deuterated dichloromethane, CD_2Cl_2.This technique determines the chemical/physical properties of a complex and can provide detailed information about a structure.

2.6 X-ray Diffraction Analysis

2.6.1 Powder X-ray Diffraction (PXRD)

PXRD is a technique used to verify and prove the identity of new phases and compounds as a unique PXRD pattern is shown for every complex due to its structural features.

The PXRD method can also determine the unit cell dimensions of a compound.[14] although in this thesis it was used solely for phase identification. All experiments were performed on a Bruker D8 Advance powder diffractometer equipped with a Lynxeye detector using CuKα-radiation (α = 1.5406 Å) at 25 °C. Samples were placed into a sample holder in the path of the X-ray beam after being manually powdered in a mortar and pestle.

Slurry experiments were also performed using 7 – 10 mL of selected halogenated guest solvents. The suspensions were stirred overnight at room temperature. After formation of a paste-like product, these mixtures were filtered on a filter paper and allowed to air dry before conducting a PXRD analysis.

The sampled were scanned over the 2θ range of 4° to 40° at a scan speed of 1.8 deg 2θ/ min.

Variable PXRD temperature was also performed on some inclusion compounds within a temperature range of 30-300 °C. The experimental PXRD patterns were compared to the calculated patterns generated from known structures using LAZY PULVERIX.[15]

2.6.2 Single Crystal X-ray Diffraction

The determination of crystal and molecular structure of compounds were performed using X-ray diffraction which is a non-destructive analytical technique. X-ray diffraction provides information such as unit cell parameters, details of site-ordering, bond lengths and bond-angles in a compound.

Refinement and interpretation are done from data obtained using X-ray analysis in order to solve a crystal structure.[16] There are four main steps in the study of crystalline materials using X-ray diffraction: crystallization, data collection, structure solution and refinement. Good quality single crystals with suitable size were mounted on a nylon loop and coated with paratone oil. Data collections were conducted using two instruments; a Nonius Kappa CCD[17]diffractometer and a Bruker KAPPA APEX 2 DUO[18] diffractometer, both using MoKα-radiation (λ = 0.71073 Å) at a temperature of 173 K. the intensity data were collected by phi scan and omega scan techniques, scaled and reduced with DENZO-SMN[19] or SAINT-Plus.[20] Absorption correction of the collected intensities was carried out with the SADABS program.[21] XPREP[22] software was utilized to confirm the space group and the input files obtained from this program was used for structure solution using SHELXS[23] program. Structures were solved by direct method using SHELX-97[24] and refined using full matrix least-squares methods in SHELXL.[24] All non-hydrogen atoms were refined isotropically or anisotropically depending on the occurrence of disorder in the structures. Hydrogen atoms were placed in geometrically calculated positions with a riding model for their isotropic temperature factors.

POVRAY in X-SEED[25] and Mercury (3.5)[26] were used to generate diagrams.

2.7 Computing Components

Platon[27]: Program which calculates the structure molecular parameters.

ConQuest[28]: Software for searching and retrieving information about compound from Cambridge Structural Database (CSD).

XPREP[22]: This program processes data from the X-ray diffractometer and determines the space group of complexes. The SHELX input files are also created.

Layer[29]: It displays the intensity data of a crystal as simulated precession photographs of the reciprocal lattice levels and the systematic absences which occur are investigated.

LAZY PULVERIX[15]: Calculates the theoretical powder X-ray diffraction pattern from single crystal X-ray diffraction data.

POVLabel[30]: Used to edit the atomic labels of POV-Ray images.

POV-Ray[30]: This program renders graphics for structures.

Section[31]: Graphical interpretation of the crystal packing by effectively cutting slices through the unit cell is given by this program. The removal of the guest molecules is done and the host compounds in van der Waals radii is shown so that cavities or channels in the structures can be studied.

MSRoll[32]: This program is utilized to calculate the void spaces in structures and can also calculate solvent volumes.

Crystal Explorer[33]: This program uses Hirshfeld surfaces[34] of molecules within a crystal structure for the determination of intermolecular interactions between molecules/crystal structures in its entirety. The extension of the weight function described by an atom in a molecule generates Hirshfeld surfaces which include the function of a molecule in a crystal.[35] Information about crystal intermolecular interactions yield by the use of Hirshfeld surface and are determined by both the enclosed molecule and its neighbours.[36]

2.8 References

1. Amombo Noa, F. M.; Bourne, S. A.; Nassimbeni, L. R. *Cryst. Growth. Des*. 2015, 15, 3271-3279.
2. Tanaka, K.; Fujimoto, D.; Altreuther, A.; Oeser, T.; Irngartinger, H.; Toda, F. *J. Chem. Soc., Perkin Trans*. 2000, 2, 2115-2120.
3. Weber, E.; Skobridis, K.; Wierig, A.; Stathi, S.; Nassimbeni, L. R.; Niven, M. L. *Angew. Chem, Int. Ed. Engl*. 1993, 32, 606-608.
4. Bourne, S. A.; Nassimbeni, L. R.; Niven, M. L.; Weber, E.; Wierig, A. *J. Chem. Soc., Perkin Trans*. *2*. 1994, 1215-1222.
5. Weber, E.; Dörpinhaus, N.; Csöregh, I. *J. Chem. Soc., Perkin Trans. 2*. 1990, 2167-2177.
6. Sprinzak, Y. *J. Am. Chem. Soc*. 1958, 80 (20), 5449-5455.
7. Weber, E.; Nitsche, S.; Wierig, A.; Csöregh, I. *Eur. J. Org. Chem*. 2002, 2002 (5), 856-872.
8. Haines, P. J. *Thermal Methods of Analysis. Blackie Academic & professional, London*. 1995.
9. Caira, M. R.; Nassimbeni, L. R. *Phase Transformations in Inclusion Compounds, Kinetics and Thermodynamics of Enclathration. In Comprehensive Supramolecular Chemistry, MacNicol, D. D.; Toda, F.; Bishop, R., Eds; Pergamon: Oxford*. 1996, Vol. 6, Chapter 5.
10. Flynn, J. H.; Wall, L. A. *J. Polym. Sci*. 1966, 4, 323-328.
11. Ozawa, T. *Bull. Chem. Soc. Jpn*. 1965, 38, 1881-1886.
12. Brown, M. E. *Introduction to Thermal Analysis: Techniques and Applications; Chapman and Hall: London,* 1988.
13. Stuart, B.; George, B.; Mclntyre, P. *Morden Infrared Spectroscopy, John Wiley & Sons, New York, USA*. 1996.
14. Karkis, S.; Fábian, L.; Friščić, T.; Jones, W. *Powder X-ray Diffraction as an Emerging Method to Structurally Characterize Organic Solids, Organic Letters*. 2007, 9, 3133-3136.
15. Klaus, Y.; Wolfgang, J.; Parthé, E. *J. Appl. Cryst*. 1977, 10, 73-74.

16. Brown, P. J.; Forsyth, J. B. *The Crystal Structure of Solids; Edward Arnold Limited, London*. 1973.
17. Collect, data collection software; Nonius: Delft, The Netherlands, 1998.
18. APEX 2, version 1.0-27; Bruker AXS Inc.: Madison, WI, 2005.
19. Otwinowski, Z.; Minor, W. *In Methods in Enzymology, Macromolecular Crystallography; Carter, C. W.; Jr, Sweet, R. M, Eds.; Academic Press:* 1997, part A, Vol. 276, pp. 307.
20. SAINT-Plus, version 7.12; Bruker AXS Inc.: Madison, Wisconsin, USA, 2004.
21. Sheldrick, G. M. SADABS: Program for Area Detector Adsorption Correction; University of Göttingen: Germany, 1996, pp. 33-38.
22. XPREP: Data Preparation & Reciprocal Space Group Exploration, version 5.1 © Bruker Analytical X-ray System, 1997.
23. Sheldrick, G. M. SHELXS-97: Program for Crystal Structure Solution; University of Göttingen: Germany, 1997.
24. Sheldrick, G. M. SHELX-97: Program for crystal Structure Solution and Refinement; University of Göttingen: Germany, 1997, pp. 1456.
25. Barbour, L. J. X-SEED-A Software Tool for Supramolecular Crystallography. *J. Supramol. Chem*. 2001, 1, 189-191.
26. Macrae, C. F.; Bruno, I, J.; Chisholm, J. A.; Edgington, P. R.; McCabe, P.; Pidcock, E.; Rodriguez-Monge, L.; Taylor, R.; Van de Streek, J.; Wood, P. A. *J. Appl. Crystallogr*. 2008, 41, 466-470.
27. Spek, A. L. PLATON: A Multipurpose Crystallographic Tool, Version 10500: e, 1980-2000.
28. ConQuest: A Program for the Search of the CSD, Version 1.19, © 2016.
29. Barbour, L. J. LAYER: A Computer Program for the Graphic Display of Intensity Data as Simulated Procession Photographs. *J. Appl. Crystallogr*. 1999, 32, 351.
30. POV-Ray for windows, Version 3.1e.watcom.win32. The Persistence of Vision Development Team, © 1991-1999.

31. Barbour, L. J. SECTION: A Computer Program for the Graphic Display of Cross Sections through a Unit Cell. *J. Appl. Crystallogr*. 1999, 32, 353.
32. Connolly, M. L. The Molecular Surface Package. *J. Mol. Graphics*. 1993, 11, 139-141.
33. Wolff, S. K.; Grimwood, D. J.; McKinnon, J. J.; Jayatilaka, D.; Spackman, M. A. Crystal Explorer 2.1. University of Western Australia, Perth. 2007.
34. Hirshfeld, F. L. Bonded Atom Fragments for Describing Molecular Charge Densities. *Theor. Chim. Acta*. 1977, 44, 129-138.
35. Spackman, M. A.; Jayatilaka, D. Hirshfeld Surface Analysis. *Cryst.Eng.Comm*. 2009, 11, 19-32.
36. The crystal Explorer Manual. http://hirshfeldsurface.net/wiki/index.php/Surface_Properties. Accessed 17 August 2016.

CHAPTER III

Halogen Bonding in Host – Guest Compounds: Structures and Kinetics of Enclathration and Desolvation

(Amombo Noa, F. M.; Bourne, S. A.; Nassimbeni, L. R. *Cryst. Growth Des.* 2015, 15 (7), 3271 – 3279).

3.1 Summary

This chapter deals with the classification of halogen···halogen interactions found in the inclusion compounds between two chosen host compounds (tetrakis-4-(bromophenyl)ethylene and its iodo-analogue) and selected halogenated methanes.

In the process of classifying this halogen···halogen interactions, the research article of Than Thu *et* al[1] was utilised indicating that there are three types of geometries observed for these interactions. Type I, which is of van der Waals type has X…X distances greater than the sum of their van der Waals radii depending on which halogen atom used. Type I interaction angles θ_1 and θ_2 are equal ($\theta_1 \approx \theta_2$). Type II is divided into two types; type II_a and type II_b interactions. These interactions are considered to be attractive and associated with crystallographic screw axes and glide planes. Here, the halogen atom becomes more polarizable. The angles between type II_a and type II_b are not that different, as the θ_1 in each type is approximately 180°, but the angle θ_2 is ≈ 90° for type II_a and ≈ 120° in type II_b.

Nine crystal structures were successfully obtained via crystallisation and characterised using single X-ray diffraction, thermal analysis and Hirshfeld surface analysis. Five of these crystal structures are homeotypes. In other words, they have same unit cell dimensions, space group, host/guest ratios and the host atoms occupied the same positions. The only difference is the guest solvents utilised for crystallisation.

The decomposition pattern of structures **2**, **3**, **5**, **6**, **7** and **8** was the same: the first peak in the DSC is due to the loss of the guest incorporated in the structures; this is followed by the melt of the host. This was not the case for compounds **4** and **9** which were obtained from diiodomethane (CH_2I_2). Their DSC traces first exhibits an endotherm which is the loss of the CH_2I_2 guest, then there is a sharp exotherm peak which implies a reaction between the host and the CH_2I_2. This occurs at the double bond of the host molecules. One of

the iodine atom in the CH_2I_2 attacked the double bond in the ethylene group of the hosts and formed a radical.

The activation energies of desolvation for all the compound used for this study were obtained using non-isothermal thermogravimetry and the results correlated with their crystal structures. It was found that the five isostructural compounds displayed similar activation energies. The structure with CCl_4 had the highest activation energy because the guests CCl_4 lie in restricted channels and CCl_4 has high boiling point (76.72 °C). The experiment was not conducted for one of the structures with CH_2I_2 because of the paucity of the material.

Kinetics of enclathration was only conducted for structures with CH_3I as guest on a specially constructed computerised balance, and their rate laws were established.

Finally, Hirshfeld surface analysis was performed on the compounds for a better understanding of the non-bonded interactions that occur in the structures via the program Crystal Explorer.

The supporting information for this article is also given after the main article.

3.2 References

1. Than Thu Bui, T.; Dahaoui, S.; Lecomte, C.; Desiraju, G. R.; Espinosa, E. *Angew. Chem., Int. Ed.* 2009, 48, 3838 – 3841.

CRYSTAL GROWTH & DESIGN

Article

pubs.acs.org/crystal

Halogen Bonding in Host–Guest Compounds: Structures and Kinetics of Enclathration and Desolvation

Francoise M. Amombo Noa, Susan A. Bourne, and Luigi R. Nassimbeni*

Centre for Supramolecular Chemistry Research, Department of Chemistry, University of Cape Town, Rondebosch 7701, South Africa

Supporting Information

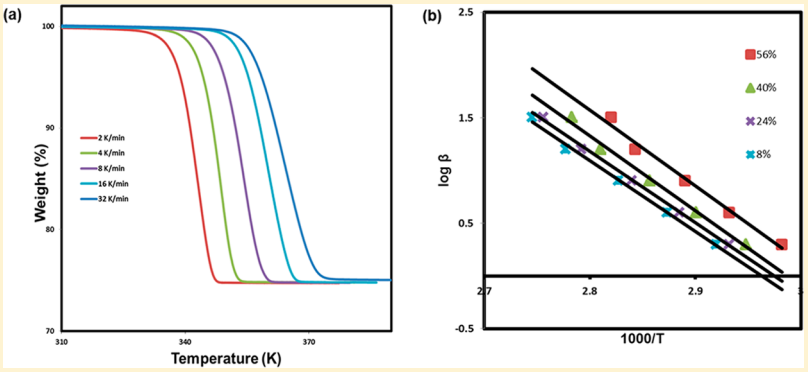

ABSTRACT: The host compounds tetrakis(4-bromophenyl) ethylene and its iodo-analogue form inclusion compounds with a series of chloro- and iodo-methanes. Their structures have been elucidated, and their nonbonded halogen···halogen contacts have been analyzed and classified. Their kinetics of desolvation have been studied, and the concomitant activation energies have been established. Five of the clathrates are isostructural and display similar activation energies of desolvation, thus correlating structure and function. The velocity of the enclathration for the solid host–methyl iodide vapor reactions and associated rate law have been established.

INTRODUCTION

The topic of halogen bonding and its importance in various aspects of crystal engineering is receiving considerable interest. Desiraju reviewed it in his book *Crystal Engineering*[1] and more recently pointed out its effects in crystal plasticity[2] and on the packing of dihalogenated phenols.[3] Halogen bonding has been likened to hydrogen bonding, and its applications in synthetic chemistry and materials science have been evaluated.[4,5] The nature of halogen bonding in the gas phase has been examined[6] and its occurrence in biological molecules such as proteins and nucleic acids has been studied.[7] Recently, a complete issue of *Crystal Growth & Design* was devoted to halogen bonding in crystal engineering.[8] This covered a variety of topics, ranging from the theoretical to the practical applications of these secondary interactions, and attests to the importance of this subject.

In this work, we present the results of the synthesis, structural characterization, and dynamic behavior of a series of inclusion compounds formed between two related hosts, tetrakis(4-bromophenyl) ethylene (**H1**) and its iodo-analogue (**H2**), with a series of halogenated methanes. The host compounds were chosen because they are the most reactive in terms of halogen bonding,[9] and the guests were selected due to their low boiling points, giving them high volatility. This feature is useful in examining their kinetics by thermal gravimetry.

Inclusion compounds of **H1** with acetone, tetrahydrofuran,[10] and *p*-xylene[11] have been reported. **H2** formed clathrates with 1,1,2,2-tetrachloroethane[9] and C_{60} fullerene/toluene solvate.[12]

The atomic numbering is given in Scheme 1. In this publication, the symbol for the element iodine is given as *I* to distinguish it from the Roman numeral I, which is used to denote "type I".

Scheme 1. Host and Guest Compounds

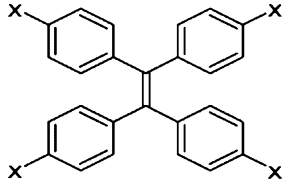

Host
H1: X = Br
H2: X = *I*

Guests
CH_2Cl_2
$CHCl_3$
CCl_4
CH_3I
CH_2I_2

EXPERIMENTAL SECTION

H1 was synthesized by exposing tetraphenylethene to bromine vapor in a desiccator for 24 h. The resulting product was recrystallized twice from a 50/50 (v/v) mixture of ethanol and chloroform.

H2 was synthesized by mixing a suspension of tetraphenylethene (8.3 g, 25 mmol), iodine (12.7 g, 50.0 mmol), and bis[trifluoroacetoxy]phenyl

Received: March 23, 2015
Revised: May 21, 2015
Published: May 26, 2015

ACS Publications © 2015 American Chemical Society

DOI: 10.1021/acs.cgd.5b00402
Cryst. Growth Des. 2015, 15, 3271–3279

iodine (26.2 g, 60.0 mmol) in chloroform (30.0 mL) and stirring at room temperature for 12 h. After the iodine color disappeared, the reaction mixture was filtered, washed with a little hexane, dried, and recrystallized from toluene to give colorless prisms.[9]

Crystal Growth. The inclusion compounds were obtained by dissolving **H1** or **H2** in the various liquid guests and allowing the solutions to evaporate. The single crystals obtained were initially analyzed by thermal gravimetry (TG), which detected the formation of the inclusion compound and yielded the host/guest ratio.

Structure Analysis. Cell dimensions were established from the intensity data measured on Nonius Kappa CCD[13] and Bruker DUO APEX II[14] diffractometers using graphite-monochromated Mo Kα radiation. The intensity data were collected by the standard φ scan and ω scan techniques, scaled, and reduced using DENZO-SMN[15] or SAINT-Plus.[16] The structures were solved by direct methods and refined by full-matrix least-squares on F^2 using SHELX-97[17] program packages. The program X-SEED[18] was used as a graphic interface. All the non-hydrogen atoms were refined anisotropically, while the guest atoms were treated isotropically or anisotropically depending on the occurrence of disorder. All hydrogen atoms were placed geometrically and with a riding model for their isotropic temperature factors.

Crystallographic data for the structures in this paper have been deposited with the Cambridge Crystallographic Centre as supplementary publication number 1055011−1055019. Copies of the data can be obtained free of charge on application to CCDC, 12 Union Road, Cambridge CB2 1EZ, U.K. (fax: (+44) 1223-336-033; e-mail: deposit@ccdc.cam.ac.uk).

Thermal Gravimetry (TG). TG data were collected on a TGA Q500 (TA Instruments) with a purge gas of dry nitrogen flowing at 60 mL min^{-1}. The kinetics of desolvation was determined by the method of Flynn and Wall,[19] in which the mass loss of the compounds was recorded at fixed heating rates β of 2, 4, 8, 16, and 32 °C min^{-1}. Plots of log β versus $1000/T$ yielded the values of the activation energies for the reactions.

The kinetics of enclathration was determined in a specially constructed balance in which a powdered sample of the host was exposed to the vapor of the volatile guest. The apparatus allows the sorption to be carried out under controlled conditions of temperature and vapor pressure. The mass gain is automatically recorded as a function of time, and the data are converted to the extent of reaction α.

$$\alpha = (m_t - m_o)/(m_\infty - m_o)$$

where m_o, m_t, and m_∞ are the masses at the start, during, and at the end of the experiment, respectively. The α−time curves may then be fitted to an appropriate rate law[20] and the rate constant thus evaluated.

Differential Scanning Calorimetry. DSC was performed for all inclusion compounds. The crystals were crushed and placed in crimped and vented pans, then analyzed using a DSC Q200 series with a purge gas of nitrogen at 60 mL min^{-1}. Samples were analyzed between 303 and 600 K for **H1** and 303−623 K for **H2** at a heating rate of 10 K min^{-1}.

RESULTS AND DISCUSSION

The character of halogen···halogen interactions has been discussed as a model derived from experimental charge density analysis.[21] The results are based on the anisotropy of the electron density distribution around the halogen nuclei and may be understood in terms of a polarization, which is positive in the polar region of the halogen atom and negative in the equatorial region. The outcome of this study suggests three types of geometries, shown in Scheme 2.

Type I interactions are of the van der Waals type, and their X···X distances are generally greater than the sum of the van der Waals radii. Type II$_a$ and II$_b$ interactions are considered as attractive, and the X···X distances are usually shorter than those of type I.

In this work, we have employed the van der Waals radii of Bondi[22] (radii in Å, H = 1.20, Cl = 1.75, Br = 1.85, I = 1.98).

Scheme 2. Halogen···Halogen Interactions

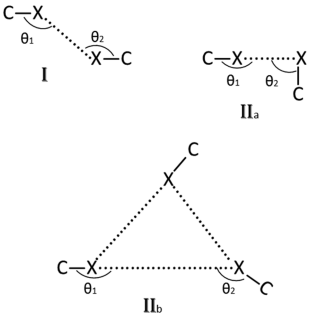

All halogen···halogen interactions are reported in Tables 2 and 4, which specify the X···X distance, angles θ_1 and θ_2, and the type of bond as shown in Scheme 2.

We recorded X···X distances that were less than the sum of the van der Waals radii +5% for interactions of type I and II$_a$ and type II$_b$. In general the type II$_b$ interactions gave reasonable nonbonded distances, but the angles θ_1/θ_2 sometimes deviated significantly from the ideal values of 180°/120°.

Structure Analysis. Crystal data and experimental and refinement parameters are given in Table 1 for the host−guest compounds with **H1**.

Structure **1** is that of a new polymorph of the apohost, the first structure of which was published by Tanaka et al.[11] That structure was obtained from *meta*-xylene and crystallizes in the space group *Pccn* with Z = 8. By contrast, this new polymorph of **H1**, obtained from acetonitrile, crystallizes in the space group $P2_1/n$ with Z = 8. The packing, shown as a projection viewed along [010], is illustrated in Figure 1. There are four Br···Br interactions, all of type IIa (Table 2).

Structure **2**, **H1·2CH$_2$Cl$_2$**, crystallizes in $P2_12_12_1$ with Z = 4. The packing is shown in Figure 2, which displays channels contiguous to the screw axis along [100] in which half the dichloromethane guests are located. The other dichloromethane guests reside in cavities. There are six X···X interactions, reported in Table 2.

Hirshfeld Surface Analysis. In order to further understand the nonbonded interactions that occur in these structures, the program Crystal Explorer[23−25] was employed, which calculates the Hirshfeld surfaces of a molecule in the structure and depicts all the molecular interactions of a targeted molecule with its neighbors.

The results for structure **2**, **H1·(2CH$_2$Cl$_2$)**, are given as an example. The host compound **H1** was selected as the target molecule, and the Hirshfed surface was calculated. The fingerprint plots for the various nonbonded interactions are shown in Figure 3a−h, and the corresponding frequency of these interactions is reported as a percentage in the legend, in which the first atom is from the targeted host and the second from any surrounding molecules.

Thus, for example, Figure 3c shows the interactions between C atoms in the targeted host and all H atoms in the surrounding hosts and guests. It shows that the closest approach, shown as peak 2, occurs at the sum of the internal and external distances from the surface $(d_i + d_e)$ = 2.95 Å, slightly longer than the sum of the van der Waals radii.

What we glean from these maps is that the packing is dominated by H···H interactions (28.1%), Figure 3b, with a closest approach at peak 1 at $(d_i + d_e)$ = 2.60 Å, somewhat longer than the sum of the van der Waals radii (2.40 Å).

DOI: 10.1021/acs.cgd.5b00402
Cryst. Growth Des. 2015, 15, 3271−3279

Table 1. Crystallographic Data and Structure Refinement Parameters of H1 and Its Inclusion Compounds

compound	1	2	3	4
code	**H1**	**H1·(2CH_2Cl_2)**	**H1·(2CH_3I)**	**H1·(1.5CH_2I_2)**
structural formula	$C_{26}H_{16}Br_4$	$C_{26}H_{16}Br_4{\cdot}2CH_2Cl_2$	$C_{26}H_{16}Br_4{\cdot}2CH_3I$	$C_{26}H_{16}Br_4{\cdot}1.5CH_2I_2$
molecular mass (g mol^{-1})	648.03	817.84	931.86	1237.92
data collection temp (K)	296(2)	173(2)	173(2)	173(2)
crystal size (mm)	0.10 × 0.13 × 0.15	0.13 × 0.14 × 0.15	0.1 × 0.11 × 0.12	0.04 × 0.07 × 0.12
space group	$P2_1/n$	$P2_12_12_1$	$P2_12_12_1$	$P2_1/n$
a (Å)	20.5195(6)	9.3805(4)	9.3728(19)	25.4217(18)
b (Å)	9.7865(3)	15.3256(6)	14.7617(3)	9.5847(6)
c (Å)	24.0043(8)	21.0238(8)	21.8708(4)	25.8099(17)
α (deg)	90	90	90	90
β (deg)	91.598(1)	90	90	103.462(1)
γ (deg)	90	90	90	90
vol ($Å^3$)	4818.57(3)	3022.42(2)	3026.01(10)	6116.04(7)
Z	8	4	4	8
D_c (g cm^{-3})	1.787	1.797	2.045	2.280
absorp coeff (mm^{-1})	6.692	5.697	7.375	8.308
θ range	1.29−26.46	1.64−27.97	1.66−26.37	1.01−27.96
reflns collected	69270	37644	12346	164831
no. data $I > 2\sigma(I)$	7362	5969	5322	10288
final R indices [$I > 2\sigma(I)$]	0.0425	0.0326	0.0584	0.0383
R indices (all data)	0.0666	0.0477	0.0709	0.0696
GOF on F^2	1.047	1.020	1.056	1.056

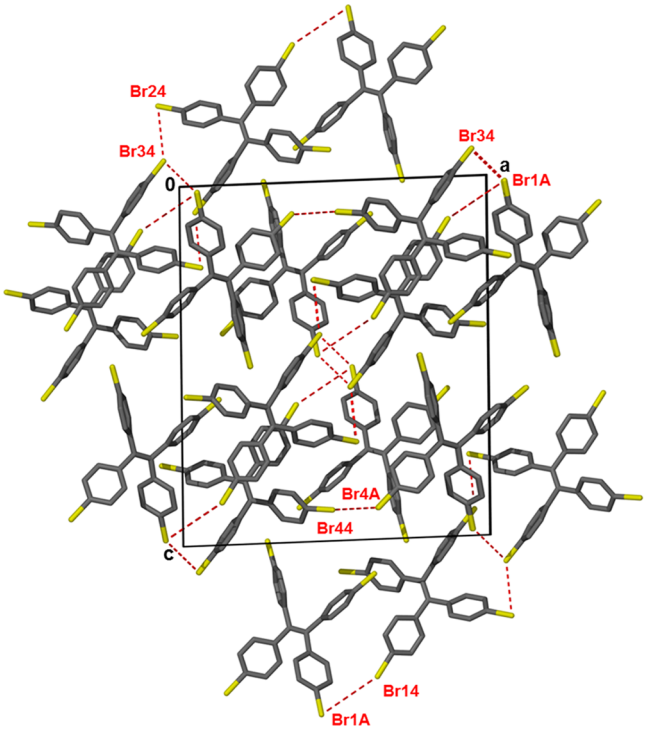

Figure 1. Packing diagram of **1** along [010] with hydrogen atoms omitted.

A striking feature is that the Br···Br interactions (6.2%), Figure 3g, and Br···Cl interactions (3.6%), Figure 3h, are buried within the fingerprint plots, peaking at approximately the sum of the van der Waals radii, as previously reported in Table 2. This puts the halogen···halogen interactions in context of the packing as a whole.

The same calculations were performed on the other structures, and similar results were obtained. The resulting percentage frequencies of the interactions are reported as tables in the Supporting Information.

Table 2. X···X Interactions of H1 with Its Inclusion Compounds

compound	X···X	d [Å]	θ_1/θ_2 [deg]	$d - \sum$vdw [Å]	%	type
1	$Br_{1A}\cdots Br_{34}$	3.706(1)	150/77	+0.006	+0.2	II_a
	$Br_{1A}\cdots Br_{14}$	3.637(1)	171/139	−0.063	−1.7	II_a
	$Br_{4A}\cdots Br_{44}$	3.681(1)	170/122	−0.019	−0.5	II_a
	$Br_{24}\cdots Br_{34}$	3.755(1)	137/80	+0.055	+1.5	II_a
2	$Br_{14}\cdots Cl_2$	3.678(2)	162/113	+0.078	+2.2	II_a
	$Br_{24}\cdots Br_{34}$	3.478(1)	169/130	−0.222	−6.0	II_a
	$Br_{24}\cdots Cl_2$	3.766(2)	162/92	+0.166	+4.6	II_a
	$Br_{34}\cdots Br_{44}$	3.762(2)	137/115	+0.062	+1.7	II_a
	$Cl_1\cdots Cl_2$	3.547(2)	155/88	+0.047	+1.3	II_a
	$Cl_2\cdots Cl_4$	3.563(2)	153/79	+0.063	+1.8	II_a
3	$Br_{14}\cdots I_2$	3.847(2)	169/113	+0.017	+0.4	II_a
	$Br_{24}\cdots Br_{34}$	3.656(7)	167/132	−0.044	−1.2	II_a
	$Br_{34}\cdots Br_{44}$	3.753(8)	127/113	+0.053	+1.4	II_a
	$I_1\cdots I_2$	4.026(8)	166/76	+0.066	+1.7	II_a
4	$Br_{1A}\cdots Br_{34}$	3.596(3)	179/114	−0.104	−2.8	II_a
	$Br_{1A}\cdots I_5$	3.760(3)	170/113	−0.070	−1.8	II_a
	$Br_{2A}\cdots Br_{14}$	3.784(3)	156/70	+0.084	+2.3	II_a
	$Br_{4A}\cdots Br_{14}$	3.635(3)	169/135	−0.065	−1.8	II_a
	$Br_{24}\cdots I_1$	3.768(3)	177/74	−0.062	−1.6	II_a
	$Br_{44}\cdots I_4$	3.734(3)	165/71	−0.096	−2.5	II_a
	$Br_{44}\cdots I_2$	4.030(3)	139/61	+0.200	+5.2	II_a
	$Br_{44}\cdots I_6$	3.725(3)	166/78	−0.105	−2.7	II_a
	$I_3\cdots I_5$	4.121(3)	163/113	+0.161	+4.1	II_a

Structure **3** is homeotypic with **2** in that the unit cell dimensions are similar, space group and host/guest ratios are the same, and the host atoms occupy the same positions. The only difference is that the CH_2Cl_2 guests are replaced with CH_3I, and the subsequent halogen···halogen contacts are reported in Table 2.

When the methyl iodide guest was replaced by methylene iodide, CH_2I_2, structure **4**, which crystallized in $P2_1/n$, was obtained. This structure contains two host and three guest molecules in the asymmetric unit, and the packing is shown in Figure 4.

DOI: 10.1021/acs.cgd.5b00402
Cryst. Growth Des. 2015, 15, 3271−3279

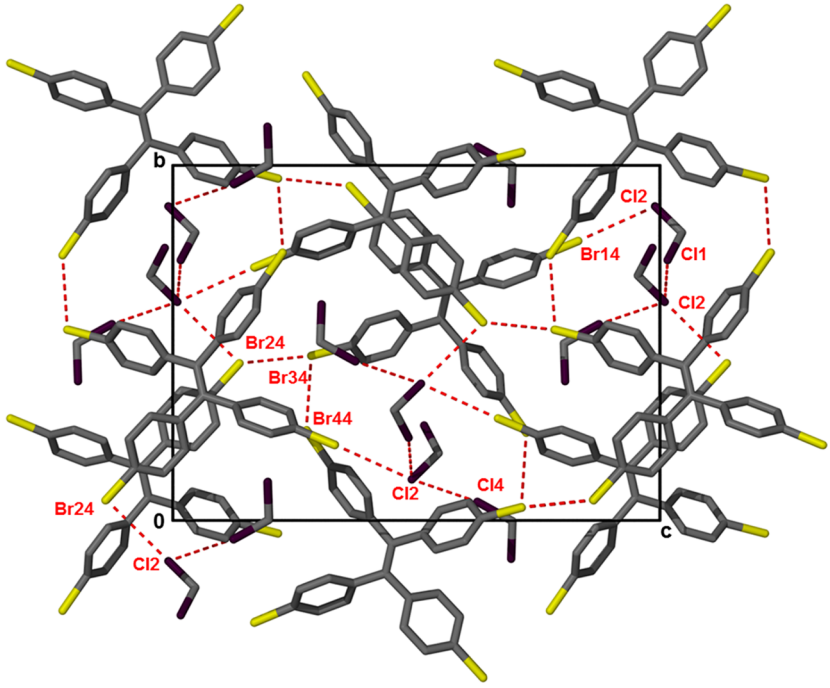

Figure 2. Packing diagram of **2** along [100] illustrating the channels and cavities in the structure.

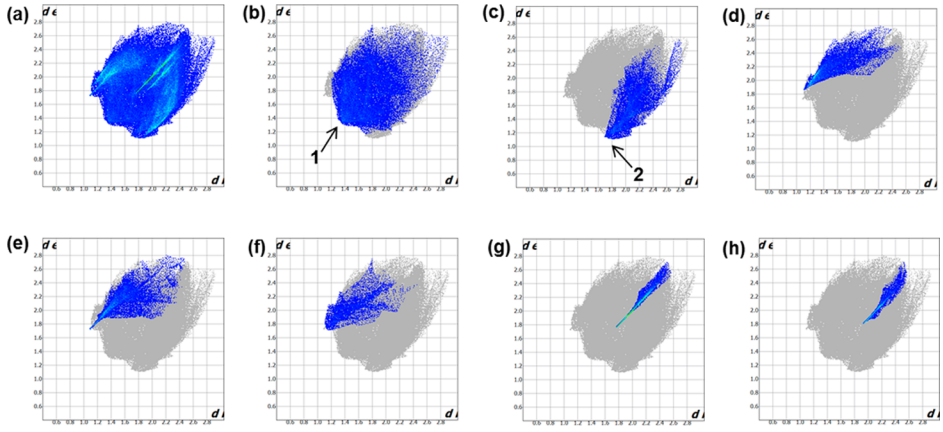

Figure 3. Two-dimensional plots for the host molecule in structure **2**: (a) overall fingerprint with **H1** as target; (b) H···H = 28.1%; (c) C···H = 10.9%; (d) H···Br = 9.9%; (e) H···Cl = 10.5%; (f) H···C = 5.3%; (g) Br···Br = 6.2%; (h) Br···Cl = 3.6%.

The guest molecules are located along constricted hourglass channels running along [010].

Structures **5**, **6**, and **7** where the Br atoms of the host have been replaced by $\mathcal{I}$, and in which the guests are CH_2Cl_2, $CH_3\mathcal{I}$, and $CHCl_3$ respectively, are also homeotypic with structure **2**. Their crystal data and experimental and refinement parameters are reported in Table 3. The halogen···halogen interactions of these homeotypic structures are listed in Table 4.

Structure **8** crystallizes in *Pbcn* with $Z = 4$. The host atoms are located on the dyads at Wyckoff position *c*, while the guests lie in channels running along [010], which are shown in Figure 5a and with van der Waals radii in Figure5b. It is interesting that there are halogen···halogen contacts between host···host, host···guest, and guest···guest molecules shown in Table 4.

The CCl_4 molecules are in restricted channels. The diagram displays the molecules with van der Waals radii. In the projection, one notes the apparent overlap of host and guest atoms.

Structure **9** crystallizes in $P2_1/c$ with $Z = 8$. The asymmetric unit contains two host and two guest molecules. $CH_2\mathcal{I}_2$ molecules are located in cavities shown in Figure 6. There are 11 halogen··· halogen interactions, whereby seven of these interactions are between host···guest molecules and four between host···host molecules. Three of the halogen···halogen interactions are of type I and eight of type II_a listed in Table 4.

Kinetics of Decomposition, Adsorption, and DSC. The decomposition of all the inclusion compounds was analyzed, and the kinetics were studied by recording the mass loss as a function of temperature at known heating rates. A typical result, that of the decomposition of **H2**·$(2CH_3\mathcal{I})$ is shown in Figure 7a, which illustrates the desolvation curves at rates varying geometrically from 2 to 32 °C min^{-1}. The corresponding semilogarithmic plot (Figure 7b) yielded straight lines for decomposition corresponding to 8%, 24%, 40%, and 56% of the extent of reaction. The concomitant activation energies varied from 122.4 to 130.9 kJ mol^{-1}. The differential scanning calorimeter (DSC) result recorded at a heating rate of 10 °C min^{-1} is shown in Figure 7c.

This displays the first endotherm at 359.4 K, corresponding to the loss of the $CH_3\mathcal{I}$ guest. The second sharper endotherm,

DOI: 10.1021/acs.cgd.5b00402
Cryst. Growth Des. 2015, 15, 3271−3279

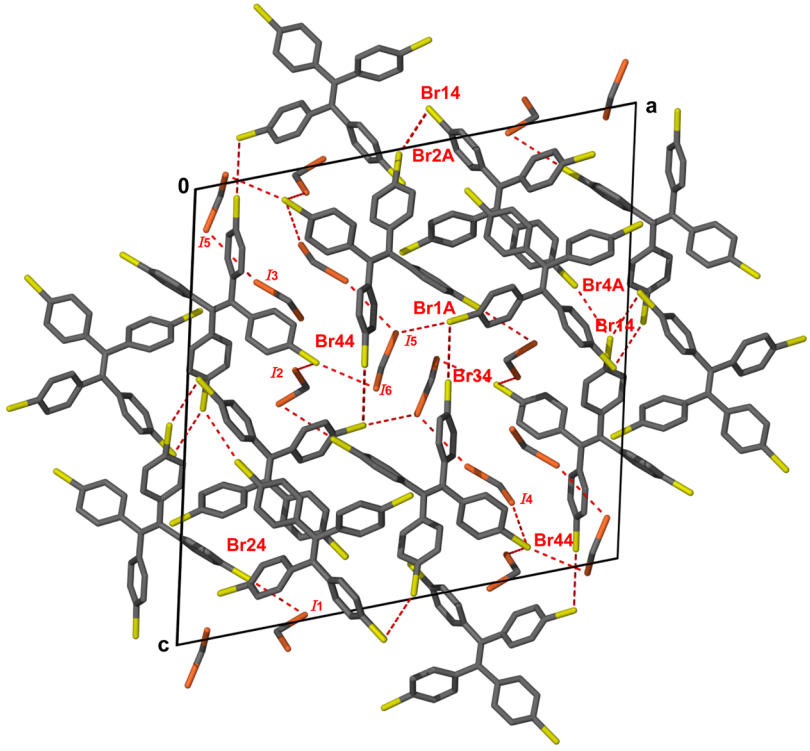

Figure 4. Packing diagram of **4** along [010] showing halogen···halogen interactions.

Table 3. Crystallographic Data and Structure Refinement Parameters of H2 Inclusion Compounds

compound	**5**	**6**	**7**	**8**	**9**
code	**H2·(2CH$_2$Cl$_2$)**	**H2·(2CH$_3$*I*)**	**H2·(2CHCl$_3$)**	**H2·(2CCl$_4$)**	**H2·CH$_2$*I*$_2$**
structural formula	$C_{26}H_{16}I_4 \cdot 2CH_2Cl_2$	$C_{26}H_{16}I_4 \cdot 2CH_3I$	$C_{26}H_{16}I_4 \cdot 2CHCl_3$	$C_{26}H_{16}I_4 \cdot 2CCl_4$	$C_{26}H_{16}I_4 \cdot CH_2I_2$
molecular mass (g mol^{-1})	1005.84	1119.86	1073.71	1143.61	1103.82
data collection temp (K)	173(2)	173(2)	173(2)	173(2)	173(2)
crystal size (mm)	0.06 × 0.14 × 0.15	0.07 × 0.10 × 0.12	0.07 × 0.12 × 0.13	0.09 × 0.10 × 0.12	0.02 × 0.06 × 0.10
space group	$P2_12_12_1$	$P2_12_12_1$	$P2_12_12_1$	*Pbcn*	$P2_1/c$
a (Å)	9.6916(19)	9.5601(19)	9.7376(19)	18.949(13)	21.2266(42)
b (Å)	15.450(3)	15.1117(3)	15.3250(3)	10.3422(7)	9.8811(2)
c (Å)	22.047(4)	22.5968(5)	22.9939(5)	17.9428(12)	29.6534(59)
α (deg)	90	90	90	90	90
β (deg)	90	90	90	90	103.043(3)
γ (deg)	90	90	90	90	90
vol (Å^3)	3301.18(11)	3264.55(12)	3431.35(12)	3516.3(4)	6059.11(2)
Z	4	4	4	4	8
D_c (g cm^{-3})	2.024	2.278	2.078	2.160	2.420
absorp coeff (mm^{-1})	4.116	5.724	4.117	4.172	6.166
θ range	1.61−27.48	3.44−27.46	1.60−27.43	2.15−28.43	1.41−27.52
reflns collected	141283	86357	107385	65710	148904
no. data $I > 2\sigma(I)$	5965	6191	7835	3290	13923
final *R* indices [$I > 2\sigma(I)$]	0.0499	0.0335	0.0427	0.0310	0.0653
R indices (all data)	0.0784	0.0490	0.0658	0.0506	0.1512
GOF on F^2	1.147	1.045	1.083	1.007	1.074

which occurs at 572.1 K, is due to the melting of the host. The peak temperatures were recorded as opposed to onset temperatures because not all the DSC profiles gave a steady baseline. The activation energies and the temperatures for the guest desolvation are given in Table 5. The results of the decomposition of the other inclusion compounds have been deposited as Supporting Information.

It is noteworthy that the activation energies of the desolvation reactions for compounds **2**, **3**, **5**, **6**, and **7** fall in a tight range of 112−138 kJ mol^{-1}. This is to be expected since they are isostructural and the three guests have normal boiling points in a small range of ∼20 K. (boiling point (K), CH_2Cl_2 = 312.8, CH_3I = 315.5, and $CHCl_3$ = 334.4).

For compound **8**, the activation energy is higher; this is because the CCl_4 molecules lie in restricted channels (Figure 4) and the boiling point of CCl_4 is higher at 349.9 K.

The only compound that did not follow this decomposition pattern, namely, loss of guest followed by melting of the host, is

DOI: 10.1021/acs.cgd.5b00402
Cryst. Growth Des. 2015, 15, 3271−3279

Table 4. X···X Interactions of H2 Inclusion Compounds

compound	X···X	d [Å]	θ_1/θ_2 [deg]	$d - \sum$vdw [Å]	%	type
5	$I_{14}\cdots I_{24}$	4.028(8)	129/118	+0.068	+1.7	II_b
	$I_{14}\cdots I_{44}$	3.794(7)	167/132	−0.166	−4.2	II_b
	$I_{24}\cdots I_{44}$	4.163(7)	173/88	+0.203	+5.1	II_b
	$Cl_1\cdots Cl_7$	3.670(7)	160/84	+0.170	+4.9	II_a
	$Cl_1\cdots Cl_2$	3.621(7)	157/89	+0.121	+3.5	II_a
6	$I_{14}\cdots I_1$	4.032(8)	171/107	+0.072	+1.8	II_a
	$I_{14}\cdots I_{24}$	4.159(8)	148/122	+0.199	+5.0	I
	$I_{14}\cdots I_2$	3.944(8)	168/128	−0.016	−0.4	II_a
	$I_{24}\cdots I_{44}$	4.127(8)	176/91	+0.167	+4.2	II_b
	$I_{24}\cdots I_{34}$	3.857(8)	166/132	−0.103	−2.6	II_b
	$I_{34}\cdots I_{44}$	4.017(8)	126/113	+0.057	+1.4	II_b
	$I_1\cdots I_4$	3.995(8)	166/75	+0.035	+0.9	II_a
	$I_2\cdots I_4$	4.156(8)	157/73	+0.196	+4.9	II_a
7	$I_{14}\cdots I_{34}$	4.023(9)	177/87	+0.063	+1.6	II_a
	$I_{24}\cdots I_{34}$	3.988(9)	164/133	+0.028	+0.7	II_a
	$I_{34}\cdots Cl_4$	3.930(9)	133/114	+0.200	+5.4	I
	$Cl_1\cdots Cl_9$	3.561(8)	141/101	+0.061	+1.7	I
	$Cl_5\cdots Cl_9$	3.666(8)	160/122	+0.166	+4.7	II_a
	$Cl_2\cdots Cl_5$	3.128(7)	174/160	−0.372	−10.6	I
8	$I_{14}\cdots I_{24}$	3.748(3)	173/95	−0.212	−5.4	II_a
	$I_{14}\cdots I_{24}$	3.952(3)	162/108	−0.008	−0.2	II_a
	$I_{14}\cdots Cl_2$	3.830(3)	142/69	+0.100	+2.7	II_a
	$I_{24}\cdots Cl_4$	3.871(3)	135/63	+0.140	+3.8	II_a
	$Cl_2\cdots Cl_4$	3.592(2)	110/103	+0.092	+2.6	I
9	$I_{14}\cdots I_{34A}$	4.056(8)	138/75	+0.096	+2.4	II_a
	$I_{14}\cdots I_4$	3.937(8)	179/88	−0.023	−0.6	II_a
	$I_{24}\cdots I_{34A}$	3.942(8)	150/146	−0.018	−0.5	I
	$I_{34}\cdots I_3$	4.011(8)	141/93	+0.051	+1.3	II_a
	$I_{34}\cdots I_4$	4.070(8)	132/111	+0.110	+2.8	I
	$I_{34}\cdots I_{34}$	3.831(8)	136/136	−0.129	−3.3	I
	$I_{44}\cdots I_{44A}$	3.910(8)	173/113	−0.050	−1.3	II_a
	$I_{44}\cdots I_3$	3.682(7)	167/79	−0.278	−7.0	II_a
	$I_{14A}\cdots I_1$	4.142(8)	139/91	+0.182	+4.6	II_a
	$I_{14A}\cdots I_2$	3.870(8)	165/98	−0.009	−2.3	II_a
	$I_{24A}\cdots I_1$	3.777(8)	174/79	−0.183	−4.6	II_a

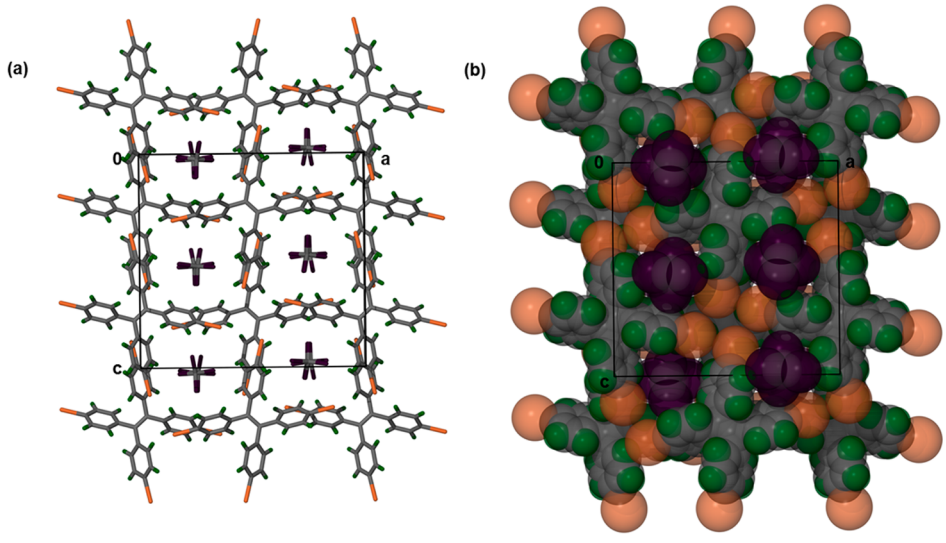

Figure 5. Packing diagram of **8** along [010] showing (a) carbon tetrachloride molecules in channels and (b) van der Waals radii crystal packing down [010].

DOI: 10.1021/acs.cgd.5b00402
Cryst. Growth Des. 2015, 15, 3271−3279

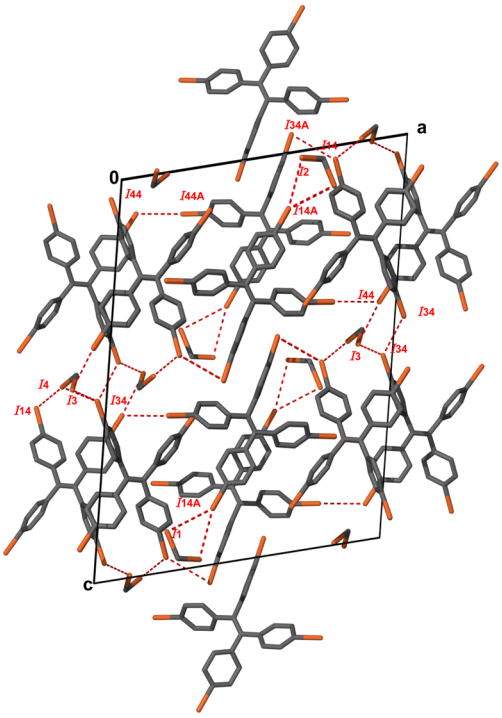

Figure 6. Packing diagram of **9** down [010] with the guest molecules located in cavities.

compound **H1·(1.5CH$_2$I$_2$)**. The DSC trace for this compound exhibits an endotherm at 336.4 K due to the loss of CH$_2$I$_2$ guest.

Table 5. Activation Energies and DSC Endotherm of H1 and H2 Inclusion Compounds

compounds	structures	E_a, kJ mol^{-1}	DSC guest release, K	DSC host melt, K
H1·(2CH$_2$Cl$_2$)	**2**	112.5−137.6	315.4	526.1
H1·(2CH$_3$I)	**3**	126.7−144.5	342.4	526.7, 531.1
H1·(1.5CH$_2$I$_2$)	**4**	72.8−83.3	336.4	decomposes
H2·(2CH$_2$Cl$_2$)	**5**	115.5−122.9	342.0	573.8
H2·(2CH$_3$I)	**6**	122.4−130.9	359.4	572.1
H2·(2CHCl$_3$)	**7**	127.1−137.9	347.7, 369.9	573.5
H2·(2CCl$_4$)	**8**	149.0−156.7	365.6	561.9
H2·CH$_2$I$_2$	**9**	*a*	368.3	450.4 (exotherm peak)

[a]Experiment not performed due to paucity of material.

This is followed by a sharp exotherm peak at 412.4 K, which implies a reaction between the host and the CH$_2$I$_2$. We surmise that this is a reaction at the double bond. The same reaction is observed in structure **9**, and we did not pursue this further.

Compound **4**, **H1·(1.5CH$_2$I$_2$)** has a significantly lower activation energy of desolvation. It was noted that the crystals obtained, very thin needles (0.04 × 0.07 × 0.12 mm^3), were very unstable and began to decompose immediately upon removal from the mother liquor. They were therefore quickly covered in paratone oil, mounted in a plastic loop, and put in the stream of cold nitrogen to minimize decomposition. The crystal instability matches the DSC result, which has the endotherm due to guest loss at 336.4 K, in comparison to the high boiling point of CH$_2$I$_2$ (454.4 K).

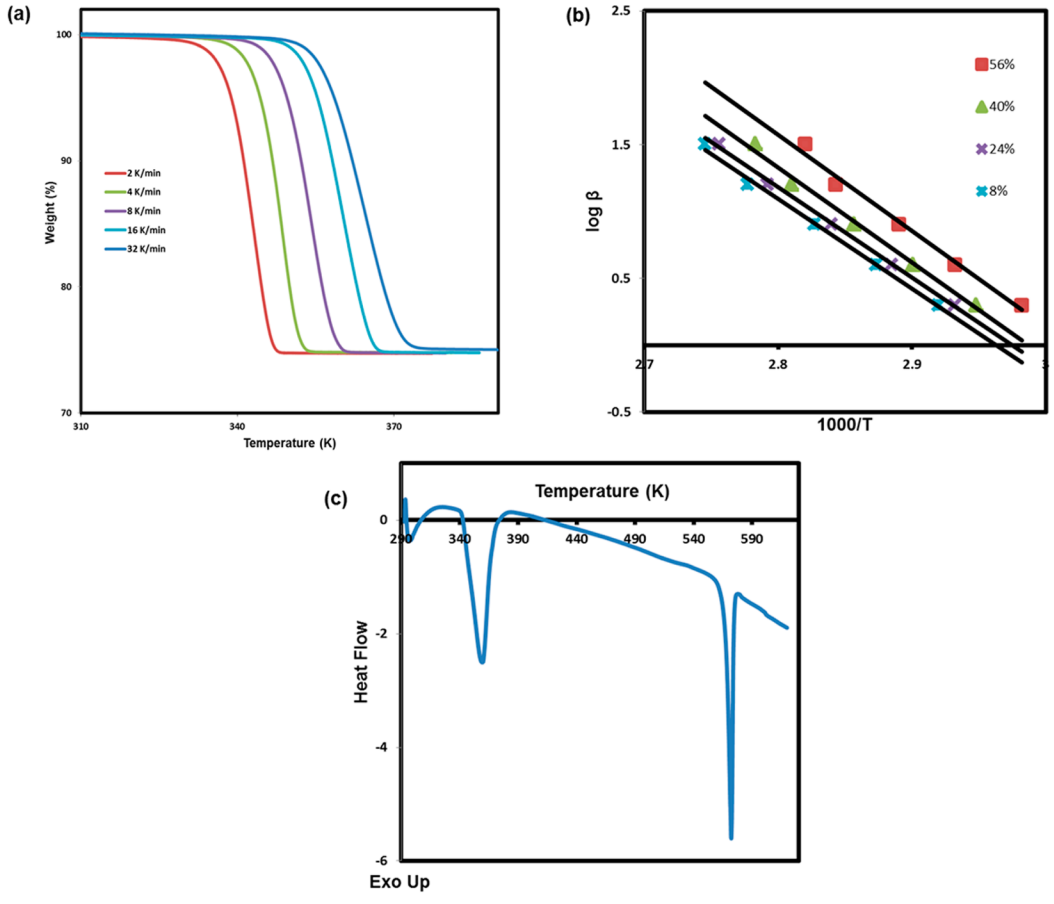

Figure 7. (a) Nonisothermal TG curves for **6**, (b) plot of log β vs the reciprocal of the temperature for **6**, and (c) DSC curve for **6**.

DOI: 10.1021/acs.cgd.5b00402
Cryst. Growth Des. 2015, 15, 3271−3279

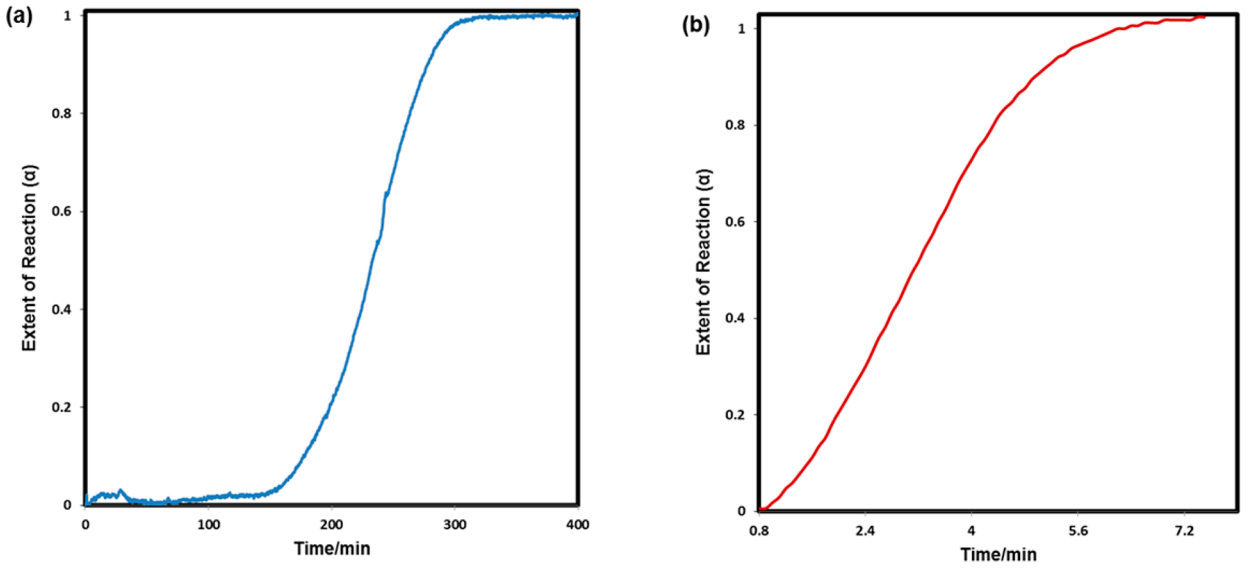

Figure 8. Kinetic curves for (a) **3** and (b) **6** at 25 °C.

The kinetics of enclathration was determined on a specially constructed balance, which consists of a Precisa four place balance the weighing mechanism of which has been separated from its electronics component and placed under an inverted desiccator. This allows the sorption of guest vapor to be carried out under controlled conditions of temperature and vapor pressure of volatile guest.

The results of the kinetics of enclathration of **H1** with CH_3I vapor at 25 °C is shown in Figure 8a, which displays the extent of reaction α versus time. The mass of CH_3I absorbed corresponded to a host/guest ratio of 1:2 as was found in the crystal structure derived by the crystallization of **H1** in pure CH_3I. The powdered host was exposed to the vapor of liquid CH_3I under atmospheric conditions.

The enclathration reaction displays a long induction period of 140 min, after which the absorption curve has a sigmoidal profile that fits the Avrami−Erofe'ev equation:

$$f(\alpha) = [-\ln(1 - \alpha)]^{1/4} = kt$$

where k is the rate constant, which has a value of 6.64×10^{-3} min^{-1} ($r = 0.998$) at 25 °C.

The kinetic curve for the reaction of **H2** with CH_3I vapor at 25 °C is shown in Figure 8b. This reaction has no induction period, follows the same kinetic mechanism as the previous case, and is much faster with $k = 1.91 \times 10^{-1}$ min^{-1} ($r = 0.997$). In contrast to the previous reaction, this host only absorbs 1 mol of CH_3I per mole of host, although the host/guest ratio of the inclusion compound derived from solution is 1:2.

CONCLUSION

The host−guest complexes formed by the host compounds tetrakis(4-bromophenyl) ethylene and its iodo-analogue with a series of halogenated methanes have been characterized. They all exhibit halogen···halogen interactions that have been classified as type I (van der Waals) or types II_a and II_b (attractive). Five of the structures, which contain the volatile guests dichloromethane, chloroform, and methyl iodide, are isostructural, with half the guest molecules located in channels and the other half in cavities. Their thermal decomposition curves are similar, with the desolvation taking place in a single step and the DSC exhibiting a corresponding guest-release endotherm. The average energies of activation of their decomposition lie in a narrow range of ∼119−135 kJ mol^{-1}, thus correlating structure and thermal behavior. The compound containing the less volatile guest carbon tetrachloride has significantly higher activation energy of desolvation. The compounds with diiodomethane form unstable crystals, yield low activation energy of desolvation, and react with the host compounds when heated.

ASSOCIATED CONTENT

Supporting Information

Triangular halogen···halogen interaction, DSC traces, kinetics of decomposition, plot of log β vs the reciprocal of the temperature, Hirshfeld surface analysis, and crystallographic data in cif format. The Supporting Information is available free of charge on the ACS Publications website at DOI: 10.1021/acs.cgd.5b00402.

AUTHOR INFORMATION

Corresponding Author

*Tel: +27 21 650 5893. Fax: +27 21 650 2569. E-mail: luigi.nassimbeni@uct.ac.za.

Notes

The authors declare no competing financial interest.

ACKNOWLEDGMENTS

We thank the University of Cape Town and the National Research Foundation (South Africa) for funding.

REFERENCES

(1) Desiraju, G. R. *Crystal Engineering*; Elsevier: Amsterdam, 1989, Chapter 6.
(2) Reddy, C. M.; Kirchner, M. T.; Gundakaram, R. C.; Padmanabhan, K. A.; Desiraju, G. R. *Chem.—Eur. J.* **2006**, *12*, 2222−2234.
(3) Mukherjee, A.; Desiraju, G. R. *IUCrJ* **2014**, *1*, 49−60.
(4) Metrangolo, P.; Neukirch, H.; Pilati, T.; Resnati, G. *Acc. Chem. Res.* **2005**, *38*, 386−395.
(5) Metrangolo, P.; Meyer, F.; Pilati, T.; Resnati, G.; Terraneo, G. *Angew. Chem., Int. Ed.* **2008**, *47*, 6114−6127.
(6) Legon, A. C. *Phys. Chem. Chem. Phys.* **2010**, *12*, 7736−7747.
(7) Auffinger, P.; Hays, F. A.; Westhof, E.; Ho, P. S. *Proc. Natl. Acad. Sci. U. S. A.* **2004**, *101*, 16789−16794.

DOI: 10.1021/acs.cgd.5b00402
Cryst. Growth Des. 2015, 15, 3271−3279

(8) Halogen Bonding in Crystal Engineering: Fundamentals and Applications, Virtual Special Issue *Crystal Growth and Design*; Vol *vi*, issue 8, **2012**, http://pubs.acs.org/page/cgdefu/vi/8.
(9) Tanaka, K.; Fujimoto, D.; Toda, F. *Tetrahedron Lett.* **2000**, *41*, 6095−6099.
(10) Tanaka, K.; Fujimoto, D.; Altreuther, A.; Oeser, T.; Irngartinger, H.; Toda, F. *J. Chem. Soc., Perkin Trans.* **2000**, *2*, 2115−2120.
(11) Tanaka, K.; Fujimoto, D.; Oeser, T.; Irngartinger, H.; Toda, F. *Chem. Commun.* **2000**, 413−414.
(12) Tanaka, K.; Caira, M. R. *J. Chem. Res.* **2002**, 642.
(13) COLLECT, data collection software; Nonius: Delft, The Netherlands, 1998.
(14) APEX 2, Version 1.0-27, Bruker AXS Inc: Madison, Wisconsin, 2005.
(15) Otwinowski, Z.; Minor, W. In *Macromolecular Crystallography, part A*; Carter, C. W. Jr.; Sweet, R. M, Eds.; Methods in Enzymology, Vol. *276*; Academic Press: San Diego, CA, 1997; p 307.
(16) SAINT-Plus, Version 7.12, Bruker AXS Inc.: Madison, Wisconsin, 2004.
(17) Sheldrick, G. M. *SHELX-97: Program for Crystal Structure Refinement*; University of Göttingen: Göttingen, Germany, 1997.
(18) Barbour, L. J. X-Seed − A software Tool for Supramolecular Crystallography. *J. Supramol. Chem.* **2001**, *1*, 189−191.
(19) Flynn, J. H.; Wall, L. A. *J. Polym. Sci.* **1966**, *4*, 323−328.
(20) Brown, M. E. *Introduction to Thermal Analysis: Techniques and Applications*; Chapman and Hall: London, 1988.
(21) Than Thu Bui, T.; Dahaoui, S.; Lecomte, C.; Desiraju, G. R.; Espinosa, E. *Angew. Chem., Int. Ed.* **2009**, *48*, 3838−3841.
(22) Bondi, A. *J. Phys. Chem.* **1964**, *68*, 441−451.
(23) Spackman, M. A.; McKinnon, J. J. *CrystEngComm* **2002**, *4*, 978−392.
(24) McKinnon, J. J.; Spackman, M. A.; Mitchell, A. S. *Acta Crystallogr.* **2004**, *B60*, 627−668.
(25) McKinnon, J. J.; Jayatilla, D.; Spackman, M. A. *Chem. Commun.* **2007**, 3814−3816.

DOI: 10.1021/acs.cgd.5b00402
Cryst. Growth Des. 2015, 15, 3271−3279

SUPPORTING INFORMATION

Halogen bonding in host-guest compounds: structures and kinetics of enclathration and desolvation.

*Francoise M. Amombo Noa, Susan A. Bourne and Luigi R. Nassimbeni**

Centre for Supramolecular Chemistry Research, Department of Chemistry, University of Cape Town, Rondebosch 7701, South Africa. Email: luigi.nassimbeni@uct.ac.za.

INDEX

Triangular halogen-halogen-halogen interactions

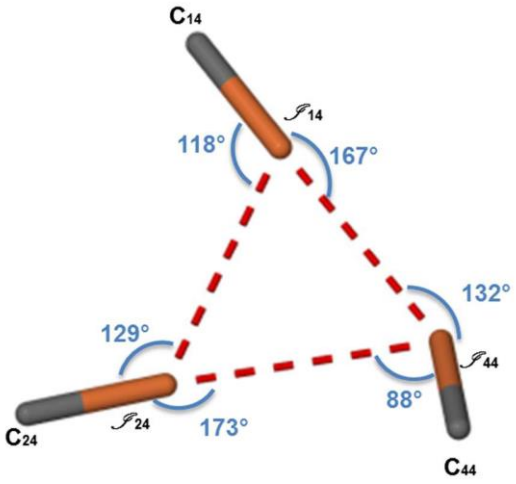

Figure S1 Example of triangular halogen-halogen interactions in structure **5**.

Thermal Analysis

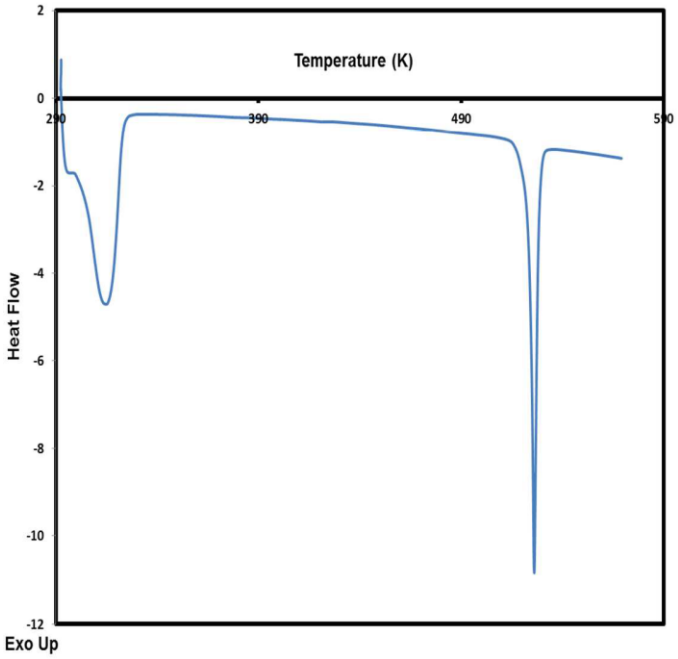

Figure S2 DSC curve of structure **2**.

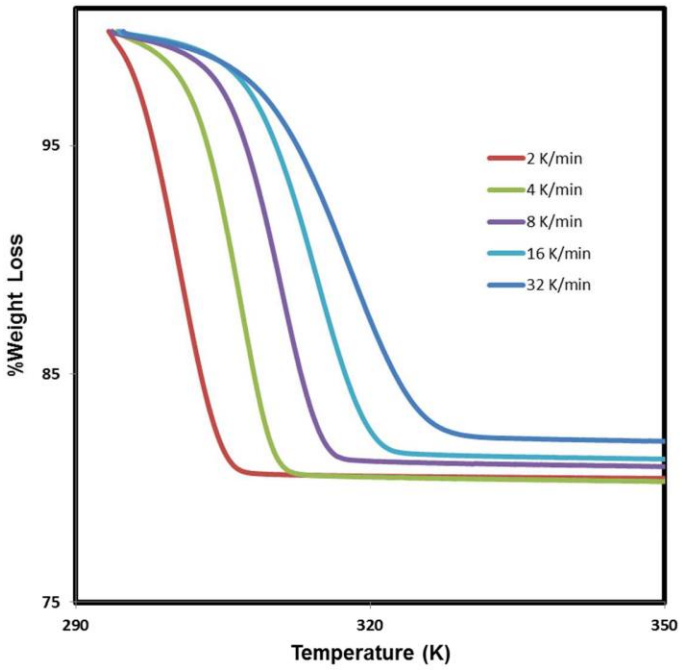

Figure S3 Non-isothermal TG curves of structure **2**.

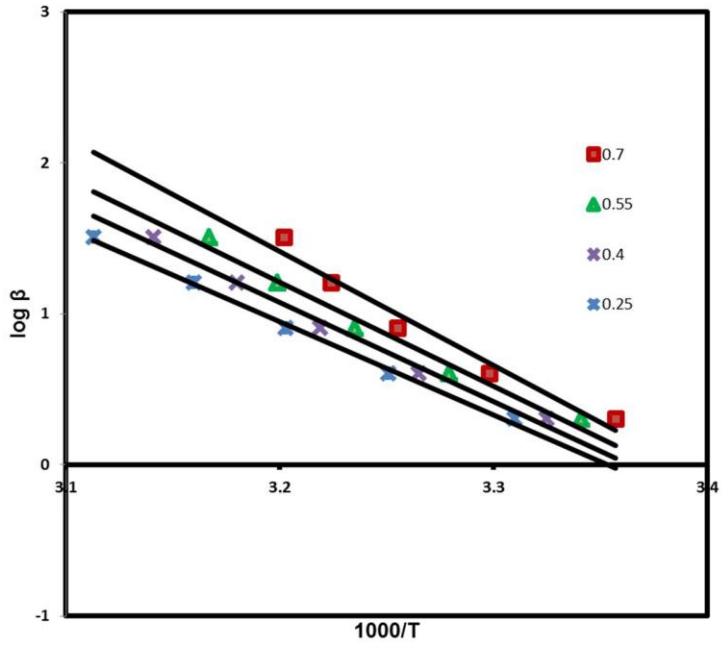

Figure S4 Plot of log *β vs.* the reciprocal of the temperature for structure **2**.

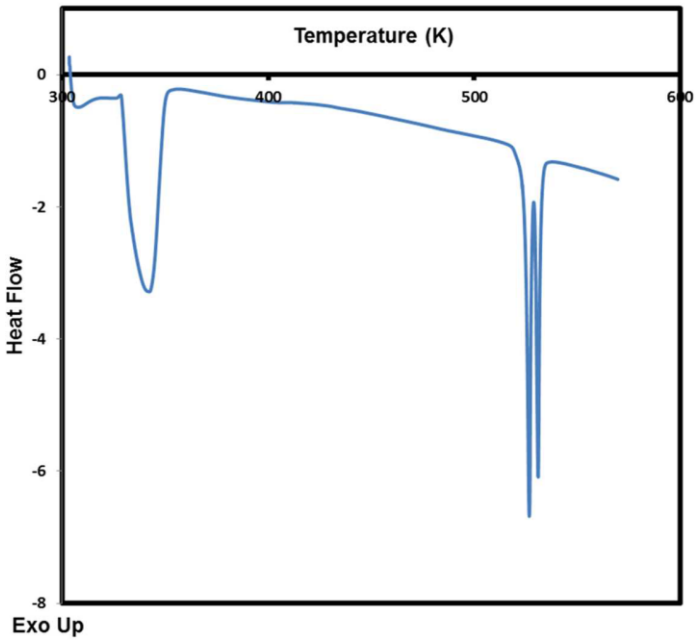

Figure S5 DSC curve of structure **3**.

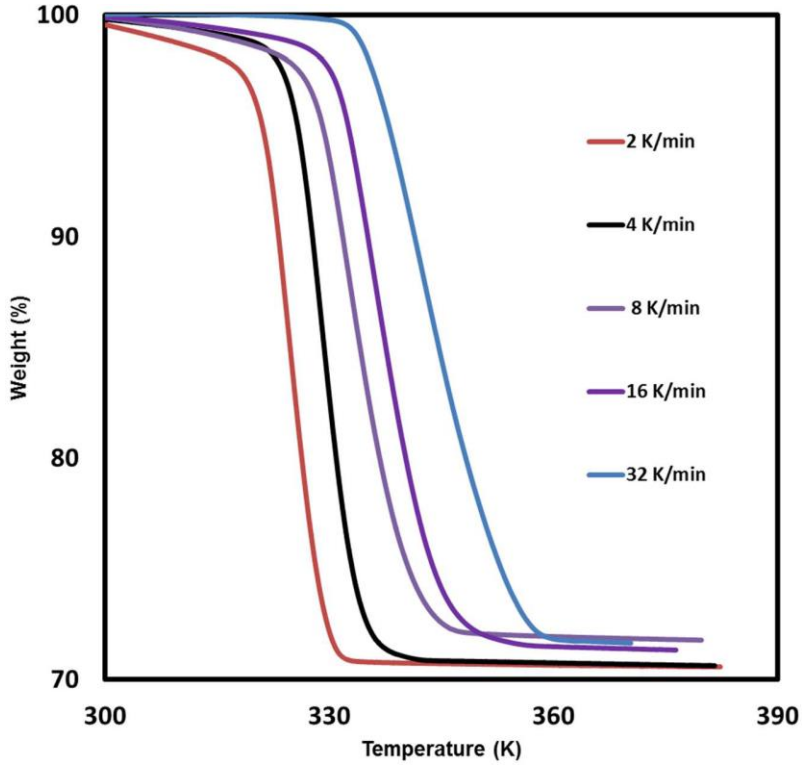

Figure S6 Non-isothermal TG curves of structure **3**.

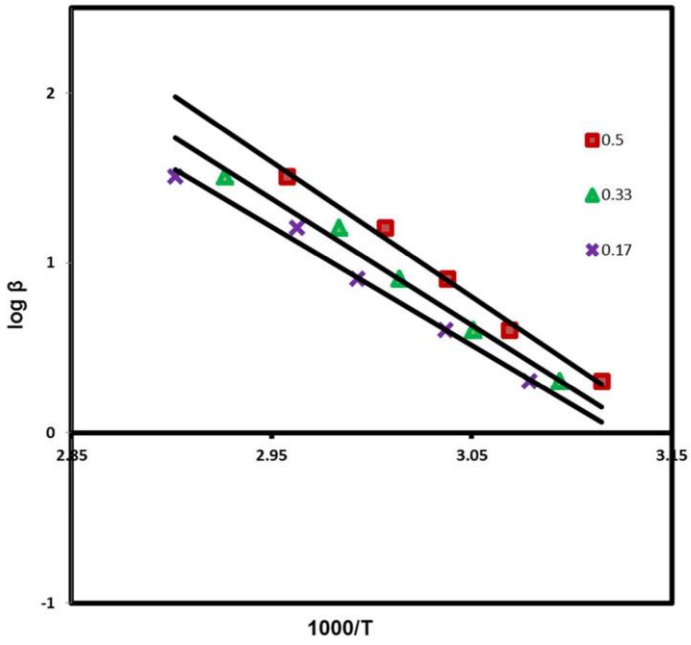

Figure S7 Plot of log β *vs.* the reciprocal of the temperature for structure **3**.

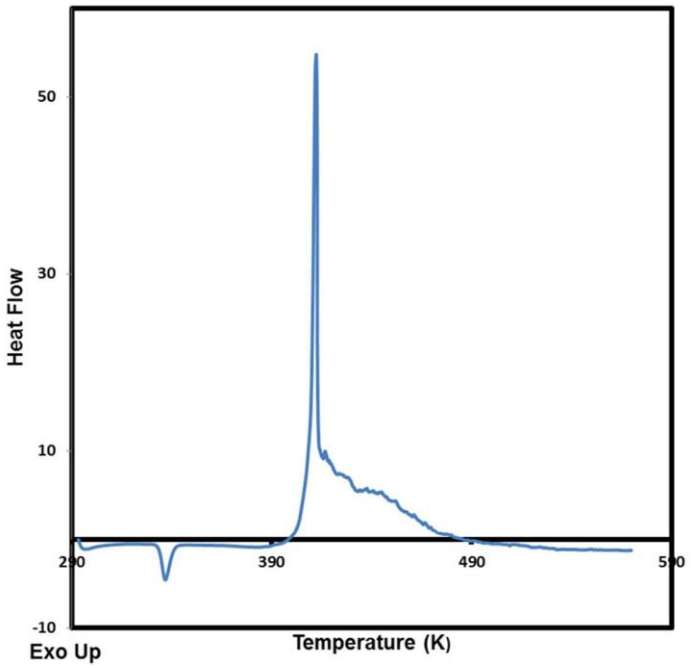

Figure S8 DSC curve of structure **4**.

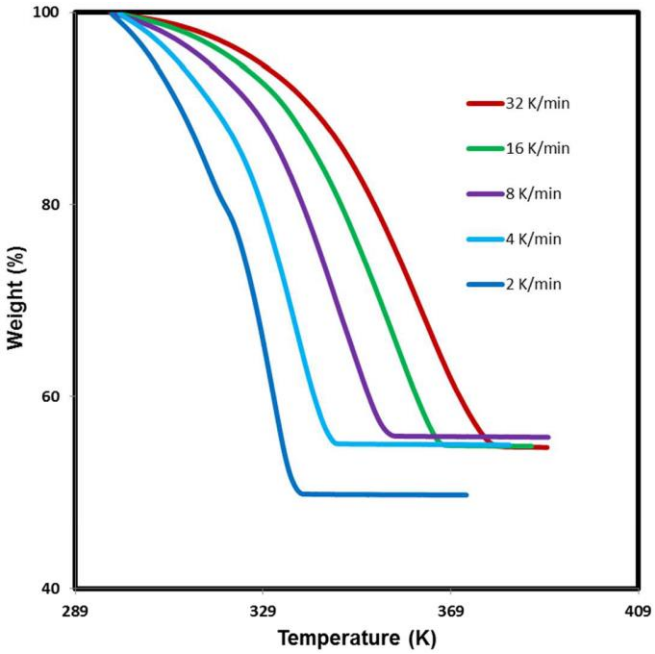

Figure S9 Non-isothermal TG curves of structure **4**.

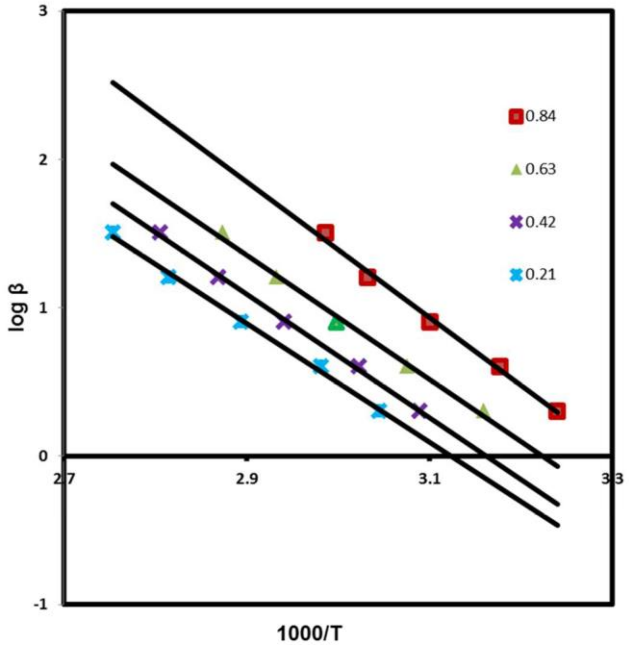

Figure S10 Plot of log β *vs.* the reciprocal of the temperature for structure **4**.

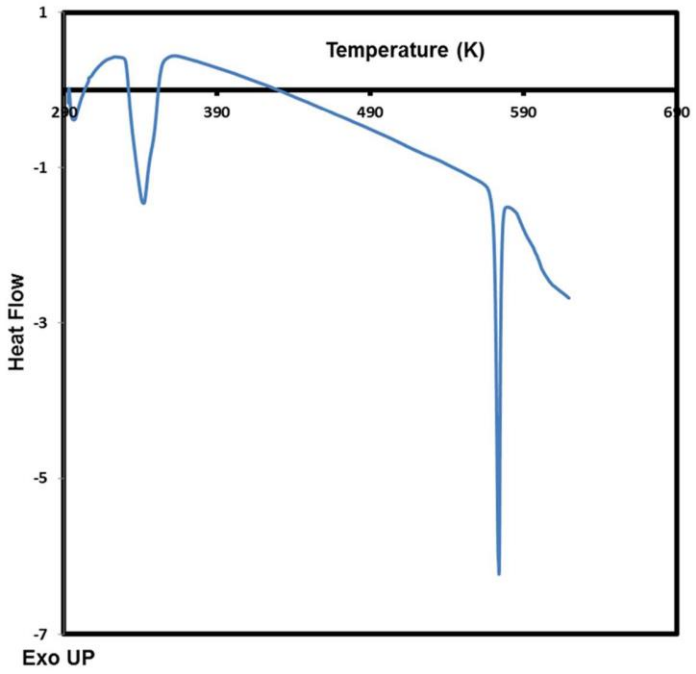

Figure S11 DSC curve of structure **5**.

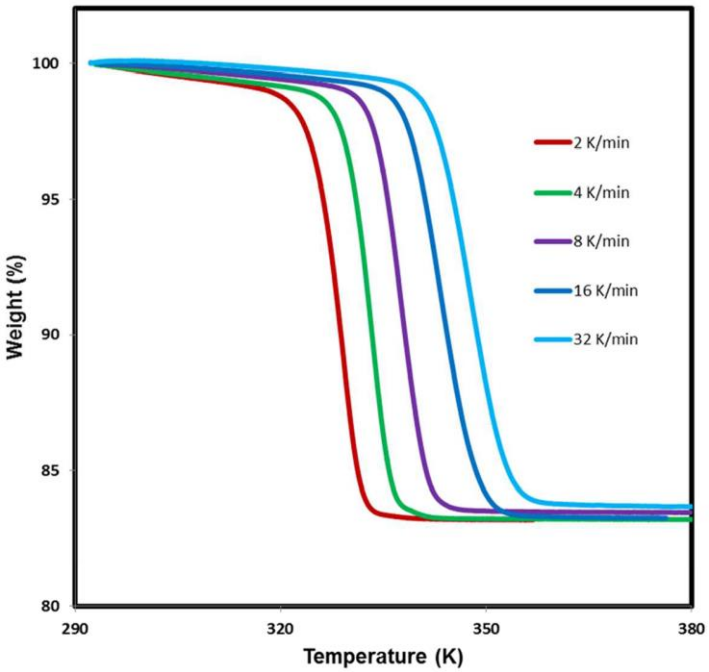

Figure S12 Non-isothermal TG curves of structure **5**.

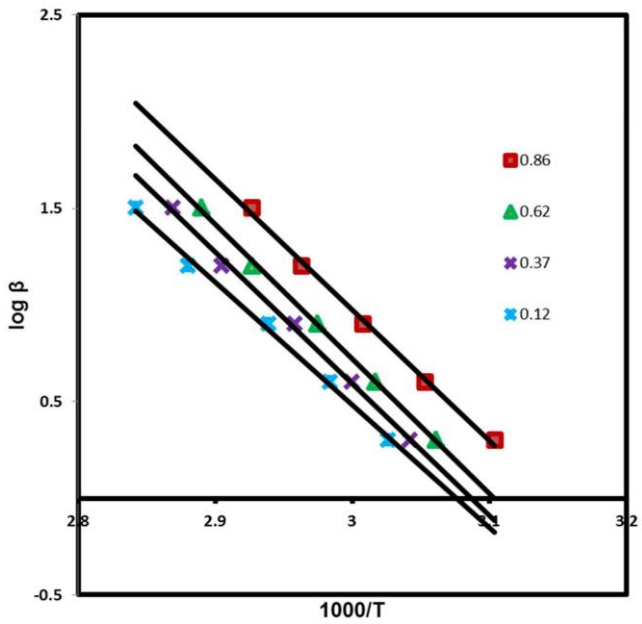

Figure S13 Plot of log β *vs.* the reciprocal of the temperature for structure **5**.

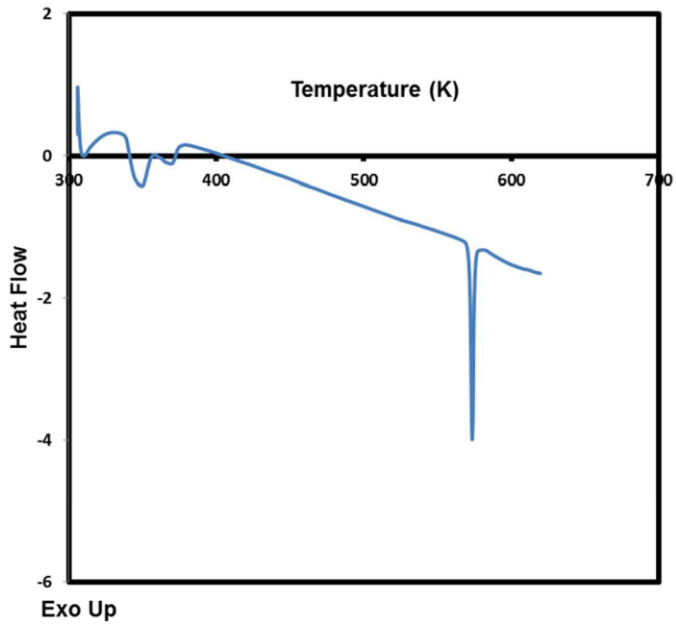

Figure S14 DSC curve of structure **7**.

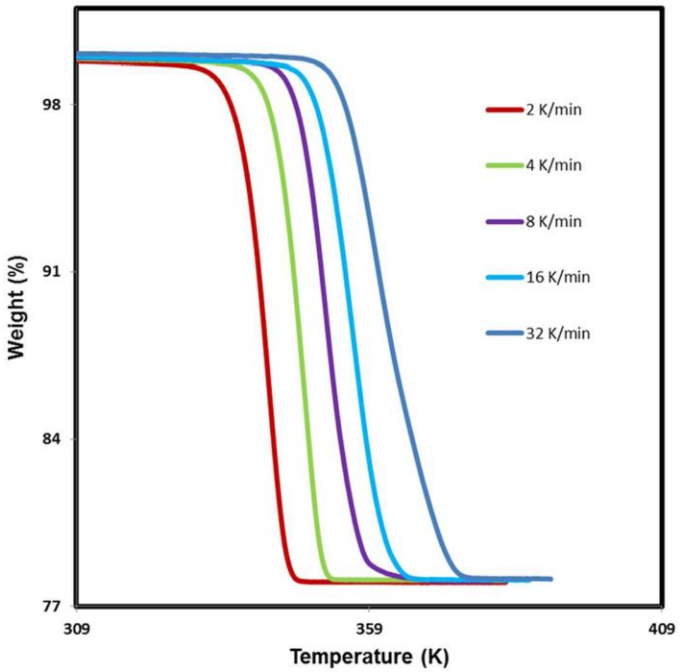

Figure S15 Non-isothermal TG curves of structure **7**.

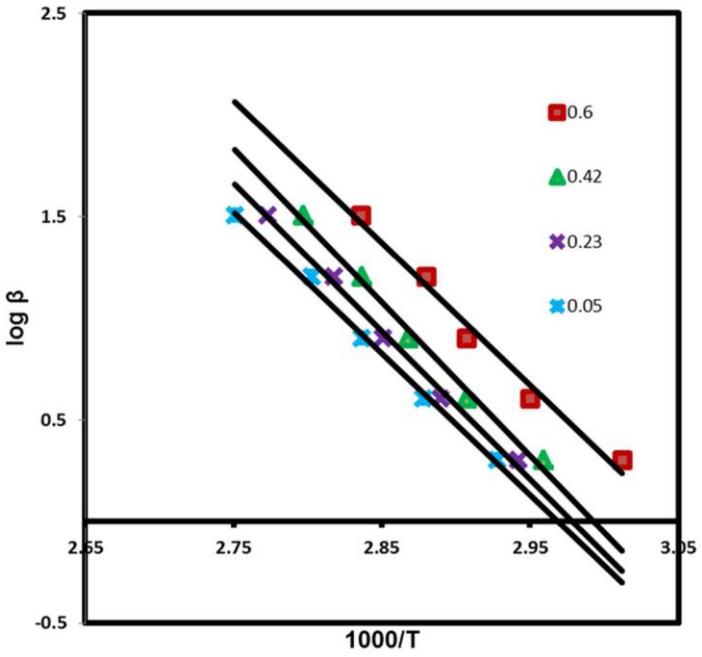

Figure S16 Plot of log *β vs.* the reciprocal of the temperature for structure **7**.

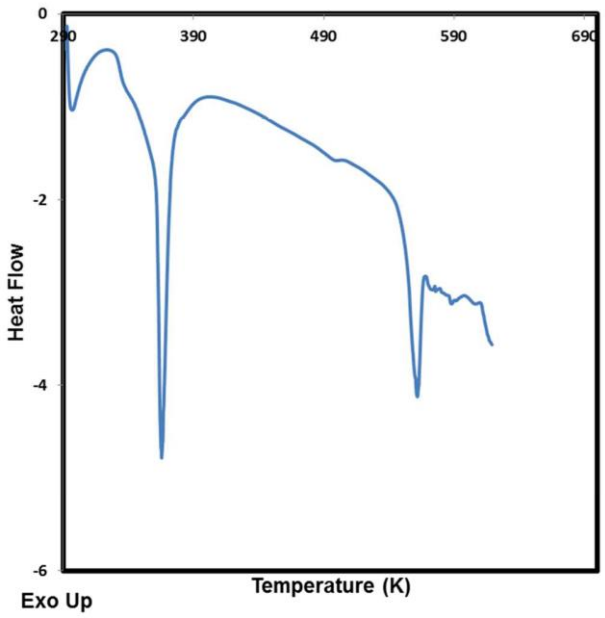

Figure S17 DSC curve of structure **8**.

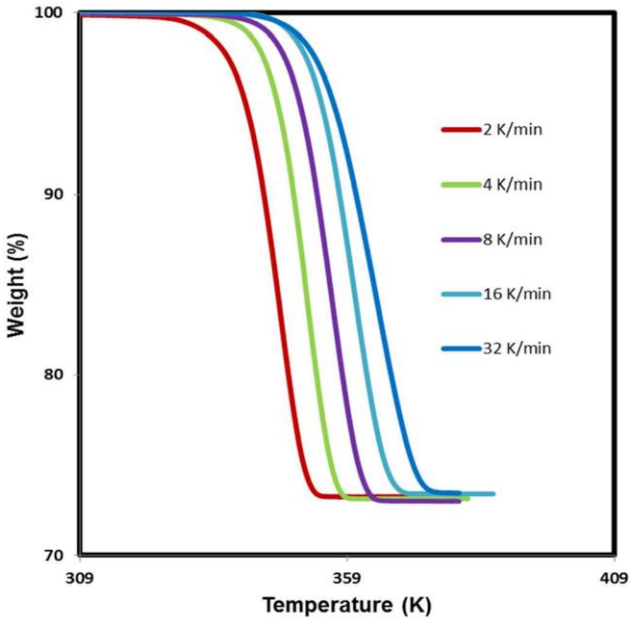

Figure S18 Non-isothermal TG curves of structure **8**.

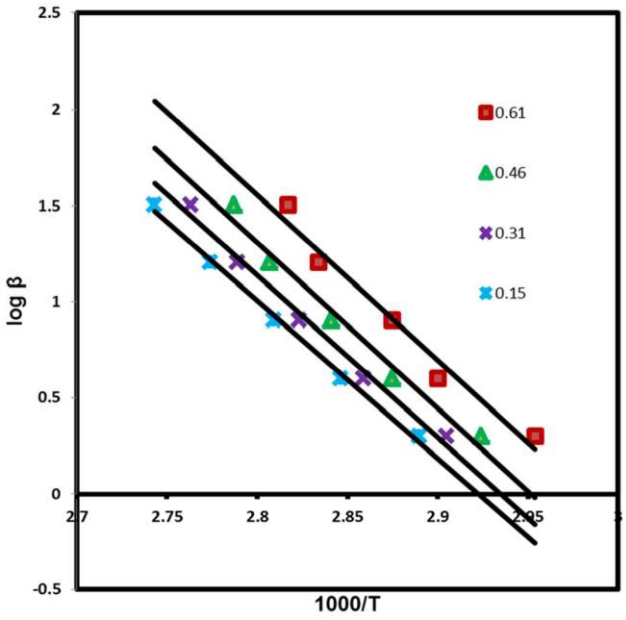

Figure S19 Plot of log β *vs.* the reciprocal of the temperature for structure **8**.

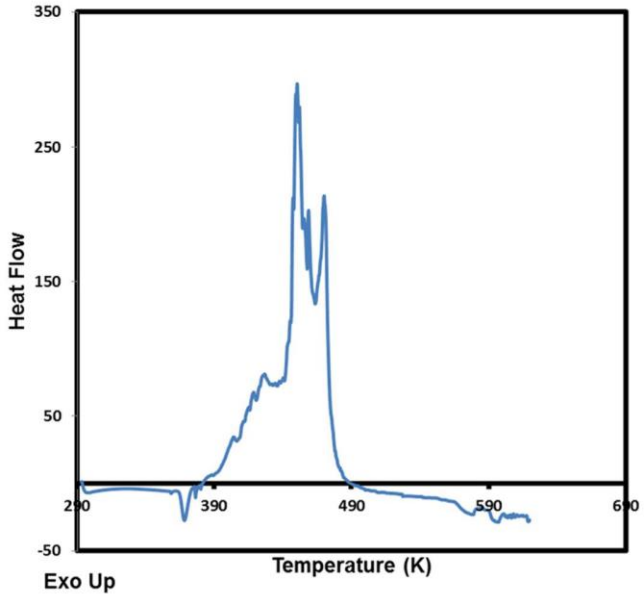

Figure S20 DSC curve of structure **9**.

Hirshfeld surface analysis

Table S1 Percentage contribution for the interactions of the first host molecule in structure **1**.

Atoms outside the host molecule .

Atoms inside the host molecule	C (%)	H (%)	Br (%)
C	0.4	9.8	4.4
H	9.0	29.6	14.7
Br	2.5	22.7	6.4

Table S2 Percentage contribution for the interactions of the second host molecule in structure **1**.

Atoms outside the host molecule.

Atoms inside the host molecule	C (%)	H (%)	Br (%)
C	0.0	11.0	1.9
H	9.2	30.3	14.1
Br	3.8	21.1	5.5

Table S3 Percentage contribution for the interactions of the host molecule in structure **3**.

Atoms with are outside the host molecule.

Atoms inside the host molecule.	C (%)	H (%)	Br (%)	$\mathscr{F}$(%)
C	0.1	13.0	1.0	0.6
H	5.2	32.3	10.9	5.2
Br	1.0	23.2	6.2	1.3

Table S4 Percentage contribution for the interaction of the first host molecule in structure **4**.

Atoms with are outside the host molecule.

Atoms inside the host molecule.	C (%)	H (%)	Br (%)	$\mathscr{F}$(%)
C	0.3	8.7	0.7	6.0
H	3.4	23.4	11.4	15.9
Br	1.2	22.8	2.4	3.6

Table S5 Percentage contribution for the interactions of the second host molecule in structure **4**.

Atoms with are outside the host molecule.

Atoms inside the host molecule.	C (%)	H (%)	Br (%)	$\mathscr{F}$(%)
C	0.6	10.5	2.7	1.1
H	9.8	28.5	10.5	3.8
Br	2.1	24.3	3.9	2.1

Table S6 Percentage contribution for the interactions of the host molecule in structure **5**.

Atoms with are outside the host molecule.

Atoms inside the host molecule.	C (%)	H (%)	$\mathscr{S}$ (%)	Cl (%)
C	0.1	9.6	1.0	3.0
H	4.6	27.7	9.2	10.1
$\mathscr{S}$	1.1	21.6	7.2	4.7

Table S7 Percentage contribution for the interactions of the host molecule in structure **6**.

Atoms outside the host molecule.

Atoms inside the host molecule.	C (%)	H (%)	$\mathscr{S}$(%)
C	0.1	11.9	1.8
H	4.5	31.9	15.2
$\mathscr{S}$	1.3	25.4	7.8

Table S8 Percentage contribution for the interactions of the host molecule in structure **7**.

Atoms with are outside the host molecule.

Atoms inside the host molecule.	C (%)	H (%)	$\mathscr{S}$ (%)	Cl (%)
C	0.1	6.6	1.1	6.4
H	4.5	20.0	9.5	16.7
$\mathscr{S}$	2.3	16.6	8.1	8.2

Table S9 Percentage contribution for the interactions of the host molecule in structure **8**.

Atoms with are outside the host molecule.

Atoms inside the host molecule.	C (%)	H (%)	$\mathscr{F}$(%)	Cl (%)
C	0.0	4.8	0.2	9.5
H	2.8	13.7	10.5	21.8
$\mathscr{F}$	0.3	19.8	10.1	5.5

Table S10 Percentage contribution for the interactions of the first host molecule in structure **9**.

Atoms outside the host molecule.

Atoms inside the host molecule.	C (%)	H (%)	$\mathscr{F}$(%)
C	0.5	9.3	5.0
H	8.3	29.4	12.2
$\mathscr{F}$	3.3	22.3	9.2

Table S11 Percentage contribution for the interactions of the second host molecule in structure **9**.

Atoms outside the host molecule.

Atoms inside the host molecule.	C (%)	H (%)	$\mathscr{F}$(%)
C	0.2	11.7	1.7
H	8.1	27.5	16.0
$\mathscr{F}$	1.1	18.1	15.4

CHAPTER IV

Guest Exchange in Halogenated Host – Guest Compounds: Structures and Kinetics.

(Amombo Noa, F. M.; Bourne, S. A.; Hong Su.; Nassimbeni, L. R. *Cryst. Growth Des*. 2016, 16 (3), 1636 – 1642).

4.1 Summary

Guest exchange in inclusion compounds is an important tool in crystal engineering as it has applications in storing volatile gases in compound, in sensing and catalysis based on inclusion. In this chapter, small halogenated solvents were used for guest storage and to prove that the inclusion compounds can accommodate solvents other than the original solvent in the structure.

Six inclusion compounds were synthesized via crystallisation of the host compound (tetrakis-4-(bromophenyl)ethylene/iodo-analogue) in a chosen guest solvent. Solvents used were 1,2-dichloroethane (DCE), benzene (BEN), iodomethane (MeI) and piperidine (PIP). A series of exchange experiments were performed on the elucidated inclusion compounds by exposing their single crystals to the vapours of the selected guests. There are two types of guest exchange obtained from this study: (i) a zeolitic exchange, where the incoming guest G_2 replaces G_1 while the host structure is retained with minor distortions; and (ii) the recrystallization exchange process where the incorporated guest molecule G_1 is desorbed from the inclusion compound, and the apohost then forms a new compound with G_2.

NMR spectroscopy was utilised to monitor the kinetic exchange which was performed in a desiccator at room temperature. The single crystals of the original inclusion were placed in a Petri dish separated from the liquid guest by a wire net.

Four further crystal structures were obtained from this exchange process, where the first exchange structure yielded an intermediate structure with the two solvents incorporated in the crystal structure and were at distinct and separate crystallographic sites. This corresponds to a zeolitic exchange.

The three other exchange structures were a simple replacement of the incorporate guest by the incoming guest. Here, the starting, intermediate and final structures had the same host: guest ratios and are isomorphous.

The rate laws were obtained for the exchange structures done with CH_3I vapour.

Thermal analysis (TG and DSC) were also carried out and all compounds showed the same pattern of decomposition which is the loss of the guest solvent followed by the melt of the host.

The original article and the supporting information are given below.

CRYSTAL GROWTH & DESIGN

Article

pubs.acs.org/crystal

Guest Exchange in Halogenated Host–Guest Compounds: Structures and Kinetics

Francoise M. Amombo Noa, Susan A. Bourne, Hong Su, and Luigi R. Nassimbeni*

Centre for Supramolecular Chemistry Research, Department of Chemistry, University of Cape Town, Rondebosch 7701, South Africa

Supporting Information

ABSTRACT: The host compounds tetrakis(4-bromophenyl) ethylene, **H1**, and its iodo-analogue (**H2**) form inclusion compounds with the guests 1,2-dichloroethane (DCE), methyl iodide (MeI), benzene (BEN), and piperidine (PIP). The structures of the host–guest compounds have been elucidated and a series of exchange experiments on these compounds were performed by exposing their single crystals to the vapors of different guests. The kinetics of the exchange was monitored by NMR spectroscopy, and the reactions were interrupted and the structures of the inclusion compounds containing both the incoming and outgoing guests were solved. In the case of **1.5H1·DCE** exchanged with MeI, the intermediate structure yields a unit cell which has quadrupled in volume and shows both DCE and MeI in distinct, different locations. In the case of BEN being exchanged with PIP, the guests occupy the same site, and the mechanism is one of isomorphous replacement.

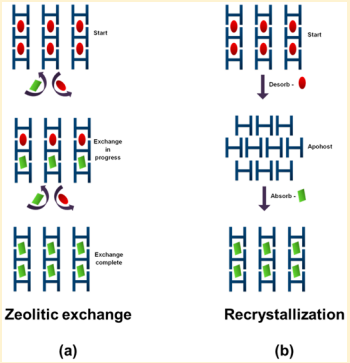

INTRODUCTION

The process of guest exchange in porous crystalline solids is of fundamental importance in heterogeneous catalysis, the selective absorption of gases and their separation, as well as controlling various properties of crystalline materials. This is especially true of Metal Organic Frameworks (MOFs), whose structure–property relations are currently receiving increasing attention.[1] This work, however, deals with guest exchange in host–guest systems, in which the host molecules crystallize as separate entities, and the geometry of the ensuing structure leaves spaces of varying topology which accommodate the guest molecules. The resulting structures are known as intercalates when host and guest molecules are in separate layers, tubulates when guests are in channels, aediculates when they form open pockets, and cryptates or true clathrates when the guest is trapped in a cage.[2] The progression of guest exchange in such systems is governed by the phenomenon of molecular recognition and depends on the nonbonded interactions which occur in the host–guest system under defined conditions of temperature and pressure. There are two possible mechanisms which govern guest exchange in inclusion compounds:

a. The host–guest system retains its structure throughout the exchange:

$$\mathrm{H}\cdot n\mathrm{G}_1(\mathrm{s},\beta) + m\mathrm{G}_2(\mathrm{l\,or\,g}) \rightarrow \mathrm{H}\cdot m\mathrm{G}_2(\mathrm{s},\beta) + n\mathrm{G}_1(\mathrm{l\,or\,g}) \quad (1)$$

The host behaves like a zeolite or a MOF and the incoming guest G_2 replaces G_1 while the host structure, the β-phase, is essentially retained with minor distortions. This is most readily achieved if there are strong similarities between the guests G_1 and G_2 with respect to molecular size and polarity.

b. The inclusion compound desorbs guest G_1 to yield the apohost in its α, nonporous phase, which in turn forms a new compound with G_2, and is in effect a recrystallization.

$$\mathrm{H}\cdot n\mathrm{G}_1(\mathrm{s},\beta) \rightarrow \mathrm{H}(\mathrm{s},\alpha) + n\mathrm{G}_1(\mathrm{l\,or\,g})$$

$$\mathrm{H}(\mathrm{s},\alpha) + m\mathrm{G}_2 \rightarrow \mathrm{H}\cdot m\mathrm{G}_2(\mathrm{s},\beta) \quad (2)$$

These mechanisms are shown schematically in Figure 1.

There are numerous studies of guest exchange in host–guest systems, both in solution and in the solid state. Solution NMR was employed to monitor the kinetics of guest exchange in an M_4L_6 host, and the mechanism was shown to require the deformation of the host structure.[3] NMR was also employed to follow guest exchange in lanthanide-mediated supramolecular cages.[4] A general discussion on the experimental methods employed in monitoring guest exchange in solids points out that the refinement of the crystal structures obtained after partial guest exchange poses special problems, and that the initial site occupancy factors should be approximately correct in order for the refinement to converge.[5] Differential scanning calorimetry (DSC) was employed to follow the exchange of cyclohexane, 1,4-dioxane and *N,N*-dimethylformamide in the inclusion compounds with a xanthenol host.[6] DSC was also used in the study of the inclusion compounds formed by the host 1,1,6,6-tetraphenylhexa-2,4-diyne-1,6-diol and the guest exchange between the guests tetrahydrofuran and thiophene.[7] Interestingly, guest exchange was used as an efficient method of β-cyclodextrin clathrate synthesis, by employing the water-free β-cyclodextrin solid phase and thus simplifying the preparative

Received: December 7, 2015
Revised: January 14, 2016
Published: January 26, 2016

ACS Publications © 2016 American Chemical Society

DOI: 10.1021/acs.cgd.5b01728
Cryst. Growth Des. 2016, 16, 1636–1642

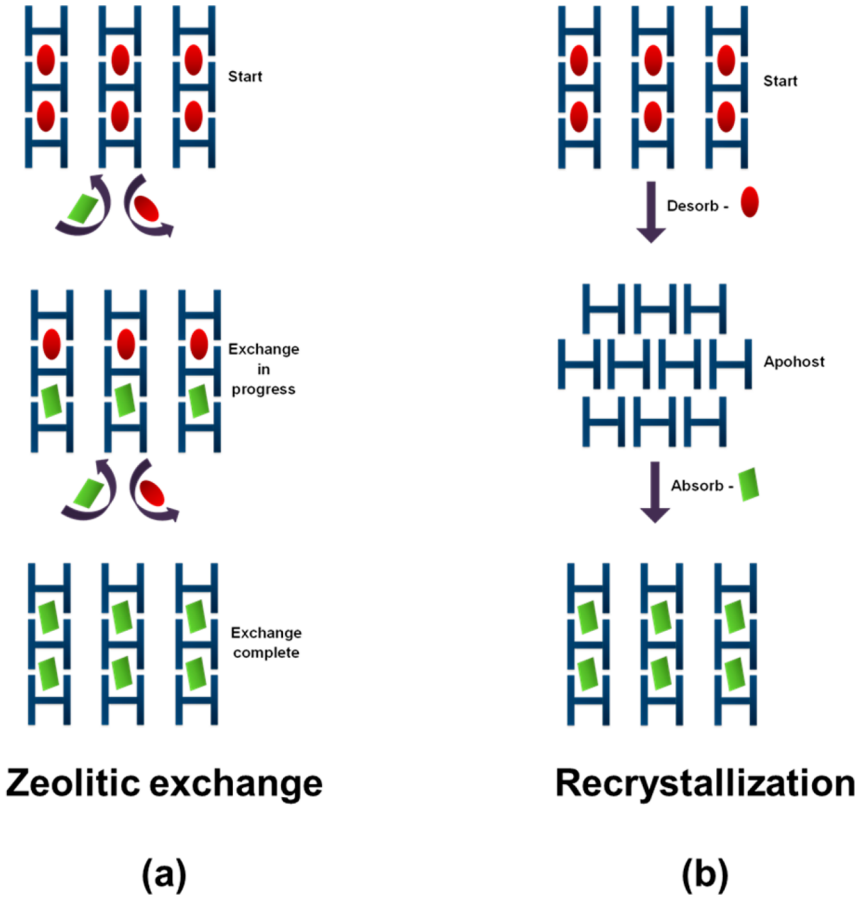

Figure 1. Schematic representation of guest exchange: (a) zeolitic exchange and (b) recrystallization.

procedure.[8] The porous metallocycle $[Ag_2L_2](BF_4)_2{\cdot}2CH_3CN$, where the ligand L is 1,4-bis (2-methylimidazol-1-ylmethyl) benzene, can carry out guest exchange by immersing the single crystal in different organic solvents such as acetone, chloroform, benzene, difluorobenzene, and toluene, while retaining the integrity of the starting single crystal (SC), thus exhibiting SC-SC transformations.[9] Recently, selective guest exchange has been demonstrated with a dinuclear wheel-and-axle metal-lorganic host, in which the original clathrate with tetrahydrofuran could be exchanged with *p*-xylene by vapor uptake, while other aromatic guests such as benzene, toluene, and *o*- and *m*-xylene only yielded partial exchanges, and *p*-cymene blocked the exchange.[10]

In this work, we present the structures (Scheme 1) and guest exchange results which occur in the inclusion compounds formed by the hosts tetrakis(4-bromophenyl) ethylene (**H1**) and its iodo-analogue (**H2**) and the guests 1,2-dichloroethane (DCE), benzene (BEN), piperidine (PIP), and methyl iodide (MeI).

Scheme 1. Host and Guest Compounds

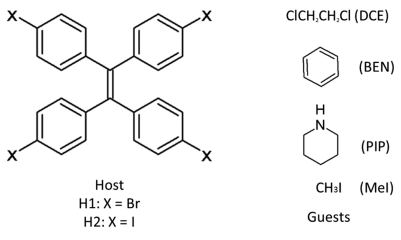

EXPERIMENTAL SECTION

All the guest compounds were purchased from Sigma-Aldrich and utilized without further purification. The host **H1** and **H2** were synthesized as described in the previous article by Nassimbeni et al.[11]

^{1}H NMR spectra were recorded on a Bruker ultrashield 400+ spectrometer. ^{1}H spectra were calibrated with respect to deuterated chloroform, $CDCl_3$, or deuterated dichloromethane, CD_2Cl_2.

Crystal Growth and Thermal Analysis. **H1** and **H2** complexes were obtained by dissolving each host compound in the chosen liquid guest. The solutions were allowed to evaporate at room temperature. Thermal analysis (TG and DSC) were conducted on the resulting crystals, and the host/guest ratio of each compound was analyzed by TG.

TG was performed on a Q500 (TA Instruments) thermal balance between 25 and 350 °C at a heating rate of 10 °C min^{-1}. A purging gas of dry nitrogen was employed at a flow rate of 60 mL min^{-1}.

DSC was performed on a Q200 series instrument with the same purge gas and heating rate as above in the temperature range of 20 to 350 °C. The crystalline samples were crushed and placed in crimped and vented pans.

Guest Exchange. The experiments were carried out in a desiccator at room temperature, as shown in Figure 2.

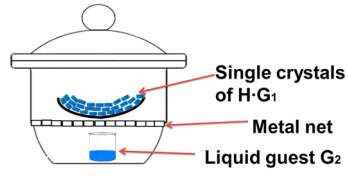

Figure 2. Desiccator in which the exchange experiment is performed.

DOI: 10.1021/acs.cgd.5b01728
Cryst. Growth Des. 2016, 16, 1636−1642

The incoming guest G_2 was placed at the bottom of the desiccator (eq 1). When the process follows a "Zeolitic" exchange, it may be represented as

$$H{\cdot}nG_1(s, \beta) \xrightarrow{mG_2(\text{lorg})} H{\cdot}xG_1{\cdot}(1-x)G_2(s, \beta) \rightarrow H{\cdot}mG_2(s, \beta) \quad (3)$$

where x is the guest mole fraction of G_1 (x = mol G_1/(molG_1 + molG_2)), x varies from 0 to 1 for a complete exchange, and its value depends on the time of exposure, the size of the crystals, and the temperature of the experiment.

In this work, all crystals described by $H{\cdot}nG_1$ and $H{\cdot}mG_2$, representing the starting and end products of the exchange reaction, were grown separately from the solutions of the host in the relevant liquid guest. The intermediate compound $H{\cdot}xG_1{\cdot}(1-x)G_2$ was grown by exposing single crystals of $H{\cdot}nG_1$ to vapors of G_2.

Single crystals of **H1·G$_1$** were placed in a Petri dish separated from the liquid guest G_2 by a wire net, which allowed G_2 vapor to attack the target crystals. The latter were selected under a microscope to be of approximately the same size. The kinetics of the exchange was monitored by sampling the exposed crystals at specific times and recording their NMR spectra. For **1.5H1·DCE/MeI** and the **H2·2DCE/MeI** exchanges, the relative quantities of the two guests were obtained by appropriate integration of the methyl hydrogen signals of the MeI versus the methylene hydrogen signals of the DCE. The crystal structures containing the mixed guests were obtained by subjecting a suitable crystal from the Petri dish at a given time of exposure to X-ray data collection.

In the cases of the exchanged reaction between BEN and PIP structures with both hosts, there was a color change of the complexes from colorless to light pink.

X-ray Crystallography. Single crystal X-ray diffraction data were collected on Nonius CCD[12] (structures **4**, **5**, **6**, **7**, and **9**) and Bruker DUO APEX[13] diffractometers (structures **1**, **2**, **3**, **8**, and **10**) using Mo Kα radiation (λ = 0.71073 Å) at a temperature of 173 K. The intensity data were collected by the phi scan and omega scan techniques, scaled, and reduced with DENZO-SMN[14] or SAINT-Plus.[15] The correction of the collected intensities for absorption was done using SADABS program.[16]

The structures were solved by direct methods using SHELX-97[17] and refined using full-matrix least-squares methods in SHELXL.[17] The graphical interface used the program X-SEED.[18] All non-hydrogen atoms were refined isotropically or anisotropically depending on the occurrence of disorder in the structures. All hydrogen atoms were placed geometrically and with a riding model for their isotropic temperature factors. Diagrams were generated using POVRAY in X-SEED[18] and Mercury (3.5).[19]

RESULTS AND DISCUSSION

Thermal Analysis. We carried out thermal gravimetry (TG) and differential scanning calorimetry (DSC) on the nonexchanged compounds.

A typical result is shown in Figure 3 for **1.5H1·DCE** which displays a single step mass loss of 9.0% (calc 9.2%) and two endotherms due to guest loss (T_{peak} = 94.8 °C) and host melt (T_{peak} = 254.2 °C). The results for all the compounds are given in Table 1. The thermal results for the other compounds have been deposited in the Supporting Information. One of the features of these compounds is that the endotherm due to guest loss was broad, and we therefore report the appropriate temperature range. The experimental guest mass losses are all within 2.0% of the calculated values, indicating the correct stoichiometries of the inclusion compounds.

Structures. An important aspect of all the structures elucidated is the secondary bonding and type of halogen···halogen interactions which occur.

Following our previous work on halogen bonding,[11] we have employed the van der Waals radii of Bondi[20] (radii in Å, H = 1.20, Cl = 1.75, Br = 1.85, I = 1.98) and we have recorded X···X distances that were less than the sum of the van der Waals radii +5%.

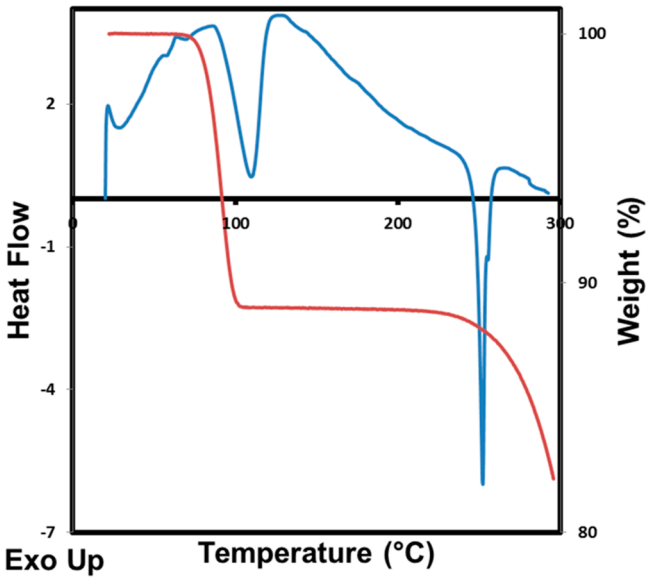

Figure 3. Thermal analysis of **1.5H1·DCE**, DSC (blue), and TG (red).

Table 1. Thermal Analysis Results

compound	1	3	5	6	8	10
code	1.5H·DCE	H1·BEN	H1·PIP	H2·2DCE	H2·BEN	H2·PIP
mass loss (obs) %	9.0	10.9	11.4	17.5	8.3	9.4
mass loss (calc) %	9.2	10.8	11.6	19.1	8.5	9.2
guest release endotherm range/°c	75–98	88–123	80–121	50–78	58–118	50–125

We have also indicated the type of halogen···halogen interactions which occur in the structures, classifying them as type I, II$_a$, or II$_b$, together with the angles θ_1 and θ_2, as explained in Figure 4. These have been deposited as Table S1 and S2 as Supporting Information. The crystal and refinement parameters of **H1** complexes are given in Table 2.

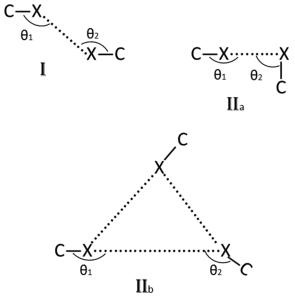

Figure 4. Halogen···halogen interactions.

In structure **1.5H·DCE**, the strongest X···X interaction is $Br_{14}\cdots Br_{2A}$, with d = 3.390 Å, which is 8.4% less than the sum of the van der Waals radii.

The structure **1.5H1·DCE**, crystallizes in $C2/c$ with Z = 8. There are eight host molecules in general positions and a further four located on diads at Wyckoff position **e**, which are disordered and carry site occupancies of 0.5. The guest 1,2-

DOI: 10.1021/acs.cgd.5b01728
Cryst. Growth Des. 2016, 16, 1636–1642

Table 2. Summary of Data Collection and Refinement Parameters of H1 Complexes and Its Exchanged Structures

compound	1	2	3	4	5
code	**1.5H1·DCE**	**6H1·3DCE·2MeI**	**H1·BEN**	**H1·0.66BEN·0.34PIP**	**H1·PIP**
structural formula	$C_{41}H_{28}Br_6Cl_2$	$C_{164}H_{114}Br_{24}Cl_6I_2$	$C_{32}H_{22}Br_4$	$C_{31.66}H_{16}N_{0.34}Br_4$	$C_{31}H_{27}Br_4N_1$
host: guest ratio	1:0.67	1:0.5:0.33	1:1	1:0.66:0.34	1:1
molecular mass (g mol^{-1})	1070.99	4468.93	726.14	728.53	733.18
data collection temp. (K)	173 (2)	173 (2)	173 (2)	173 (2)	173 (2)
crystal system	monoclinic	monoclinic	orthorhombic	orthorhombic	orthorhombic
space group	*C*2/*c*	*C*2/*c*	$P2_12_12_1$	$P2_12_12_1$	$P2_12_12_1$
a (Å)	38.5159 (3)	74.1035 (9)	9.8464 (2)	9.8189 (2)	9.7255 (19)
b (Å)	9.0807 (8)	18.1775 (2)	16.3660 (3)	16.3509 (3)	16.3721 (3)
c (Å)	24.4698 (2)	24.4586 (3)	17.6458 (4)	17.6309 (4)	18.1482 (4)
α (deg)	90	90	90	90	90
β (deg)	112.352 (2)	105.345 (2)	90	90	90
γ (deg)	90	90	90	90	90
volume (Å^3)	7975.4(11)	31771.6 (7)	2843.5 (10)	2830.7 (10)	2889.6 (10)
Z	8	8	4	4	4
D_c, calc density (g cm^{-3})	1.797	1.868	1.696	1.710	1.685
absorption coefficient (mm^{-1})	6.251	6.584	5.680	5.707	5.591
θ range	2.29−26.85	-	4.42−27.48	3.91−27.53	2.44−27.48
reflections collected	44839	-	6475	90191	70310
no data $I > 2\sigma(I)$	6005	-	5164	5895	5478
final *R* indices $[I > 2\sigma(I)]$	0.0513	-	0.0320	0.0317	0.0299
R indices (all data)	0.0806	-	0.0520	0.0382	0.0444
goodness-of-fit on F^2	1.022	-	1.023	1.045	1.014
CCDC no.	1438627	-	1438628	1438629	1438630

dichloroethane (DCE) is disordered, also with site occupancy factor of 0.5, and displays (Host)-Br···Cl-(Guest) contacts. The packing of **1.5H·DCE** is shown in Figure 5, viewed along [010].

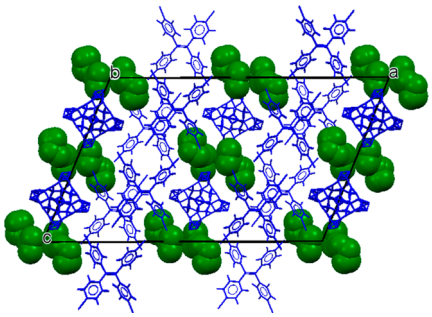

Figure 5. Crystal packing along [010] with the DCE (green) molecules in van der Waals radii for **1.5H·DCE**.

Crystals of **1.5H1·DCE** were subjected to the vapors of MeI as discussed in the Experimental Section. The kinetic result is given in Figure 6, which displays the % mole fraction of MeI (mol MeI/(mol MeI + mol DCE)) in the structure and represents the complete exchange.

$$\textbf{1.5H1·DCE}(s) \xrightarrow{\text{MeI}} \textbf{H1·2MeI}(s)$$

The structure of **H1·2MeI**, which crystallizes in the space group $P2_12_12_1$, has recently been published.[11]

The reaction follows the Prout-Tompkins equation

$$\alpha = \ln[\alpha/(1-\alpha)] = kt$$

where α is the extent of reaction, and k is the rate constant. At 25 °C we obtained $k = 1.03 \times 10^{-1}$ min^{-1} ($r = 0.994$ for an α range of (0.05 to 0.95).

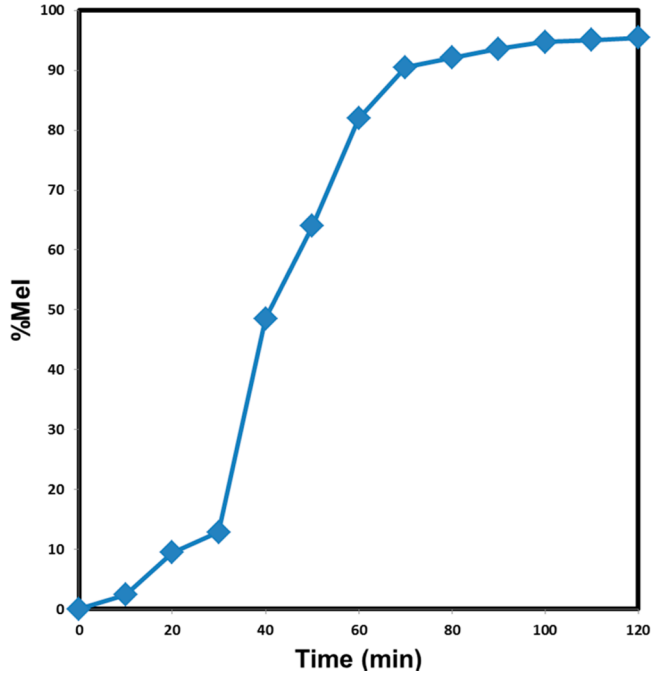

Figure 6. Exchange kinetic curves of **6H·3DCE·2MeI** at 25 °C.

We exposed single crystals of **1.5H1·DCE** to MeI vapor for 40 min and then removed a single crystal from the Petri dish in the desiccator. NMR analysis of these crystals yielded a guest mole fraction of 48.6% MeI. This was a difficult experiment, because within a few further minutes the single crystals turned opaque, their edges were indistinct, and the crystals became a wet powder. We repeated this procedure four times in order to choose the best single crystal for intensity data collection. We report the guest exchanged structure for **6H·3DCE·2MeI**. This

DOI: 10.1021/acs.cgd.5b01728
Cryst. Growth Des. 2016, 16, 1636−1642

structure did not refine satisfactorily and not all the reflection data could be indexed.

Further analysis of the reflection data allowed some of the reflections to be indexed with the unit cell parameters of the starting **1.5H1·DCE**. In fact we solved the structure using these reflections and we obtained the same results as before for this starting structure.

For structure **6H·3DCE·2MeI**, we obtained sufficient detail from the electron density maps to locate the positions of the incoming MeI guest molecules, but the final residual factor was a poor 18% and therefore only the unit cell parameters are reported. In this structure the unit cell lengths of **a** and **b** are double those of structure **1.5H1·DCE**, the starting compound. This exchanged structure is shown in projection along [010] in Figure 7, which displays the results of the exchange after 40

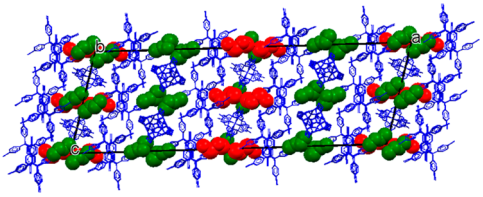

Figure 7. Packing diagram of **6H·3DCE·2MeI** along [010] with DCE (green) and MeI (red) molecules in van der Waals radii.

min. Half of the eight DCE molecules which were originally located about the centers of inversion at Wyckoff position **a** have been replaced by MeI. The other eight DCE molecules placed about the centers of inversion at Wyckoff position **c** remain unexchanged. The asymmetric unit of this exchanged compound comprises 6 host, 3 DCE, and 2 MeI molecules. The guest mole fraction of MeI is thus 40%, in fair agreement with that measured by NMR (48%).

A second view of the structures obtained from the guest exchange is shown in Figure 8a,b. Four unit cells of **1.5H1·**

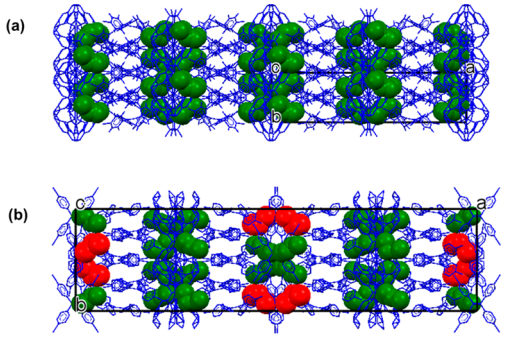

Figure 8. (a) Four unit cells of **1.5H1·DCE** viewed along [001] and (b) structure **6H·3DCE·2MeI** viewed along [001] with DCE (green) and MeI (red).

DCE, viewed along [001], are shown in Figure 8a, while the exchanged structure **6H·3DCE·2MeI** is displayed in Figure 8b. There are three notable short contacts in structure **6H·3DCE·2MeI**: $Br_{1F}\cdots Br_{4C}$ (d = 3.354 Å), $Br_{4F}\cdots Br_{4D}$ (d = 3.469 Å), and $Br_{44}\cdots Br_{3A}$ (d = 3.412 Å).

The second exchange experiment was carried out on the benzene inclusion compound of **H1** which was exposed to piperidine vapor at 25 °C using the method previously described. The three structures **H1·BEN**, **H1·0.66BEN·0.34PIP**, and **H1·PIP** are isostructural as reported in Table 2. Crystals of the exchanged structure were analyzed after 18 h and NMR results (CD_2Cl_2 solvent) yielded guest mole fraction of 66% benzene and 34% piperidine. We accepted these values for the site occupancy factors of BEN and PIP, respectively. A projection of the **H1·BEN** structure is shown in Figure 9, viewed along [100].

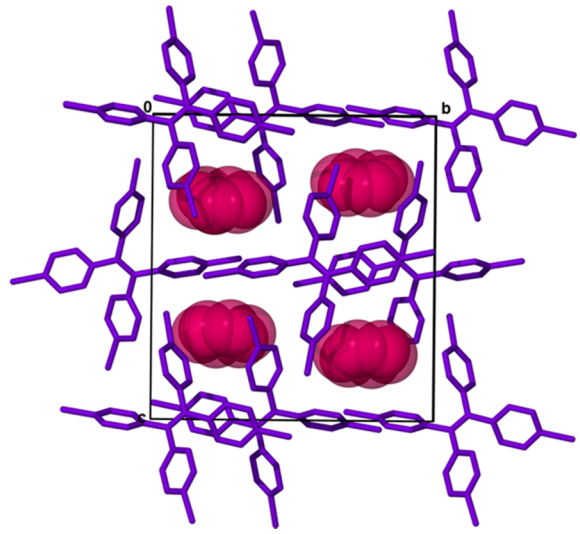

Figure 9. Packing diagram of **H1·BEN** along [100] with BEN molecules in van der Waals radii.

The mixed guest structure **H1·0.66BEN·0.34PIP**, displays the two guests sharing the same site (Figure 10). The guest atoms were refined with independent isotropic temperature factors and their H atoms were not modeled.

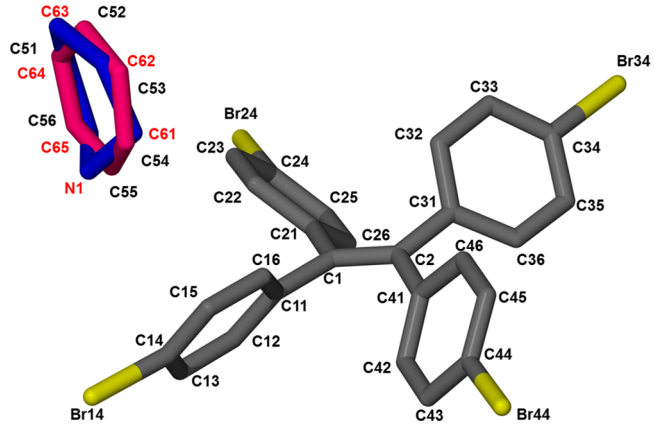

Figure 10. Asymmetric unit of **H1·0.66BEN·0.34PIP** showing BEN (pink) and PIP (blue) molecules.

The third exchange experiment was carried out with **H2**.

$$\mathbf{H2\cdot 2DCE} \xrightarrow[40\text{min}]{\text{MeI}} \mathbf{H2\cdot 1.22DCE\cdot 0.78MeI}$$

The kinetic curve is displayed in Figure 11.

We interpreted this exchange as occurring in two distinct steps, which we treated as separate reactions: Step 1 (t = 0 to 40 min) the kinetics followed the decreasing volume law $kt = 1 - (1 - \alpha)^{1/3}$, with $k = 1.99 \times 10^{-2}$ min^{-1} (r = 0.996). Step 2 (t = 50 to 120 min) the same law applies, with $k = 3.75 \times 10^{-2}$ min^{-1} (r = 0.999). It is noteworthy that after 120 min the

DOI: 10.1021/acs.cgd.5b01728
Cryst. Growth Des. 2016, 16, 1636−1642

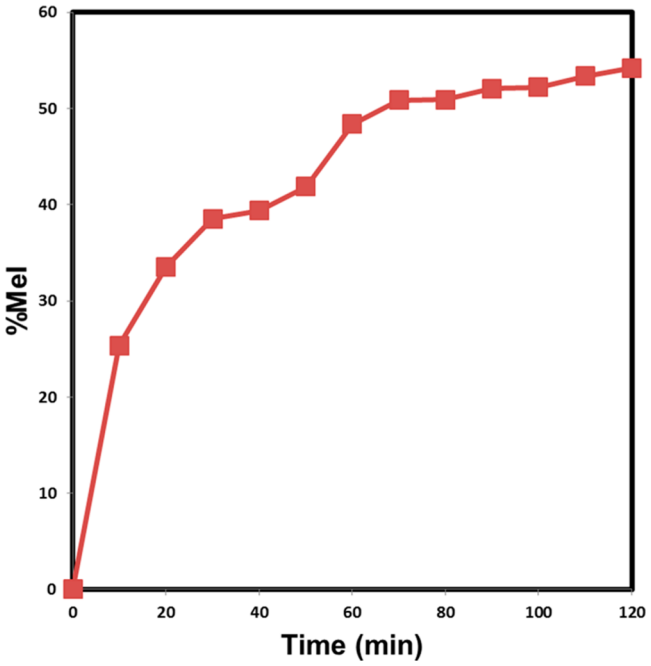

Figure 11. Exchange kinetic curve of **H2·1.22DCE·0.78MeI** at 25 °C.

kinetic curve had virtually flattened at %MeI ≈ 50, which may be interpreted as

$$\textbf{H2·2DCE} \xrightarrow[120\ \text{min}]{\text{MeI}} \textbf{H2·DCE·MeI}$$

The crystal data for these structures (Table 3) and for the **H2·2MeI** which has been published[11] shows them to be isostructural, all crystallizing in the space group $P2_12_12_1$.

For structure **H2·2DCE**, one of the DCE guest molecules is disordered. In the exchanged structure **H2·1.22MeI·0.78MeI**, the host:guest ratio remains at 1:2. One of the DCE molecules is unaffected, while the other shares its location with MeI. There are two significant nonbonded interactions in structure **H2·2DCE**: $I_{24}\cdots I_{34}$ (d = 3.797 Å) which is between the host molecules and $I_{34}\cdots Cl_6$ (d = 3.561 Å) between the host and the guest molecules.

We adopted the result of NMR analysis (DCE = 61%, MeI = 39%) and allocated site occupancies of 0.22 (DCE) and 0.78 (MeI) to the partially exchanged guest. The overall formula for the compound is thus **H2·1.22DCE·0.78MeI**. The only nonbonded interaction in this structure is between the host molecules with $I_{14}\cdots I_{44}$ at 3.795 Å.

The fourth exchange experiment in which the inclusion compound of **H2** with BEN was exchanged with PIP vapor over 24 h yielded similar results to the **H1** analogues. The three inclusion compounds of **H2** are isostructural to each other and to the corresponding **H1** structures, hold the host:guest ratio 1:1, and crystallize in $P2_12_12_1$. The BEN and PIP molecules share the same sites and the NMR analysis (BEN = 25%, PIP = 75%) was employed for the site occupancy factors. The packing is similar to that shown in Figure 10. The structures **H2·BEN** and **H2·0.25BEN·0.75PIP** also have very distinct interactions which occur between the host molecules with corresponding distances of 3.775 and 3.780 Å, respectively (see Table S2 in the Supporting Information).

CONCLUSION

Four guest exchange experiments were carried out on the inclusion compounds formed between the similar halogenated hosts **H1** and **H2**. Only the first exchange experiment, in which **1.5H1·DCE** was exposed to MeI vapor, yielded an intermediate structure which contains both DCE and MeI guests in distinct

Table 3. Summary of data collection and refinement parameters of H2 complexes and its exchanged structures

compound	6	7	8	9	10
code	**H2·2DCE**	**H2·1.22DCE·0.78MeI**	**H2·BEN**	**H2·0.25BEN·0.75PIP**	**H2·PIP**
structural formula	$C_{30}H_{24}Cl_4I_4$	$C_{29.22}H_{23.22}Cl_{2.44}I_{4.78}$	$C_{32}H_{22}I_4$	$C_{31.25}H_{25.75}I_4N_{0.75}$	$C_{31}H_{27}N_1I_4$
host:guest ratio	1:2	1:1.22:0.78	1:1	1:0.25:0.75	1:1
molecular mass (g mol^{-1})	1033.89	1067.42	914.10	919.38	921.14
data collection temp. (K)	173 (2)	173 (2)	173 (2)	173 (2)	173 (2)
crystal system	orthorhombic	orthorhombic	orthorhombic	orthorhombic	orthorhombic
space group	$P2_12_12_1$	$P2_12_12_1$	$P2_12_12_1$	$P2_12_12_1$	$P2_12_12_1$
a (Å)	9.6614 (19)	9.6677 (19)	9.9574 (5)	9.9613 (2)	9.7573 (6)
b (Å)	15.7829 (3)	15.7470 (3)	16.9715 (9)	17.0037 (3)	17.0805 (10)
c (Å)	22.3714 (5)	22.3413 (5)	18.0787 (9)	18.1250 (4)	18.5836 (11)
α (deg)	90	90	90	90	90
β (deg)	90	90	90	90	90
γ (deg)	90	90	90	90	90
volume (Å^3)	3411.3 (12)	3401.2 (12)	3055.2 (3)	3070.0 (11)	3097.1 (3)
Z	4	4	4	4	4
D_c, calc density (g cm^{-3})	2.013	2.085	1.987	1.989	1.975
absorption coefficient (mm^{-1})	3.986	4.581	4.098	4.080	4.044
θ range	3.87−27.50	2.59−27.48	1.65−28.32	2.65−27.47	1.62−28.33
reflections collected	82014	106228	50526	136650	84489
no data $I > 2\sigma(I)$	5323	6560	6534	6072	6997
final R indices [$I > 2\sigma(I)$]	0.0541	0.0529	0.0291	0.0314	0.0306
R indices (all data)	0.0945	0.0659	0.0401	0.0438	0.0366
goodness-of-fit on F^2	1.057	1.075	1.019	1.113	1.038
CCDC no.	1438631	1438632	1438633	1438634	1438635

DOI: 10.1021/acs.cgd.5b01728
Cryst. Growth Des. 2016, 16, 1636−1642

and separate crystallographic sites, showing that the exchange mechanism occurred via an enlarged cell which quadrupled in volume.

The second exchange experiment was performed on the benzene inclusion compound of **H1** which was exposed to piperidine vapor. In this experiment, the starting material **H1·BEN**, the intermediate product **H1·2/3BEN·1/3PIP**, and the final product **H1·PIP** are isomorphous and the guests occupy the same sites. Therefore, the exchange mechanism is a simple replacement of the existing guest by the incoming guest, while the host structure remains unaltered, as depicted in Figure 10.

The third and fourth exchange experiments which were carried out on the starting inclusion compounds of **H2** with DCE and BEN were exchanged with MeI and PIP, respectively, and displayed the same mechanism as the second exchange. The starting, intermediate, and final compounds held the same host:guest ratios and are isomorphous.

■ ASSOCIATED CONTENT

Supporting Information

The Supporting Information is available free of charge on the ACS Publications website at DOI: 10.1021/acs.cgd.5b01728.

X···X interactions tables, thermal analysis results (PDF)

Accession Codes

CCDC 1438627−1438635 contains the supplementary crystallographic data for this paper. These data can be obtained free of charge via www.ccdc.cam.ac.uk/data_request/cif, or by emailing data_request@ccdc.cam.ac.uk, or by contacting The Cambridge Crystallographic Data Centre, 12, Union Road, Cambridge CB2 1EZ, UK; fax: +44 1223 336033.

■ AUTHOR INFORMATION

Corresponding Author

*E-mail: luigi.nassimbeni@uct.ac.za. Tel: +27 21 650 5893. Fax: +27 21 650 2569.

Notes

The authors declare no competing financial interest.

■ ACKNOWLEDGMENTS

We thank the University of Cape Town and the National Research Foundation (South Africa) for funding.

■ ABBREVIATIONS

BEN, benzene; DCE, 1,2-dichloroethane; MeI, methyl iodide; PIP, piperidine

■ REFERENCES

(1) Li, J.-R.; Kuppler, J.; Zhon, H.-C. *Chem. Soc. Rev.* **2009**, *38*, 1477−1504.
(2) Weber, E.; Josel, H.-P. *J. Inclusion Phenom.* **1983**, *1*, 79−85.
(3) Davis, A. V.; Raymond, K. N. *J. Am. Chem. Soc.* **2005**, *127*, 7912−7919.
(4) El-Aroussi, B.; Guénée, L.; Pal, P.; Hamacek, J. *Inorg. Chem.* **2011**, *50*, 8588−8597.
(5) Nassimbeni, L. R.; Su, H. *CrystEngComm* **2013**, *15*, 7396−7401.
(6) Jacobs, A.; Faleni, N.; Nassimbeni, L. R.; Taljaard, J. H. *Cryst. Growth Des.* **2007**, *7* (6), 1003−1006.
(7) Caira, M. R.; Nassimbeni, L. R.; Toda, F.; Vujovic, D. *J. Chem. Soc. Perkin Trans. 2.* **2001**, 2119−2124.
(8) Gorbatchuk, V. V.; Gatiatulin, A. K.; Ziganshin, M. A.; Gubaidullin, A. T.; Yakimova, L. S. *J. Phys. Chem. B* **2013**, *117*, 14544−14556.
(9) Du Plessis, M.; Smith, V. J.; Barbour, L. J. *CrystEngComm* **2014**, *16*, 4126−4132.
(10) Bacchi, A.; Bourne, S. A.; Cantoni, G.; Cavallone, S. A. M.; Mazza, S.; Mehlana, G.; Pelagatti, P.; Righi, L. *Cryst. Growth Des.* **2015**, *15*, 1876−1888.
(11) Amombo Noa, F. M.; Bourne, S. A.; Nassimbeni, L. R. *Cryst. Growth Des.* **2015**, *15*, 3271−3279.
(12) *COLLECT*, data collection software; Nonius: Delft, The Nettherlands, 1998.
(13) *APEX 2*, v 1.0−27, Bruker AXS Inc.: Madison, WI, 2005.
(14) Otwinowski, Z.; Minor, W. In *Methods in Enzymology, Macromolecular Crystallography*; Carter, C. W., Jr; Sweet, R. M, Eds.; Academic Press, 1997; part A, pp *276*, 307.
(15) *SAINT-Plus*, v 7.12; Bruker AXS Inc., Madison, WI, 2004.
(16) Sheldrick, G. M. *SADABS: Program for area detector adsorption correction*; University of Göttingen, Germany, 1996; pp 33−38.
(17) Sheldrick, G. M. *SHELX-97: Program for Crystal Structure Solution and Refinement*; University of Göttingen, Germany, 1997; p 1456.
(18) Barbour, L. J. X-Seed − A software Tool for Supramolecular Crystallography. *J. Supramol. Chem.* **2001**, *1*, 189−191.
(19) Macrae, C. F.; Bruno, I. J.; Chisholm, J. A.; Edgington, P. R.; McCabe, P.; Pidcock, E.; Rodriguez-Monge, L.; Taylor, R.; Van de Streek, J.; Wood, P. A. Mercury CSD 3.5.1-New Features for the Visualization and Investigation of Crystal Structures. *J. Appl. Crystallogr.* **2008**, *41*, 466−470.
(20) Bondi, A. *J. Phys. Chem.* **1964**, *68*, 441−451.

DOI: 10.1021/acs.cgd.5b01728
Cryst. Growth Des. 2016, 16, 1636−1642

SUPPORTING INFORMATION

Guest Exchange in Halogenated Host-Guest Compounds: Structures and Kinetics.

*Francoise M. Amombo Noa, Susan A. Bourne, Hong Su and Luigi R. Nassimbeni**

Centre for Supramolecular Chemistry Research, Department of Chemistry, University of Cape Town, Rondebosch 7701, South Africa. Email: luigi.nassimbeni@uct.ac.za.

Table S1. X···X interactions in **H1** compounds.

Compound	X···X	*d* [Å]	θ_1/θ_2 [°]	*d*-Σvdw [Å]	%	Type
1	$Br_{14}\cdots Br_{2A}$	3.390 (3)	157/122	-0.31	-8.4	I
	$Br_{14}\cdots Br_{4A}$	3.766 (3)	174/94	0.066	+1.8	II_a
	$Br_{34}\cdots Br_{1A}$	3.621 (3)	140/76	-0.079	-2.1	II_a
	$Br_{3A}\cdots Cl_4$	3.566 (3)	151/86	-0.034	-0.9	II_a
	$Br_{4A}\cdots Cl_3$	3.766 (3)	74/73	+0.166	+4.6	I
2	$Br_{1E}\cdots Br_{4B}$	3.570 (4)	140/77	-0.13	-3.5	II_a
	$Br_{1F}\cdots Br_{4C}$	3.354 (4)	155/125	-0.346	-9.4	I
	$Br_{2F}\cdots Br_{4D}$	3.699 (5)	172/110	-0.001	-0.03	II_a
	$Br_{3F}\cdots Br_{4C}$	3.815 (5)	175/117	+0.115	+3.1	II_a
	$Br_{4E}\cdots Br_{24}$	3.653 (4)	136/73	-0.047	-1.3	II_a
	$Br_{4F}\cdots Br_{4D}$	3.469 (4)	155/122	-0.231	-6.2	I
	$Br_{1A}\cdots Br_{2C}$	3.740 (5)	129/76	+0.04	+1.1	II_a
	$Br_{2B}\cdots Br_{4A}$	3.720 (5)	175/92	+0.02	+0.5	II_a
	$Br_{4B}\cdots Br_{1E}$	3.570 (4)	140/77	-0.13	-3.5	II_a
	$Br_{44}\cdots Br_{3A}$	3.412 (4)	161/124	-0.288	-7.8	II_a
	$Br_{3E}\cdots Cl_6$	3.734 (5)	147/141	+0.134	+3.7	I
	$Br_{3F}\cdots Cl_3$	3.753 (5)	142/111	+0.153	+4.3	I
	$Br_{1B}\cdots I_1$	3.771 (5)	128/82	-0.059	-1.5	II_a
	$Br_{4A}\cdots I_1$	3.897 (5)	78/77	+0.067	+1.7	I
3	$Br_{14}\cdots Br_{44}$	3.896 (8)	129/105	+0.196	+5.3	I
	$Br_{24}\cdots Br_{44}$	3.620 (7)	145/146	-0.08	-2.2	I
4	$Br_{14}\cdots Br_{44}$	3.883 (8)	129/105	+0.183	+4.9	I
	$Br_{24}\cdots Br_{44}$	3.617 (7)	144/146	-0.083	-2.2	I
5	$Br_{24}\cdots Br_{44}$	3.722 (8)	142/142	+0.022	+0.6	I
	$Br_{14}\cdots Br_{44}$	3.817 (8)	138/108	+0.117	+3.2	I

Table S2. X···X interactions in **H2** compounds.

Compound	X···X	*d* [Å]	θ_1/θ_2 [°]	*d*-Σvdw [Å]	%	Type
6	$I_{14}\cdots I_{24}$	4.153 (8)	138/118	+0.193	+4.9	I
	$I_{24}\cdots I_{34}$	3.797 (7)	165/133	-0.163	-4.1	II_a
	$I_{24}\cdots Cl_4$	3.699 (7)	117/62	-0.031	-0.8	II_a
	$I_{34}\cdots Cl_1$	3.895 (8)	162/86	+0.165	+4.4	II_a
	$I_{34}\cdots Cl_6$	3.561 (7)	160/112	-0.169	-4.5	II_a
	$I_{44}\cdots Cl_6$	3.901 (8)	80/70	+0.171	+4.6	I
	$Cl_1\cdots Cl_5$	3.610 (7)	135/79	+0.11	+3.1	II_a
7	$I_{14}\cdots I_{24}$	4.150 (8)	129/118	+0.19	+4.8	I
	$I_{14}\cdots I_{44}$	3.795 (7)	164/133	-0.165	-4.2	II_a
	$I_{34}\cdots Cl_3$	3.795 (7)	126/62	+0.065	+1.7	II_a
	$I_{44}\cdots Cl_2$	3.852 (8)	161/86	+0.122	+3.3	II_a
	$Cl_1\cdots Cl_4$	3.467 (7)	164/119	-0.033	-0.9	II_a
8	$I_{14}\cdots I_{34}$	3.775 (2)	150/148	-0.185	-4.7	I
	$I_{14}\cdots I_{24}$	4.095 (2)	158/60	+0.135	+3.4	II_a
9	$I_{14}\cdots I_{34}$	3.780 (8)	150/148	-0.18	-4.5	I
	$I_{34}\cdots I_{44}$	4.101 (9)	158/60	+0.141	+3.6	II_a
10	$I_{14}\cdots I_{44}$	4.066 (3)	139/110	+0.106	+2.7	I
	$I_{24}\cdots I_{44}$	3.942 (2)	146/146	-0.018	-0.5	I
	$I_{34}\cdots I_{44}$	4.067 (3)	154/64	+0.107	+2.7	II_a

Thermal analysis

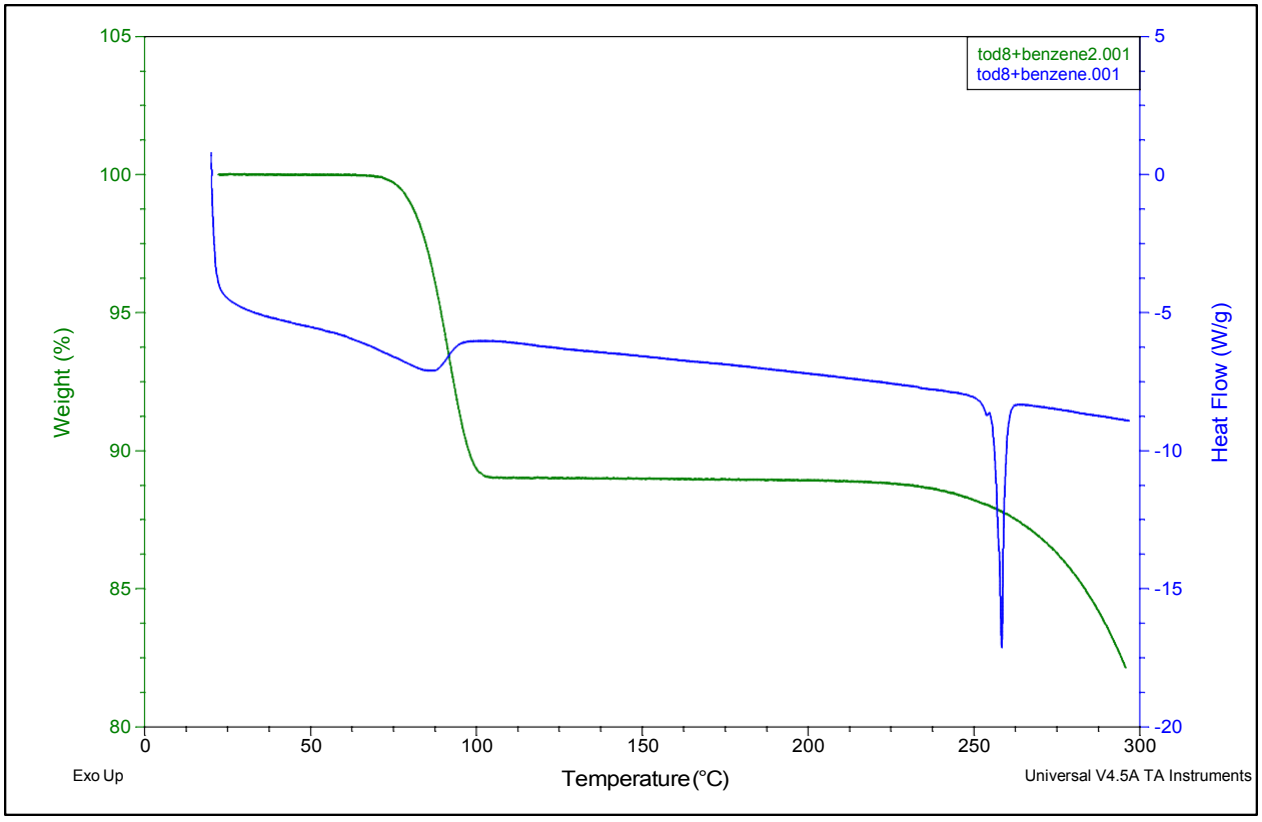

Figure S1 DSC and TG plots of **3**.

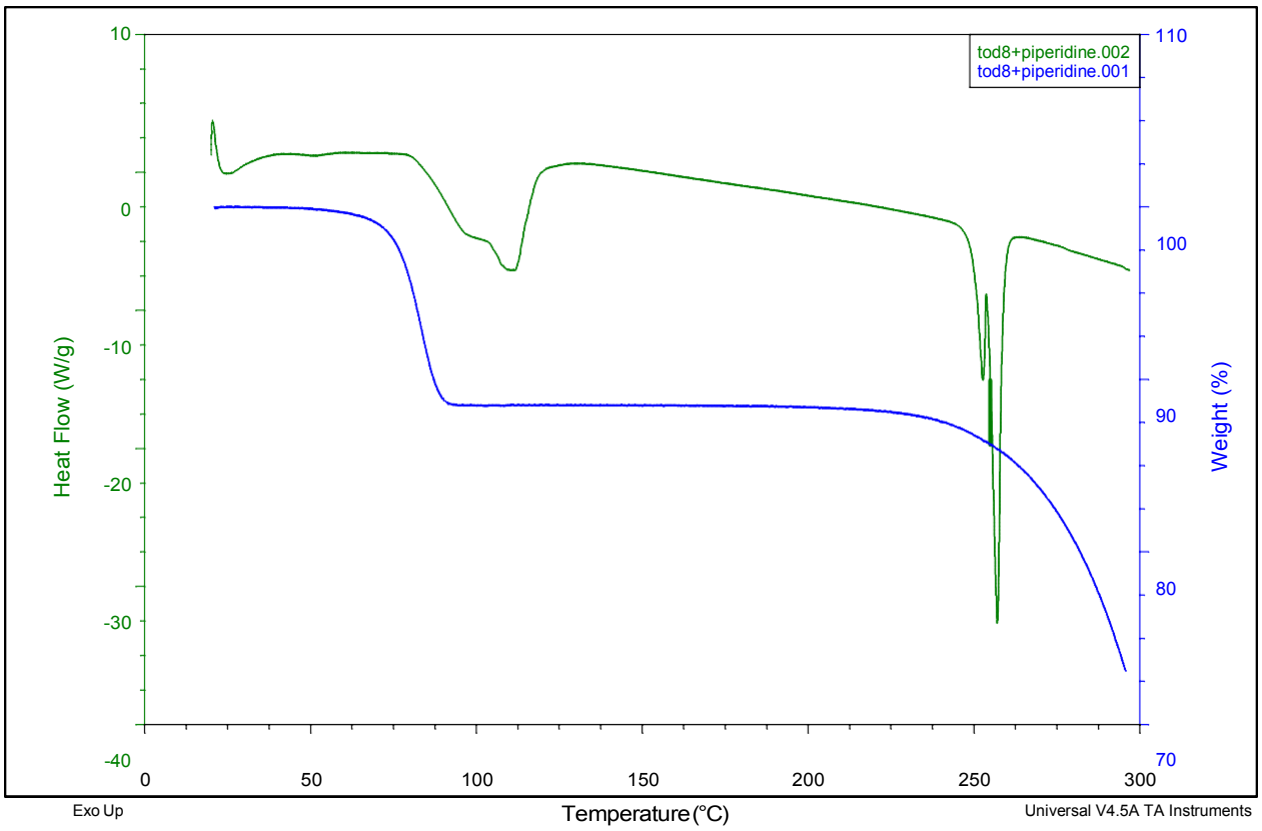

Figure S2 DSC and TG plots of **5**.

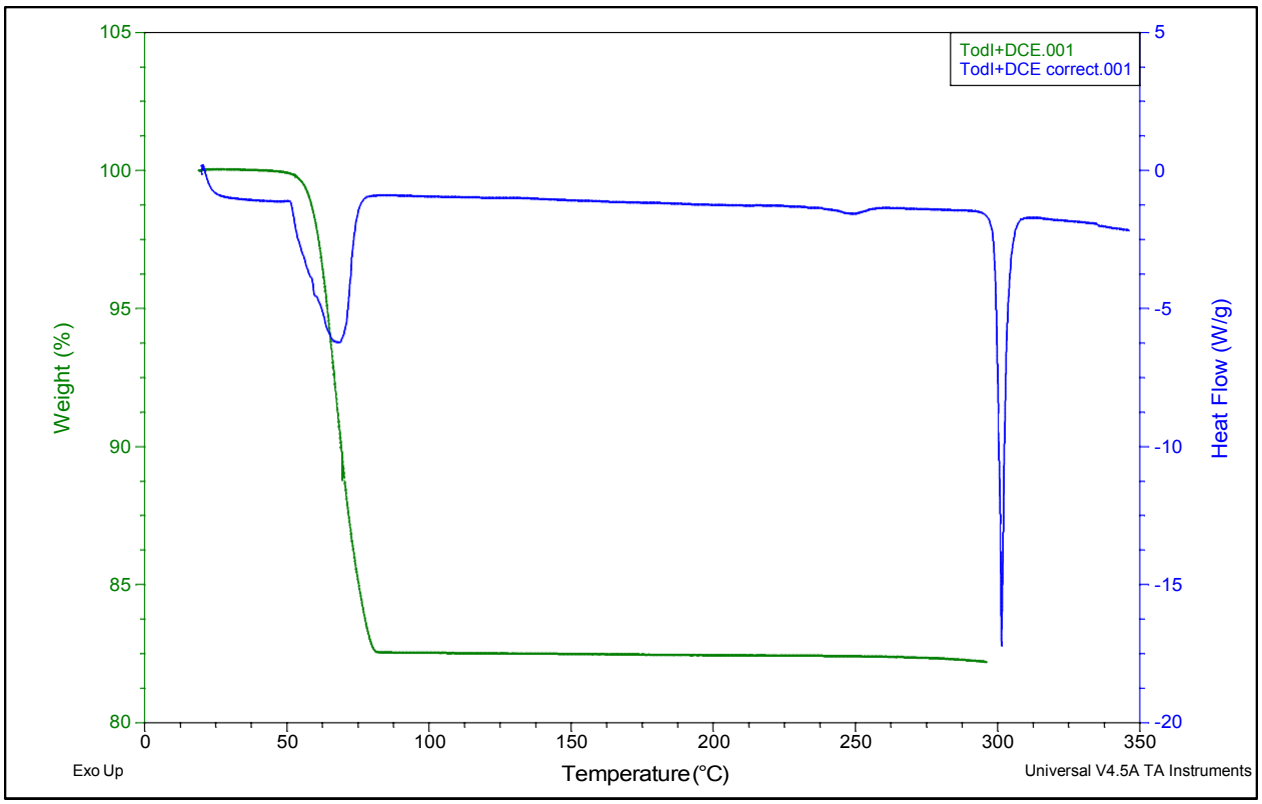

Figure S3 DSC and TG plots of **6**.

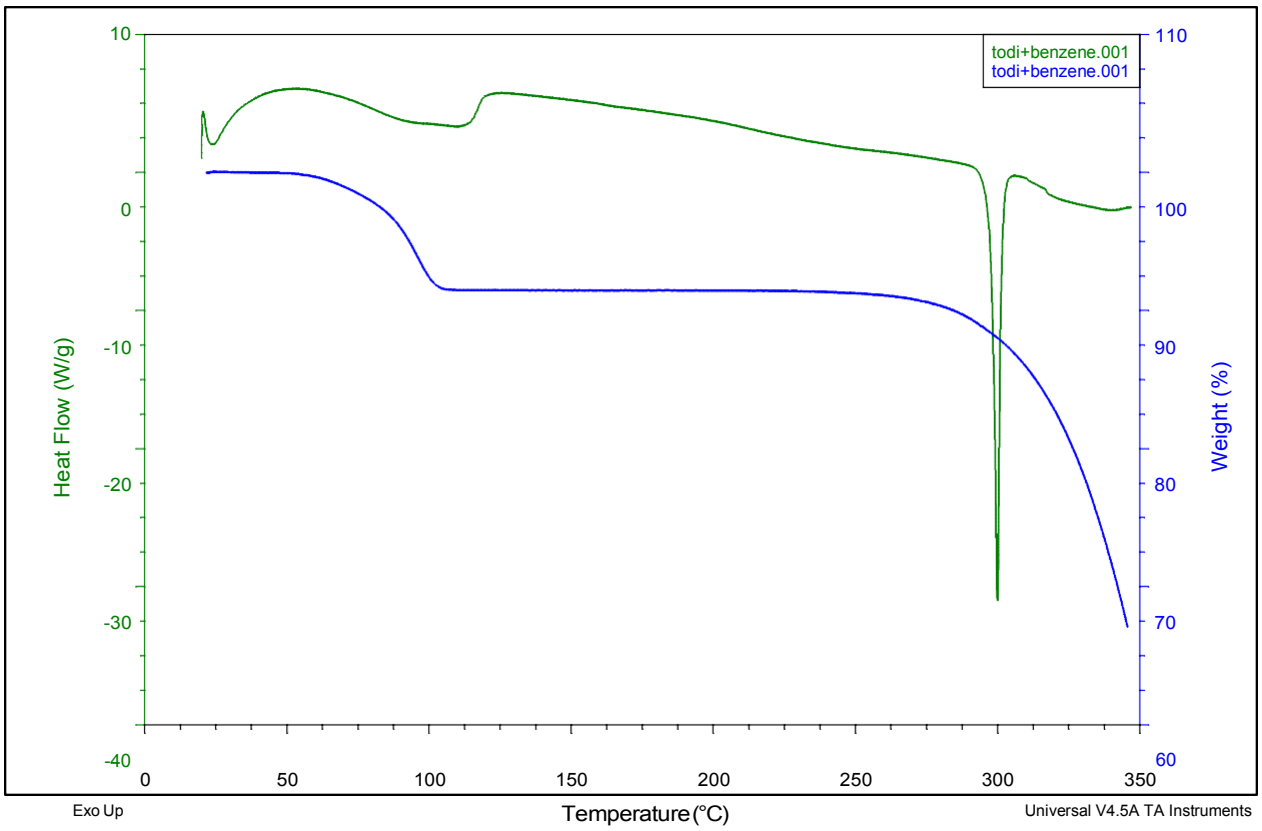

Figure S4 DSC and TG plots of **8**.

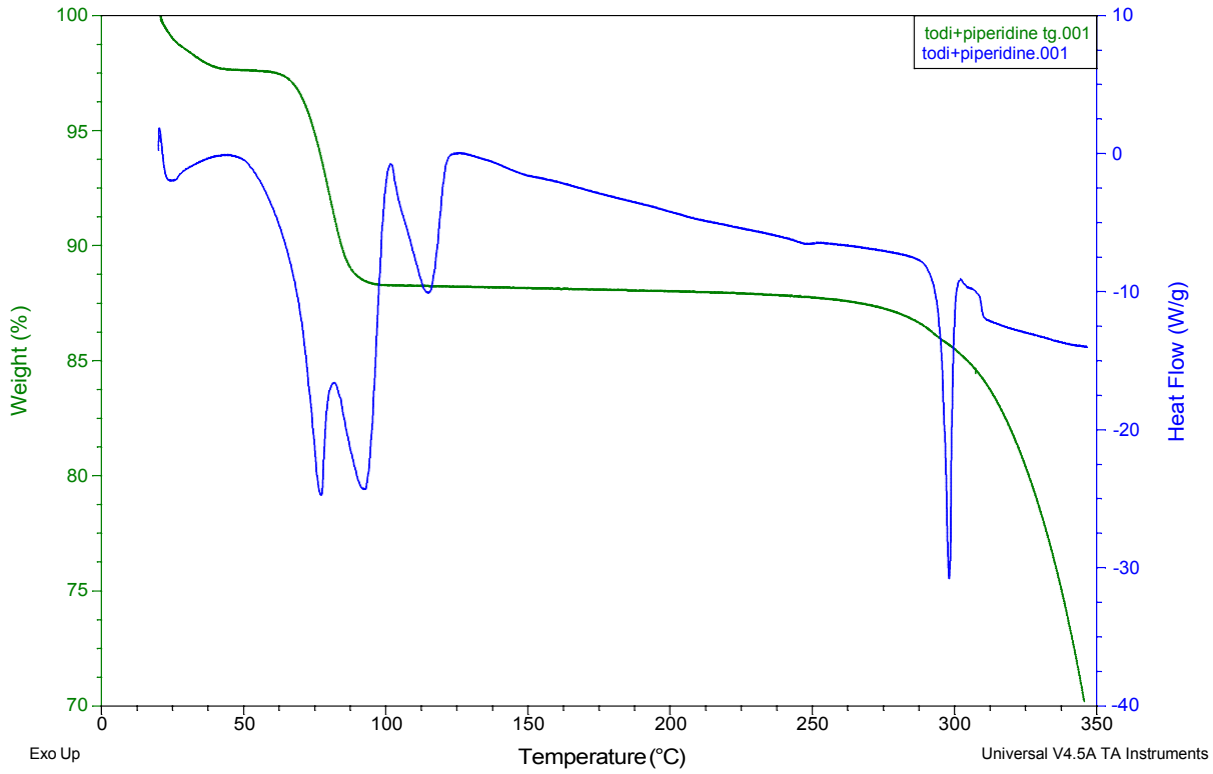

Figure S5 DSC and TG plots of **10**.

CHAPTER V

Halogen – Bonding, Isomorphism, Polymorphism and Kinetics of Enclathration in Host – Guest Compounds

(Amombo Noa, F. M.; Bourne, S. A.; Hong Su.; Nassimbeni, L. R. *Cryst. Growth Des*. 2017. DOI:10.1021/acs.cgd.7b00521).

5.1 Summary

Eight inclusion compounds of the host tetrakis-4-(bromophenyl)ethylene and its iodoanalogue were synthesised and successfully characterised by X-ray diffraction, thermal analysis and kinetics of enclathration by suspension. Only the obtained inclusions between tetrakis-4-(bromophenyl)ethylene and selected guest solvents (3-brompyridine (3BrPY) and 3-picoline (3PIC)) were subjected to the analysis of kinetics of enclathration. The velocity of enclathration for solid host – 3BrPY/3PIC vapour reactions and associated rate law at both 25 °C and 35 °C were established.

The iodo host formed two polymorphs with 3PIC; one with a 1: 1 ratio and the other with a 2: 2 ratio. Both polymorphs crystallised in the same vial, having different crystal size morphologies and colour. They were solved in different space groups, but belong to the same crystal system. The 1: 1 polymorph had a block-like shape and was a colourless crystal, but the 2: 2 polymorph on the other hand crystallised as little pink needles.

The two polymorphs have showed different packings and void topologies which correlate with their DSC profiles.

CRYSTAL GROWTH & DESIGN

Article

pubs.acs.org/crystal

Halogen-Bonding, Isomorphism, Polymorphism, and Kinetics of Enclathration in Host–Guest Compounds

Francoise M. Amombo Noa, Susan A. Bourne, Hong Su, and Luigi R. Nassimbeni*

Centre for Supramolecular Chemistry Research, Department of Chemistry, University of Cape Town, Rondebosch 7701, South Africa

Supporting Information

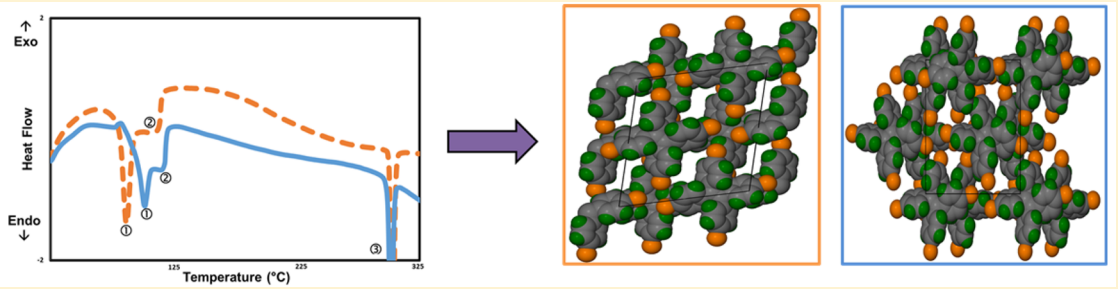

ABSTRACT: The inclusion compounds formed by the host tetrakis(4-bromphenyl) ethylene and its iodo-analogue have been characterized. Their structures have been elucidated and the halogen···halogen interactions recorded. The iodo-host forms two polymorphs with 3-picoline and their structures have different void topologies which correlate with the corresponding DSC profiles. The kinetics of enclathration by the bromo-host was carried out in aqueous suspension for the 3-picoline and the 3-brompyridine guests yield distinctly different results.

INTRODUCTION

There has been a considerable increase in publications dealing with "halogen bonding". Since the year 2000, there have been ~200 papers a year appearing in the literature, attesting to the importance of the topic. Desiraju reviewed its importance in his book on Crystal Engineering[1] and pointed out its effects on crystal plasticity[2] and on the packing patterns of dihalogenated phenols.[3] Halogen bonding has been compared to hydrogen bonding and its various applications highlighted.[4,5]

A definitive review, entitled The Halogen Bond, has appeared,[6] and it describes several aspects of the field, including the nature of this bond, its relevance to crystal engineering, soft materials, biomolecular systems, and other special topics. Recently, halogen bonding in hypervalent iodine and bromine derivatives has been described.[7]

In a previous article in this journal we discussed the importance of halogen bonding and briefly reviewed its relevance in various aspects of crystal engineering[8] and host–guest chemistry. In particular, the host compound tetrakis-(4-bromophenyl)ethylene (**H1**) and its iodo-analogue (**H2**) have been previously shown to be reactive in terms of forming halogen···halogen bonds,[9] and recently their structures with a series of mono-carbon halogenated guests have been elucidated, their secondary interactions classified, and their kinetics of decomposition measured. These hosts were further employed to characterize their inclusion compounds with dichoroethane, methyl iodide, benzene, and piperidine and to monitor their kinetics of guest exchange.[10] Inclusion chemistry is a useful technique for separating compounds with similar boiling points, where traditional methods such as distillation are impractical. The method depends on the selectivity of a host compound for a given guest molecule in a mixture and has been successfully employed in the separation of isomers such as the xylenes,[11] toluidines,[12] and so forth.

In this work, we present the structures which occur by the enclathration by these hosts of the substituted pyridines shown in Scheme 1.

EXPERIMENTAL SECTION

The host molecules **H1** and **H2** were synthesized as described in our previous paper.[8] The guest solvents utilized were obtained

Scheme 1. Host and Guest Compounds Studied

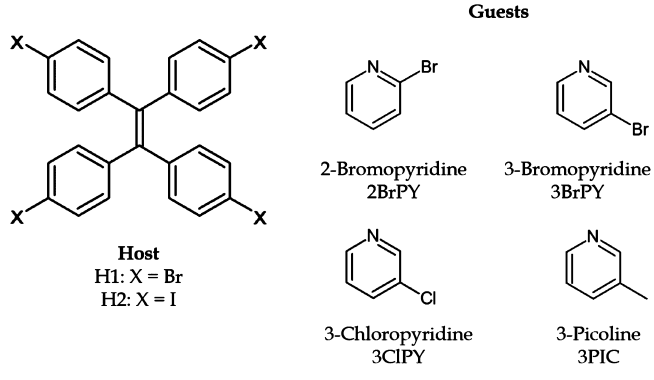

Received: April 12, 2017
Revised: July 11, 2017
Published: August 2, 2017

ACS Publications © 2017 American Chemical Society

DOI: 10.1021/acs.cgd.7b00521
Cryst. Growth Des. 2017, 17, 4647–4654

Table 1. Crystallographic Data Parameters of H1 Inclusions

Compound	H1·(2BrPY)	H1·1.5(3BrPY)	H1·1.5(3ClPY)	H1·1.5(3PIC)
Structural formula	$C_{31}H_{20}Br_5N$	$C_{33.5}H_{22}Br_{5.5}N_{1.5}$	$C_{33.5}H_{22}Br_4Cl_{1.5}N_{1.5}$	$C_{35}H_{26.5}Br_4N_{1.5}$
Host:Guest ratio	1:1	1:1.5	1:1.5	1:1.5
Molecular mass (g mol^{-1})	805.98	885.03	818.34	787.72
Data collection temp. (K)	173 (2)	173 (2)	173 (2)	173 (2)
Crystal system	Monoclinic	Monoclinic	Monoclinic	Monoclinic
Space group	$P2_1/n$	$P2_1/n$	$P2_1/n$	$P2_1$/n
a (Å)	14.6785 (3)	16.5232 (3)	16.5262 (3)	16.5506 (3)
b (Å)	9.3025 (19)	9.453 (9)	9.3912 (19)	9.3279 (19)
c (Å)	21.9821 (4)	20.3947 (4)	20.3678 (4)	20.3914 (4)
α (deg)	90	90	90	90
β (deg)	103.384 (3)	91.523 (3)	90.98 (3)	90.087 (3)
γ (deg)	90	90	90	90
Volume (Å^3)	2920.2 (11)	3184.4 (11)	3160.7 (10)	3148.07 (11)
Z	4	4	4	4
D_c, calc density (g cm^{-3})	1.833	1.846	1.720	1.662
Absorption coefficient (mm^{-1})	6.902	6.962	5.244	5.139
θ range	2.67−27.87	2.00−26.74	1.57−27.47	3.44−27.54
Reflections collected	117026	12846	13972	13957
No data $I > 2$ sigma (I)	4490	5291	5626	5145
Final R indices [$I > 2$ sigma (I)]	R_1 = 0.0600	R_1 = 0.0842	R_1 = 0.0415	R_1 = 0.0433
	wR_2 = 0.1415	wR_2 = 0.2449	wR_2 = 0.1024	wR_2 = 0.1093
R indices (all data)	R_1 = 0.1002	R_1 = 0.1022	R_1 = 0.0616	R_1 = 0.0748
	wR_2 = 0.1613	wR_2 = 0.2573	wR_2 = 0.1130	wR_2 = 0.1200
Goodness-of-fit on F^2	1.034	1.048	1.030	1.045
CCDC no.	1543290	1543291	1543292	1543293

Table 2. Crystallographic Data Parameters of H2 Inclusions

Compound	H2·(3BrPY)	H2·(3ClPY)	H2·(3PIC)A	H2·(3PIC)B
Structural formula	$C_{31}H_{20}Br_1I_4N$	$C_{31}H_{20}Cl_1I_4N$	$C_{32}H_{23}I_4N$	$C_{32}H_{23}I_4N$
Host:Guest ratio	1:1	1:1	1:1	1:1
Molecular mass (g mol^{-1})	993.99	949.53	929.11	929.11
Data collection temp. (K)	173 (2)	173 (2)	173 (2)	173 (2)
Crystal system	Monoclinic	Monoclinic	Monoclinic	Monoclinic
Space group	$C2/c$	$C2/c$	$C2/c$	$P2_1$
a (Å)	20.0216 (4)	20.0875 (4)	20.1602 (4)	9.6949 (19)
b (Å)	9.4839 (19)	9.4185 (19)	9.3808 (19)	18.652 (4)
c (Å)	16.9984 (3)	16.9553 (3)	16.9782 (3)	17.1292 (3)
α (deg)	90	90	90	90
β (deg)	105.369 (3)	105.595 (3)	105.159 (3)	94.634 (3)
γ (deg)	90	90	90	90
Volume (Å^3)	3112.3 (2)	3089.7 (2)	3099.2 (2)	3087.3 (11)
Z	4	4	4	4
D_c, calc density (g cm^{-3})	2.121	2.041	1.991	1.999
Absorption coefficient (mm^{-1})	5.309	4.141	4.043	4.058
θ range	2.80−27.45	3.83−27.87	4.87−27.86	1.62−27.17
Reflections collected	93984	90850	100895	7298
No data $I > 2$ sigma (I)	2938	2884	3071	6445
Final R indices [$I > 2$ sigma (I)]	R_1 = 0.0282	R_1 = 0.0329	R_1 = 0.0287	R_1 = 0.0420
	wR_2 = 0.0638	wR_2 = 0.0690	wR_2 = 0.0618	wR_2 = 0.0902
R indices (all data)	R_1 = 0.0389	R_1 = 0.0525	R_1 = 0.0401	R_1 = 0.0537
	wR_2 = 0.0688	wR_2 = 0.0772	wR_2 = 0.0673	wR_2 = 0.0951
Goodness-of-fit on F^2	1.105	1.127	1.153	1.054
CCDC no.	1543294	1543295	1543296	1543297

commercially and employed without further purification. Crystal growth was conducted by dissolving the host molecule in the selected guest at ambient temperature and allowing the solvent to evaporate.

Crystal Structure Analysis. X-ray diffraction analysis was performed on suitable single crystals selected by utilizing a polarized light optical microscope. Data for structures **H1·(2BrPY)**, **H1·1.5(3BrPY)**, **H1·1.5(3PIC)**, **H2·(3BrPY)**, **H2·(3ClPY)**, and **H2·(3PIC)A** were collected using a Nonius Kappa CCD.[13] Data for structures **H1·1.5(3ClPY)** and **H2·(3PIC)B** were collected using a Bruker DUO APEX[14] diffractometer utilizing Mo Kα radiation (λ = 0.71073 Å) at a temperature of 173 K. The intensity data were collected by the phi scan and omega scan techniques, scaled and

DOI: 10.1021/acs.cgd.7b00521
Cryst. Growth Des. 2017, 17, 4647−4654

reduced with DENZO-SMN[15]/ SAINT-Plus.[16] The integration and reduction of data were performed with a multiscan method executed with the SADABS program.[17] The determination of the space groups was done using XPREP implemented in APEX II. The structures were solved by direct methods using SHELX-97[18] and refined using full-matrix least-squares methods in SHELXL.[18] The graphical interface used was the program X-SEED.[19] All non-hydrogen atoms were refined anisotropically. All hydrogen atoms were placed geometrically and with a riding model for their isotropic temperature factors. Diagrams were generated using POVRAY in X-SEED.[19]

RESULTS AND DISCUSSION

Initial experiments were aimed at separating the picoline isomers, but it was noted that **H1** would only enclathrate 3PIC and solutions of **H1** with 2-picoline (2PIC) and 4-picoline (4PIC) yielded the apohost upon slow evaporation. Similarly, equimolar mixtures of 2PIC/3PIC and 3PIC/4PIC yielded the inclusion compound **H1·1.5(3PIC)** while the 2PIC/4PIC mixture again yielded the apohost. Therefore, **H1** is selective to 3PIC. The same results were obtained when using **H2** as host.

We therefore pursued the investigation with the halogenated pyridines shown in Scheme 1 in which the Cl or Br substituent has a similar volume to the methyl group of the picolines.

Crystal data and refinement parameters are given in Tables 1 and 2.

Inclusion Compounds with H1. Structure **H1·(2BrPY)** crystallizes in $P2_1/n$ with $Z = 4$. The host displays a propeller conformation in which the torsion angles are shown in Figure 1

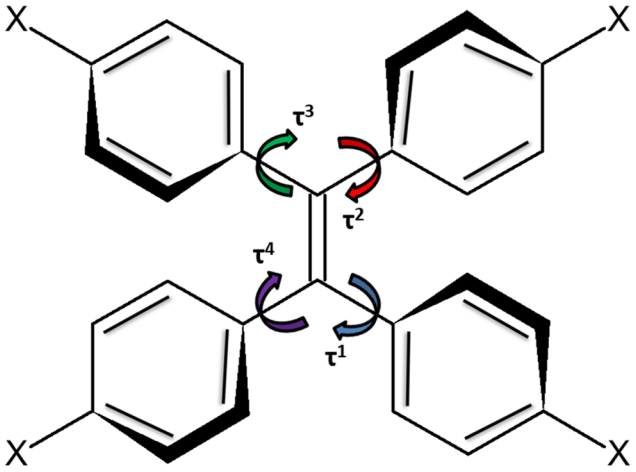

Figure 1. Propeller conformation of the host compounds.

have been recorded. For example, in structure **1**, the torsion angles are $\tau^1 = 42.3°$, $\tau^2 = 48.5°$, $\tau^3 = 44.8°$, $\tau^4 = 60.3°$ ranging over 18°. This propeller conformation is remarkably constant in all eight structures, and the torsion angles recorded have been deposited in Table S1 in the Supporting Information.

The host molecules lie in planes perpendicular to the *b*-axis. Following our previous methodology for interactions involving halogens, we employed the van der Waals radii of Bondi[20] (radii in Å, H = 1.20, Cl = 1.75, Br = 1.85, I = 1.98) and recorded X···X distances that were less than the sum of the van der Waals radii +5%. The geometric classification into types I, II_a, and II_b derived from Than Thu Bui et al.[21] are recorded in the Table S2.

In this structure there is a (Host)Br_{14}···Br_1(Guest) interaction of 3.696 (8) Å and (Host)Br_{14}···Br_{24}(Host) of 3.711 (8) Å. The packing is shown in Figure 2.

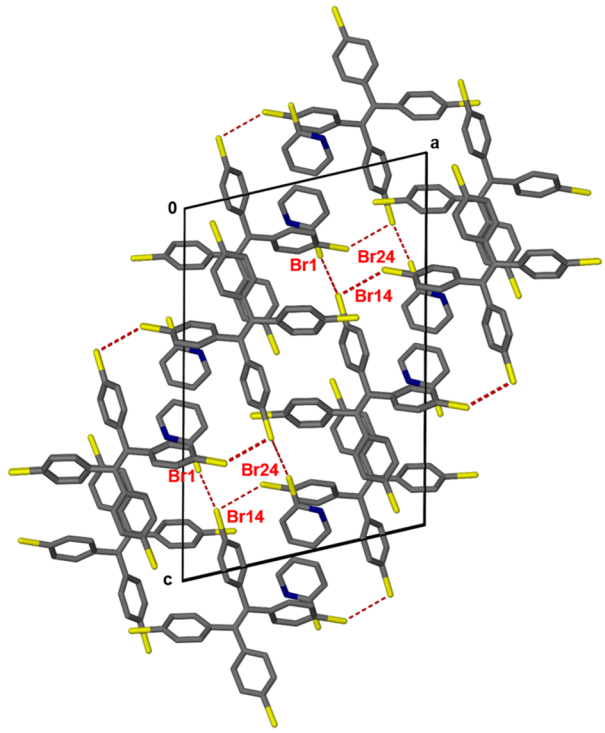

Figure 2. Packing diagram of **H1·(2BrPY)** viewed along [010], showing the Br···Br interactions.

Structure **H1·1.5(3BrPY)** has a different host:guest ratio from structure **H1·(2BrPY)**. The host and one guest molecule lie in a general position, but a second guest is disordered and is located on a center of inversion at Wyckoff position *b*. The packing is shown in Figure 3 and is characterized by host molecules lying in the *a*−*c* plane and the 3BrPY guests in channels running along [010] or located at inversion centers with site occupancies of 0.5. There are two Br···Br interactions

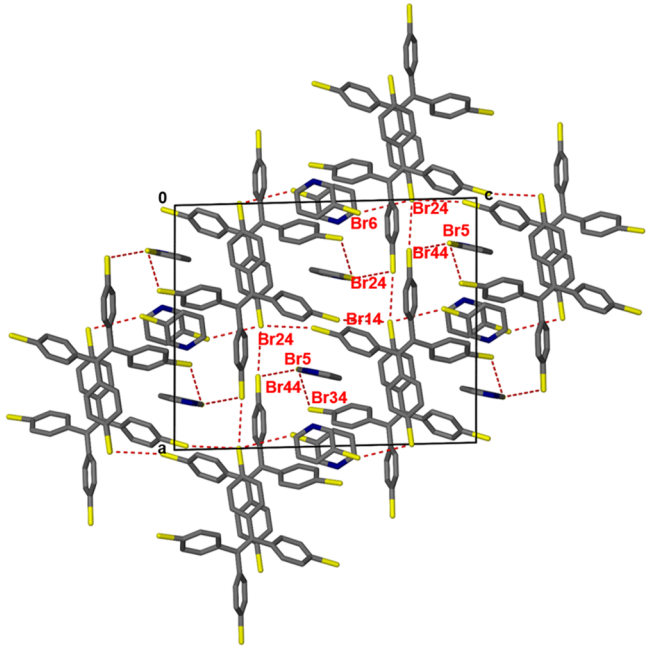

Figure 3. Crystal packing of **H1·1.5(3BrPY)**, down [010], showing the halogen···halogen interactions which occur in the structure.

DOI: 10.1021/acs.cgd.7b00521
Cryst. Growth Des. 2017, 17, 4647−4654

between host molecules and three between host and guest moieties. These are listed in Table 3.

Table 3. Halogen Interactions of H1/H2 Inclusion Compounds

Compound	X···X	d [Å]
H1·(2BrPY)	$Br_1\cdots Br_{14}$	3.696 (8)
	$Br_{14}\cdots Br_{24}$	3.711 (8)
H1·1.5(3BrPY)	$Br_{14}\cdots Br_{24}$	3.605 (14)
	$Br_{24}\cdots Br_{44}$	3.494 (15)
	$Br_{34}\cdots Br_5$	3.899 (2)
	$Br_{44}\cdots Br_5$	3.843 (2)
	$Br_{24}\cdots Br_6$	3.766 (3)
H1·1.5(3ClPY)	$Br_{14}\cdots Br_{24}$	3.631 (11)
	$Br_{24}\cdots Br_{44}$	3.486 (11)
	$Br_{34}\cdots Cl_5$	3.865 (3)
	$Br_{44}\cdots Cl_5$	3.779 (3)
	$Br_{24}\cdots Cl_6$	3.745 (6)
H1·1.5(3PIC)	$Br_{14}\cdots Br_{24}$	3.739 (10)
	$Br_{24}\cdots Br_{44}$	3.483 (9)
	$Br_{34}\cdots C_{55}$	3.788 (5)
	$Br_{44}\cdots C_{55}$	3.715 (5)
	$Br_{34}\cdots C_{65}$	3.838 (5)
H2·(3BrPY)	$I_{14}\cdots I_{24}$	3.912 (8)
	$I_{14}\cdots I_{24}$	4.031 (9)
	$I_{24}\cdots I_{24}$	4.048 (9)
H2·(3ClPY)	$I_{14}\cdots I_{24}$	3.929 (9)
	$I_{14}\cdots I_{24}$	4.066 (9)
	$I_{24}\cdots I_{24}$	4.000 (9)
H2·(3PIC)A	$I_{14}\cdots I_{24}$	3.935 (9)
	$I_{14}\cdots I_{24}$	4.098 (9)
	$I_{24}\cdots I_{24}$	3.977 (9)
H2·(3PIC)B	$I_{14}\cdots I_{24}$	4.003 (9)
	$I_{14A}\cdots I_{24}$	3.907 (8)
	$I_{14A}\cdots I_{44}$	4.153 (9)
	$I_{34}\cdots I_{44A}$	4.031 (9)
	$I_{34A}\cdots I_{44A}$	3.956 (8)
	$I_{24A}\cdots N_1$	3.414 (7)
	$I_{44}\cdots N_2$	3.506 (8)

Structures **H1·1.5(3ClPY)** and **H1·1.5(3PIC)** are isomorphous with structure **H1·1.5(3BrPY)**, as can be seen from the unit cell parameters listed in Table 1.

We have listed the five Br···Br interactions (two host···host and three host···guest contacts) in Table 3. This table also contains the corresponding X···X interactions of structure **H1·1.5(3ClPY)**. With regard to structure **H1·1.5(3PIC)**, where the 3PIC guest contains no halogen, we accepted the volume of the methyl moiety given by Kitaigorosky[22] as 23.5 Å^3. This yields a van der Waals radius of 1.78 Å which we assigned to the corresponding carbon atom. It is interesting that the positions of the 3PIC guests do not match those of the halogenated guests in structures **H1·1.5(3BrPY)** and **H1·1.5(3ClPY)**. The positions of the disordered guest match, but while the centers of the pyridyl rings of the ordered guests are similar, the positions of the methyl group does not correspond to those of the halogens in structures **H1·1.5(3BrPY)** and **H1·1.5-(3ClPY)**. Therefore, structure **H1·1.5(3PIC)** is not strictly isomorphous to those of **H1·1.5(3BrPY)** and **H1·1.5(3ClPY)** by virtue of the 3PIC guest rotating its position relative to the host molecules. Despite this there are close $H_3C\cdots Br$ contacts recorded in Table 3.

Inclusion Compounds with H2. Structure **H2·(3BrPY)** crystallizes in $C2/c$ with $Z = 4$. The host lies on the diad at Wyckoff position *e* and the 3BrPY guest is disordered about the center of inversion at Wyckoff position *d*. Structures **H2·(3BrPY)**, **H2·(3ClPY)** and **H2·(3PIC)A** are isomorphous with respect to both the host and guest atomic positions. These three structures do not exhibit X···X between host and guest moieties. The host···host halogen interactions are similar and are listed in Table 3. The packing of **H2·(3BrPY)**, shown in Figure 4 viewed along [010], is characterized by host layers lying in the *ac* planes and stabilized by I···I interactions. The 3BrPY guests are located in channels running in the [010] directions.

The structures of H2 with 3PIC form two polymorphs **H2·(3PIC)A** and **H2·(3PIC)B**, which grew concomitantly. **H2·(3PIC)A**, crystallized as colorless blocks while **H2·(3PIC)B** yielded needles of pale pink color. The two polymorphs were

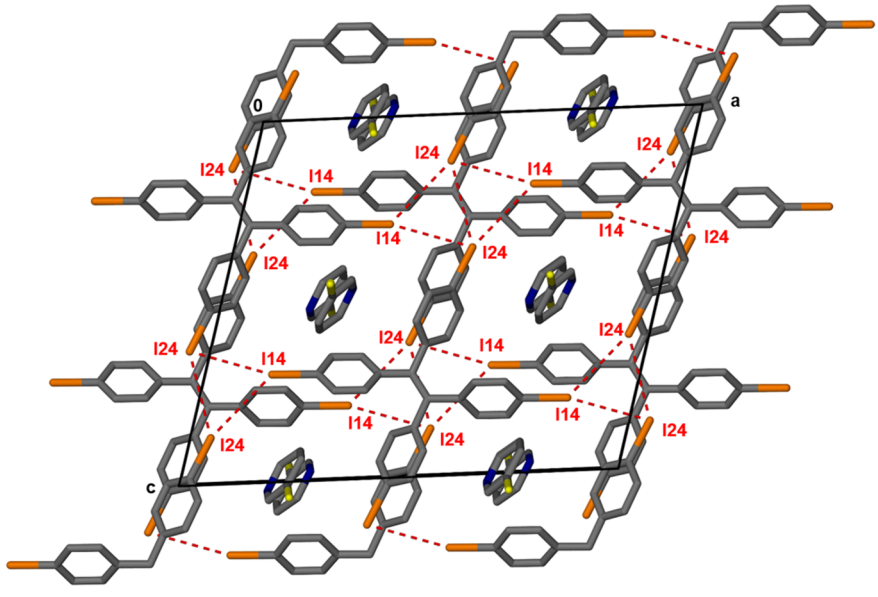

Figure 4. Illustration of the I···I interactions occurring in structure **H2·(3BrPY)**, with the packing diagram viewed down [010].

DOI: 10.1021/acs.cgd.7b00521
Cryst. Growth Des. 2017, 17, 4647−4654

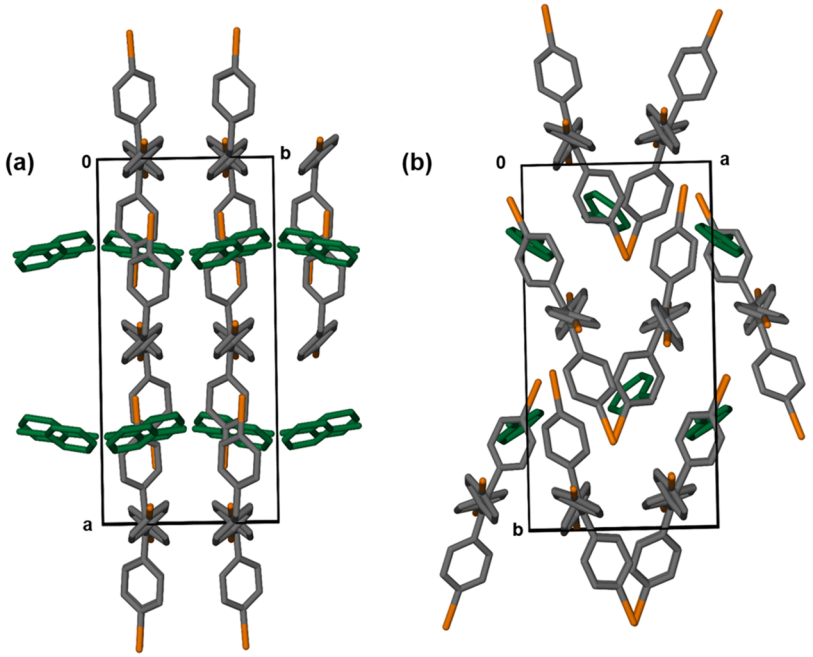

Figure 5. Comparison of the packing diagram of the two polymorphs **H2·(3PIC)A** and **H2·(3PIC)B** viewed along [001].

readily separated under the microscope for X-ray, TG, and DSC experiments. **H2·(3PIC)B** crystallizes in $P2_1$, with $Z = 4$, $Z' = 2$. The packing, however, is different from that of **H2·(3PIC)A**. Figure 5 shows structure **H2·(3PIC)A** and **H2·(3PIC)B** viewed along their respective c axes which are of similar lengths. In structure **H2·(3PIC)B**, the alignment of the host molecule is different and in addition to the I···I interactions there are (Host)I···N(Guest) contacts which are listed in Table 3. In the Supporting Information, Table S2 illustrates all the halogen bonds in the structures which are classified as type I, II_a, and II_b.

We carried out a survey of the Cambridge Structural Database (CSD) and noted a number of inclusion compounds of H1 and H2 with a variety of guests which have similar cell parameters and packings.

Inclusion compounds of **H1** with CH_2Cl_2,[8] CH_3I,[8] THF,[23] and acetone[23] with the following reference codes KUWYEI, KUWYIM, XALCAO, and XALBUH, respectively, have been reported previously and shown to be nearly isomorphous with the **H1** compounds obtained in this research. All of these compounds including those of this study have similar cell parameters except for their β angles. These compounds all crystallized in $P2_12_12_1$ with two molecules of each guest on the asymmetric unit.

Inclusion compounds with **H2** with similar structures had guests 1,1,2,2-tetrachloroethane (GUHQIJ)[9] and were similar to **H2·(2BrPY)**, while the following four compounds were similar to **H2·(3PIC)B**: with carbon tetrachloride (KUWJIN),[8] piperidine/benzene (LACSIU),[10] piperidine (LACSOA),[10] and benzene (LADCAX).[10]

Thermal Analysis. The results of thermal gravimetry (TG) and differential scanning calorimetry (DSC) are presented in Table 4. The experimental values of the thermal gravimetry are highly satisfactory, with differences between calculated and experimental values being generally within 1%. The DSC curves exhibit two endotherms corresponding to guest loss (labeled ① and ②).

Table 4. Thermal Analysis

	TG		DSC		
Structure	Expt %	Calc %	Guest T_{peak1}/ °C	Guest T_{peak2}/ °C	Host T_{melt}/ °C
H1·(2BrPY)	21.3	19.6	68.2	129.7	255.7
H1·1.5(3BrPY)	26.8	26.8	86.5	126.4	256.0
H1·1.5(3ClPY)	20.4	20.8	72.6	99.3	255.7
H1·1.5(3PIC)	17.7	17.7	99.9	123.7	256.4
H2·(3BrPY)	15.3	15.9	130.3	143.9	301.4
H2·(3ClPY)	11.8	12.0	116.0	121.0	301.8
H2·(3PIC)A	10.0	10.0	86.1	112.0	302.7
H2·(3PIC)B	-	10.0	101.3	117.0	302.0

These are broad and we therefore recorded their peak temperatures T_{peak} as opposed to their onset temperatures T_{on}. The third endotherms ③ due to host melting are very consistent in their T_{melt} temperatures for **H1** and **H2**. A typical TG/DSC profile, that of **H1·1.5(3BrPY)**, is shown in Figure 6. The remaining profiles have been deposited as additional information.

The DSC results of the two polymorphs of **H2** with 3PIC, structure **H2·(3PIC)A**, and **H2·(3PIC)B** are interesting and are shown Figure 7. Both polymorphs show a double endotherm due to guest loss, but those of the second polymorph, structure **H2·(3PIC)B**, are displaced by 15.2 and 5.0 °C to higher temperature, showing that polymorph II is the more stable. This correlates with the corresponding structures **H2·(3PIC)A** and **H2·(3PIC)B**.

The structures of the two polymorphs, **H2·(3PIC)A** and **H2·(3PIC)B**, are characterized by host molecules in layers and the 3PIC guests located in highly constricted channels of hourglass shape. These are shown in Figure 8a,b in which the guest molecules have been removed and the host atoms are shown in van der Waals representation.

Kinetics of Enclathration. The kinetics of enclathration of the solid **H1** with 3PIC and 3BrPY as vapors was extremely slow, and so we measured the reactions with the solid host in

DOI: 10.1021/acs.cgd.7b00521
Cryst. Growth Des. 2017, 17, 4647−4654

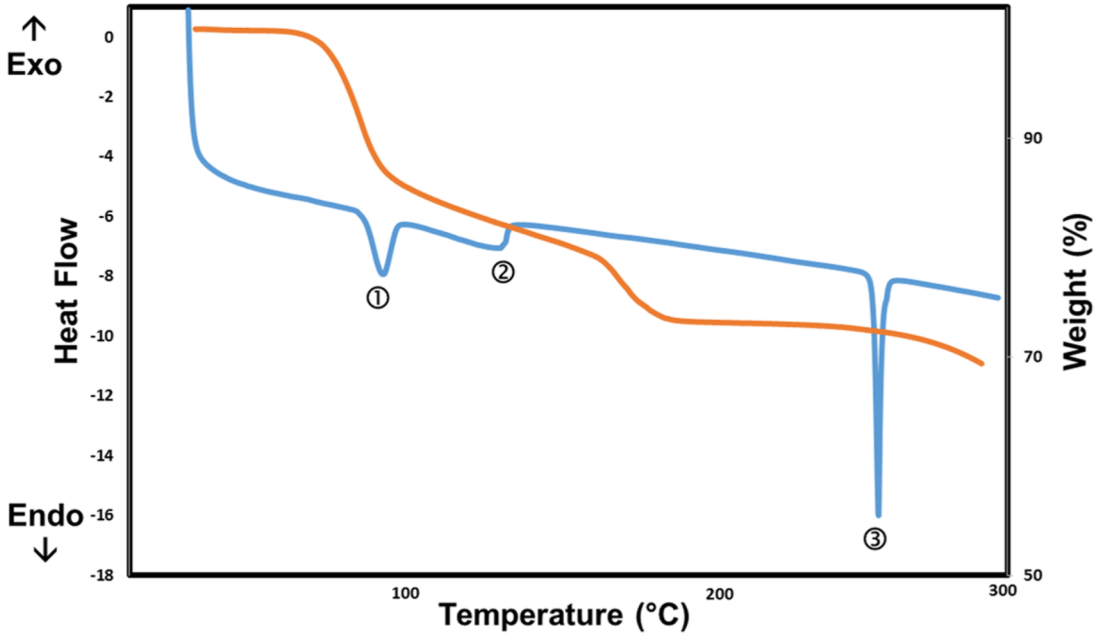

Figure 6. Thermal analysis curves of structure **H1·1.5(3BrPY)** illustrating the thermal events.

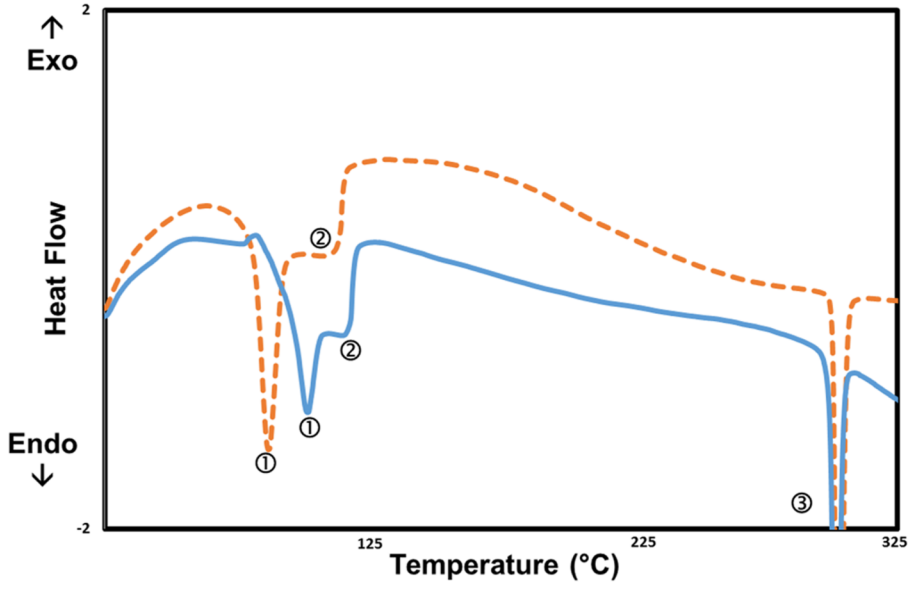

Figure 7. DSC curves of structures **H2·(3PIC)A** (orange) and **H2·(3PIC)B** (blue) illustrating the different endotherms in the two polymorphs.

suspension of a solution of the guests in water (75% guest by weight). The solid host **H1** was stirred vigorously and remained in suspension throughout the experiment at a fixed temperature. Samples were removed at fixed times and subjected to thermal gravimetry to measure the progress of the reaction. The curves for the enclathration of 3PIC carried out at 25 and 35 °C are shown in Figure 9a. The kinetics follows the Avrami–Erofe'ev eq A2,[24] with $k = 4.63 \times 10^{-3}$ min^{-1} (25 °C) and 1.20×10^{-2} min^{-1} (35 °C).

The curves for the enclathration of 3BrPY, shown in Figure 9b are more interesting. For the reaction at 25 °C, the kink in the curve, which occurs at a Guest/Host ratio at ~1, shows that this is a two-step reaction, the first step yielding a G/H of 1:1, followed by the second step with a final G/H of ~1.5:1 which corresponds to the stoichiometry of the crystal structure. The kinetic results for the reaction at 35 °C also show a kink in the curve, but this is less pronounced. For the reaction at 25 °C the first step from 0 to 150 min, again follows the Avrami–Erofe'ev eq A2[24] with $k = 2.14 \times 10^{-2}$ min^{-1}, and the second step from 150 to 300 min followed the same law with $k = 6.28 \times 10^{-3}$ min^{-1}. The reaction at 35 °C was more difficult to analyze due to the paucity of experimental points. The kinetics are linear form 0 to 45 min with $k = 2.22 \times 10^{-2}$ min^{-1}, while the second step from 45 to 150 min follows the Prout–Tompkins[15] equation

$$\ln(\alpha/1 - \alpha) = kt \qquad \text{with } k = 6.73 \times 10^{-2}\text{min}^{-1}$$

CONCLUSION

The host compounds tetrakis(4-bromophenyl) ethylene and its iodo-analogue form inclusion compounds with halogenated pyridines and 3-picoline. These host molecules display a

DOI: 10.1021/acs.cgd.7b00521
Cryst. Growth Des. 2017, 17, 4647–4654

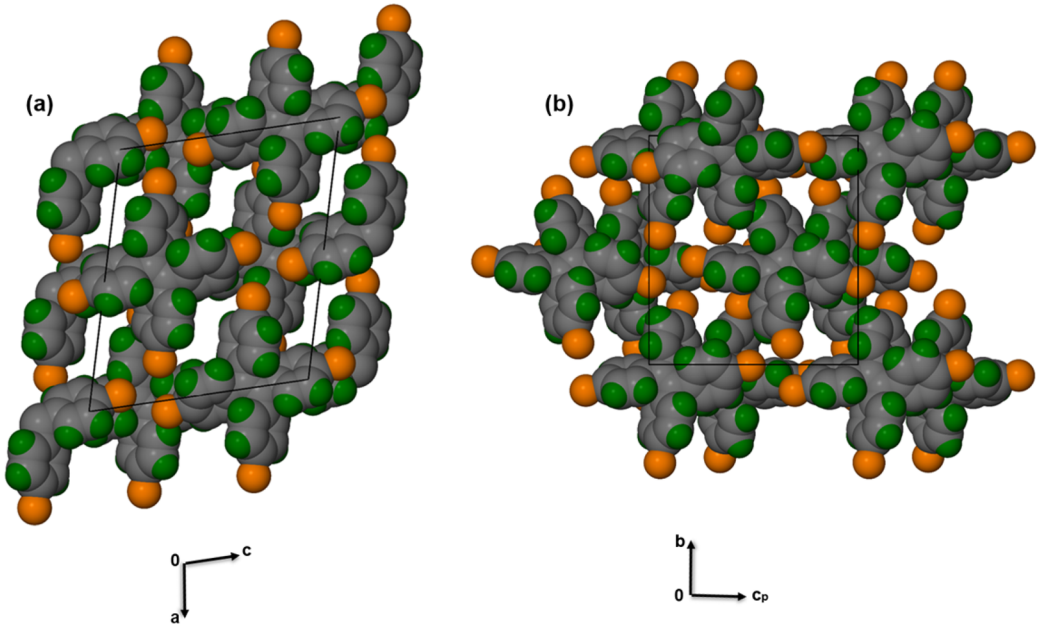

Figure 8. van der Waals radii representation of (a) **H2·(3PIC)A** shown down [010] and (b) **H2·(3PIC)B** shown down [100] with the 3PIC molecules removed to illustrate the highly constricted hourglass shaped channels in the structures. The channel restrictions in **H2·(3PIC)B** are the more severe.

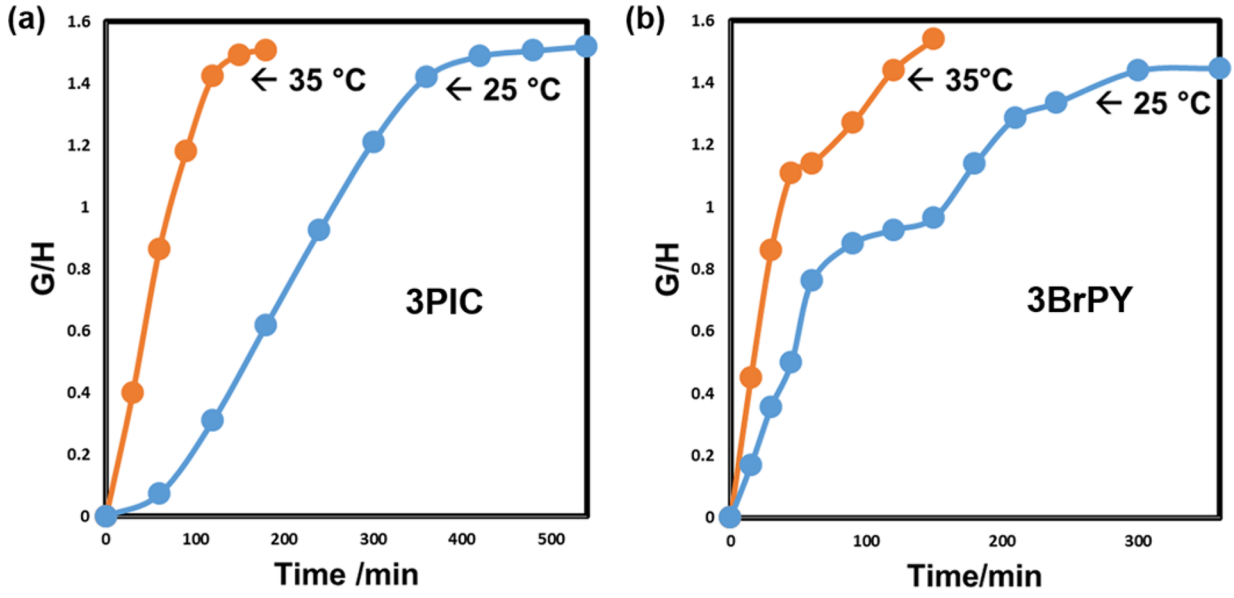

Figure 9. Kinetics of suspension at 25 and 35 °C of **H1** with (a) 3PIC **H1·1.5(3PIC)** and (b) 3BrPY **H1·1.5(3BrPY)**.

propeller conformation which remains practically constant in all the clathrate structures. The iodo-host forms two polymorphs with the 3-picoline guest. These display dissimilar DSC profiles which correlate with their structures. Their kinetics of guest enclathration in aqueous suspensions are distinctly different, with the 3BrPY guest displaying a two-step reaction.

■ ASSOCIATED CONTENT

Supporting Information

The Supporting Information is available free of charge on the ACS Publications website at DOI: 10.1021/acs.cgd.7b00521.

Torsion angles of **H1**/**H2** inclusion compounds, halogen interactions of **H1**/**H2** inclusion compounds, TG/DSC events (PDF)

Accession Codes

CCDC 1543290−1543297 contain the supplementary crystallographic data for this paper. These data can be obtained free of charge via www.ccdc.cam.ac.uk/data_request/cif, or by emailing data_request@ccdc.cam.ac.uk, or by contacting The Cambridge Crystallographic Data Centre, 12 Union Road, Cambridge CB2 1EZ, UK; fax: +44 1223 336033.

■ AUTHOR INFORMATION

Corresponding Author

*E-mail: luigi.nassimbeni@uct.ac.za. Tel: +27 21 650 5893. Fax: +27 21 650 2569.

ORCID

Francoise M. Amombo Noa: 0000-0001-8361-3432

DOI: 10.1021/acs.cgd.7b00521
Cryst. Growth Des. 2017, 17, 4647−4654

Susan A. Bourne: 0000-0002-2491-2843
Luigi R. Nassimbeni: 0000-0001-8714-8646

Notes

The authors declare no competing financial interest.

■ ACKNOWLEDGMENTS

We thank the University of Cape Town and the National Research Foundation (South Africa) for funding.

■ REFERENCES

(1) Desiraju, G. R. *Crystal Engineering*; Elsevier: Amsterdam, 1989, Chapter 6.
(2) Reddy, C. M.; Kirchner, M. T.; Gundakaram, R. C.; Padmanabhan, K. A.; Desiraju, G. R. *Chem. - Eur. J.* **2006**, *12*, 2222−2234.
(3) Mukherjee, A.; Desiraju, G. R. *IUCrJ.* **2014**, *1*, 49−60.
(4) Metrangolo, P.; Neukirch, H.; Pilati, T.; Resnati, G. *Acc. Chem. Res.* **2005**, *38*, 386−395.
(5) Metrangolo, P.; Meyer, F.; Pilati, T.; Resnati, G.; Terraneo, G. *Angew. Chem., Int. Ed.* **2008**, *47*, 6114−6127.
(6) Cavallo, G.; Metrangolo, P.; Milani, R.; Pilati, T.; Priimagi, A.; Resnati, G.; Terraneo, G. *Chem. Rev.* **2016**, *116*, 2478−2601.
(7) Cavallo, G.; Murray, J. S.; Politzer, P.; Pilati, T.; Ursini, M.; Resnati, G. *IUCrJ.* **2017**, *4*, 411−419.
(8) Amombo Noa, F. M.; Bourne, S. A.; Nassimbeni, L. R. *Cryst. Growth Des.* **2015**, *15*, 3271−3279.
(9) Tanaka, K.; Fujimoto, D.; Toda, F. *Tetrahedron Lett.* **2000**, *41*, 6095−6099.
(10) Amombo Noa, F. M.; Bourne, S. A.; Su, H.; Nassimbeni, L. R. *Cryst. Growth Des.* **2016**, *16*, 1636−1642.
(11) Nassimbeni, L. R.; Bathori, B. N.; Patel, L. D.; Su, H.; Weber, E. *Chem. Commun.* **2015**, *51*, 3627−3629.
(12) Caira, M. R.; Nassimbeni, L. R.; Toda, F.; Vujovic, D. *J. Chem. Soc., Perkin Trans. 2.* **1999**, 2681−2684.
(13) *Collect, data collection software*; Nonius: Delft, The Netherlands, 1998.
(14) *APEX 2*, v 1.0−27; Bruker AXS Inc.: Madison, WI, 2005.
(15) Otwinowski, Z.; Minor, W. In *Methods in Enzymology, Macromolecular Crystallography*, Carter, C. W., Jr; Sweet, R. M, Eds.; Academic Press: 1997; Part A, Vol. *276*, p 307.
(16) *SAINT-Plus*, v 7.12; Bruker AXS Inc.: Madison, Wisconsin, USA, 2004.
(17) Sheldrick, G. M. *SADABS; Program for Area Detector Adsorption Correction*; University of Göttingen: Germany, 1996; p 33−38.
(18) Sheldrick, G. M. *SHELX-97; Program for crystal Structure Solution and Refinement*; University of Göttingen: Germany, 1997; p 1456.
(19) Barbour, L. J. X-SEED; A Software Tool for Supramolecular Crystallography. *J. Supramol. Chem.* **2001**, *1*, 189−191.
(20) Bondi, A. *J. Phys. Chem.* **1964**, *68*, 441−451.
(21) Than Thu Bui, T.; Dahaoui, S.; Lecomte, C.; Desiraju, G. R.; Espinosa, E. *Angew. Chem., Int. Ed.* **2009**, *48*, 3838−3841.
(22) Kitaigorodsky, A. I. *Molecular Crystals and Molecules*; Academic Press; New York and London, 1973; Chapter 1.
(23) Tanaka, K.; Fujimoto, D.; Altreuther, A.; Oeser, T.; Irngartinger, H.; Toda, F. *J. Chem. Soc., Perkin Trans. 2.* **2000**, 2115−2120.
(24) Brown, M. E. *Introduction to Thermal Analysis: Techniques and Applications*; Chapman and Hall: London, 1988.

DOI: 10.1021/acs.cgd.7b00521
Cryst. Growth Des. 2017, 17, 4647−4654

SUPPORTING INFORMATION

*Francoise M. Amombo Noa, Susan A. Bourne, Hong Su and Luigi R. Nassimbeni**

Centre for Supramolecular Chemistry Research, Department of Chemistry, University of Cape Town, Rondebosch 7701, South Africa. Email: luigi.nassimbeni@uct.ac.za.

Table S1. Torsion Angles of H1/H2 Inclusion Compounds.

	1	**2**	**3**	**4**
C_{12}-C_{11}-C_1-C_2 **τ^1/°**	+42.3	+52.0	+52.1	+51.8
C_{46}-C_{41}-C_2-C_{31} **τ^2/°**	+48.5	+48.2	+48.8	+48.8
C_{32}-C_{31}-C_2-C_1 **τ^3/°**	+44.8	+54.9	+54.3	+55.3
C_{22}-C_{21}-C_1-C_{11} **τ^4/°**	+60.3	+46.5	+47.2	+49.2
	5	**6**	**7**	
C_{16}-C_{11}-C_1-C_{21} **τ^1/°**	+47.8	+47.7	+48.2	
C_{26}-C_{21}-C_1-$C_{1'}$ **τ^2/°**	+46.8	+45.8	+46.4	
$C_{16'}$-$C_{11'}$-$C_{1'}$-$C_{21'}$ **τ^3/°**	+47.8	+47.7	+48.2	
$C_{26'}$-$C_{21'}$-$C_{1'}$-C_1 **τ^4/°**	+46.8	+45.8	+46.4	
	8		**8'A**	
C_{12}-C_{11}-C_1-C_2 **τ^1/°**	+47.6	C_{12A}-C_{11A}-C_{1A}-C_{2A} **τ^1/°**	+50.1	
C_{46}-C_{41}-C_2-C_{31} **τ^2/°**	+54.9	C_{46A}-C_{41A}-C_{2A}-C_{31A} **τ^2/°**	+39.7	
C_{32}-C_{31}-C_2-C_1 **τ^3/°**	+54.6	C_{32A}-C_{31A}-C_{2A}-C_{1A} **τ^3/°**	+56.7	
C_{22}-C_{21}-C_1-C_{11} **τ^4/°**	+45.9	C_{22A}-C_{21A}-C_{1A}-C_{11A} **τ^4/°**	+41.7	

Table S2. Halogen Interactions of **H1**/**H2** Inclusions Compounds

Compound	X···X	*d* [Å]	θ_1/θ_2 [deg]	*d*-∑vdw [Å]	%	Type
1	$Br_1\cdots Br_{14}$	3.696 (8)	155/124	-0.004	-0.1	II_a
	$Br_{14}\cdots Br_{24}$	3.711 (8)	143/95	+0.011	+0.3	II_a
2	$Br_{14}\cdots Br_{24}$	3.605 (14)	166/101	-0.095	-2.6	II_a
	$Br_{24}\cdots Br_{44}$	3.494 (15)	166/163	-0.206	-5.6	I
	$Br_{34}\cdots Br_5$	3.899 (2)	118/85	+0.199	+5.4	I
	$Br_{44}\cdots Br_5$	3.843 (2)	156/91	+0.143	+3.9	II_a
	$Br_{24}\cdots Br_6$	3.766 (3)	145/96	+0.066	+1.8	II_a
3	$Br_{14}\cdots Br_{24}$	3.631 (11)	167/102	-0.069	-1.9	II_a
	$Br_{24}\cdots Br_{44}$	3.486 (11)	167/164	-0.214	-5.8	I
	$Br_{34}\cdots Cl_5$	3.865 (3)	118/86	+0.265	+7.4	I
	$Br_{44}\cdots Cl_5$	3.779 (3)	156/90	+0.179	+5.0	II_a
	$Br_{24}\cdots Cl_6$	3.745 (6)	150/93	+0.145	+4.0	II_a
4	$Br_{14}\cdots Br_{24}$	3.739 (10)	167/104	+0.039	+1.1	II_a
	$Br_{24}\cdots Br_{44}$	3.483 (9)	169/168	-0.217	-5.9	I
	$Br_{34}\cdots C_{55}$	3.788 (5)	136/98	+0.158	+4.4	I
	$Br_{44}\cdots C_{55}$	3.715 (5)	163/101	+0.085	+2.3	II_a
	$Br_{34}\cdots C_{65}$	3.838 (5)	120/80	+0.208	+5.7	I
5	$I_{14}\cdots I_{24}$	3.912 (8)	162/78	-0.048	-1.2	II_b
	$I_{14}\cdots I_{24}$	4.031 (9)	163/134	+0.071	+1.8	II_b
	$I_{24}\cdots I_{24}$	4.048 (9)	139/139	+0.088	+2.2	II_b
6	$I_{14}\cdots I_{24}$	3.929 (9)	163/78	-0.031	-0.8	II_b
	$I_{14}\cdots I_{24}$	4.066 (9)	163/134	+0.106	+2.7	II_b
	$I_{24}\cdots I_{24}$	4.000 (9)	139/139	+0.04	+1.0	II_b
7	$I_{14}\cdots I_{24}$	3.935 (9)	164/78	-0.025	-0.6	II_b
	$I_{14}\cdots I_{24}$	4.098 (9)	161/134	+0.138	+3.5	II_b
	$I_{24}\cdots I_{24}$	3.977 (9)	140/140	+0.017	+0.4	II_b
8	$I_{14}\cdots I_{24}$	4.003 (9)	158/65	+0.043	+1.1	II_a
	$I_{14A}\cdots I_{24}$	3.907 (8)	144/113	-0.053	-1.3	I
	$I_{14A}\cdots I_{44}$	4.153 (9)	157/87	+0.193	+4.9	II_a
	$I_{34}\cdots I_{44A}$	4.031 (9)	137/101	+0.071	+1.8	I
	$I_{34A}\cdots I_{44A}$	3.956 (8)	154/64	-0.004	-0.1	II_a
	$I_{24A}\cdots N_1$	3.414 (7)	154/132	-0.116	-3.3	I
	$I_{44}\cdots N_2$	3.506 (8)	155/140	-0.024	-0.7	I

Thermal Analysis

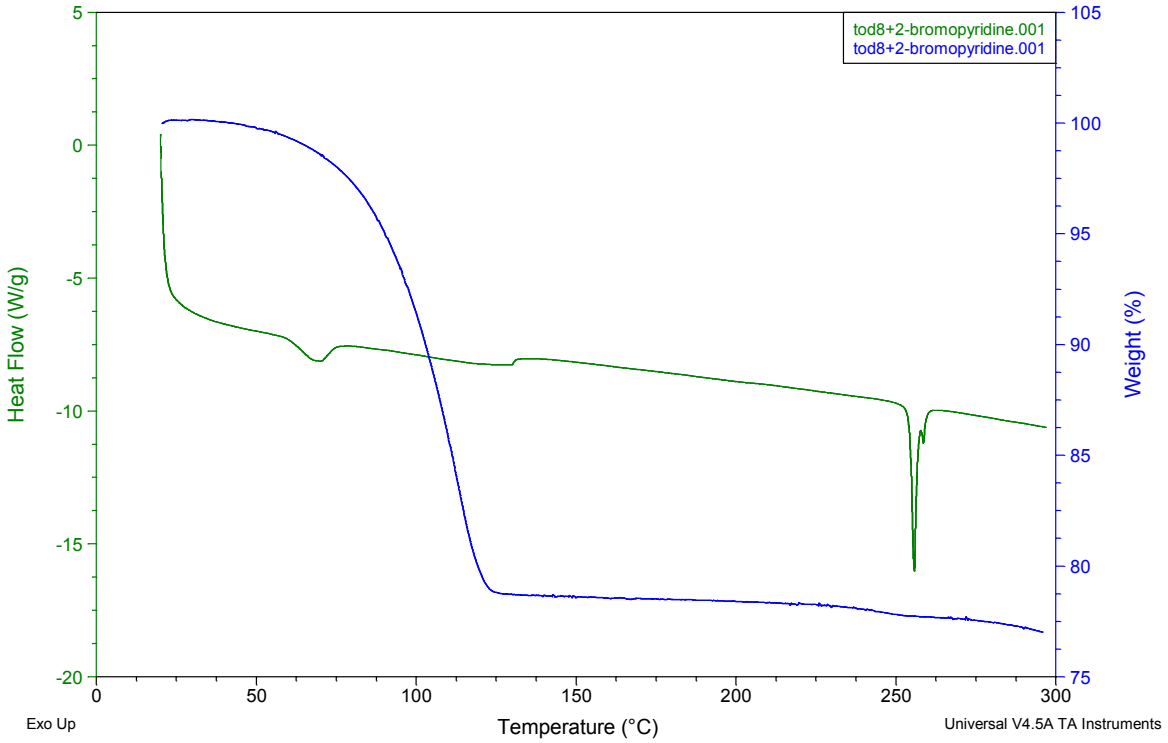

Figure S1. DSC and TG plots of **1**.

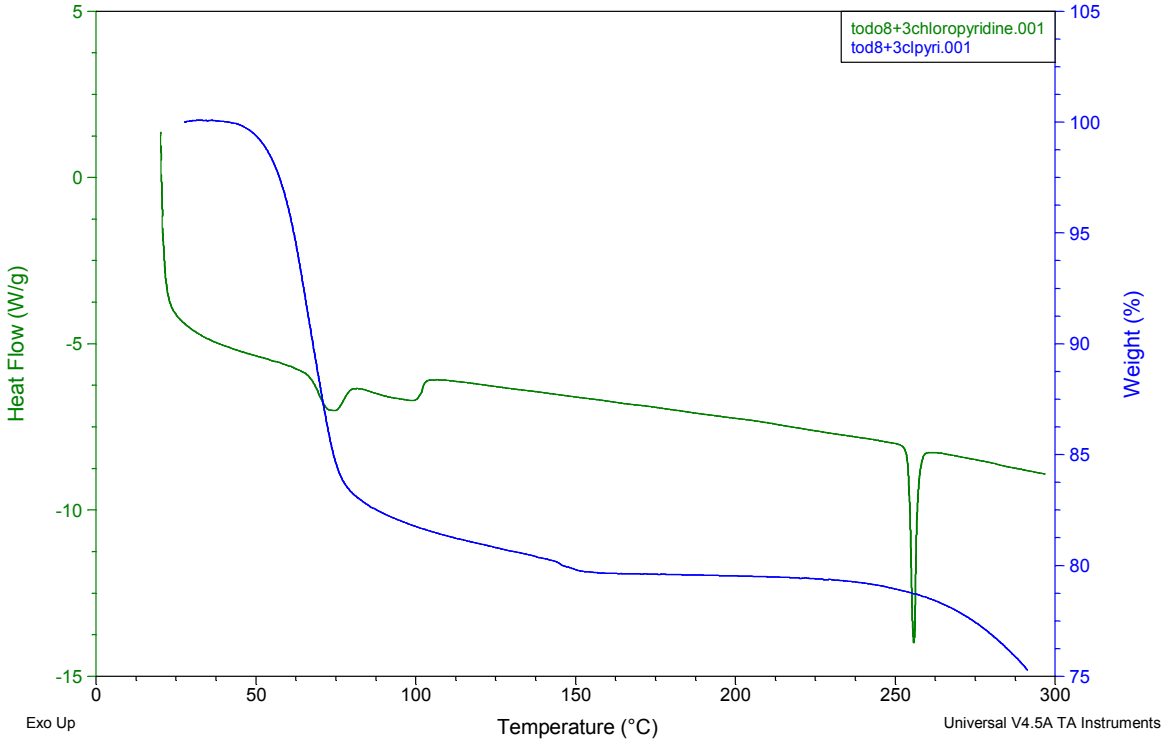

Figure S2. DSC and TG plots of **3**.

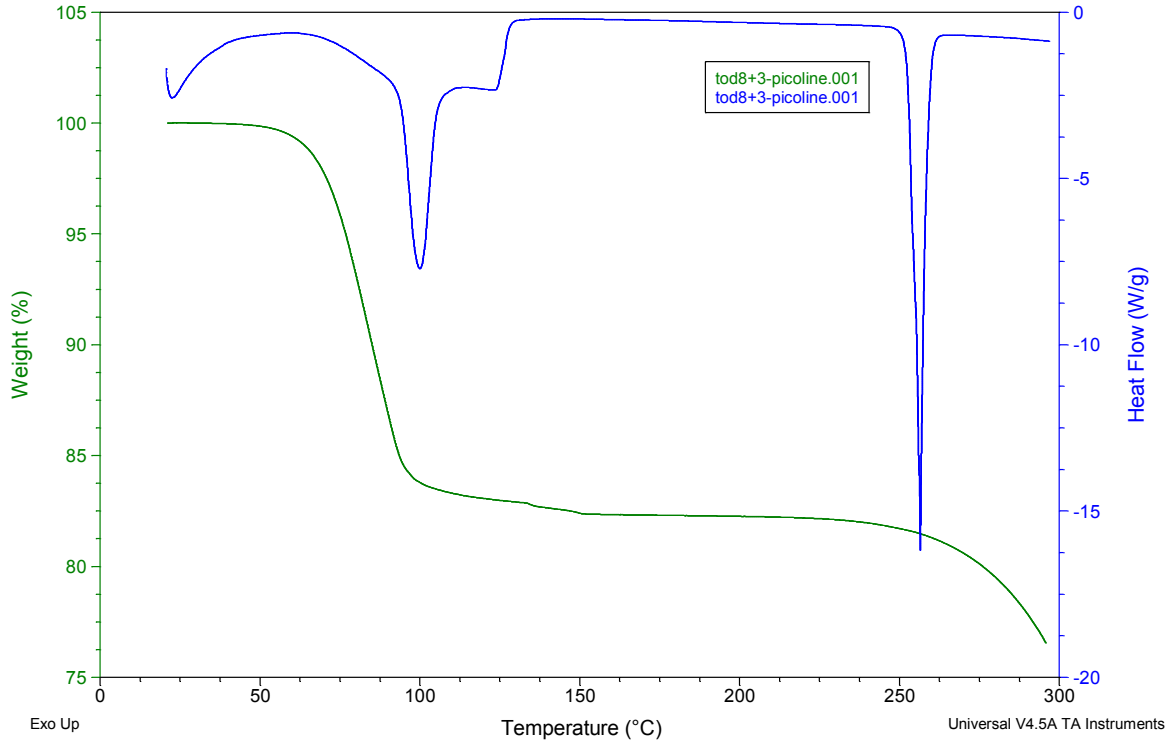

Figure S3. DSC and TG plots of **4**.

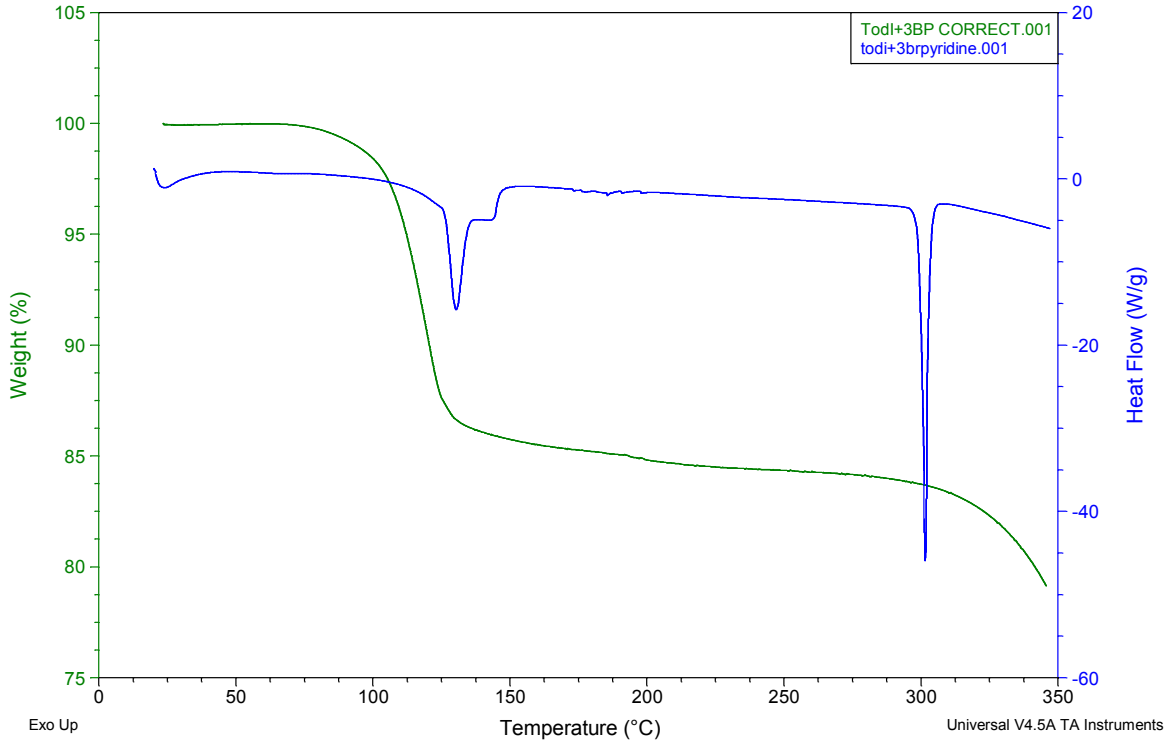

Figure S4. DSC and TG plots of **5**.

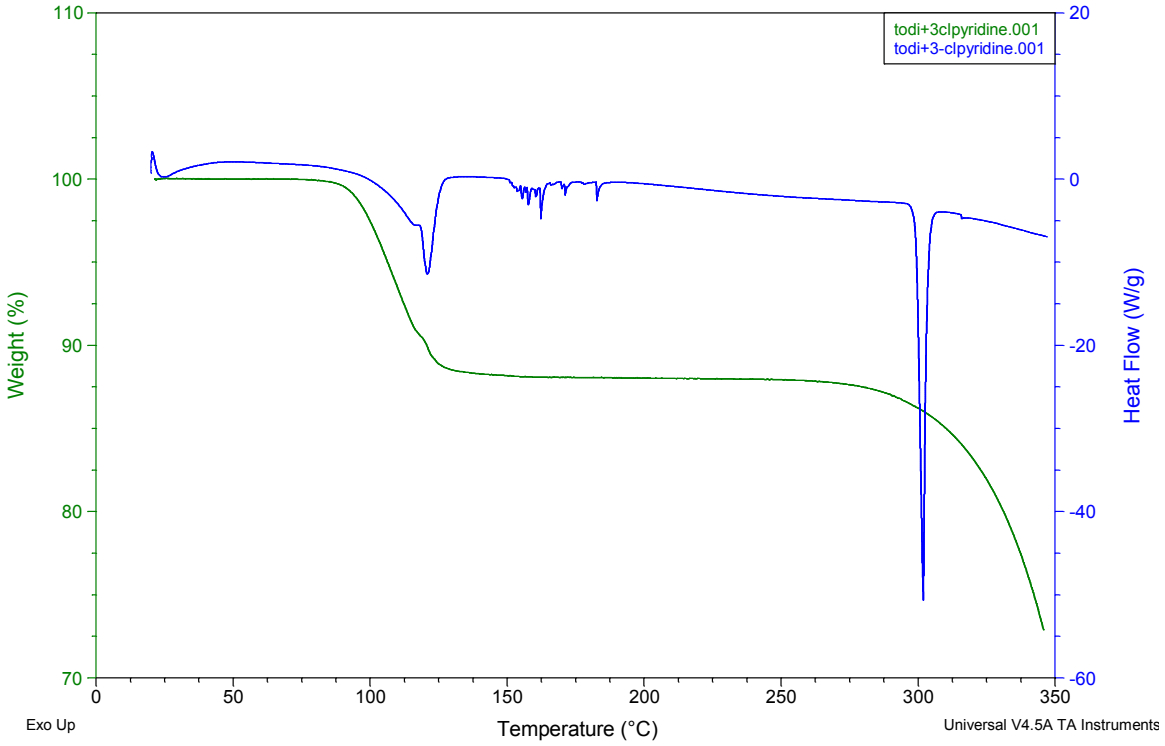

Figure S5. DSC and TG plots of **6**.

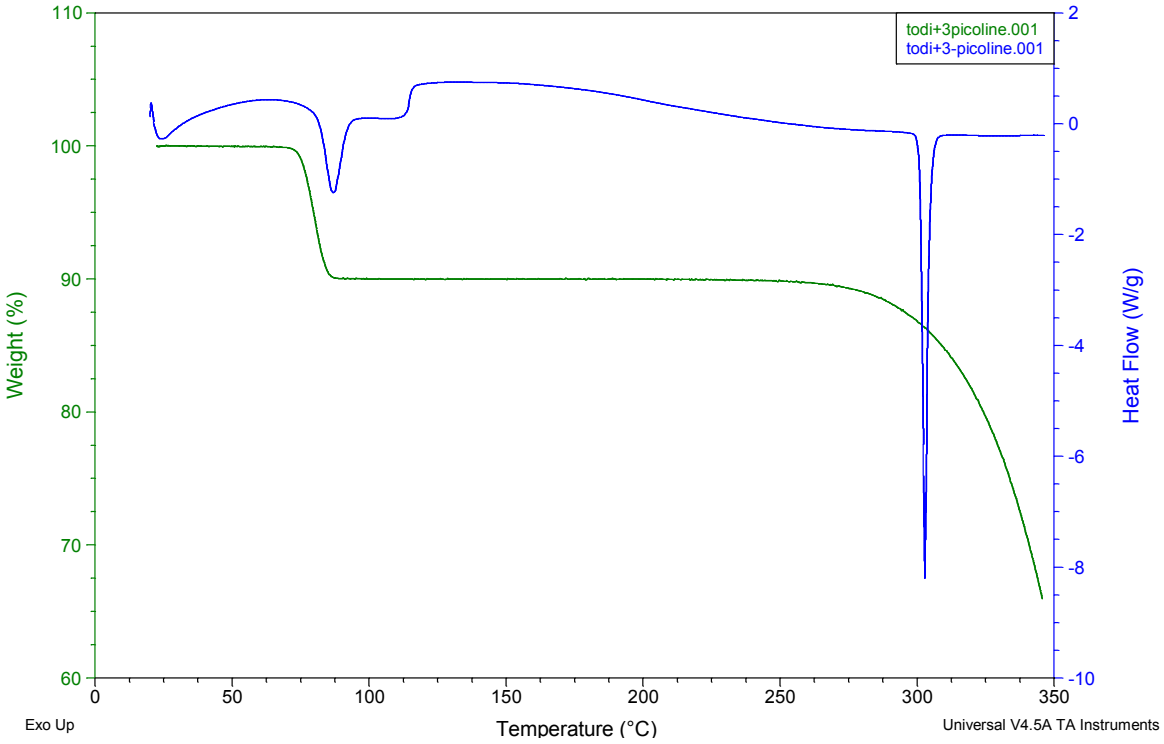

Figure S6. DSC and TG plots of **7**.

CHAPTER VI

Hydrogen Bonding versus Halogen Bonding in Host – Guest Compounds

(Amombo Noa, F. M.; Bourne, S. A.; Hong Su.; Weber, E.; Nassimbeni, L. R. *Cryst. Growth Des.* 2016, 16 (8), 4765 – 4771).

6.1 Summary

Three similar but different host compounds **H1**: 9,9′-(biphenyl-2,2′-diyl) difluorenl-9-ol, **H2**: 2,2′,7,7′-tetrabromo-9,9′-(biphenyl-2,2′-diyl) difluoren-9-ol and **H3**: 2,2′,7,7′-tetra-tert-butyl-9,9′-(1,4-phenylene)-dipfluoren-9-ol were used in this study to form inclusion compounds with 3-brompyridine (3BrPY) and 3-chloropyridine (3ClPY). This was done to compare the interactions (hydrogen bond and halogen bond) found in these structures.

Six structures were obtained by crystallisation with either 3BrPY and 3ClPY. They were characterised by single X-ray diffraction, thermal analysis, variable powder X-ray diffraction, Hirshfeld surface analysis an IR spectroscopy.

In the structure analysis of all the compounds, the hydrogen bonding motif (Host)O-H⋯O(Host)-H⋯N(Guest) was predominated over the halogen⋯halogen interactions which appeared to have secondary importance. Structures of **H2** with 3BrPY and its chloro-analogue contained more halogen⋯halogen interactions than the other structures because the host compound also contains substituted Br on each fluorenyl moiety.

While **H1** and **H2** adopt the *trans* conformation to form an intramolecular H-bond, this is not possible for **H3.** The obtained inclusion compounds cannot form an intramolecular H-bond, due to the bulk of the *t*-butyl substituents. For this reason the host adopts a *cis*-conformation to allow two adjacent molecules to form H-bonds in a dimer arrangement.

The first compound (**1**) in the thermal analysis case did not follow the decomposition pattern of the rest of structures. Its TG curve showed multi-steps which are due to the loss of the 3BrPY and its DSC traces has two endotherm peaks labelled as A and B. This is followed by a series of small peaks and the melt of the host at a melting point which is not originally the host melting point.

However, thermal analysis for compounds **2**, **3**, **4**, **5** and **6** were more or less the same, showing three endotherm peaks on their DSC's where the first two

peaks are attributed to the loss of the guest solvents in the structures, followed by the melt of the hosts. Multiple steps mass loss which are due to the guests on the TG's of compounds **2**, **3**, **5** and **6** were observed except for compound **4** which gave rise to only one mass loss on its TG.

To understand what is going on in this structure, Hot-Stage Microscopy and variable powder x-ray diffraction were also conducted for more clarification.

Hirshfeld surface analysis was utilised to compared the packing of the structures of **H1** and **H2** using the program Crystal Explorer in other to discern the effect of the Br atoms on **H2**. H⋯H interactions were greater for **H1** inclusion compounds than for **H2** compounds, this is due to the Br⋯Br interaction which was only seen in **H2** complexes.

Finally, IR spectroscopy was performed in all the obtained crystals and host compounds to confirm the presence of the host-guest hydrogen bond.

The original article and the supporting information are provided below.

CRYSTAL GROWTH & DESIGN

Article

pubs.acs.org/crystal

Hydrogen Bonding versus Halogen Bonding in Host–Guest Compounds

Francoise M. Amombo Noa,[†] Susan A. Bourne,[†] Hong Su,[†] Edwin Weber,[‡] and Luigi R. Nassimbeni*[,†]

[†]Centre for Supramolecular Chemistry Research, Department of Chemistry, University of Cape Town, Rondebosch 7701, South Africa

[‡]Institut für Organishe Chemie, TU Bergakademie Freiberg, Leipziger Strasse 29, D-09596 Freiberg/Sachs, Germany

Supporting Information

ABSTRACT: The similarity and differences of the three host compounds **H1** = 9,9′-(biphenyl-2,2′-diyl)difluoren-9-ol, **H2** = 2,2′,7,7′-tetrabromo-9,9′-(biphenyl-2,2′-diyl)difluoren-9-ol, and **H3** = 2,2′,7,7′-tetra-*tert*-butyl-9,9′-(1,4-phenylene)-difluoren-9-ol which form inclusion compounds with 3-bromopyridine and its chloro-analogue guest are compared with respect to hydrogen bonding and halogen bonding. In all cases the hydrogen bonding motif (Host)O–H···O(Host)–H···N(Guest) predominates while the halogen···halogen interactions are of secondary importance in the packing of the structures. The structural data are supported by thermal analysis, Hirshfeld surface analysis, and IR spectroscopy.

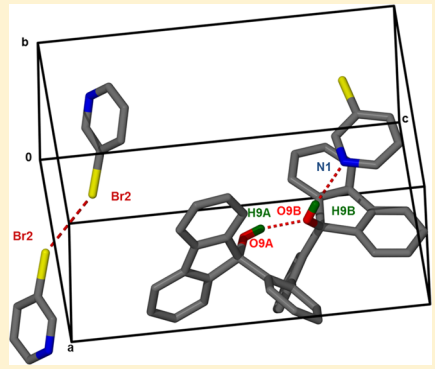

INTRODUCTION

The similarities and differences between hydrogen bonding and halogen bonding have attracted considerable interest. Both these intermolecular interactions are deemed important to the field of crystal engineering and the design of new solids with specific properties. An important review by Metrangolo and Resnati[1] points out the strong similarities between hydrogen bonding, a well-established secondary bond, and that afforded by halogen bonding. They indicate that they are complementary and that they can coexist.[2] Nangia has studied the packing of a series of 4-iodopyridine cocrystals with 4-nitrobenzoic acid, 3,5-dinitrobenzoic acid, as well as 4-nitrobenzamide and 4-iodobenzamide,[3] and the competing demands of halogen and hydrogen bonding were examined.[3] The complementary halogen and hydrogen bonding which occurs in structures of organo iodides with thioamides exhibits N–H···S and S···I interactions.[4]

A computational study of the complexes formed by hypohalous acids (HOX, X = F, Cl, Br) with formaldehydes found H···O and X···O contacts. The bond lengthening and shortening of the secondary interactions were analyzed, and the study concluded that the contribution from the electrostatic energy was larger in the H-bonded than in the X-bonded complexes.[5] The Cambridge Structural Database has been employed to analyze the interactions between molecules containing *p*-X-phenyl moieties (X = CH_3, F, Cl, Br, I, CH_2Cl_2) and electron rich atoms (halogen, N, O, P, S, As, Se, Te). The results show that the halogen bonding is highly directional and is potentially competitive with hydrogen bonding.[6] An extensive study of iodopyridinium tetrahalocuprate(II) salts, $(nIP)_2CuX_4$, with X = Cl and Br, and nIP = the iodopyridinium cation with n = 2, 3, 4, has been carried out. The crystallographic study was backed by theoretical calculations and concluded that as the halogen···halogen bonds became stronger as the corresponding N–H···X halogen bonds became weaker.[7] An interesting innovation is the use of halogen bonding in the design of functional materials. The high directionality of halogen bonding has been employed in the development of azobenzene-containing polymers for light-induced surface patterning, and the iodoethynyl moiety has been identified as an important component in future photoactive materials.[8] A series of cocrystals formed between acridine and *ortho*- or *meta*-halogen-substituted benzoic acids has been examined. The number and strengths of the hydrogen and halogen bonds were correlated with the melting points of the cocrystals.[9]

The interplay of the supramolecular motifs of polypyridyl metal complexes and halogen bonding has been analyzed, and the study concluded that it is possible to influence the aggregation of metal complexes by encapsulation in various halogen-bonded networks.[10]

Aakeröy has made a significant contribution to the hydrogen- versus halogen-bonding discussion in a series of publications dealing with several aspects of this subject. A group of compounds derived from pyridine and aminopyrimidines with iodo- and bromo-substituted benzoic acids allowed the precise analysis of hydrogen and halogen nonbonded interactions.[11]

Received: June 10, 2016
Revised: June 29, 2016
Published: July 13, 2016

ACS Publications © 2016 American Chemical Society

DOI: 10.1021/acs.cgd.6b00886
Cryst. Growth Des. 2016, 16, 4765–4771

Avoiding structural interference between the two kinds of secondary bonds is shown to be possible provided care is taken in designing tectons with appropriate geometric and electrostatic complementarity.[12,13] The ligands 3,3′-azobipyridine and 4,4′-azobipyridine were crystallized with a series of bifunctional donor molecules containing a halogen bond donor (I, Br) as well as a hydrogen bond donor (acid, phenol, oxime). It was found that the final result depended on the binding site of the acceptor molecule.[14]

The competitive nature of H-bonding and X-bonding was examined in two recent publications. Five heteroaryl-2-imidazoles were cocrystallized with 15 halogen-bond donors. The conclusion was that the X-bond is formed with the best acceptor site, showing that X-bonding can compete with strong H-bonding.[15] Recently a systematic study was performed in which molecules containing both H- and X-bond donors were crystallized with various monotopic and ditopic asymmetric acceptor molecules. The resulting crystals were examined by IR spectroscopy and X-ray diffraction, and the conclusions were derived with the additional information obtained from electrostatic potential considerations. The possibility of predicting the likely primary synthons in such a situation was enunciated.[16] This is a seminal publication which is likely to influence future research on this subject.

In this work we present the results of the cocrystals obtained between the host molecules and guests shown in Scheme 1.

Scheme 1. Host and Guest Compounds[a]

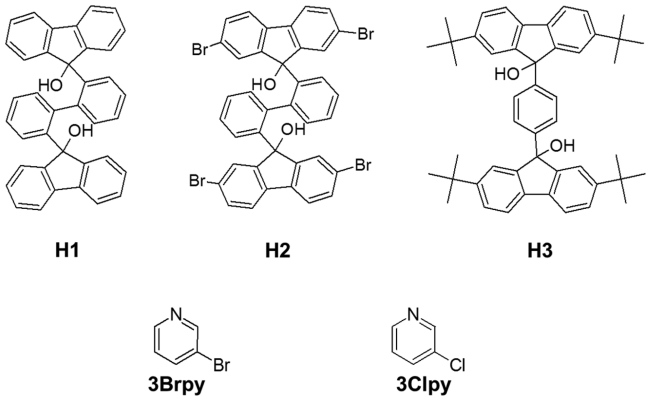

[a]**H1** = 9,9′-(Biphenyl-2,2′-diyl)difluoren-9-ol; **H2** = 2,2′,7,7′-tetrabromo-9,9′-(biphenyl-2,2′-diyl)difluoren-9-ol; **H3** = 2,2′,7,7′-tetra-*tert*-butyl-9,9′-(1,4-phenylene)difluoren-9-ol; **3Brpy** = 3-bromopyridine; **3Clpy** = 3-chloropyridine; Structure **1** = **H1·2(3Brpy)**; Structure **2** = **H1·2(3Clpy)**; Structure **3** = **H2·2(3Brpy)**; Structure **4** = **H2·2(3Clpy)**; Structure **5** = H3·2.5(3Brpy); Structure **6** = H3·2.5(3Clpy).

H1 and **H2** are similar in that the fluorenyl moiety in **H1** is substituted at two positions with Br. **H3** has a phenylene spacer between the fluorenyl groups, which are substituted with *tert*-butyl moieties at two positions. All three contain hydroxyl groups, making them useful and bulky diol compounds, which have proven to be a successful class of hosts in the synthesis of coordinato-clathrates.[17]

The hosts were chosen to study the relative importance of hydrogen versus halogen bonding in these systems, which were crystallized in the presence of the same guests: 3-bromopyridine and 3-chloropyridine.

EXPERIMENTAL SECTION

Materials. The host compounds **H1**,[18] **H2**,[19] and **H3**[20] were prepared following literature procedures. Single crystals of the inclusion compounds were obtained by dissolving these three host compounds in 3-bromopyridine or 3-chloropyridine, and allowing them to crystallize by slow evaporation.

X-ray Crystallography. Single crystal X-ray diffraction data were collected on a Nonius CCD[21] diffractometer for structure **4** and on a Bruker DUO APEX[22] diffractometer for structures **1**, **2**, **3**, **5**, and **6** using Mo Kα radiation (λ = 0.71073 Å) at a temperature of 173 K. The intensity data were collected by the phi scan and omega scan techniques, scaled, and reduced with DENZO-SMN[23] or SAINT-Plus.[24] The correction of the collected intensities for absorption was done using the SADABS program.[25]

The structures were solved by direct methods using SHELX-97[26] and refined using full-matrix least-squares methods in SHELXL.[26] The graphical interface used the program X-SEED.[27] All non-hydrogen atoms were refined isotropically or anisotropically depending on the occurrence of disorder in the structures. All hydrogen atoms were placed geometrically and with a riding model for their isotropic temperature factors. The O−H distances in the host compounds were fixed using the suggested formulas by Lusi and Barbour,[28] who studied the neutron data of the D−H···A systems, where D and A are donor and acceptor atoms. They derived correlation formulas which yield sensible positions of the H atoms in such systems, based on the distances between the donor and acceptor atoms. Diagrams were generated using POVRAY in X-SEED.[27]

Variable temperature PXRD scans were carried out on a Bruker D8 Advance powder diffractometer, scanning between 2θ 4° and 40°, at a scan speed of 1.8 deg 2θ min^{-1}.

RESULTS AND DISCUSSION

Structure **1**, **H1·2(3Brpy)**, crystallizes in the space group $P\bar{1}$ with Z = 2. The crystal data and refinement parameters for **1**−**6** are given in Table 1. The conformation of the host compound is governed by the intermolecular H-bond O9A−H9A···O9B and is characterized by the three torsion angles τ^1 (C10A−C11A−C11B−C10B), τ^2 (O9A−C9A−C10A−C11A), and τ^3 (O9B−C9B-C10B−C11B) shown in Figure 1. Table 2 summarizes the torsion angles for structures **1**−**4** containing this type of host.

The packing pattern for structures **1**−**4** is governed by the motif given schematically in Figure 2, which displays the intramolecular O−H···O of the host and the intermolecular (Host)−OH···N(Guest−site I). Site I, as defined by the midpoint of the pyridyl ring, lies at fractional coordinates *x*, *y*, *z* ≈ 0.29, 0.34, 0.89.

The second guest is not hydrogen bonded and lies at site II (*x*, *y*, *z* ≈ 0.38, 0.10, 0.11), but displays a Br···Br interaction with *d* = 3.50 Å. The geometry of the halogen···halogen (X···X) interactions is well established, and we have adopted the nomenclature established by Espinosa et al.[29] The van der Waals radii of Bondi[30] (radii in Å, H = 1.20, Cl = 1.75, Br = 1.85, I = 1.98, C = 1.70, N = 1.55, and O = 1.52) were employed, and we recorded the distances that were ≤ the sum of the van der Waals radii +5%. The asymmetric unit of structure **1** is shown in Figure 3, and displays the Host···Guest (Site I) as well as the Guest 2 (Site II), which has the Br···Br interaction across a center of inversion.

Structure **2**, in which the 3-chloropyridine guest replaces the 3-bromopyridine, is isomorphous to structure **1**. The host conformational parameters, the intramolecular H-bond and the (Host)−OH···N(Guest) H-bond, are similar to those of structure **1**, and the X···X interaction is the secondary bond Cl···Cl of 3.50 Å.

DOI: 10.1021/acs.cgd.6b00886
Cryst. Growth Des. 2016, 16, 4765−4771

Table 1. Crystallographic Data Parameters of the Host−Guest Complexes Studied

Compound	1	2	3	4	5	6
Code	**H1·2(3Brpy)**	**H1·2(3Clpy)**	**H2·2(3Brpy)**	**H2·2(3Clpy)**	**H3·2.5(3Brpy)**	**H3·2.5(3Clpy)**
Structural formula	$C_{48}H_{34}Br_2N_2O_2$	$C_{48}H_{34}Cl_2N_2O_2$	$C_{48}H_{30}Br_6N_2O_2$	$C_{48}H_{30}Br_4Cl_2N_2O_2$	$C_{60.5}H_{64}Br_{2.5}N_{2.5}O_2$	$C_{60.5}H_{64}Cl_{2.5}N_{2.5}O_2$
Host:Guest ratio	1:2	1:2	1:2	1:2	1:2.5	1:2.5
Molecular mass (g mol^{-1})	830.62	741.67	1146.14	1057.28	1057.92	946.77
Data collection temp (K)	173(2)	173(2)	173(2)	173(2)	173(2)	173(2)
Crystal system	Triclinic	Triclinic	Triclinic	Triclinic	Triclinic	Triclinic
Space group	$P\bar{1}$	$P\bar{1}$	$P\bar{1}$	$P\bar{1}$	$P\bar{1}$	$P\bar{1}$
a (Å)	8.3362(4)	8.2734(6)	9.9893(5)	10.0124(2)	12.6824(14)	12.6874(2)
b (Å)	14.9151(8)	14.908(10)	13.2183(7)	13.1044(3)	14.2258(15)	14.2151(2)
c (Å)	15.0908(8)	15.0045(10)	17.2447(8)	17.2882(4)	15.6077(16)	15.6234(3)
α (deg)	81.152(10)	81.366(10)	105.991(10)	106.146(3)	88.720(2)	88.467(3)
β (deg)	83.376(10)	83.341(10)	90.916(10)	91.110(3)	73.366(2)	73.364(3)
γ (deg)	85.262(10)	85.037(10)	105.326(10)	105.410(3)	85.890(2)	86.403(3)
Volume (Å^3)	1837.6(16)	1812.83(2)	2101.4(18)	2089.8(7)	2691.12(5)	2694.4(8)
Z	2	2	2	2	2	2
D_o, calc density (g cm^{-3})	1.501	1.359	1.812	1.680	1.306	1.167
Absorption coefficient (mm^{-1})	2.250	0.224	5.775	4.022	1.921	0.189
θ range	1.37−28.33	1.38−28.35	1.67−28.40	2.47−26.76	1.36−27.97	1.36−26.40
Reflections collected	38483	52387	57766	17633	72134	37165
No. data $I > 2\sigma(I)$	6988	7193	7920	5719	9658	6341
Final R indices $[I > 2\sigma(I)]$	0.0343	0.0510	0.0320	0.0339	0.0632	0.0835
R indices (all data)	0.0527	0.0656	0.0534	0.0764	0.0851	0.1413
Goodness-of-fit on F^2	1.039	1.034	1.027	0.994	1.057	1.048
CCDC no.	1483233	1483234	1483235	1483236	1483237	1483238

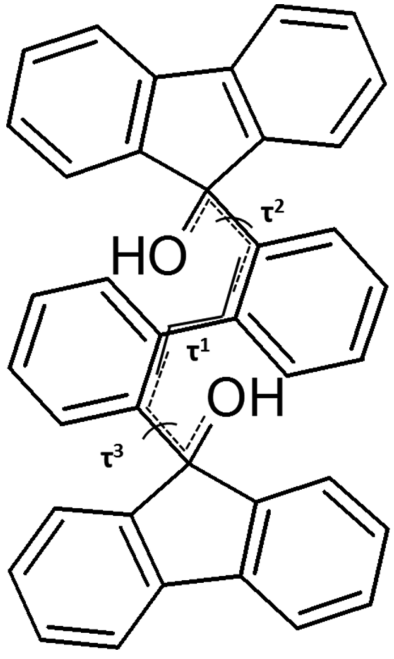

Figure 1. Conformation of the host compounds **H1**, **H2**.

Table 2. Torsion Angles Describing Host H1 and H2 Conformations

Compound	τ^1/deg	τ^2/deg	τ^3/deg
1	89.9(2)	−25.2(2)	−34.5(2)
2	90.8(2)	−25.5(2)	−33.4(2)
3	91.3(3)	−21.1(3)	−16.2(3)
4	92.0(7)	−20.9(7)	−16.0(7)

Structure **3** contains host molecules which have been doubly substituted with Br on each fluorenyl moiety. The internal host

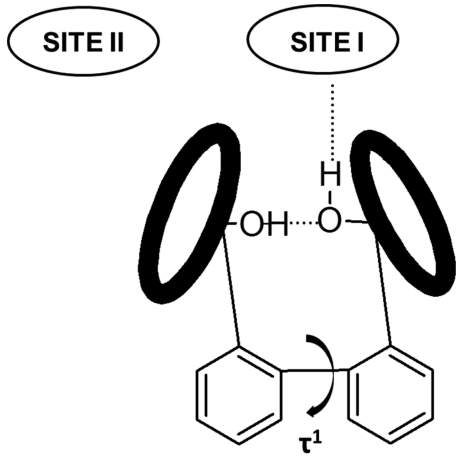

Figure 2. Schematic representation of the host conformations. The fluorenyl moieties are shown as bold ovals, while the guests are located as sites I and II.

conformation is similar to structure **1** (Table 2), but there are additional X···X contacts. These are listed in Table 3 and are shown as dotted lines in the projection of the structures, viewed down [100] in Figure 4. Structure **4** is isomorphous to structure **3** and has similar hydrogen bonds and X···X bonds, although the Br···Cl interactions are weaker than their corresponding Br···Br contacts.

The host in structures **5** and **6** comprises two fluorenyl moieties connected by a phenylene spacer and decorated by *tert*-butyl groups on the fluorenyl moieties. The stoichiometry displays a host:guest ratio of 1:2.5. One of the guests is disordered and is located on a center of inversion at Wyckoff position c. For structure **5**, the *tert*-butyl group is disordered over two positions, with site occupancies of 73% and 27%. Interestingly, the hydroxyl moieties of the host display a *cis*-

DOI: 10.1021/acs.cgd.6b00886
Cryst. Growth Des. 2016, 16, 4765−4771

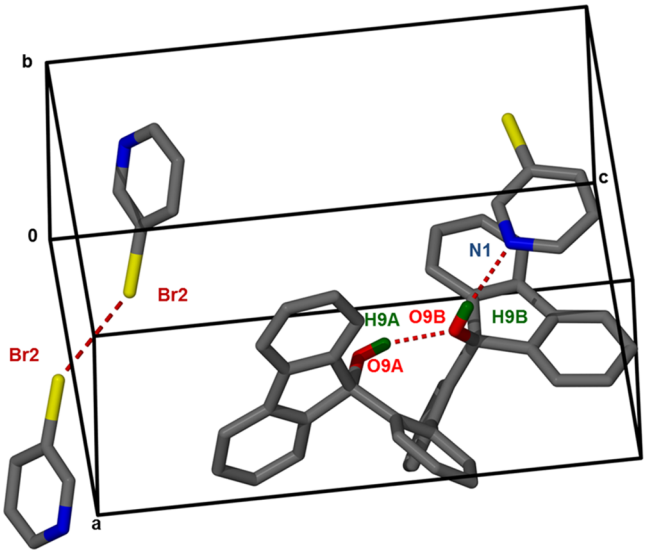

Figure 3. Host molecule in structure **1** showing the intramolecular bonding to one guest and the Br···Br interaction of the second guest.

conformation and two host molecules arrange themselves about a center of inversion at Wyckoff position b so that the result reproduces the motif shown previously in structures **1**–**4** (Figure 5).

This is shown in Figure 6. The structural motif is essentially that of a dimer comprising two H-bonded host molecules arranged about a center of inversion, with the guests attached as H-bonded appendages (in graphset notation this is $R_2^2(18)$ $D_1^1(3)$),[31] while the other guests do not display H-bonding to the host molecules.

Thermal Analysis. Each inclusion compound was subjected to thermal gravimetry (TG) and differential scanning calorimetry (DSC), using TA Instruments TGA Q500 and DSC Q200. The temperature range was 25 °C to 350 °C at a constant heating rate of 10 °C min^{-1}, and the purging gas was dry N_2 flowing at 60 mL min^{-1}.

The TG/DSC trace for **H1·2(3Brpy)** is shown in Figure 7(a) and is described in detail because the result is atypical of this series of compounds. The TG curve is complex, showing that the loss of the 3-bromopyridine is a multistep process. This is reflected in the DSC curve, which shows two distinct endotherms labeled **A** and **B**, peaking at 100.1 and 129.0 °C, respectively. This is followed by a series of small peaks between 138 and 250 °C, at which point we obtained endotherm **C** corresponding to a melting point of the host at 252.2 °C. This endotherm, however, does not correspond to the melting point of the apohost, which is 286.7 °C. We therefore subjected the compound to the hot stage miscroscopy (HSM) and noted a number of events which could not be discerned from the DSC trace alone. The HSM shows bubbles escaping the crystal of this compound which correspond to endotherms **A** and **B**. At approximately 205 °C we observed a first melting which corresponds to the area of multiple endothermic peaks. The second melting corresponded with endotherm **C**. This was followed by a recrystallization and a third melting at ≈304 °C. Neither of these latter two phenomena are discernible in the DSC trace.

In addition, we carried out a complete powder X-ray diffraction analysis (PXRD) at variable temperatures from 30 to 300 °C in steps of 10 °C. There are three changes in the diffraction pattern which occur in the ranges (80°−90°), (130°−140°), and (250°−260°). These equate to the three endotherms **A**, **B**, and **C** in Table 4. The variable temperature PXRD patterns have been added to the Supporting Information as Figure S5.

The TG/DSC of **H1·2(3Clpy)**, shown in Figure 7(b), is easier to interpret. It again shows a complex TG curve in that the guest loss occurs in two steps. The DSC trace exhibits the two corresponding endotherms **A** and **B**. The third endotherm **C** peaks at 294.6 °C and is associated with the melt of the host. We also carried out HSM analysis on this compound, and we observed the bubbles of the guest loss corresponding to endotherms **A** and **B** and the final melting point of the host at endotherm **C**.

Table 3. Hydrogen and Halogen Bonding Studied

Compound	Donor (D)	Acceptor (A)	D···A/Å	D−H/Å	H···A/Å	D−H···A /deg	X···X	d/Å	θ_1/θ_2	$D - \sum$vdw/Å	%
1	O9A	O9B	2.749(2)	0.971(1)	1.801(1)	165(7)	$Br_2\cdots Br_2$	3.501(2)	148/148	−0.200	−5.4
	O9B	N1	2.909(2)	0.953(1)	1.988(1)	162(7)	-	-	-	-	-
2	O9A	O9B	2.757(1)	0.957(1)	1.819(1)	166(1)	$Cl_2\cdots Cl_2$	3.499(3)	148/148	−0.001	−0.03
	O9B	N1	2.920(1)	0.960(1)	1.966(1)	172(1)	-	-	-	-	-
3	O9A	O9B	2.688(2)	0.978(1)	1.728(1)	166(1)	$Br_1\cdots Br_3$	3.817(2)	140/112	+0.117	+3.2
	O9B	N1	2.724(3)	0.992(1)	1.748(1)	167(1)	$Br_2\cdots Br_4$	3.590(2)	76/33	−0.110	−3.0
							$Br_3\cdots Br_6$	3.891(2)	119/80	+0.191	+5.2
							$Br_5\cdots$O9A	3.447(2)	172/107	+0.077	+2.3
4	O9A	O9B	2.718(2)	0.972(1)	1.755(1)	170(1)	$Br_1\cdots Br_3$	3.795(9)	141/112	+0.095	+2.6
	O9B	N1	2.732(3)	0.993(1)	1.747(1)	171(1)	$Br_2\cdots Br_4$	3.587(8)	158/78	−0.113	−3.1
							$Br_2\cdots Cl_1$	3.865(2)	130/73	+0.265	+7.4
							$Br_3\cdots Cl_2$	3.904(3)	120/80	+0.304	+8.4
							$Cl_1\cdots$O9A	3.526(2)	172/106	+0.256	+7.8
5	O9A	O9B[a]	2.792(2)	0.965(1)	1.830(4)	175(3)	-	-	-	-	-
	O9B[a]	N1	2.766(3)	0.981(1)	1.793(7)	171(4)	-	-	-	-	-
6	O9A	O9B[a]	2.784(3)	0.965(11)	1.822(5)	175(4)	-	-	-	-	-
	O9B	N1	2.776(4)	0.973(11)	1.811(8)	171 (4)	-	-	-	-	-

[a] $-x, -y, 1 - z$.

DOI: 10.1021/acs.cgd.6b00886
Cryst. Growth Des. 2016, 16, 4765−4771

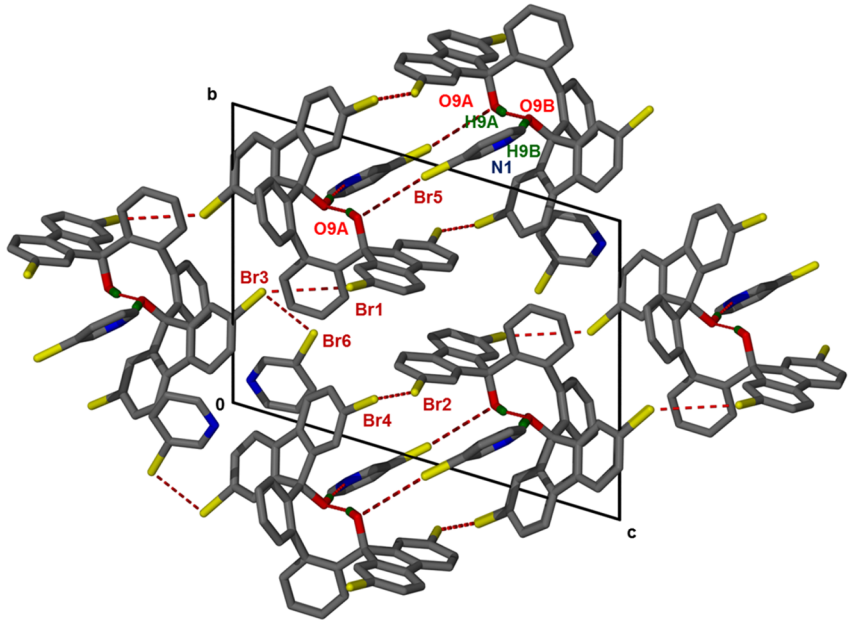

Figure 4. Structure **3** viewed along [100]. H-bonds and X-bonds are shown in dotted lines.

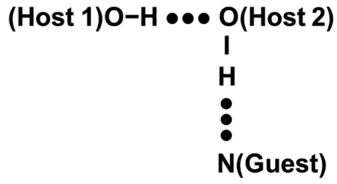

Figure 5. Hydrogen bonding motif in structures **1**–**4**.

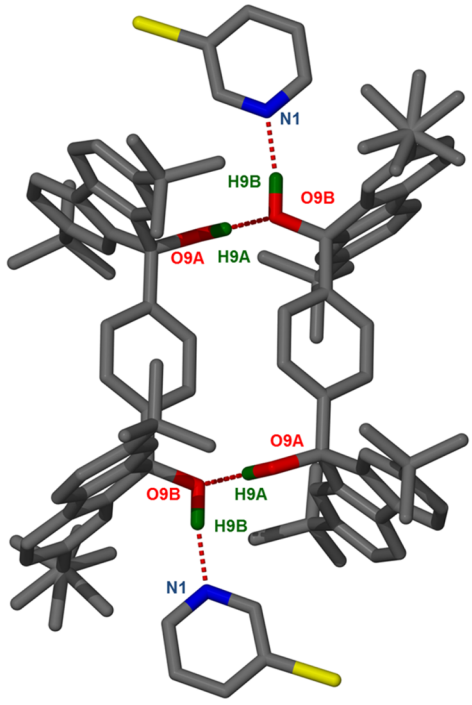

Figure 6. Hydrogen bonding in structure **5**.

The results of all the thermal analyses are given in Table 4. The observed versus calculated mass losses are in good agreement, as are the pairs of endotherms corresponding to the melting point of **H2** and **H3**. The difference in the melting points of **H1** has been discussed above. The interesting point of Table 4 lies in the comparison of the peak temperatures of **H1·2(3Brpy)** at 100.1 °C and of **H2·2(3Brpy)** at 141.3 °C. This shows that the guest of the latter compound is held more tightly than in the former, and it may be surmised that this is because it displays a Br···Br interaction in addition to the host–guest H-bonding. The same phenomenon is discernible for structures **2** and **4**, and can be applied to the second endotherms **B**.

For structures **5** and **6**, the complex first endotherms correspond to the loss of 1.5 guests which are not hydrogen bonded, while the second endotherm **B** peaks at a considerably higher temperature in both compounds and is associated with the H-bonded guests. The thermal TG/DSC traces for the compounds corresponding to structures **3**–**6** have been deposited as Supporting Information.

Hirshfeld Surface Analysis. We compared the packing of structures **1** and **3** by using the program CrystalExplorer[32−34] in order to discern the effect of the Br atoms on **H2**. In each analysis the Hirshfeld surface was drawn round the host molecules, and the resulting fingerprint plots are shown in Figure 8(a) and (b) while the percentage of the reciprocal contacts are given in Table 5a and b. The spikes labeled ① in both structures correspond to the (Host)O–H···N(Guest) H-bonds. The important feature, however, is the peak corresponding to the H···H interactions, labeled ② in Figure 8, which is much stronger in structure **1** (53.7%) than in structure **3** (33.7%), as given by Table 5a and b. This differential is also reflected in the C···H interactions labeled ③ and amounting to 28.8% and 17.8% for structures **1** and **3**, respectively. This is due to the Br···Br interactions, which only occur in structure **3** (4.9%) and which have the effect of keeping the host molecules apart, reducing their H···H and C···H contacts.

Infrared Spectroscopy. We confirmed the presence of host–guest hydrogen bonding by IR spectroscopy. We measured the spectra on a PerkinElmer FT-IR C88996 spectrometer, including the spectrum of the apohost **H1**, whose crystal structure has been previously elucidated.[35] The

DOI: 10.1021/acs.cgd.6b00886
Cryst. Growth Des. 2016, 16, 4765−4771

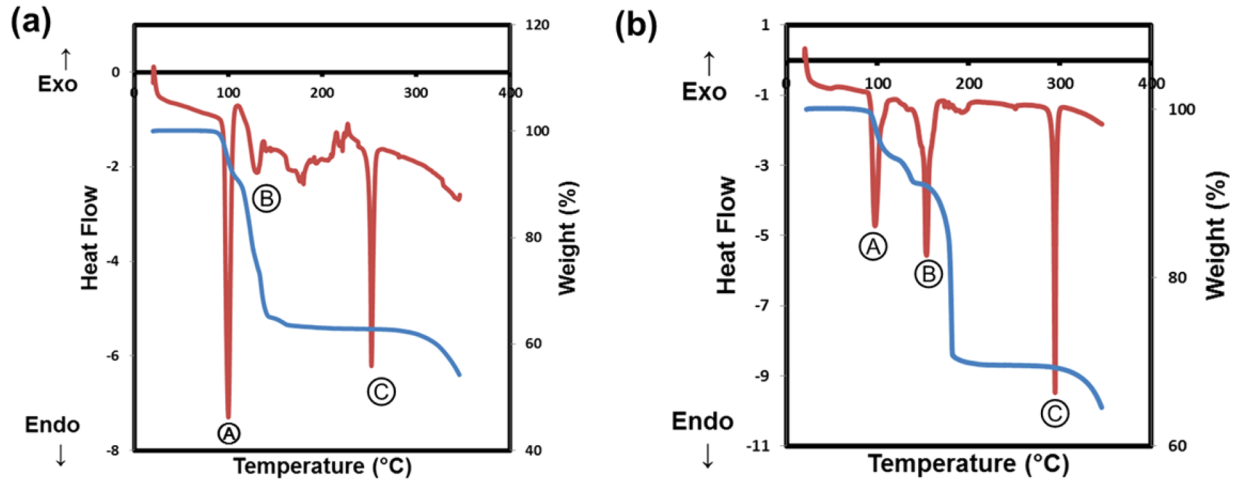

Figure 7. TG (blue) and DSC (red) traces for **H1·2(3Brpy)** and **H2·2(3Brpy)**.

Table 4. Thermal Analysis Results

Structure	Compound	Mass loss obsd %	Mass loss calc %	Tpeak/°C Endo A	Tpeak/°C Endo B	Tpeak/°CEndo C
1	**H1·2(3Brpy)**	36.7	38.1	100.1	129.0	252.2
2	**H1·2(3Clpy)**	30.1	30.6	97.1	153.7	294.6
3	**H2·2(3Brpy)**	27.5	27.6	141.3	166.3	358.3
4	**H2·2(3Clpy)**	20.8	21.5	130.6	156 (trace)	359.0
5	**H3·2.5(3Brpy)**	36.3	37.3	98.0	174.4	331.2
6	**H3·2.5(3Clpy)**	29.1	30.0	97.9	170.3	331.8

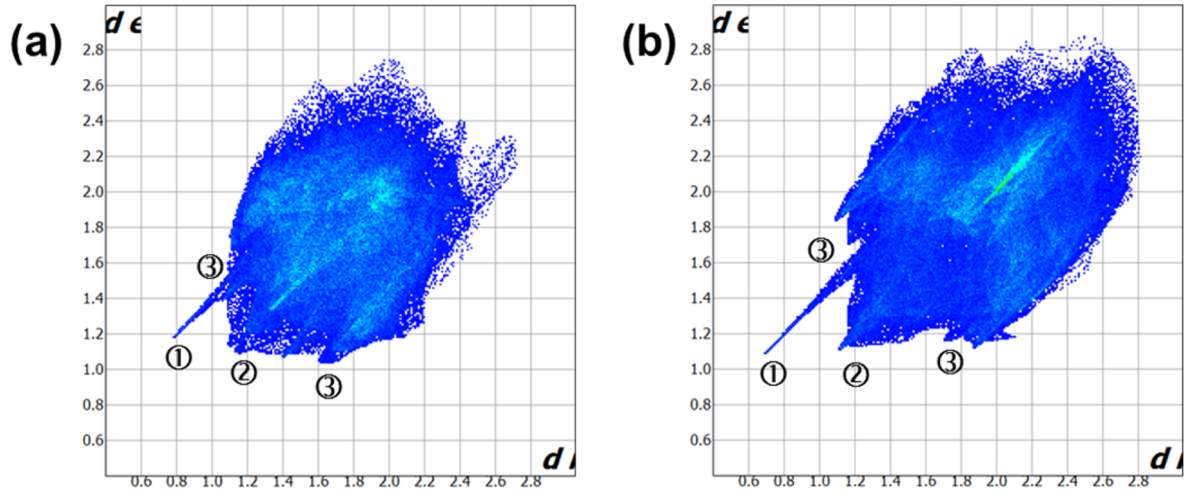

Figure 8. Fingerprint plots with **H1** in structure 1 and **H2** in structure **2** as targets. Spikes labeled ①, ②, and ③ correspond to H···N, H···H, and C···H interactions, respectively.

structure crystallizes in $P2_1/c$ with $Z = 8$ and has two molecules in the asymmetric unit. Each displays a conformation similar to that of **H1** in this work, with an intramolecular (Host)O−H···O−H(Host) hydrogen bond. However, the second hydroxyl group is not hydrogen bonded to another host molecule. The IR spectrum of the **H1** apohost displayed an absorption peak at 3417.5 cm^{-1}, corresponding to the "free" hydroxyl group, and a second peak at 3056 cm^{-1}, assigned to the hydroxyl moiety which takes part in the intramolecular H-bond.

For the compound **H1·2(3Brpy)**, structure **1**, the IR spectrum displays a peak at 3055.1 cm^{-1}, corresponding to the intramolecular H-bond, and one at 3340.9 cm^{-1}, assigned to the (Host)···N(Guest) H-bond. The IR spectra of all the compounds follow the pattern described above, and the results and the assignments of the absorption peaks are given in the Supporting Information (Table S1).

■ CONCLUSION

The compounds **H1**, **H2**, and **H3** are successful host compounds which display both similarities and differences. All three carry hydroxyl moieties rendering them good H-bond donors. **H2**, in addition, carries four Br atoms, giving it the possibility of halogen···halogen interactions with the guests 3-bromopyridine and 3-chloropyridine, to which all the hosts were exposed.

H1 displayed an intramolecular (Host)O−H···O−H(Host) H-bond and an O−H···N(Guest) H-bond. This motif was repeated with **H2**, which in addition displays a number of X···X

DOI: 10.1021/acs.cgd.6b00886
Cryst. Growth Des. 2016, 16, 4765−4771

Table 5. Percentage Interactions between Host Atoms (in) and Guest Atoms (out) in (a) Structure 1 and (b) Structure 3

	Out %				
In	C	H	O	N	Br
		(a) Structure **1**			
C	4.5	28.8	0.0	0.2	1.9
H	28.8	53.7	3.8	2.2	4.9
O	0.0	3.8	0.0	0.0	0.0
		(b) Structure **3**			
C	2.7	17.8	0.0	0.5	10.9
H	17.8	33.7	1.1	3.1	24.8
O	0.0	1.1	0.0	0.0	0.6
Br	10.9	24.8	0.6	0.0	4.9

interactions. **H3**, which by virtue of its phenyl spacer cannot form an intramolecular H-bond, nevertheless achieves the same hydrogen bonding motif as **H1** and **H2** by forming dimers. This hydrogen bonding synthon dominates the packing of these three structures, showing the X···X interactions to be of secondary importance in the assembly of the structures. The crystallographic results are complemented by packing analyses, thermal data, and IR spectroscopy.

■ ASSOCIATED CONTENT

Supporting Information

The Supporting Information is available free of charge on the ACS Publications website at DOI: 10.1021/acs.cgd.6b00886.

TG/DSC traces, variable temperature PXRD patterns, and IR wavenumber table (PDF)

Accession Codes

CCDC 1483233−1483238 contain the supplementary crystallographic data for this paper. These data can be obtained free of charge via www.ccdc.cam.ac.uk/data_request/cif, or by emailing data_request@ccdc.cam.ac.uk, or by contacting The Cambridge Crystallographic Data Centre, 12 Union Road, Cambridge CB2 1EZ, UK; fax: +44 1223 336033.

■ AUTHOR INFORMATION

Corresponding Author

*Tel: +27 21 650 5893. Fax: +27 21 650 2569. E-mail: luigi.nassimbeni@uct.ac.za.

Notes

The authors declare no competing financial interest.

■ ACKNOWLEDGMENTS

We thank the University of Cape Town and the National Research Foundation (South Africa) for funding.

■ REFERENCES

(1) Metrangolo, P.; Neukirch, H.; Pilati, T.; Resnati, G. *Acc. Chem. Res.* **2005**, *38*, 386−395.
(2) Metrangolo, P.; Resnat, G. *Science* **2008**, *321*, 918−919.
(3) Saha, B. K.; Nangia, A.; Jaskólski, M. *CrystEngComm* **2005**, *7* (58), 355−358.
(4) Arman, H. D.; Gieseking, L.; Hanks, T. W.; Pennington, W. T. *Chem. Commun.* **2010**, *46*, 1854−1856.
(5) Li, Q.; Xu, X.; Liu, T.; Jing, B.; Li, W.; Cheng, J.; Gong, B.; Sun, J. *Phys. Chem. Chem. Phys.* **2010**, *12*, 6837−6843.
(6) Mooibroek, T. J.; Gamez, P. *CrystEngComm* **2013**, *15*, 4565−4570.
(7) Awwadi, F. F.; Taher, D.; Haddad, S. F.; Turnbull, M. M. *Cryst. Growth Des.* **2014**, *14*, 1961−1971.
(8) Saccone, M.; Dichiarante, V.; Forni, A.; Goulet-Hanssens, A.; Cavallo, G.; Vapaavuori, J.; Terraneo, G.; Barrett, J. C.; Resnati, G.; Metrangolo, P.; Priimagi, A. *J. Mater. Chem. C* **2015**, *3*, 759−768.
(9) Kowalska, K.; Trzybiński, D.; Sikorski, A. *CrystEngComm* **2015**, *17*, 7199−7212.
(10) Pfrunder, M. C.; Micallef, A. S.; Rintoul, L.; Arnold, D. P.; McMurtrie, J. *Cryst. Growth Des.* **2016**, *16*, 681−695.
(11) Aakeröy, C. B.; Schultheiss, N. C.; Rajbanshi, A.; Desper, J.; Moore, C. *Cryst. Growth Des.* **2009**, *9* (1), 432−441.
(12) Aakeröy, C. B.; Chopade, P. D.; Ganser, C.; Desper, J. *Chem. Commun.* **2011**, *47*, 4688−4690.
(13) Aakeröy, C. B.; Chopade, P. D.; Ganser, C.; Desper, J. *Cryst. Growth Des.* **2011**, *11*, 5333−5336.
(14) Aakeröy, C. B.; Panikkattu, S.; Chopade, P. D.; Desper, J. *CrystEngComm* **2013**, *15*, 3125−3136.
(15) Aakeröy, C. B.; Wijethunga, T. K.; Haj, M. A.; Desper, J.; Moore, C. *CrystEngComm* **2014**, *16*, 7218−7225.
(16) Aakeröy, C. B.; Spartz, C. L.; Dembowski, S.; Dwyre, S.; Desper, J. *IUCrJ* **2015**, *2*, 498−510.
(17) Weber, E. In *Inclusion Compounds*; Atwood, J. L., Davies, J. E. D., MacNicol, D. D., Eds.; Oxford University Press: Oxford, 1991; Vol *4*.
(18) Weber, E.; Skobridis, K.; Wierig, A.; Stathi, S.; Nassimbeni, L. R.; Niven, M. L. *Angew. Chem., Int. Ed. Engl.* **1993**, *32*, 606−608.
(19) Bourne, S. A.; Nassimbeni, L. R.; Niven, M. L.; Weber, E.; Wierig, A. *J. Chem. Soc., Perkin Trans. 2* **1994**, 1215−1222.
(20) Weber, E.; Nitsche, S.; Wierig, A.; Csöregh, I. *Eur. J. Org. Chem.* **2002**, *2002*, 856−872.
(21) *COLLECT*, data collection software; Nonius: Delft, The Netherlands, 1998.
(22) *APEX 2*, Version 1.0-27; Bruker AXS Inc.: Madison, WI, 2005.
(23) Otwinowski, Z.; Minor, W. In *Methods in Enzymology, Macromolecular Crystallography*; Carter, C. W., Jr., Sweet, R. M, Eds.; Academic Press: 1997; part A, Vol. *276*, p 307.
(24) *SAINT-Plus*, Version 7.12; Bruker AXS Inc.: Madison, Wisconsin, USA, 2004.
(25) Sheldrick, G. M. *SADABS: Program for Area Detector Adsorption Correction*; University of Göttingen: Germany, 1996; pp 33−38.
(26) Sheldrick, G. M. *SHELX-97: Program for Crystal Structure Solution and Refinement*; University of Göttingen: Germany, 1997; p 1456.
(27) Barbour, L. J. X-Seed − A Software Tool for Supramolecular Crystallography. *J. Supramol. Chem.* **2001**, *1*, 189−191.
(28) Lusi, M.; Barbour, L. J. *Cryst. Growth Des.* **2011**, *11*, 5515−5521.
(29) Bui, T. T. T.; Dahaoui, S.; Lecomte, C.; Desiraju, G. R.; Espinosa, E. *Angew. Chem., Int. Ed.* **2009**, *48*, 3838−3841.
(30) Bondi, A. *J. Phys. Chem.* **1964**, *68*, 441−451.
(31) Etter, M. C.; MacDonald, J. C.; Bernstein, J. *Acta Crystallogr., Sect. B: Struct. Sci.* **1990**, *B46*, 256−262.
(32) Spackman, M. A.; McKinnon, J. J. *CrystEngComm* **2002**, *4*, 378−392.
(33) McKinnon, J. J.; Spackman, M. A.; Mitchell, A. S. *Acta Crystallogr., Sect. B: Struct. Sci.* **2004**, *B60*, 627−668.
(34) McKinnon, J. J.; Jayatilla, D.; Spackman, M. A. *Chem. Commun.* **2007**, 3814−3816.
(35) Skobridis, K.; Theodorou, V.; Seichter, W.; Weber, E. *Cryst. Growth Des.* **2010**, *10*, 862−869.

DOI: 10.1021/acs.cgd.6b00886
Cryst. Growth Des. 2016, 16, 4765−4771

SUPPORTING INFORMATION

Hydrogen Bonding *versus* Halogen Bonding in Host-Guest Compounds.

Francoise M. Amombo Noa,[a] *Susan A. Bourne,*[a] *Hong Su,*[a] *Edwin Weber*[b] *and Luigi R. Nassimbeni* [a]*

[a]Centre for Supramolecular Chemistry Research, Department of Chemistry, University of Cape Town, Rondebosch 7701, South Africa. Email: luigi.nassimbeni@uct.ac.za.

[b]Institut für Organishe Chenie, TU Bergakademie Freiberg, Leipziger Strasse 29, D – 09596 Freiberg/Sachs, Germany.

Thermal Analysis

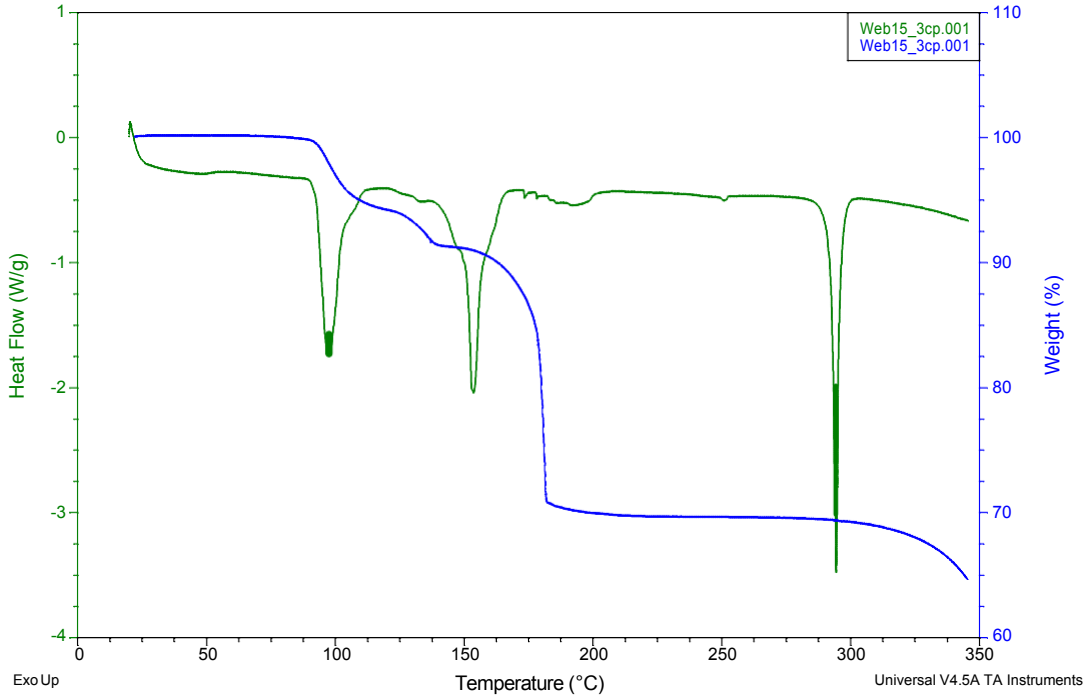

Figure S1 DSC and TG plots for **2**.

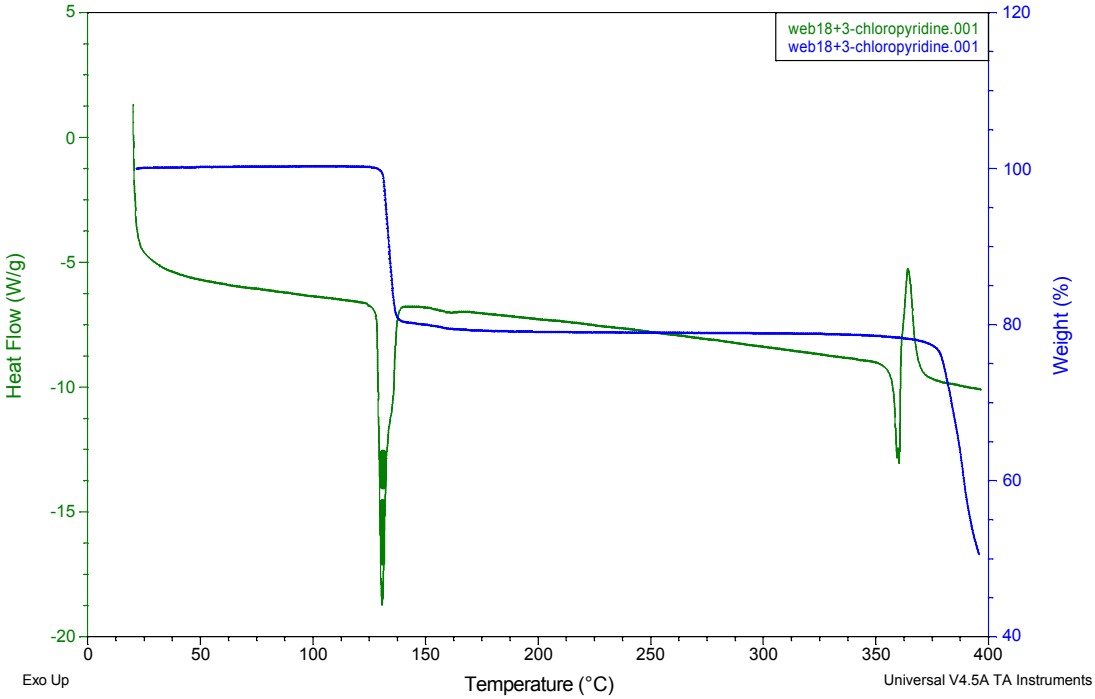

Figure S2 DCS and TG plots for **4**.

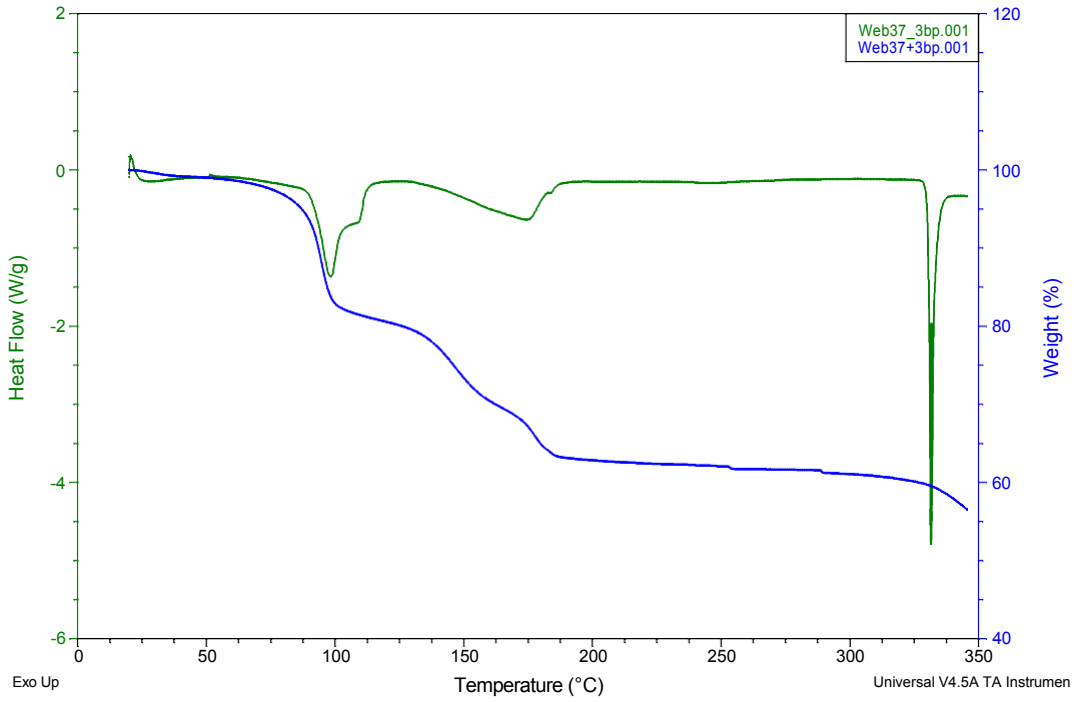

Figure S3 DSC and TG plots for **5**.

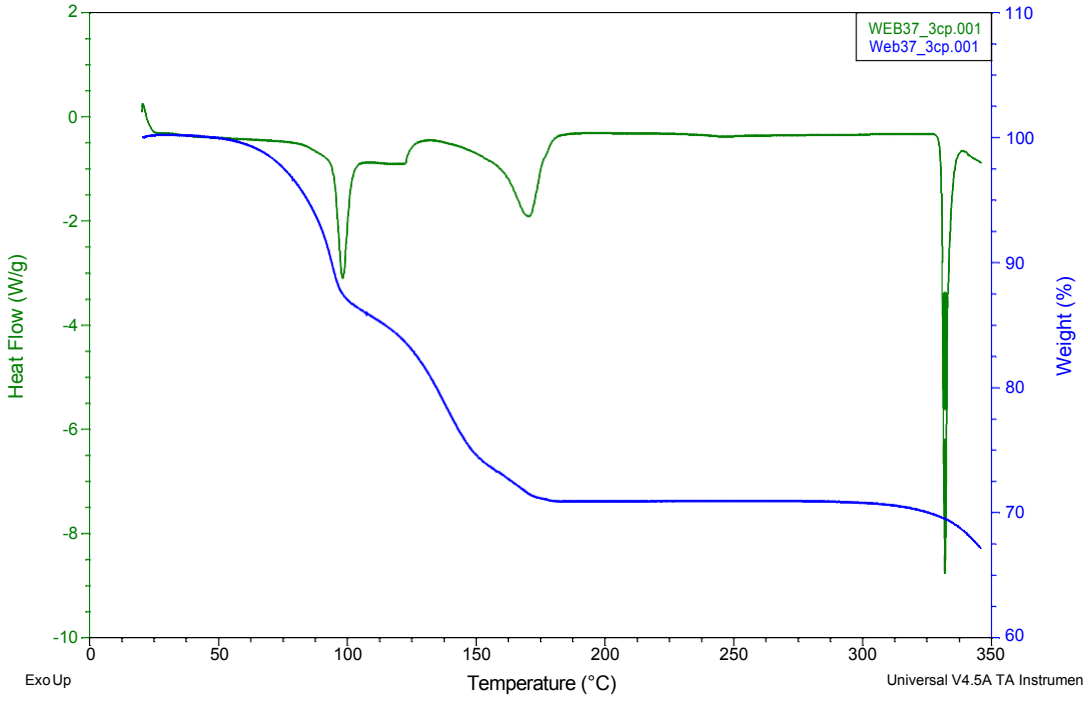

Figure S4 DSC and TG plots for **6**.

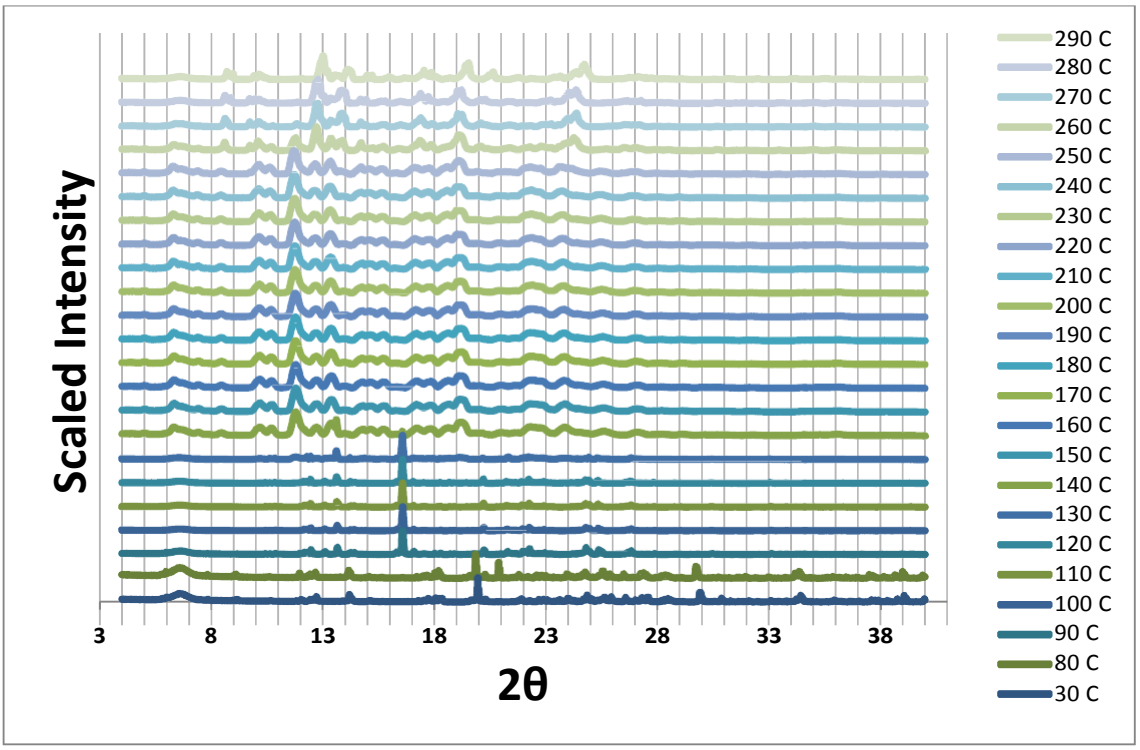

Figure S5. Variable temperature PXRD patterns of **H1•2(3Brpy)** in the range of 30-290 °C.

Table S1: IR wavenumbers

Compound	Crystal structure	Peak 1 (cm^{-1})	Assignemt	Peak 2 (cm^{-1})	Assignment
H1 apohost	Reference 32	3417.5	'Free' O-H	3056.2	Intramolecular O-H···O
H1·2(3Brpy)	**1**	3340.9	O-H···N	3055.1	O-H···O
H1·2(3Clpy)	**2**	3341.5	O-H···N	3060.3	O-H···O
H2 apohost	**-**	3558.9	'Free' O-H	2975.2	O-H···O
H2·2(3Brpy)	**3**	3250.1	O-H···N	3150.2	O-H···O
H2·2(3Clpy)	**4**	3255.9	O-H···N	2989.5	O-H···O
H3 apohost	-	3628.0	'Free' O-H	3297.1	O-H···O
H3·2.5(3Brpy)	**5**	3320.2	O-H···N	3032.1	O-H···O
H3·2.5(3Clpy)	**6**	3310.6	O-H···N	3053.9	O-H···O

CHAPTER VII

Secondary Interactions in Halogenated Werner Clathrates

(Amombo Noa, F. M.; Bourne, S. A.; Hong Su.; Nassimbeni, L. R. *Cryst. Growth Des*. 2017, 17 (4), 1876 – 1883).

7.1 Summary

Werner clathrates are coordination complexes with the general formula MX_2A_4, where M is a divalent cation (Cr, Co, Fe, Mn, Ni, Fe), X denotes anionic ligands (NCS^-, NCO^-, NO_3^-, Cl^-, Br^-, I^-, H_2O, CH_3CN) and A is usually a neutral base, such as substituted pyridines, α-arylkyamines or isoquinoline.

Eight halogenated Werner clathrates were synthesised by crystallisation of the $NiBr_2/NiCl_2/NiI_2$ with 3PIC/4PIC/4IPY as neutral bases and $H_2O/MeOH/CH_3CN$ as solvents. In some of these Werner clathrates moles of I_2 were added to the synthesis to form polyiodide Werner clathrates.

The structures were characterised via single x-ray diffraction, thermal analysis and solid vapour kinetics of formation. When analysing the structures, halogen⋯halogen interactions and hydrogen bonds were both present. The last two Werner complexes (**7** and **8**) were the polyiodide complexes, where each contain two separate tri-iodide molecules. In the last structure, the polyiodide complex is disordered over three positions.

Thermal analysis of all the obtained compounds was different and for some was very complex. The most important ones were discussed in the main manuscript and the rest in the supporting information.

Kinetics of formation was carried out in a desiccator at 80 °C for $NiBr_2$ and $NiCl_2$ with 4PIC. Their rate laws were established and the results revealed that the compound formed between $NiBr_2$ and 4PIC reaction was slower than the one obtained from $NiCl_2$ and 4PIC. This is due to the steric hindrance poser by Br^- versus the Cl^- ions on the Ni^{2+} ion.

The original article and the supporting information is provided below.

CRYSTAL GROWTH & DESIGN

Article

pubs.acs.org/crystal

Secondary Interactions in Halogenated Werner Clathrates

Francoise M. Amombo Noa, Susan A. Bourne, Hong Su, and Luigi R. Nassimbeni*

Centre for Supramolecular Chemistry Research, Department of Chemistry, University of Cape Town, Rondebosch 7701, South Africa

Supporting Information

ABSTRACT: Halogenated Werner clathrates which contain Cl, Br, and I as part of the host and guest moieties have been synthesized and characterized by single X-ray diffraction, thermal analysis, and solid−vapor kinetics of formation. The compounds derived from NiI_2 are ionic, forming I^- salts and which yielded tri-iodide anions by the addition of I_2. Secondary interactions involving halogen···halogen and hydrogen bonds have been fully characterized and the structures were correlated with the thermal decomposition results.

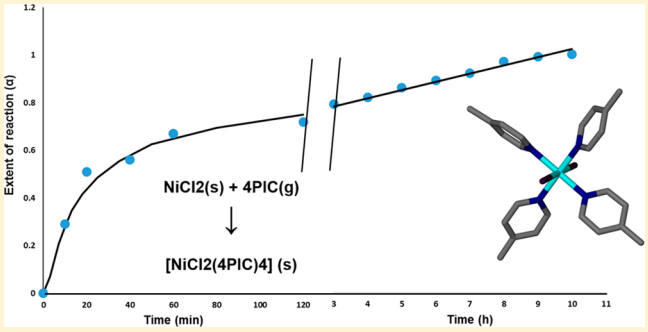

INTRODUCTION

Werner clathrates are coordination compounds of general formula MX_2A_4, where M is a divalent cation (Fe, Co, Ni, Zn, Mn, Hg, Cr), X is an anionic ligand (NCS^-, NCO^-, CN^-, NO_3^-, Cl^-, Br^-, I^-) and A is a neutral base, typically a substituted pyridine, α-arylalkylamine, or isoquinoline. These compounds were found to be efficient hosts which enclathrated a variety of aromatic guest molecules.[1] Significant work employing α-arylakylamines was also undertaken as the neutral bases showed that these hosts also formed inclusion compounds with the xylenes, ethyltoluenes, diethylbenzenes, cymenes, and other substituted benzenes. Fundamental work on the physical chemistry of these compounds was carried out by J. Lipkowski, who has reviewed their fundamental properties,[2,3] and outlined their structures, absorption isotherms, thermal properties, phase studies, and kinetics of guest enclathration and desorption. Soldatov[4] revisited the host compound $[Ni(NCS)_2(4\text{-methylpyridine})_4]$ and studied its polymorphic phases and their reactivity toward guests. Lusi and Barbour[5] employed the phenyl derivative $[Ni(NCS)_2(4\text{-phenylpyridine})_4]$ to discriminate between xylene isomers.

Barbour et al. also used solid−solid grinding methods to synthesize $[NiCl_2(4\text{-PhPy})_4]$, $[CoCl_2(4PhPy)_4]$, the solid solution $[Ni_{0.5}Co_{0.5}Cl_2(4PhPy)_4]$, and studied their clathrates with the isomers of xylene as guests.[6] More recently, Wicht[7,8] has investigated the inclusion of xylenes by $[Ni(NCS)_2(isoquinoline)_4]$ and has explored the host $[Ni(NCS)_2(4\text{-vinylpyridine})_4]$ in its clathrate formation with a series of polyaromatic hydrocarbons. The host formed by $Ni(NCS)_2$ and the mixed ligands isoquinoline/4-phenylpyridine has been utilized to discriminate the xylene isomers and the desorption kinetics and packing properties have been examined.[9]

Significant contributions in the study of the structures and properties of transition metal coordination compounds which exhibit guest inclusion properties have been made by Iwamoto and Nishikiori. They studied Hofmann-type inclusion compounds which are formed by various combinations of amine or amine−metal(II) tetracyanometallate (II) hosts and aromatic guests.[10,11]

Iwamoto reviewed this subject[12] and discussed their history, structures, and thermal properties and summarized how the original compound can be modified to yield related clathrates.

In this work we discuss the secondary interactions occurring in the eight crystal structures **H1**−**H8** which are described in Scheme 1 with the various guests. The general formula MX_2A_4 has M = Ni (II), X = Cl^-, Br^-, H_2O, CH_3CN and several of the compounds are salts with I^- or I_3^-. Following our previous publication[13] we employed the van der Waals radii of Bondi[14] (radii in Å, H = 1.20, C = 1.70, O = 1.52, Cl = 1.75, Br = 1.85, I = 1.98). For halogen···halogen interactions we recorded X···X distances that were less than or equal to the sum of the van der Waals radii plus 5%. The same criterion was adopted for C−H···A interactions (A = O, Cl, Br).

EXPERIMENTAL SECTION

Synthesis and Characterization of Compounds 1−8. The chemicals utilized for this study were purchased from Sigma-Aldrich and used without further purification.

$[NiBr_2(4PIC)_4]$ (1). $NiBr_2$ (40 mg, 0.183 mmol) was dissolved in 10 mL of distilled water, and then 5 mL of 4-picoline (4PIC) and 10 mL of methanol (MeOH) were added to the solution. The mixture was heated at 60 °C for 20 min. The solution was filtered and allowed to evaporate. Blue crystals were obtained after a week.

$[NiCl_2(4PIC)_4]\cdot 1/2H_2O$ (2). $NiCl_2\cdot 6H_2O$ (40 mg, 0.168 mmol) was dissolved in a 50:50 (v/v) mixture of methanol and water as a solvent, and 7 mL of 4PIC was added to the solution. Green crystals were obtained via slow evaporation under ambient temperature after a week, yielding a hydrate of compound **2**.

Received: December 16, 2016
Revised: February 9, 2017
Published: February 13, 2017

ACS Publications © 2017 American Chemical Society

DOI: 10.1021/acs.cgd.6b01844
Cryst. Growth Des. 2017, 17, 1876−1883

Chart 1. Host and Guest Compounds Studied

Compound number	Host	Guest	
1	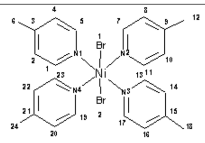	-	Apohost
Tetra(4-methylpyridine)nickel(II) dibromide **H1**			
2	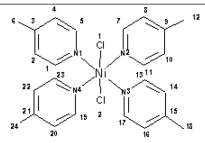	½H2O	Hemihydrate
Dichlorido tetra(4-methylpyridine)nickel(II) hemihydrate **H2·½H$_2$O**			
3	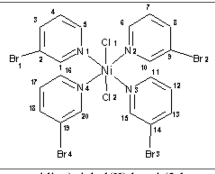		Clathrate
Dichlorido tetra(3-bromopyridine)nickel(II) hemi (3-bromopyridine) clathrate **H3·½(3BrPY)**			
4	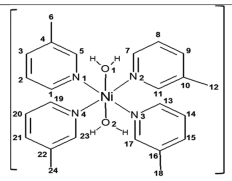	$2I^-$	Salt
Diaquatetra(3-methylpyridine)nickel(II) diiodide **H4^{2+}·2I$^-$**			
5	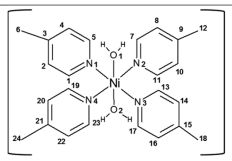	 2.5H$_2$O	Clathrate of Salt
Diaquatetra(4-methylpyridine)nickel(II) diiodide – di(4-methylpyridine) – (water) **H5^{2+}·2I$^-$·2(4PIC)·2.5H$_2$O**			
6	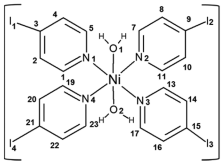		Clathrate of Salt
Diaquatetra(4-iodopyridine)nickel(II) diiodide – tri(4-iodopyridine) **H6^{2+}·2I$^-$·3(4IPY)**			
7	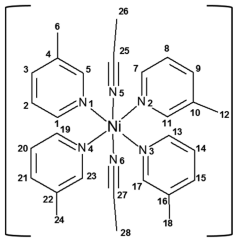	-	Salt
Di(acetonitrile) tetra(3-methylpyridine) bis(tri-iodide) **H7^{2+}·2I$_3^-$**			
8	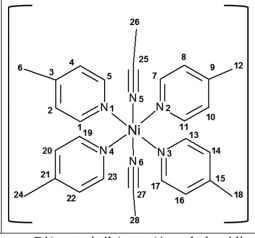	-	Salt
Di(acetonitrile) tetra(4-methylpyridine) bis(tri-iodide) **H8^{2+}·2I$_3^-$**			

*[NiCl$_2$(3Brpy)$_4$]·1/2(3BrPY) (**3**).* NiCl$_2$·6H$_2$O (40 mg, 0.168 mmol) was dissolved in a 50:50 (v/v) mixture of MeOH and water, and 7 mL of 3-bromopyridine (3BrPY) was also added to the solution. The dilute solution was left to evaporate and green crystals were obtained after 10 days.

*[Ni(H$_2$O)$_2$(3PIC)$_4$]$^{2+}$2I$^-$ (**4**).* NiI$_2$ (40 mg, 0.128 mmol) was dissolved in 15 mL of distilled water, and 7 mL of 3-picoline (3PIC) in MeOH. The two solutions were mixed, heated at approximately 60 °C, and filtered. Blue crystals were obtained after few days.

*[Ni(H$_2$O)$_2$(4PIC)$_4$]$^{2+}$2I$^-$·2(4PIC)·2.5H$_2$O (**5**).* NiI$_2$ (40 mg, 0.128 mmol) was dissolved in 15 mL of distilled water and 7 mL of 4PIC in MeOH. The same conditions as compound **4** were used and a pentahydrate was yielded as blue crystals after 30 days.

*[Ni(H$_2$O)$_2$(4Ipy)$_4$]$^{+2}$2I$^-$·3(4IPY) (**6**).* The complex was prepared by dissolving 40 mg (0.128 mmol) of NiI$_2$ in distilled water and 104.96 mg (0.512 mmol) of 4-iodopyridine (4-IPY) in MeOH, and the two mixtures were added in a vial. The solution was allowed to slowly evaporate at ambient temperature, and black crystals were obtained after a month.

*[Ni(CH$_3$CN)$_2$(3PIC)$_4$]$^{2+}$2I$_3^-$ (**7**) and [Ni(CH$_3$CN)$_2$(4PIC)$_4$]$^{2+}$2I$_3^-$ (**8**).* These compounds were obtained by dissolving a mole of NiI$_2$ (40 mg, 0.128 mmol) in distilled water and 1 mol of iodine (I$_2$: 32.51 mg, 0.128 mmol) in acetonitrile. The two solutions were mixed and 7 mL of 3PIC/4PIC was added to the blend. Brown crystals were obtained from the solutions after 3 days.

Thermal Analysis. TG and DSC were performed on a Q500 (TA Instrument) and on a Q200 series instrument, respectively. A purge gas of dry nitrogen was employed at a flow rate of 60 mL min^{-1}. Thermal analysis experiments were conducted from 20 to 450 °C for all samples at a heating rate of 10 °C min^{-1}.

Structure Analysis. Single crystals used for X-ray diffraction analysis were selected utilizing a polarized light optical microscope. NiBr$_2$ and NiI$_2$ structures (**1**, **4**, **5**, **6**, **7**, and **8**) data collection was conducted using a Bruker DUO APEX[15] and NiCl$_2$ complexes (**2** and **3**) on a Nonius CCD[16] diffractometer using Mo Kα radiation (λ = 0.71073 Å) at a temperature of 173 K. The intensity data were collected by the phi scan and omega scan techniques, scaled and reduced with DENZO-SMN[17] or SAINT-Plus.[18] The integration and reduction of data were performed with a multiscan method executed in SADABS program.[19] The determination of the complexes space group was done using XPREP implemented in APEX II. The structures were solved by direct methods using SHELX-97[20] and refined using full-matrix least-squares methods in SHELXL.[20] The graphical interface used the program X-SEED.[21] All non-hydrogen atoms were refined anisotropically. All hydrogen atoms were placed geometrically and with a riding model for their isotropic temperature factors. Diagrams were generated using POVRAY in X-SEED.[21]

RESULTS AND DISCUSSION

The crystals and refinement parameters are given in Table 1 and Table 2.

Structure **1**, the **H1** apohost, crystallizes in the space group $P\bar{1}$ with Z = 4 and Z' = 2; therefore, there are two molecules in the asymmetric unit. In each molecule the Ni atom exhibits octahedral geometry, with the axial Br ligands in *trans* configuration and the four 4-picolines in the equatorial positions. There are 11 C−H···Br intermolecular interactions with less than the sum of the van der Waals radii, the strongest being C$_{12}$−H$_{12C}$···Br$_1$ at 2.74 Å. There are no direct Br···Br intermolecular contacts. The remaining interactions for this and the other seven structures have been deposited in the Supporting Information, Table S1. The asymmetric unit is shown in Figure 1, which also displays the C−H···Br close contact.

Structure **2**, **H2·1/2H$_2$O**, crystallizes in $P2_1/c$ with Z = 8 and Z' = 2. There are two host molecules and one water in the asymmetric unit. The water molecules are hydrogen bonded to

DOI: 10.1021/acs.cgd.6b01844
Cryst. Growth Des. 2017, 17, 1876−1883

Table 1. Crystallographic Data Parameters of Nickel Complexes 1−4

Compound	1	2	3	4
Structural formula	$C_{24}H_{28}Br_2N_4Ni$	$C_{24}H_{29}Cl_2N_4O_{0.5}Ni$	$C_{22.5}H_{18}Br_{4.5}Cl_2\ N_4Ni$	$C_{24}H_{32}I_2N_4O_2Ni$
Molecular mass (g mol^{-1})	591.03	511.12	840.62	721.05
Data collection temp (K)	173 (2)	173 (2)	173 (2)	173 (2)
Crystal system	Triclinic	Monoclinic	Monoclinic	Monoclinic
Space group	$P\bar{1}$	$P2_1/c$	$P2_1/c$	$C2/c$
a (Å)	9.5909 (8)	17.0277 (3)	17.7920 (4)	15.6556 (12)
b (Å)	15.4528 (12)	17.4155 (4)	20.9985 (4)	8.8991 (7)
c (Å)	17.3609 (14)	17.0023 (3)	15.6144 (3)	20.4433 (16)
α (deg)	88.9794 (14)	90	90	90
β (deg)	88.3828 (15)	92.484 (3)	100.805 (3)	96.103 (2)
γ (deg)	80.1832 (13)	90	90	90
Volume (Å^3)	2534.1 (4)	5037.2 (2)	5730.2 (2)	2832.0 (4)
Z	4	8	8	4
D_c Calc density (g cm^{-3})	1.549	1.348	1.948	1.691
Absorption coefficient (mm^{-1})	3.937	1.003	7.160	2.891
F(000)	1192	2136	3232	1416
θ range	1.17−27.14	1.67−28.61	1.87−27.46	2.00−28.38
Reflections collected	64506	70440	259020	42409
No data I > 2σ(I)	8520	8377	10353	3530
Final R indices [I > 2σ(I)]	0.0340	0.0426	0.0504	0.0320
R indices (all data)	0.0546	0.0824	0.0699	0.0423
Goodness-of-fit on F^2	1.023	1.018	1.037	1.052
CCDC No.	1522998	1522999	1523000	1523001

Table 2. Crystallographic Data Parameters of Nickel Complexes 5−8

Compound	5	6	7	8
Structural formula	$C_{36}H_{51}I_2N_6O_{4.5}Ni$	$C_{35}H_{32}I_9N_7O_2Ni$	$C_{28}H_{34}I_6N_6Ni$	$C_{28}H_{34}I_6N_6Ni$
Molecular mass (g mol^{-1})	952.34	1783.49	1274.70	1274.70
Data collection temp (K)	173 (2)	173 (2)	173 (2)	173 (2)
Crystal system	Monoclinic	Triclinic	Monoclinic	Orthorhombic
Space group	$P2_1$	$P\bar{1}$	$P2_1/n$	$Pnna$
a (Å)	11.6560 (12)	8.2998 (7)	14.6626 (8)	16.5289 (12)
b (Å)	11.1644 (12)	14.5104 (12)	12.4450 (7)	15.7022 (12)
c (Å)	32.4356 (33)	20.5166 (17)	21.3397 (12)	15.4692 (11)
α (deg)	90	93.249 (2)	90	90
β (deg)	93.930 (2)	93.249 (2)	94.676 (2)	90
γ (deg)	90	96.641 (2)	90	90
Volume (Å^3)	4211.0 (8)	2445.4 (4)	3881.0 (4)	4014.9 (5)
Z	4	2	4	4
D_c Calc density (g cm^{-3})	1.502	2.422	2.181	2.109
Absorption coefficient (mm^{-1})	1.970	6.115	5.299	5.122
F(000)	1916	1624	2360	2360
θ range	1.26−28.39	1.42−28.30	1.63−27.15	1.80−27.59
Reflections collected	93295	69014	57007	73098
No data I > 2σ(I)	16533	10680	6101	3575
Final R indices [I > 2σ(I)]	0.0369	0.0303	0.0498	0.0281
R indices (all data)	0.0578	0.0360	0.0807	0.0445
Goodness-of-fit on F^2	1.021	1.057	1.069	1.052
CCDC No.	1523002	1523003	1523004	1523005

the Cl_1 atoms and form a bridge about the center of inversion at Wyckoff position *d*, giving an $R_4^2(8)$ H-bonding motif[22] as shown in Figure 2. There are five C−H···Cl and three C−H···O contacts (Table S1).

Structure **3**, **H3·1/2(3Brpy)** crystallizes in $P2_1/c$ with $Z = 8$. There are thus eight host and four guest molecules in the unit cell. There are several halogen···halogen interactions of which the most prominent are Br_4···Cl_2 (d = 3.225 (7) Å) and Br_7···Cl_4 (d = 3.239 (7) Å). There is only one X···X interaction involving the 3-bromopyridine guest, to another symmetry related guest. The remaining ten such interactions are all between the host molecules (Table S1).

Structure **4** was obtained by mixing nickel iodide with 3-picoline in aqueous methanol (50:50 v/v). The resulting crystalline compound is a salt, with the host as a $[\mathbf{Ni(H_2O)_2(3PIC)_4}]^{2+}$ cation and two iodide anions. This structure crystallizes in $C2/c$ with $Z = 4$ and the Ni^{2+} ion located on a diad at Wyckoff position *e*. The coordination of the Ni ions remains as octahedral, with the two water molecules at the axial

DOI: 10.1021/acs.cgd.6b01844
Cryst. Growth Des. 2017, 17, 1876−1883

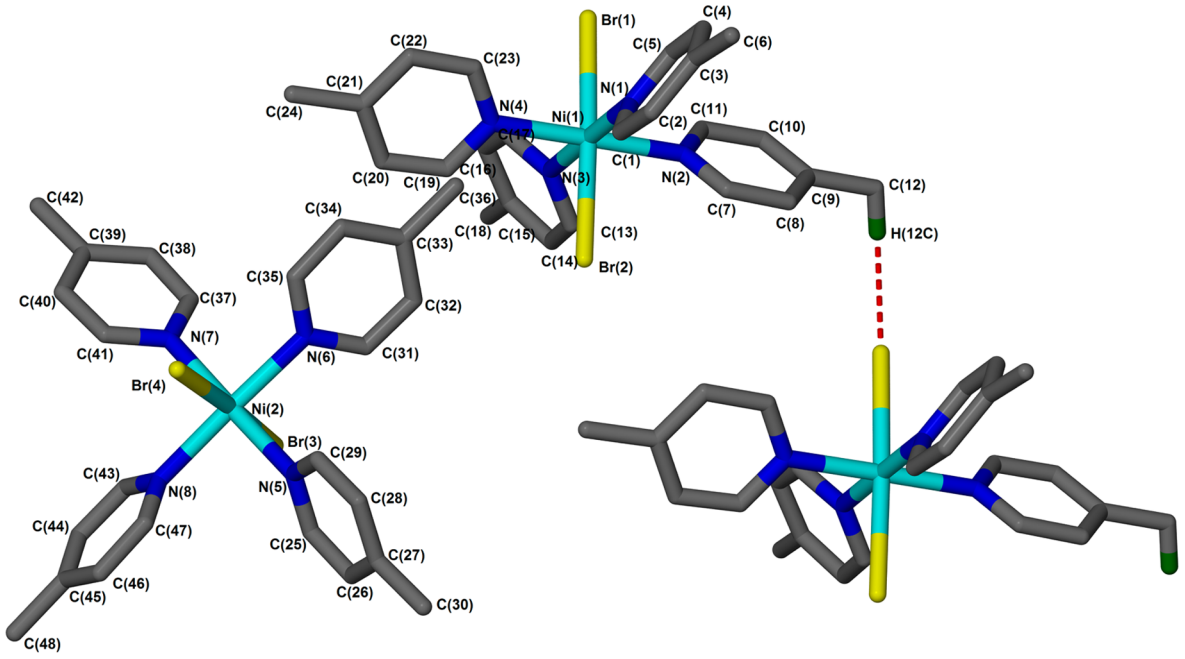

Figure 1. View of the apohost **H1** illustrating the two labeled molecules of the asymmetric unit. The third molecule shows the intermolecular C–H···Br contact.

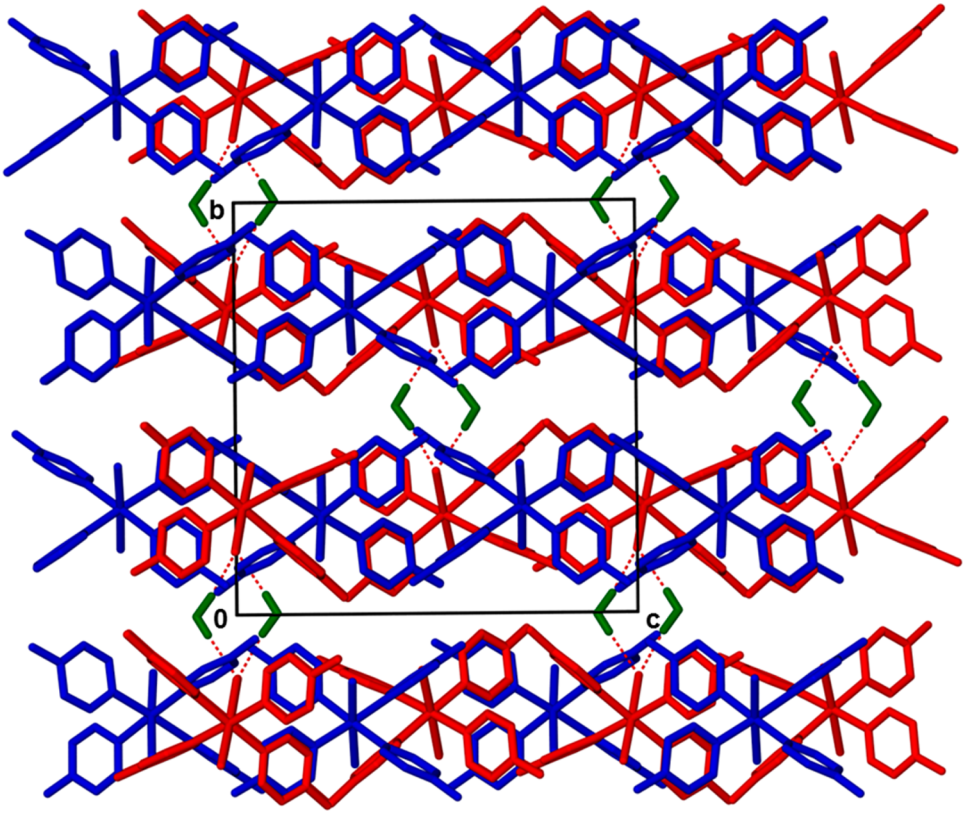

Figure 2. Packing diagram of **H2·1/2H$_2$O** down [100] with the two host molecules in red/blue and the water in green.

positions. The waters are hydrogen-bonded to the I^- anions as shown in Figure 3.

Structure **5**, crystallizes in the space group $P2_1$ with $Z = 4$, with the asymmetric unit comprising two host cations, four iodide anions, four 4-picolines, and five waters. None of these moieties are disordered. The hydrogen bonds that occur between the water ligands bound to the central Ni ion, the waters of crystallization, and the iodide anions are listed in Table S1 (Supporting Information). Not all the hydrogen atoms in the water molecules of crystallization could be satisfactorily located; therefore, we listed all H-bonds by inspection of O···O and O···I^- distances. The packing is characterized by alternating layers of host molecules which

DOI: 10.1021/acs.cgd.6b01844
Cryst. Growth Des. 2017, 17, 1876–1883

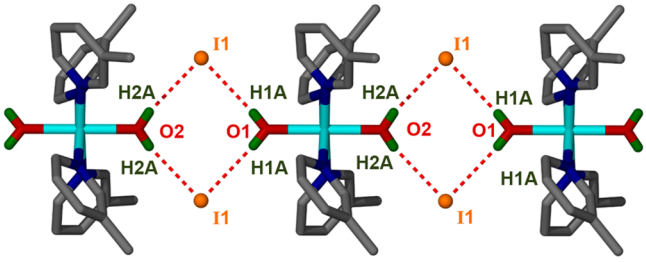

Figure 3. Hydrogen bonding ribbon of compound **4**.

sandwich {I^-, 4PIC, and H_2O} moieties in the *ab* planes. This is shown in Figure 4.

Structure **6**, crystallizes in $P\bar{1}$ and comprises one host cation, two iodides, and three guest molecules of 4-iodopyridine. The packing is stabilized by a series of $R_4^2(8)$ hydrogen bonding interactions which form ribbons of $[\mathbf{H6}]^+$with I^- running along [100] (Figure 5). Table S1 also lists five I···I interactions.

Structure **7** crystallizes in $P2_1/n$. The asymmetric unit comprises one host cation and two I_3^- anions. The Ni^{2+} exhibits octahedral coordination, with the acetonitrile moieties in axial positions, and the 3PIC bases in equatorial positions. Two tri-iodide anions are located in general position, but they do not display any close interactions.

Structure **8** crystallizes in *Pnna*. The asymmetric unit comprises half a host cation, and two separate half tri-iodides. The Ni^{2+} lies on a diad at Wyckoff position *d*. The first tri-iodide anion has I − I distances of 2.97 ($I_1 - I_2$) Å and 2.88 ($I_2 - I_3$) Å which are within normal range. However, the second tri-iodide lies across a diad and is disordered over three positions shown in blue, red, and green of Figure 6.

Thermal Analysis. TG and DSC traces were obtained for all the compounds **1**−**8**. The detailed results are discussed for compounds **1**, **3**, **5**, and **8** because they yielded the more interesting results. The results for compounds **2**, **4**, **6**, and **7** have been deposited in the Supporting Information. Table 3 gives a summary of the thermal results. For structure **1**, the TG trace and its corresponding DSC is given in Figure 7. The TG shows three desorption events. The first curve (a), corresponds to the loss of two 4-picoline ligands, closely followed by curve (b) due to one of 4PIC and a third loss (c) again due to one picoline. The corresponding DSC endotherms are shown as peaks A, B, and C. Since these peaks are generally broad or complex, we report the peak temperatures or ranges as opposed

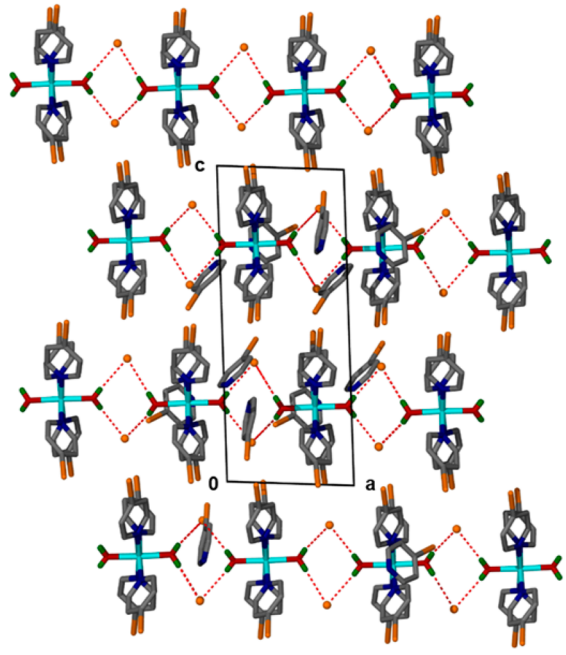

Figure 5. Packing of structure **6** displaying O−H···I^- hydrogen bond.

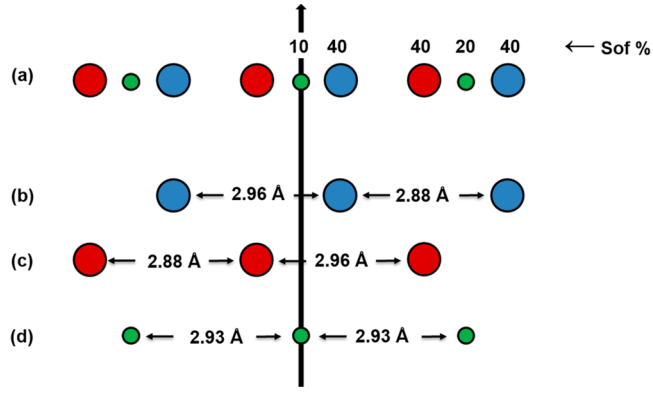

Figure 6. Schematic representation of the disordered tri-iodide anion located on a diad. (a) Shows the site occupancies of the individual atoms making up the components of the I_3^-. (b,c,d) Unpacking the three components to reveal the interatomic bond lengths (Å) in the three constituents of I_3^-.

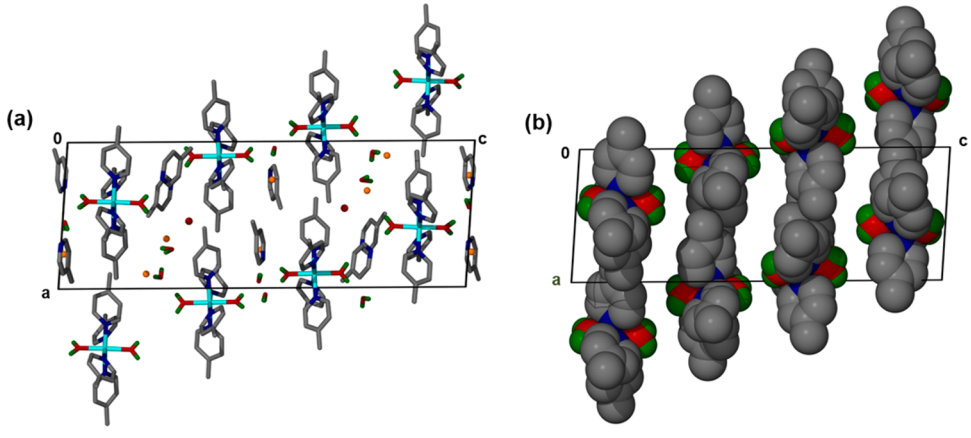

Figure 4. Packing of structure **5**. (a) Showing hosts and guests; (b) showing only the host molecules in van der Waals representation.

DOI: 10.1021/acs.cgd.6b01844
Cryst. Growth Des. 2017, 17, 1876−1883

Table 3. Thermal Analysis Results of the Nickel Complexes

structure	molecular formula	TG step a % obs (calc)	TG step b % obs (calc)	TG step c % obs (calc)	DSC T_{peak} A/°C	DSC T_{peak} B/°C	DSC T_{peak} C/°C
1	$[NiBr_2(4PIC)_4]$	31.0 (31.5)	16.3 (15.8)	15.7 (15.8)	210.0	225.4	297.1−335.0
2	$[NiCl_2(4PIC)_4]\cdot 1/2H_2O$	1.84 (1.76)	54.4 (54.7)	18.2 (18.2)	94.2	209.4	297.3−348.0
3	$[NiCl_2(3Brpy)_4]\cdot 1/2(3Brpy)$	45.2 (47.0)	21.0 (18.8)	18.5 (18.8)	101.5−146.5	268.7	329.8
4	$[Ni(H_2O)_2(3PIC)]\ I^-$	30.8 (30.2)	12.8 (12.9)	13.3 (12.9)	137.0−171.9	186.5	225.0
5	$[Ni(H_2O)_2(4PIC)_4]^{2+}2I^-\cdot 2(4PIC)\cdot 2.5H_2O$	26.7 (28.1)	20.3 (19.6)	19.7 (19.6)	61.2−92.9	126.7	198.8−225.1
6	$[Ni(H_2O)_2(4Ipy)_4]^{2+}2I^-\cdot 3(4Ipy)$	82.5 (83.1)	-	-	87.6	145.3 Exotherm	272.7
7	$[Ni(ACN)_2(3PIC)_4]^{2+}2I_3^-$	74.0 (75.5)	-	-	135.2	154.3	247.7−275.5
8	$[Ni(ACN)_2(4PIC)_4]^{2+}2I_3^-$	15 (14.6)	58.1 (60.9)	-	160.4	254.9−270.3 Exotherm	282.2

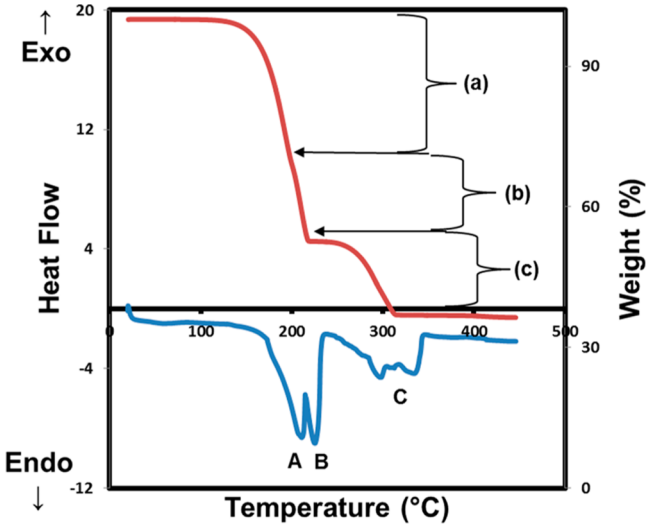

Figure 7. TG and DSC traces for structure **1**.

to the onset temperatures T_{on}. This method was adopted for the remaining compounds **2** to **8**.

The guest molecule 1/2(3BrPY) and two ligated (3BrPY) in structure **3**, correspond to the first desorption step (a). The two other steps ((b) and (c)) are due to the loss of the remaining 3Brpy in the structure as illustrated in Figure 8. There are four endotherms in the DSC trace of **3**, the first two peaks at 101.5 and 146.5 °C are associated with the desorption of 2.5 mol of the 3BrPY labeled **A** in the corresponding figure. The third and the fourth peaks at 268.7 and 329.8 °C (**B** and **C**) are due to the loss of the two remaining 3-bromopyridine moieties.

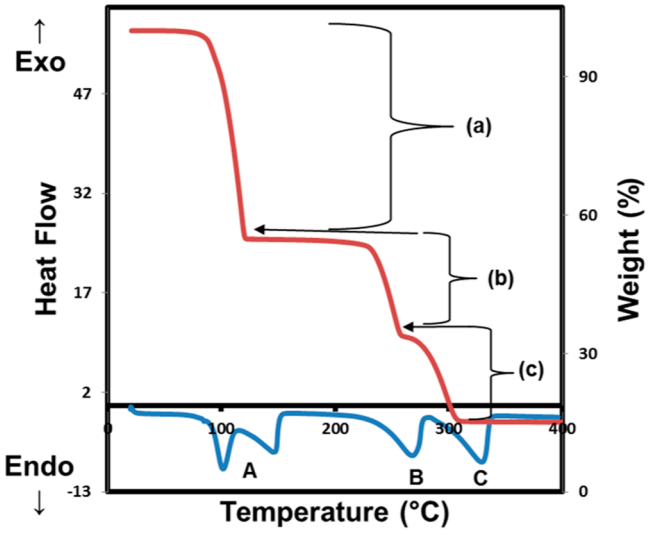

Figure 8. TG and DSC traces of structure **3**.

There is a good agreement between the experimental and the calculated percentage weight loss obtained for the TG results for structure **5**. The first step (a) is the mass loss of all the waters and the two free 4PIC guest molecules, followed with the release of the four remaining ligated 4PIC in two steps (b) and (c). The complexity of the DSC events results in four peaks: one at 61.2 °C which is the release of the water molecules, the second at 92.9 °C is the release of the guest 4PIC, the third and fourth at 126.74 and 198.8 °C corresponding to the 4 molecules of 4PIC in the crystal, respectively. These thermal events are represented in Figure 9.

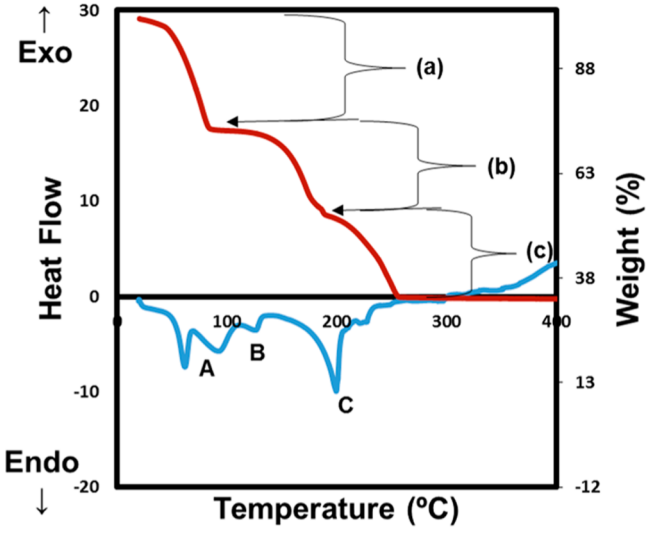

Figure 9. TG and DSC traces of structure **5**.

In the case of **8**, the first TG step is due to the loss of two of the 4PIC molecules and the second step is the release of the remaining two 4PIC, acetonitrile, and the decomposition of the $2I_3^-$ to $2I_2+2I^-$. The DSC is characterized by one endotherm (A) at 160.4 °C due to 4PIC. There are two exotherms (B), one at 254.9 °C, another at 270.3 °C, which indicate a rearrangement of the remaining structure and a sharp peak (C) at 282.2 °C corresponding to $CH_3CN/4PIC/I_2$ desorption. The results are shown in Figure 10.

Kinetics of Adsorption. The kinetics of solid−vapor host formation **H1**, $[NiBr_2(4PIC)_4]$ was also monitored by exposing solid $NiBr_2$ to the vapor of 4-picoline. The sample

DOI: 10.1021/acs.cgd.6b01844
Cryst. Growth Des. 2017, 17, 1876−1883

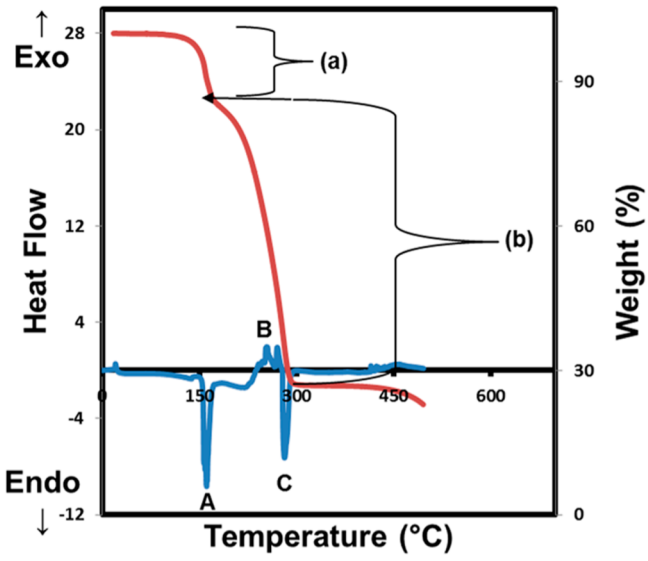

Figure 10. TG and DSC traces for structure **8**.

apparatus consisted of a desiccator in which liquid 4-picoline was placed in the bottom well and powdered $NiBr_2$ was thinly spread in the Petri dish resting on a metal net above the 4-picoline.[23] The $NiBr_2$ powder was sieved and the fraction between 90 and 106 μm was selected. The experiment was carried out in an oven at 80 °C and samples were measured at selected time intervals and subjected to thermogravimetric analysis. The procedure was repeated with $NiCl_2$ and the results are shown in Figure 11.

The solid–vapor reaction

$$NiBr_2(s) + 4PIC(vap) \rightarrow [NiBr_2(4PIC)_4](solid)$$

shows that the mass increase versus time is linear and is therefore a zero order reaction

$$\alpha = kt$$

where the extent of reaction, α, is defined as $m_t - m_o/m_\infty - m_o$ in which m_t = mass at time t, m_o = mass at start of reaction and m_∞ = mass at end of reaction; k, the rate constant = 9.52 × 10^{-2} min^{-1}. The α-time curves were fitted to an appropriate rate law[24] and the rate constant for both reactions were evaluated.

The reaction with $NiCl_2$, however, behaves differently. For the first 120 min it is fast and follows the three-dimensional diffusion law

$$[1 - (1 - \alpha)^{1/3}]^2 = kt$$

with k = 4.04 × 10^{-3}, after which it is linear with k = 5.72 × 10^{-4} min^{-1}. We surmise that the slower initial reaction of the 4PIC with $NiBr_2$ is due to the greater steric hindrance posed by Br^- versus the Cl^-ions on the Ni^{2+} ion.

CONCLUSION

A series of Werner hosts of general formula NiX_2A_4, where X = Cl, Br, I, and A is a substituted pyridine have been synthesized. The compounds with X = I are ionic, forming iodide salts. These hosts formed inclusion compounds with picoline and halogenated pyridines as guests. Two novel compounds containing the tri-iodide anion were also characterized. The nonbonded interactions have been analyzed and the thermal analysis (TG/DSC) results interpreted in terms of the structures of the inclusion compounds. The kinetics of solid–vapor reactions for the formation of the hosts $NiBr_2$ and $NiCl_2$ yield different results which may be interpreted in terms of steric hindrance to the Ni^{2+} ion.

ASSOCIATED CONTENT

Supporting Information

The Supporting Information is available free of charge on the ACS Publications website at DOI: 10.1021/acs.cgd.6b01844.

Geometry of intermolecular interactions; thermal analysis with TG/DSC events (PDF)

Accession Codes

CCDC 1522998–1523005 contains the supplementary crystallographic data for this paper. These data can be obtained free of charge via www.ccdc.cam.ac.uk/data_request/cif, or by emailing data_request@ccdc.cam.ac.uk, or by contacting The Cambridge Crystallographic Data Centre, 12, Union Road, Cambridge CB2 1EZ, UK; fax: +44 1223 336033.

AUTHOR INFORMATION

Corresponding Author

*E-mail: luigi.nassimbeni@uct.ac.za. Tel: +27 21 650 5893. Fax: +27 21 650 2569.

ORCID

Francoise M. Amombo Noa: 0000-0001-8361-3432

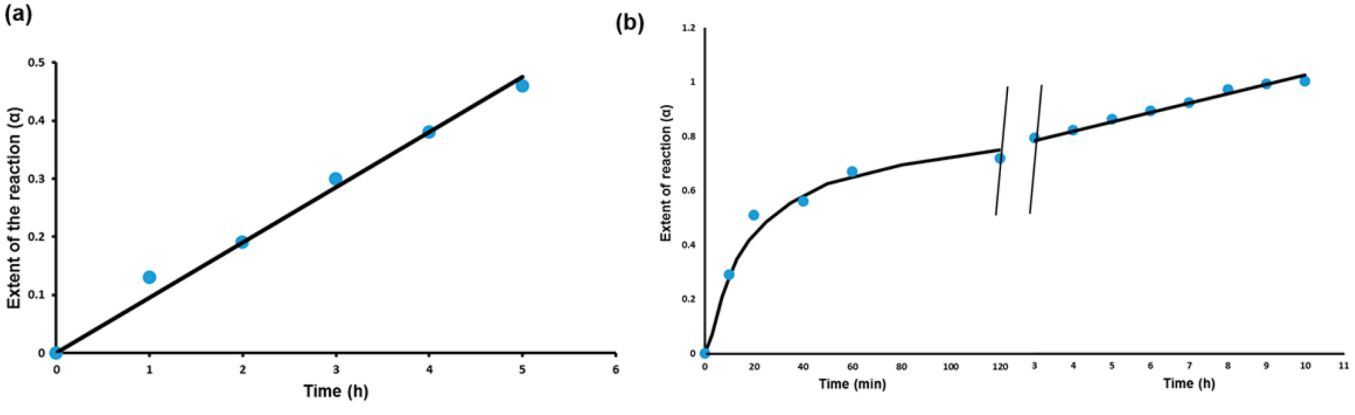

Figure 11. Kinetic curves for the absorption of 4PIC vapor by (a) $NiBr_2$ and (b) $NiCl_2$.

DOI: 10.1021/acs.cgd.6b01844
Cryst. Growth Des. 2017, 17, 1876–1883

Susan A. Bourne: 0000-0002-2491-2843
Luigi R. Nassimbeni: 0000-0001-8714-8646

Notes

The authors declare no competing financial interest.

■ ACKNOWLEDGMENTS

We thank the University of Cape Town and the National Research Foundation (South Africa) for funding.

■ REFERENCES

(1) Schaeffer, W. D.; Dorsey, W. S.; Skinner, D. A.; Christian, C. G. *J. Am. Chem. Soc.* **1957**, *79*, 5870−5876.
(2) Lipkowski, J. In *Inclusion Compounds*, Atwood, J. L.; Davies, J. E. D.; MacNicol, D. D., Eds.; Academic Press: New York, 1984; Vol. *1*, Chapter 3.
(3) Lipkowski, J. In *Comprehensive Supramolecular Chemistry*, Atwood, J. L.; Davies, J. E. D.; MacNicol, D. D.; Vögtle, F., Eds.; Elsevier: Oxford, 1996; Vol. *6*, Chapter 20.
(4) Soldatov, D. V.; Enright, G. D.; Ripmeester, J. A. *Cryst. Growth Des.* **2004**, *4*, 1185−1194.
(5) Lusi, M.; Barbour, L. J. *Angew. Chem., Int. Ed.* **2012**, *51*, 3928−3931.
(6) Batisai, E.; Lusi, M.; Jacobs, T.; Barbour, L. J. *Chem. Commun.* **2012**, *48*, 12171−12173.
(7) Wicht, M. M.; Bathori, N.; Nassimbeni, L. R. *Dalton Trans.* **2015**, *44*, 6863−6870.
(8) Wicht, M. M.; Su, H.; Bathori, N.; Nassimbeni, L. R. *CrystEngComm* **2016**, *18*, 2509−2516.
(9) Wicht, M. M.; Bathori, N.; Nassimbeni, L. R. *Polyhedron* **2016**, *119*, 127−1133.
(10) Nishikiori, S.; Iwamoto, T. *J. Inclusion Phenom.* **1984**, *2*, 341−349.
(11) Nishikiori, S.; Iwamoto, T. *Anal. Sci.* **1988**, *4*, 25−30.
(12) Iwamoto, T. In *Inclusion Compounds*, Atwood, J. L.; Davies, J. E. D.; MacNicol, D. D., Eds.; Academic Press: New York, 1984; Vol. *1*, Chapter 2.
(13) Amombo Noa, F. M. A; Bourne, S. A.; Nassimbeni, L. R. *Cryst. Growth Des.* **2015**, *15*, 3271−3279.
(14) Bondi, A. *J. Phys. Chem.* **1964**, *68*, 441−451.
(15) *APEX 2*, v 1.0−27; Bruker AXS Inc.: Madison, WI, 2005.
(16) *Collect*, data collection software; Nonius: Delft, The Netherlands, 1998.
(17) Otwinowski, Z.; Minor, W. In *Methods in Enzymology, Macromolecular Crystallography*, Carter, C. W., Jr; Sweet, R. M, Eds.; Academic Press, 1997; part A, Vol. *276*, p 307.
(18) *SAINT-Plus*, v 7.12; Bruker AXS Inc.: Madison, Wisconsin, USA, 2004.
(19) Sheldrick, G. M. *SADABS; Program for Area Detector Adsorption Correction*; University of Göttingen, Germany, 1996; pp 33−38.
(20) Sheldrick, G. M. *SHELX-97; Program for crystal Structure Solution and Refinement*; University of Göttingen, Germany, 1997; p 1456.
(21) Barbour, L. J. *J. Supramol. Chem.* **2001**, *1*, 189−191.
(22) Etter, M. C.; MacDonald, J. C.; Bernstein, J. *Acta Crystallogr., Sect. B: Struct. Sci.* **1990**, *46*, 256−262.
(23) Amombo Noa, F. M. A; Bourne, S. A.; Su, H.; Nassimbeni, L. R. *Cryst. Growth Des.* **2016**, *16*, 1636−1642.
(24) Brown, M. E. *Introduction to Thermal Analysis: Techniques and Applications*; Chapman and Hall: London, 1988.

DOI: 10.1021/acs.cgd.6b01844
Cryst. Growth Des. 2017, 17, 1876−1883

SUPPORTING INFORMATION

*Francoise M. Amombo Noa, Susan A. Bourne, Hong Su and Luigi R. Nassimbeni**

Centre for Supramolecular Chemistry Research, Department of Chemistry, University of Cape Town, Rondebosch 7701, South Africa. Email: luigi.nassimbeni@uct.ac.za.

Thermal Analysis.

Structure **2** TG also shown three mass losses. The first loss (a) is attributed to half a molecule of water incorporated in structure playing the role of a bridge connecting the host compounds in the structure. The second weight loss (b) is due to three moles of the 4PIC and the last loss is the release of one 4PIC. The DSC trace of **2** correlated with the TG weight loss where water molecule is released at 94.2 ºC followed by the three 4PIC molecules at 209.4 ºC and the one 4PIC at a range temperature of 297.3 – 348.0 ºC.

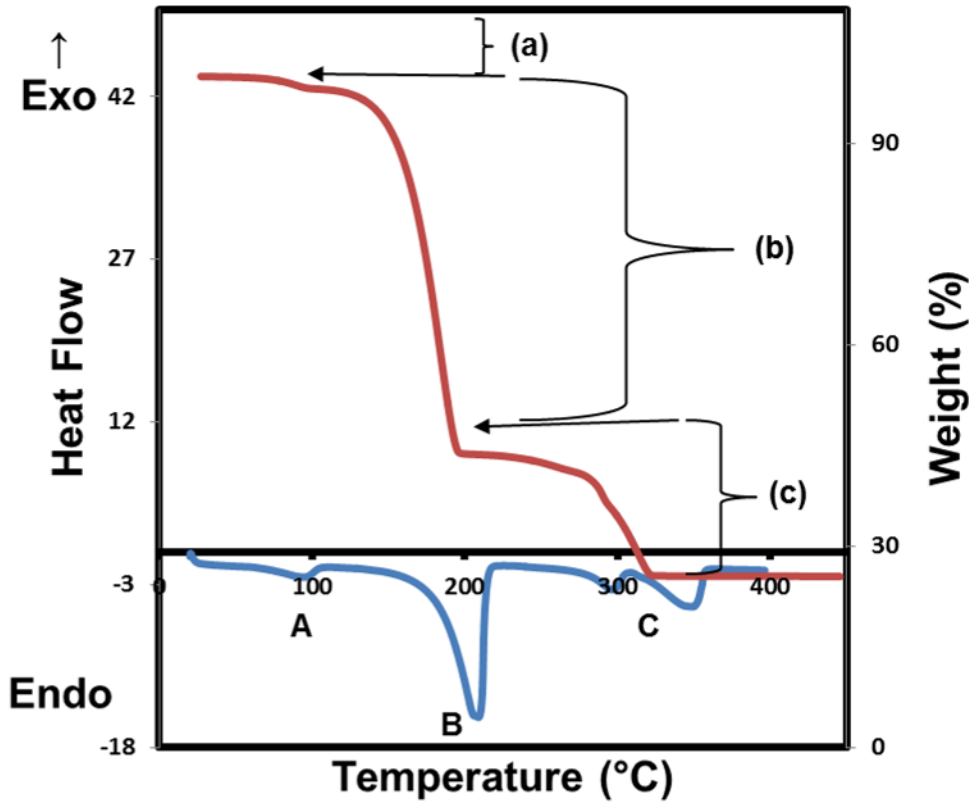

Figure S1. TG and DSC traces of structure **2**.

The heating of the crystals of structure **4**, while conducting TG analysis falls into three distinct steps: (a) evaporation of the water molecules and the release of two moles of the 3-picoline (3PIC) in the structure; (b) and (c) the release of the two remaining 3PIC, in which the calculated and the experiment mass losses are within 0.6 %. The DSC trace which is very complex kind of correlates with the TG steps, where the first two endotherms which range from

137. 9 ºC to 171.9 ºC correspond to the release of the water and the two 3PIC. The third and the four peaks at 186.5 ºC and 225.0 ºC are the desorption of the two remaining 3PIC.

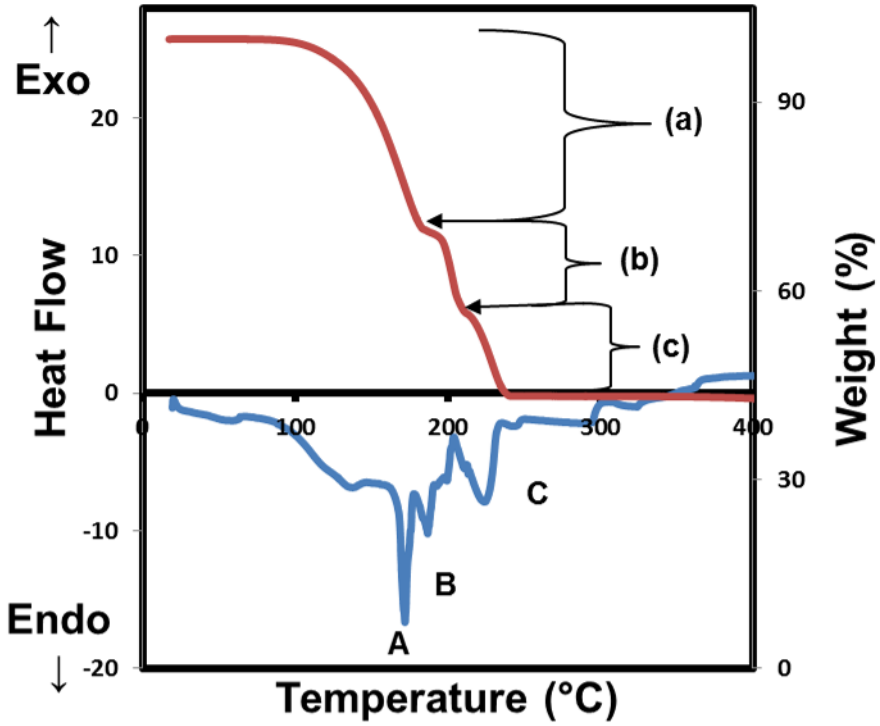

Figure S2. TG and DSC traces of structure **4**.

The inclusion compound **6** has one step for it TG. This step corresponds to the loss of both the water and the 4-iodopyridine (4Ipy). The first DSC endotherm at 87.6 ºC corresponds to the dissolution of the compound upon the release of the water, followed by one exotherm at 145.3 ºC which can be attributed to the rearrangement of the structure and finally the decomposition of the inclusion compound at 272.7 ºC.

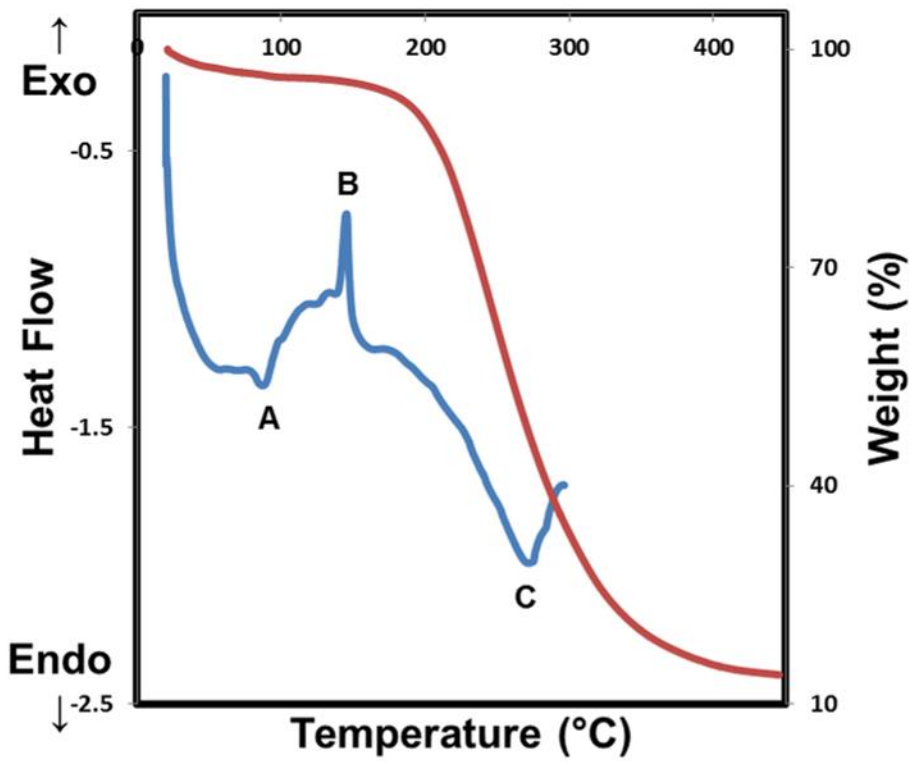

Figure S3. TG and DSC traces of structure **6**.

Structure **7**, TG follows the same pattern as in **6** due to only one step corresponding to the loss of acetonitrile, 3PIC and I_2. The DSC events are complexed showing endotherms at 135.2 ºC, 154.3 ºC and 247.7 – 275.5 ºC. This trace has a complex decomposition event.

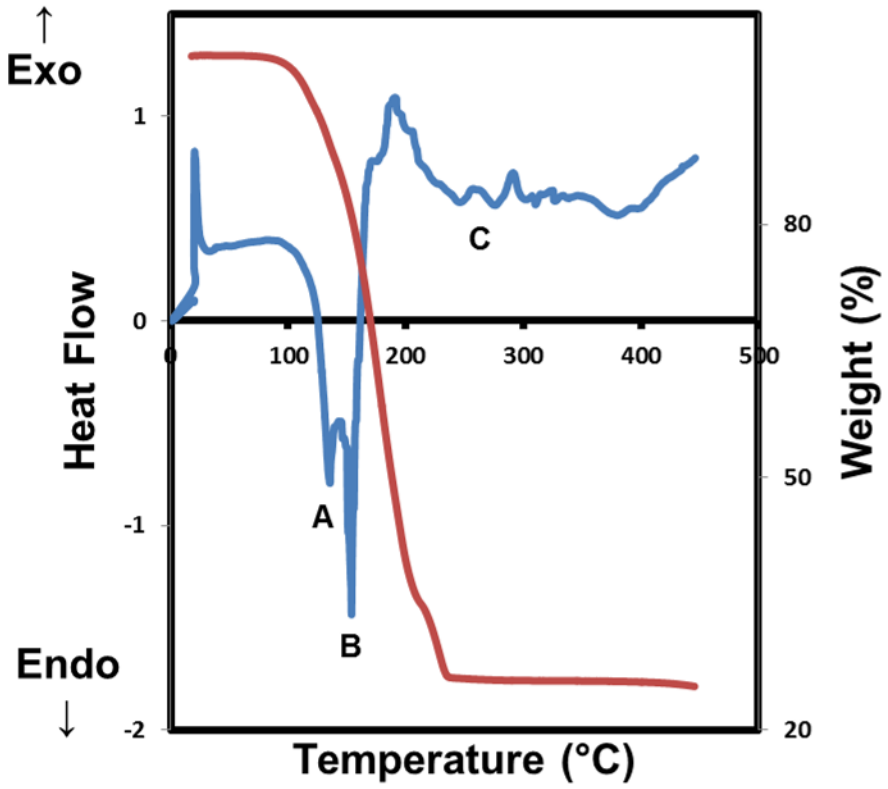

Figure S4. TG and DSC traces of structure **7**.

Table S1: Geometry of Intermolecular Interactions.

Compound	D-H···A	D-H/Å	H···A/Å	D···A/Å	D-H···A/°	X···X/ X···Y	d[Å]	θ_1/θ_2	d-Σvdw [Å]	%
1	C_{10}-H_{10}···Br_1[a]	0.950	3.210	4.020	144	-	-	-	-	-
	C_{12}-H_{12C}···Br_1[b]	0.980	2.742	3.722	179	-	-	-	-	-
	C_{48}-H_{48A}···Br_1[c]	0.980	3.110	4.017	154	-	-	-	-	-
	C_2-H_2···Br_2[d]	0.950	3.053	3.888	148	-	-	-	-	-
	C_{24}-H_{24B}···Br_2[e]	0.980	2.987	3.960	172	-	-	-	-	-
	C_6-H_{6A}···Br_3[d]	0.980	3.032	4.001	170	-	-	-	-	-
	C_{24}-H_{24A}···Br_3[c]	0.980	3.121	4.061	161	-	-	-	-	-
	C_{38}-H_{38}···Br_3[c]	0.950	2.980	3.883	159	-	-	-	-	-
	$C_{42}H_{42B}$···Br_3[c]	0.980	3.068	4.013	162	-	-	-	-	
	C_{26}-H_{26}···Br_4[b]	0.950	3.188	4.024	148	-	-	-	-	-
	C_{46}-H_{46}···Br_4[f]	0.950	2.995	3.895	158	-	-	-	-	-
	C_{48}-H_{48B}···Br_4[f]	0.980	3.053	3.999	163	-	-	-	-	-
2	O_1-H_{1A}···Cl_1[g]	0.935 (4)	2.285 (4)	3.219 (2)	176	Cl_1···O_1	3.219 (2)	176/132	-0.051	-1.6
	O_1-H_{1B}···Cl_1[h]	1.089 (6)	2.234 (6)	3.318 (2)	173	Cl_1···O_1	3.318 (2)	173/122	+0.048	+1.5
	C_{12}-H_{12C}···Cl_1[i]	0.980	3.105	3.872	136	-	-	-	-	-
	C_{24}-H_{24A}···Cl_2[g]	0.980	2.956	3.935	177	-	-	-	-	-
	C_{48}-H_{48A}···Cl_2	0.980	2.820	3.782	167	-	-	-	-	-
	C_6-H_{6C}···Cl_4[j]	0.980	2.737	3.593	146	-	-	-	-	-
	C_{12}-H_{12A}···Cl_4[g]	0.980	2.765	3.683	156	-	-	-	-	-
	C_{12}-H_{12A}···O_1[a]	0.980	2.743	3.541	139	-	-	-	-	-
	C_{18}-H_{18C}···O_1[a]	0.980	2.450	3.415	168	-	-	-	-	-
	C_{23}-H_{23}···O_1[g]	0.950	2.805	3.349	117	-	-	-	-	-
3	C_{27}-H_{27}···Br_2[k]	0.950	3.165	3.705	118	-	-	-	-	-
	C_3-H_3···Br_4[l]	0.950	3.137	3.939	143	-	-	-	-	-
	C_{20}-H_{20}···Br_4[m]	0.950	3.114	3.902	142					
	C_{18}-H_{18}···Br_7[n]	0.950	3.194	4.077	158	-	-	-	-	-
	C_{35}-H_{35}···Br_7[d]	0.950	3.038	3.881	149	-	-	-	-	-
	C_7-H_7···Cl_1[g]	0.950	3.091	3.846	138	-	-	-	-	-
	C_{22}-H_{22}···Cl_1[k]	0.950	2.801	3.526	134	-	-	-	-	-
	C_{38}-H_{38}···Cl_1[l]	0.950	3.019	3.702	130	-	-	-	-	-
	C_{32}-H_{32}···Cl_2	0.950	2.976	3.537	119	-	-	-	-	-
	C_{33}-H_{33}···Cl_2	0.950	2.769	3.433	128	-	-	-	-	-
	C_{28}-H_{28}···Cl_3[g]	0.950	2.730	3.473	136	-	-	-	-	-
	C_{53}-H_{53}···Cl_3[i]	0.950	2.686	3.621	168	-	-	-	-	-
	C_1-H_1···N_9[b]	0.950	2.520	3.296	139	-	-	-	-	-
	-	-	-	-	-	Br_1···Br_4	3.899 (9)	93/92	+0.199	+5.4
	-	-	-	-	-	Br_1···Br_7	3.889 (9)	72/70	+0.189	+5.1
	-	-	-	-	-	Br_1···Br_8	3.552 (8)	168/103	-0.148	-4.0
	-	-	-	-	-	Br_2···Br_5	3.639 (8)	165/93	-0.061	-1.6
	-	-	-	-	-	Br_3···Br_5	3.845 (9)	101/92	+0.145	+3.9

	-	-	-	-	-	$Br_3\cdots Br_8$	3.783 (9)	111/100	+0.083	+2.2
	-	-	-	-	-	$Br_4\cdots Br_6$	3.863 (9)	146/120	+0.163	+4.4
	-	-	-	-	-	$Br_9\cdots Br_9$	3.660 (8)	156/156	-0.040	-1.1
	-	-	-	-	-	$Br_4\cdots Cl_2$	3.225 (7)	177/124	-0.375	-10.4
	-	-	-	-	-	$Br_6\cdots Cl_2$	3.524 (8)	158/112	-0.076	-2.1
	-	-	-	-	-	$Br_7\cdots Cl_4$	3.239 (7)	177/127	-0.461	-10.0
4	C_1-$H_1\cdots I_1^{j}$	0.950	3.117	3.855	136	-	-	-	-	-
	C_3-$H_3\cdots I_1^{o}$	0.950	3.271	3.955	131	-	-	-	-	-
	C_9-$H_9\cdots I_1^{p}$	0.950	3.205	4.150	174	-	-	-	-	-
	C_{11}-$H_{11}\cdots I_1$	0.950	3.231	4.031	143	-	-	-	-	-
	C_{12}-$H_{12B}\cdots I_1$	0.980	3.348	4.270	158	-	-	-	-	-
	O_1-$H_{1A}\cdots I_1^{q}$	0.750 (4)	2.776 (4)	3.522 (2)	174	$I_1\cdots O_1$	3.522 (2)	174/132	+0.022	+0.6
	O_2-$H_{2A}\cdots I_1^{r}$	0.755 (4)	2.774 (4)	3.475 (2)	163	$I_1\cdots O_2$	3.475 (2)	163/132	-0.025	-0.7
5	C_2-$H_2\cdots I_1^{s}$	0.950	3.271	4.027	138	-	-	-	-	-
	C_{37}-$H_{37}\cdots I_1$	0.950	3.225	4.164	170	-	-	-	-	-
	C_6-$H_{6A}\cdots I_2^{s}$	0.950	3.318	4.100	138	-	-	-	-	-
	C_{11}-$H_{11}\cdots I_2^{t}$	0.950	3.301	4.249	177	-	-	-	-	-
	C_{12}-$H_{12B}\cdots I_2^{v}$	0.980	3.055	3.985	159	-	-	-	-	-
	C_{50}-$H_{50}\cdots I_2^{v}$	0.950	3.278	4.145	153	-	-	-	-	-
	C_{54B}-$H_{54B}\cdots I_2^{v}$	0.980	3.339	4.231	152	-	-	-	-	-
	C_{42}-$H_{42C}\cdots I_3^{w}$	0.980	3.264	4.085	142	-	-	-	-	-
	C_{48}-$H_{48A}\cdots I_3^{x}$	0.980	3.300	4.118	142	-	-	-	-	-
	C_{70}-$H_{70}\cdots I_3^{e}$	0.950	3.226	4.105	155	-	-	-	-	-
	C_{72}-$H_{72B}\cdots I_3^{e}$	0.980	3.308	4.226	157	-	-	-	-	-
	C_{36}-$H_{36B}\cdots I_4$	0.980	3.241	4.172	159	-	-	-	-	-
	C_{38}-$H_{38}\cdots I_4^{j}$	0.950	3.323	4.223	159	-	-	-	-	-
	C_{42}-$H_{42B}\cdots I_4^{j}$	0.980	3.295	4.230	160					
	C_{65}-$H_{65}\cdots I_4^{b}$	0.950	3.236	4.135	159	-	-	-	-	-
	O_1-$H_{1A}\cdots O_5$	0.738 (4)	1.959 (5)	2.691 (5)	171	-	-	-	-	-
	O_1-$H_{1B}\cdots I_2^{t}$	0.788 (5)	2.674 (5)	3.457 (4)	173	$I_2\cdots O_1$	3.457 (4)	173/128	-0.043	-1.2
	O_2-$H_{2A}\cdots O_6$	0.817 (5)	1.910 (5)	2.725 (5)	175	-	-	-	-	-
	O_2-$H_{2B}\cdots N_{11}$	0.862 (4)	1.915 (4)	2.769 (5)	170	-	-	-	-	-
	O_3-$H_{3A}\cdots O_9$	0.934 (6)	1.790 (6)	2.688 (5)	160	-	-	-	-	-
	O_3-$H_{3B}\cdots I_3$	0.723 (4)	2.746 (5)	3.467 (4)	176	$I_3\cdots O_3$	3.467 (4)	176/127	-0.033	-0.9
	O_4-$H_{4A}\cdots I_1$	0.839 (3)	2.669 (3)	3.508 (3)	177	$I_1\cdots O_4$	3.508 (3)	177/129	+0.008	+0.2
	O_4-$H_{4B}\cdots N_{10}^{j}$	0.715 (4)	2.040 (4)	2.738 (5)	165	-	-	-	-	-
	O_5-$H_{5A}\cdots I_2^{s}$	0.976 (8)	2.627 (8)	3.553 (4)	158	$I_2\cdots O_5$	3.553 (4)	158	+0.053	+1.5
	O_5-$H_{5B}\cdots N_9^{y}$	0.772 (4)	2.001 (4)	2.771 (6)	175	-	-	-	-	-
	O_6-$H_{6AA}\cdots I_4^{b}$	0.810 (6)	2.798 (6)	3.580 (5)	163	$I_4\cdots O_6$	3.580 (5)	163/116	+0.08	+2.3
	O_6-$H_{6BB}\cdots I_1^{s}$	0.735 (5)	2.910 (5)	3.644 (5)	177	$I_1\cdots O_6$	3.644 (5)	177/116	+0.144	+4.1
	O_9-$H_{9A}\cdots N_{12}$	0.703 (7)	2.066 (7)	2.764 (6)	172	-	-	-	-	-
	O_9-$H_{9B}\cdots I_3^{z}$	0.798 (4)	2.788 (4)	3.547 (4)	160	$I_3\cdots O_9$	3.547 (4)	160	+0.047	+1.3
6	C_{34}-$H_{34}\cdots I_1^{aa}$	0.950	3.336	3.935	123	-	-	-	-	-
	C_{22}-$H_{22}\cdots I_2$	0.950	3.368	4.272	160	-	-	-	-	-

	C_{10}-H_{10}···I_3^{ab}	0.950	3.356	4.162	144	-	-	-	-	-
	C_{17}-H_{17}···I_4^{aa}	0.950	3.275	4.143	153	-	-	-	-	-
	C_{25}-H_{25}···I_4^{j}	0.950	3.337	4.229	157	-	-	-	-	-
	C_1-H_1···I_5	0.950	3.234	3.932	132	-	-	-	-	-
	C_{10}-H_{10}···I_8	0.950	3.248	3.623	106	-	-	-	-	-
	C_{11}-H_{11}···I_8^{e}	0.950	3.044	3.948	160	-	-	-	-	-
	C_5-H_5···I_9^{e}	0.950	3.191	3.988	143	-	-	-	-	-
	C_{16}-H_{16}···I_9	0.950	2.994	3.925	167	-	-	-	-	-
	C_{35}-H_{35}···I_9^{v}	0.950	3.371	4.305	168	-	-	-	-	-
	O_1-H_{1A}···I_8	0.784 (6)	2.752 (6)	3.525 (3)	169	I_8···O_1	3.525 (3)	169	+0.025	+0.7
	O_1-H_{1B}···I_9	0.829 (6)	2.759 (7)	3.586 (3)	177	I_9···O_1	3.586 (3)	177	+0.086	+2.5
	O_2-H_{2A}···I_8^{b}	0.824 (7)	2.625 (7)	3.424 (3)	164	I_8···O_2	3.424 (3)	164	-0.076	-2.2
	O_2-H_{2B}···I_9^{b}	0.706 (6)	2.711 (6)	3.413 (3)	173	I_9···O_2	3.413 (3)	173	-0.087	-2.5
	-	-	-	-	-	I_1···I_9	3.593 (3)	169	-0.367	-9.3
	-	-	-	-	-	I_2···I_8	3.578 (3)	175	-0.382	-9.6
	-	-	-	-	-	I_3···I_8	3.595 (3)	172	-0.365	-9.2
	-	-	-	-	-	I_4···I_9	3.589 (3)	172	-0.371	-9.4
	-	-	-	-	-	I_5···I_8	3.713 (3)	170	-0.247	-6.2
7	C_1-H_1···I_5^{ac}	0.950	3.372	4.069	132	-	-	-	-	-
	C_2-H_2···I_4^{ac}	0.950	3.369	4.222	150	-	-	-	-	-
	C_6-H_{6B}···I_1^{ac}	0.980	3.223	4.193	171	-	-	-	-	-
	C_6-H_{6C}···I_5^{ad}	0.980	3.234	3.980	134	-	-	-	-	-
	C_6-H_{6C}···I_6^{ad}	0.980	3.338	4.291	165	-	-	-	-	-
	C_7-H_7···I_4^{ad}	0.950	3.079	3.855	140	-	-	-	-	-
	C_{12}-H_{12B}···I_6^{ac}	0.980	3.320	3.905	120	-	-	-	-	-
	C_{12}-H_{12C}···I_3^{e}	0.980	3.243	4.166	158	-	-	-	-	-
	C_{17}-H_{17}···I_1^{e}	0.950	3.337	4.252	162	-	-	-	-	-
	C_{18}-H_{18A}···I_5^{ae}	0.980	3.283	4.087	140	-	-	-	-	-
	C_{18}-H_{18B}···I_2^{e}	0.980	3.155	4.036	150	-	-	-	-	-
	C_{19}-H_{19}···I_3^{ac}	0.950	3.086	3.925	148	-	-	-	-	-
	C_{24}-H_{24C}···I_6^{ae}	0.980	3.274	4.130	147	-	-	-	-	-
	C_{26}-H_{26A}···I_6^{ac}	0.980	3.059	3.855	139	-	-	-	-	-
	C_{26}-H_{26B}···I_3^{ac}	0.980	3.030	3.795	136	-	-	-	-	-
	C_{28}-H_{28A}···I_1^{af}	0.980	3.345	4.121	137	-	-	-	-	-
	C_{28}-H_{28A}···I_2^{af}	0.980	3.205	4.160	165	-	-	-	-	-
	C_{28}-H_{28B}···I_4^{ad}	0.980	3.202	3.945	134	-	-	-	-	-
	C_{28}-H_{28C}···I_1^{e}	0.980	3.190	3.907	131	-	-	-	-	-
	C_{15}-H_{15}···I_5^{ag}	0.950	3.310	3.774	112	-	-	-	-	-
8	C_1-H_1···I_6	0.950	3.209	4.108	159	-	-	-	-	-
	C_2-H_2···I_4	0.950	2.977	3.823	149	-	-	-	-	-
	C_2-H_2···I_4^{ah}	0.950	3.277	4.198	164	-	-	-	-	-
	C_5-H_5···I_1	0.950	3.219	3.989	140	-	-	-	-	-
	C_6-H_{6C}···I_5^{ai}	0.980	3.214	4.092	150	-	-	-	-	-
	C_6-H_{6C}···I_6^{ai}	0.980	3.176	4.099	158	-	-	-	-	-
	C_7-H_7···I_5^{aj}	0.950	3.148	3.957	144	-	-	-	-	-
	C_7-H_7···I_6^{aj}	0.950	3.169	3.792	125	-	-	-	-	-
	C_8-H_8···I_6^{aj}	0.950	3.121	3.761	126	-	-	-	-	-
	C_{10}-H_{10}···I_2^{aa}	0.950	3.164	3.944	140	-	-	-	-	-
	C_{14}-H_{14A}···I_5^{aj}	0.980	3.296	4.055	136	-	-	-	-	-
	C_{14}-H_{14A}···I_6^{aj}	0.980	2.986	3.865	150	-	-	-	-	-

	C_{16}-$H_{16B}\cdots I_3^{aa}$	0.980	3.073	3.942	148	-	-	-	-	-
	C_{16}-$H_{16C}\cdots I_6$	0.980	3.360	4.011	126	-	-	-	-	-

CHAPTER VIII: CONCLUSION

8.1 Conclusion

When molecules contain halogen atoms, halogen bonding has a great deal of impact in almost all the fields where design and manipulation of aggregation phenomena play an important role. Dumas *et* al[1] introduced halogen bonding as an attractive donor-acceptor interaction that involve halogen atoms which are functioning as a Lewis acid.

The first crystallographic data of a halogenated compound was conducted by Hassel *et* al[2] demonstrating halogen bonding (XB) as a powerful tool in driving the self-assembly of endless chains of alternating donor and acceptor[3] using the bromine and *p*-dioxane structure.

Halogen and hydrogen bonding are comparable in strengths,[4] both interactions are highly directional and have similar binding geometry, where the halogen atoms are directly linked to donor atoms with a bonding direction which coincides with the axes of lone-pair orbitals in inclusion compounds donor molecules.

XB is of specific type due to its interaction strength and directionality. There are two types of XB interactions: type I and type II, where type II is sub-divided into type II_a and type II_b. Type I interactions often occur around a crystallographic inversion centre, are generally symmetrical and are of van der Waals type. Type II interactions however, are linked with crystallographic screw axes and glide planes and are usually associated with polarisation. These type II interactions are unsymmetrical.

This study contributes to the body of work on co-existence of halogen⋯halogen interactions and possible competition between hydrogen and halogen bonding in host-guest systems.

Elucidation and refinement of the obtained complexes were performed using single crystal X-ray diffraction (as listed in Table 8.1). PXRD, thermal analyses (TG, DSC and HSM), IR and NMR spectroscopy, kinetics of desolvation and enclathration and Hirshfeld surface analysis.

Two halogenated host compounds; tetrakis–4–(bromophenyl)ethylene (**H1**) and tetrakis–4–(iodophenyl)ethylene (**H2**) were successfully synthesised[5] and used in the formation of inclusion compounds illustrated in Chapters 3, 4 and 5.

The classification of halogen bonding was made in Chapter 3, where the two hosts mentioned above were utilised in combination with selected halogenated methanes to form new inclusion compounds. Here, five structures (**H1·(2CH_2Cl_2)**, **H1·(2CH_3I)**, **H2·(CH_2Cl_2)**, **H2·(2CH_3I)** and **H2·(2$CHCl_3$)** are isostructural. These five compounds have similar unit cell dimensions, space group, host/guest ratios and the host atoms occupy the same positions. Their activation energies of desolvation fall in a tight range of 112 – 138 kJ/mol. Their thermal analyses (TG and DSC) decomposition patterns are similar, where the first endotherm peak in the DSC is due to the release of the guest and the second endotherm peak which is the melt of the host. The inclusion of tetrakis–4–(iodophenyl)ethylene with carbon tetrachloride (CCl_4) was found to have a higher energy because the CCl_4 molecules lie in restricted channels and CCl_4 also has the highest boiling point which is 349.9 K. Compounds of these two hosts with diiodomethane (CH_2I_2) did not follow the decomposition pattern of the other compounds. These diiodomethane structures showed lower activation of energies. This was because their crystals were very unstable and started to decompose when removed from their mother liquor. The DSC analysis of these compounds had exothermic peaks which are due to a reaction in the double bond of the host compounds, producing radicals.

Solid host methyliodide vapour reactions were carried out for the kinetics of enclathration where **H1·(2CH_3I)** was successfully synthesised with the same ratio as in the co-crystallisation process. However, when exposing tetrakis–4–(iodophenyl)ethylene to the CH_3I vapour, a 1: 1 ratio of the inclusion was made instead of the 1: 2 ratio as in the co-crystallisation. The rate laws of both above compounds were established.

Guest exchange which is an important tool in crystal engineering was conducted in Chapter 4. Two mechanisms were obtained during the process, which are zeolotic exchange and recrystallization. The first guest exchange reaction was between tetrakis–4–(bromphenyl)ethylene complex with 1, 2-dichloroethane (**1.5H1·DCE**) and the vapour of CH_3I gave rise to an intermediate structure (**6H1·3DCE·2MeI**). This intermediate contains both DCE and CH_3I guests which are distinct and are in separate crystallographic sites with an enlargement in the unit cell which quadrupled in volume. The three other guest exchange reactions were just a recrystallization process, where the incoming guest replaces the existing guest while the host structure remains undestroyed by the mechanism. The rate laws of the complexes with CH_3I were determined. The starting, intermediate and final compounds held the same host/guest ratios and are isomorphous for the second, third and fourth exchange reactions. This is not the case for the first exchange reaction, as the starting, intermediate and final inclusions each have different ratios, and the final product crystallised in a different space group.

The separation of picoline isomers was the main aim in Chapter 5, but when **H1** was dissolved in 2-picoline (2PIC) or 4-picoline (4PIC), the apohost was obtained. However, it only made an inclusion compound with 3-picoline (3PIC). The same results were obtained with **H2**. We therefore pursued the investigation with halogenated substituted pyridines such as 2 –bromopyridine (2BrPY), 3-bromopyridine (3BrPY) and 3-chloropyridine (3ClPY). The classification of all the halogen bond interactions found in the structures was made and two polymorphs yielded from 3PIC as with **H2**. These two polymorphs grew concomitantly, with one as a colourless block, the other as pale pink needles. They crystallised in different space groups as illustrated in Table 8.1 and the 3PIC guests are located in highly constricted channels of hour-glass shape. For their thermal analysis, they both have a double endotherm due to guest loss, where those of the pink needles polymorph are displayed by 15.2 °C and 5.0 °C higher in temperature. Kinetics of enclathration by suspension of H1 host with 3BrPY and 3PIC were

conducted at two specific temperatures 25 °C and 35 °C for each complex and their rate laws were established.

Hydrogen bonding was shown to be dominated by X···X interactions in Chapter 6. Three similar but different host compounds which were synthesised by Weber *et* al[6-10] were utilised in the competition between hydrogen and halogen bonding. It also demonstrated that, if the host molecules were chosen carefully, halogen bonding between unlike components can be favoured over hydrogen bonding.

Halogenated Werner clathrates were synthesised by dissolving $NiCl_2 \cdot 6H_2O$, $NiBr_2$, NiI_2 in chosen picolines and halogenated substituted pyridines. These complexes presented interactions such as C-H···Br, C-H···Cl, C-H···I, C-H···O, C-H···N, O-H···Cl and O-H···I. Werner clathrates obtained with NiI_2 formed salts giving rise to iodide anions. Further adding of I_2 in these Werner clathrates yielded tri-iodide anions. There were two complexes which included the tri-iodide anions. Their asymmetric units comprise two of these tri-iodide anions, and in one of the structures, the tri-iodide was disordered over three positions as illustrated in Chapter 7 (Figure 6 in the paper). All of these compounds resulted in complex thermal analyses; where some of these Werner hosts showed three desorption events, all due to the guest loss, and the same was illustrated in their DSC profiles. Kinetics of enclathration was also performed for compounds composed of $NiCl_2$/$NiBr_2$ with 4PIC and their rate laws were obtained.

Finally, the concept of halogen bonding contributes to an explanation of some aspects of the reactivity in host-guest compounds and with all this research dealing with interactions, we can say halogen bonding has opened a new perspective in supramolecular chemistry.

Table 8.1: Summary of the investigated inclusion compounds.

Complex	Complex ratio	Space group
H1	-	$P2_1/n$
H1·(2CH_2Cl_2)	1: 2	$P2_12_12_1$
H1·(2CH_3I)	1: 2	$P2_12_12_1$
H1·(1.5CH_2I_2)	2: 3	$P2_1/n$
H2·(2CH_2Cl_2)	1: 2	$P2_12_12_1$
H2·(2CH_3I)	1: 2	$P2_12_12_1$
H2·(2$CHCl_3$)	1: 2	$P2_12_12_1$
H2·(2CCl_4)	1: 2	$Pbcn$
H2·(CH_2I_2)	1: 1	$P2_1/c$
1.5H1·DCE	3: 2	$C2/c$
6H1·3DCE·2MeI	6: 3: 2	$C2/c$
H1·BEN	1: 1	$P2_12_12_1$
H1·0.66BEN·0.34PIP	1: 0.66: 0.34	$P2_12_12_1$
H1·PIP	1: 1	$P2_12_12_1$
H2·2DCE	1: 2	$P2_12_12_1$
H2·1.22DCE·0.78MeI	1: 1.22: 0.78	$P2_12_12_1$
H2·BEN	1: 1	$P2_12_12_1$
H2·0.25BEN·0.75PIP	1: 0.25: 0.75	$P2_12_12_1$
H2·PIP	1: 1	$P2_12_12_1$
H1·(2BrPY)	1: 1	$P2_1/n$
H1·1.5(3BrPY)	1: 1.5	$P2_1/n$
H1·1.5(3ClPY)	1: 1.5	$P2_1/n$
H1·1.5(3PIC)	1: 1.5	$P2_1/n$
H2·(3BrPY)	1; 1	$C2/c$
H2·(3ClPY)	1: 1	$C2/c$
H2·(3PIC)A	1: 1	$C2/c$
H2·(3PIC)B	1: 1	$P2_1$
H1·2(3BrPY)	1: 2	$P\bar{1}$
H1·2(3ClPY)	1: 2	$P\bar{1}$
H2·2(3BrPY)	1: 2	$P\bar{1}$
H2·2(3ClPY)	1: 2	$P\bar{1}$
H3·2.5(3BrPY)	1: 2.5	$P\bar{1}$
H3·2.5(3ClPY)	1: 2.5	$P\bar{1}$
[$NiBr_2$(4PIC)$_4$]	-	$P\bar{1}$
[$NiCl_2$(4PIC)$_4$]·½H_2O	1: ½	$P2_1/c$
[$NiCl_2$(3Brpy)$_4$]·½(3BrPY)	1: ½	$P2_1/c$
[Ni(H_2O)$_2$(3PIC)$_4$]$^{2+}$2I$^-$	½: 2	$C2/c$
[Ni(H_2O)$_2$(4PIC)$_4$]$^{2+}$2I$^-$·2(4PIC)·2.5H_2O	1: 2: 2: 2.5	$P2_1$
[Ni(H_2O)$_2$(4Ipy)$_4$]$^{+2}$2I$^-$·3(4IPY)	1: 2: 3	$P\bar{1}$
[Ni(CH_3CN)$_2$(3PIC)$_4$]$^{2+}$2I_3^-	1: 2	$P2_1/n$
[Ni(CH_3CN)$_2$(4PIC)$_4$]$^{2+}$2I_3^-	1: 2	$Pnna$

8.2 References

1. Dumas, J. M.; Gomel, L.; Guerin, M. *Molecular Interactions Involving Organics Halides. In the Chemistry of Functional Groups, Supplement* D; Wiley: New York, 1983, 985 – 1020.
2. Hassel, O.; Hvoslef, J. *Acta. Chem*. 1954, 74 (3), 811 – 824.
3. Hassel, O. *Science*. 1970, 170, 497 – 502.
4. Metrangolo, P.; Resnati, G. *Halogen Bonding: A paradigm in Supramolecular Chemistry*. *Chem. Eur. J*. 2001, 7, 2511 – 2519.
5. Amombo Noa, F. M.; Bourne, S. A.; Nassimbeni, L. R. *Cryst. Growth Des*. 2015, 15, 3271 – 3279.
6. Weber, E.; Skobridis, K.; Wierig, A.; Stathi, S.; Nassimbeni, L. R.; Niven, M. L. *Angew. Chem, Int. Ed. Engl*. 1993, 32, 606-608.
7. Bourne, S. A.; Nassimbeni, L. R.; Niven, M. L.; Weber, E.; Wierig, A. *J. Chem. Soc., Perkin Trans*. *2*. 1994, 1215-1222.
8. Weber, E.; Dörpinhaus, N.; Csöregh, I. *J. Chem. Soc., Perkin Trans. 2*. 1990, 2167-2177.
9. Sprinzak, Y. *J. Am. Chem. Soc*. 1958, 80 (20), 5449-5455.
10. Weber, E.; Nitsche, S.; Wierig, A.; Csöregh, I. *Eur. J. Org. Chem*. 2002, 2002 (5), 856-872.

Appendices

The supplementary material for all crystal structures elucidated in this thesis can be found on the attached CD-ROM in the directory 'APPENDIX'. Five files are included for each structure, namely:

nreport. HTML	Report generated from data collection
Filename. HKL	Contains reflection data
Filename. FCF	Contains tables of observed and calculated structure factors
Filename. RES	Can be used for visualisation of the structure and packing features using an appropriate program such as X-SEED or Platon
Filename. CIF	The Crystallographic Information File

The structure files can be found in a directory named after the relevant compounds and in a subdirectory named after the structure name code.